BEHAVIOURS OF

FUNCTIONALLY GRADED SANDWICH

MICRO- BEAMS AND PLATES

LUAN CONG TRINH

PhD

2017

BEHAVIOURS OF FUNCTIONALLY GRADED SANDWICH MICRO- BEAMS AND PLATES

LUAN CONG TRINH

A thesis submitted in partial fulfilment

of the requirements of the

University of Northumbria at Newcastle

for the degree of

Doctor of Philosophy

Research undertaken in the

Faculty of Engineering & Environment

October 2017

ABSTRACT

Functionally graded materials (FGMs) are a novel class of materials having unique characteristics formed of two or more constituent phases with a continuously variable composition. The introduction of these materials to the sandwich structures creates more potentials to the structural applications with the ability of tailoring the material properties as well as the possibility of avoiding the delamination and stress concentration in conventional sandwich structures. With the rapid development of technology, it is now common to use FGMs in micro/nanoelectromechanical systems, e.g. thin films, sensors, actuators and other devices. At these scales, the use of experimentation to understand the structural behaviours is difficult and highly time-consuming, whilst the molecular modelling is computationally very expensive for the scales that are popular to structural engineers. Therefore, higher-order continuum theories, which were developed from the classical continua, become very popular in modelling micro/nano-scale structures. Based on one of these higher-order continuum theories namely the modified couple stress theory, this thesis aims to develop the analytical methods, i.e. Navier and state space based solutions, to analyse the static, free vibration and buckling behaviours of FG and FG-sandwich beams and plates. The governing equations and appropriate boundary conditions are developed for these structural behaviours of beams and plates at both micro- and macro- scales using the variational principle. Numerical results are computed using MATLAB and verified with the published results to demonstrate the accuracy and efficiency of the developed theoretical formulation. The numerical applications include:

- the free vibration and buckling behaviours of FG and FG sandwich macrobeams under arbitrary boundary conditions and mechanical/thermal loads,
- the static, free vibration and buckling behaviours of simply supported FG microbeams, and the free vibration behaviour of bidirectional FG microbeams under arbitrary boundary conditions,
- the static, free vibration and buckling behaviours of simply supported FG-sandwich microplates under mechanical/thermal loads,
- the static, free vibration and buckling behaviours of FG-sandwich microplates with two opposite simply supported edges and various boundary conditions for other edges.

The outcomes from this thesis emphasize the need of including couple stress in analyzing the structural behaviours of FG beams and plates at microscales. Some of them are presented at the first time and can be used as the benchmark results for numerical methods. These analytical methods can also be combined with other strong form methods to analyse various types of complex structures.

TABLE OF CONTENT

LIST OF TABLES

LIST OF FIGURES

This thesis is dedicated to my family

ACKNOWLEDGEMENT

Firstly, I wish to express my great gratitude to my supervisor, Dr. Thuc Vo, who provides excellent supports with constant encouragement, valuable guidance and additional resources. Alongside the inspiring discussions and proper suggestions to my project, he also provides me with precious advice and unrivalled knowledge base to expedite and enrich my life. Without his wholehearted help, this work would never have been finished.

I would like to sincerely thank Dr. Huu-Tai Thai at Latrobe University for the initial MATLAB codes, and Dr. Trung-Kien Nguyen at HCMC University of Technology and Education for introducing me to the scholarship, and their collaborations. I am also grateful to Dr. Fawad Inam for co-supervising, Dr. Benoit Huard for his discussions on mathematical background, and my friends Hoang Nguyen, Fadi Kahwash at Northumbria and Kien Nguyen at Caltech for their supports in my project.

In addition, I gratefully acknowledge the financial supports from Northumbria University at Newcastle for conducting this research. Many thanks are due to Dr. Adelaja Osofero, for accepting me to this scholarship and initial supports for my PhD project. I also thank HCMC University of Technology and Education for arranging me time to pursue this study.

I would like to express my most profound gratefulness to my parents for supporting me throughout life. Thank you does not seem enough for all their love, dedication and supports.

Finally, my deepest appreciation goes to my wife Ngoc-Diem and my daughter Bao-Vy for their love, dedication and encouragement during past years, which has allowed me to finish this thesis.

Northumbria University, Newcastle Luan Cong Trinh

October 2017

DECLARATION

I declare that the work contained in this thesis has not been submitted for any other award and that it is all my own work. I also confirm that this work fully acknowledges opinions, ideas and contributions from the work of others. Any ethical clearance for the research presented in this thesis has been approved. Approval has been sought and granted by the Faculty Ethics Committee RE-EE-14-150105-54aa7f4db6468 on 21/9/2015.

I declare that the Word Count of this Thesis is 40,000 words, excluding the References and Appendices.

Name: Luan Cong Trinh

Signature:

Date: 11th October 2017

CHAPTER 1

INTRODUCTION

1.1 Purpose and scope

Functionally Graded Materials (FGMs) are a class of composite materials in which the material properties vary gradually from one position to the other. Such materials are created from the exploitation of basic material elements into various organic and inorganic compounds to produce advanced polymers and elastomers, alloys, glasses and ceramics. The gradation process of this kind of materials can create the industrial products with smooth and continuous properties, hence avoids the stress concentration, cracking and delamination phenomena occurred in conventional composites. These striking features are appealing to the researchers in developing the advanced theories and analysis methods to predict more accurate behaviour of FG materials/structures. The combination of FGMs and sandwich structures, often referred to as FG-sandwich structures, has become even more attractive due to the designable material properties and the possibility to eliminate the delamination which occurs in conventional composite structures. Many applications of FGMs can be found in aerospace structures [1], cutting tools [2], actuators, transducers [3] and biomedical installations. An insightful introduction to the applications of FGMs is presented in [4].

Recent developments in technology require the knowledge of small-scale structural elements which are commonly presented in MEMS and NEMS such as thin films, nano-probes, sensors, actuators and other devices. It is evidenced from experiments [5-7] that when the dimensions of these structures are reduced to a certain value, the size effects in structural behaviours can be observed. There are several approaches to inspect these effects including the experimentation, atomistic or molecular dynamics simulation and higher-order continuum mechanics. Although two former methods can provide more accurate prediction, the latter has been employed widely due to the computational efficiency. Because of the coupling effects regarding the higher-order gradients of displacements, there are some challenges in integrating the analysis of microstructures to commercial software for common use. Moreover, the continuous variation of material properties in FGM leads to difficulties in using finite element packages to analyse the structural behaviours of these materials, particularly in terms of generating the stiffness matrices. Therefore, developing the effective and accurate theoretical approaches to solve these problems is one of the primary motivations of this study. The main objectives of this thesis include:

a. To develop a unified shear deformation theory in connection with the modified couple stress theory to investigate the size dependent behaviours of FG-sandwich beams and plates. The thesis concentrates on the higher-order shear deformation theories including the thickness stretching effects, i.e. quasi-3D theories, which are significant in very thick beams and plates.

b. To develop the analytical solutions, i.e. the Navier and state space based solutions, for the analysis of the static bending, free vibration and buckling behaviours of FG-sandwich beams and plates. This thesis also considers the effects of different factors such as non-classical boundary conditions and thermal environment as well as the axial and thickness variation of material properties in beams.

1.2 Background

This section presents some generic knowledge about FGMs and FG-sandwich structures, thermal environment and the size-dependent analysis of microstructures.

1.2.1 Functionally graded materials and FG-sandwich structures

The idea of FGMs can be observed in most of organisms in nature. Apart from some examples given in Fig. 1.1 for a tree cross-section and skin structure, the gradual variation of constituent phases can be seen in other configurations, such as shells, bones, teeth, cells, etc.

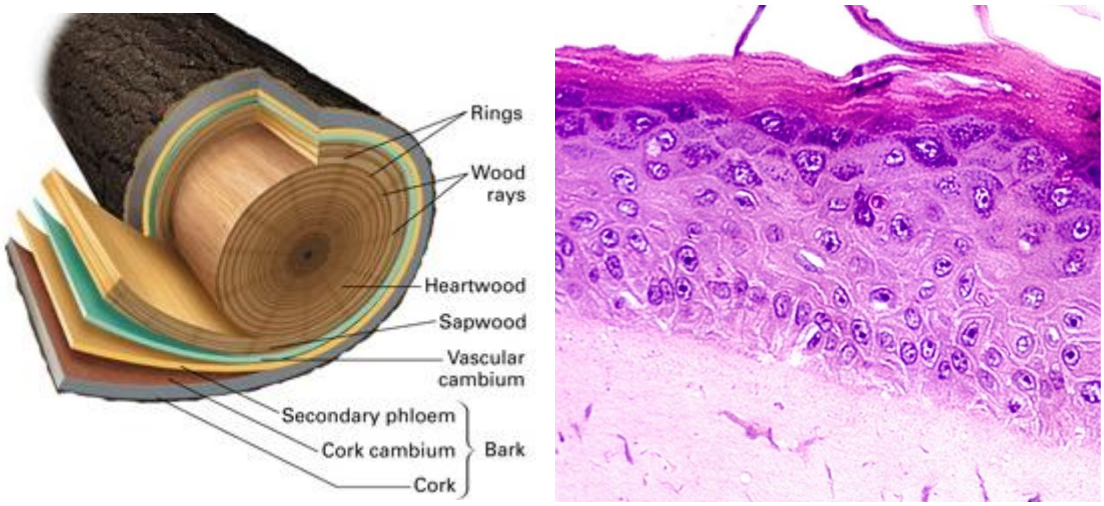

a. Tree cross-section [1] *b. Skin*[2]

Fig. 1. 1: FGMs in nature.

In the mid-1980s, Japanese researchers conceived the concept of FGM to an aerospace application to advance the material properties using in the thermal barrier coating [8]. Since

[1] www.sflonews.files.wordpress.com/2014/11/tree-cross-section.jpg
[2] www.igb.fraunhofer.de/en/press-media/press-releases/1999/skin-cosmetic-research.html

then, there are a large number of publications have been dedicated to analyse the behaviours of these materials. Following section is the effective material properties of FGMs and different types of FG-sandwich structures which are considered in this thesis.

1.2.1.1 Effective material properties of FGMs (homogenisation schemes)

The effective material properties of FGMs, which are microscopic heterogeneous, can be obtained using homogenisation techniques. Two of the most popular techniques include the rule of mixture (Voigt model [9, 10]) and Mori-Tanaka model [11]. The effective material properties can be determined using these two schemes as follow. By considering a FG beam with the geometries and co-ordinates illustrated in Fig. 1.2, the effective material properties can be determined as follows:

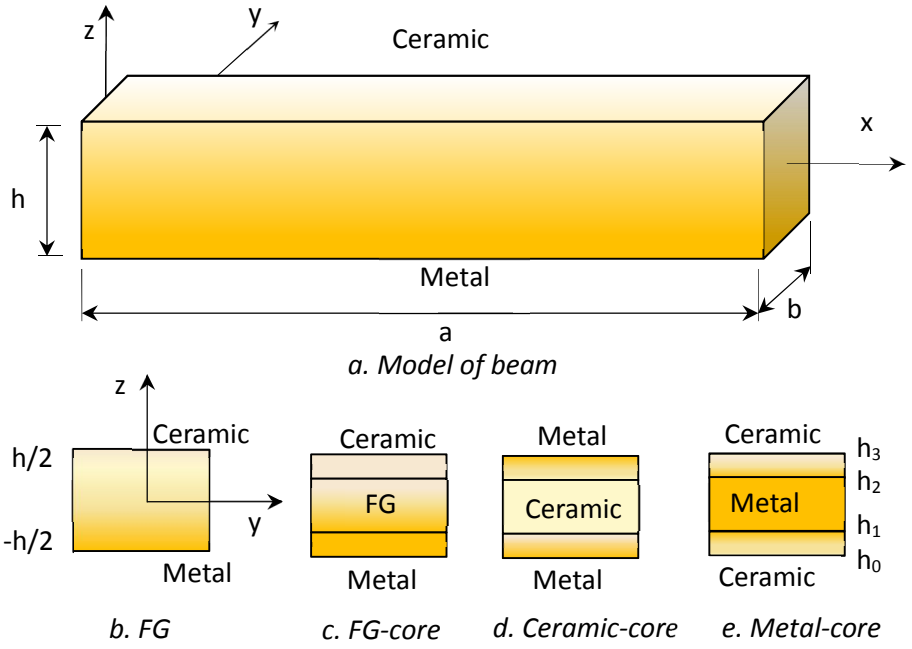

Fig. 1. 2: Geometries, co-ordinates and cross-sections of FG-sandwich beams

a. Rule of mixture (Voigt model)

According to the rule of mixture, the effective material properties of FG structures can be expressed as:

$$P_e = P_m V_m + P_c V_c \tag{1. 1}$$

where P_m and P_c are the material properties of metal and ceramic, and V_m and V_c represent the volume fraction of metal and ceramic, which depend on the types of FG structures as presented in the next section.

b. Mori-Tanaka scheme

According to Mori-Tanaka scheme [12], the effective bulk modulus K_e and shear modulus G_e are given by:

$$\frac{K_e - K_m}{K_c - K_m} = \frac{V_c}{1 + V_m \dfrac{K_c - K_m}{K_m + \frac{4}{3}G_m}} \tag{1. 2a}$$

$$\frac{G_e - G_m}{G_c - G_m} = \frac{V_c}{1 + V_m \dfrac{G_c - G_m}{G_m + \dfrac{G_m\left(9K_m + 8G_m\right)}{6\left(K_m + 2G_m\right)}}} \tag{1. 2b}$$

The effective Young's modulus E_e and Poisson's ratio ν_e are then defined as:

$$E_e = \frac{9K_eG_e}{3K_e + G_e} \tag{1. 3a}$$

$$\nu_e = \frac{9K_e - 2G_e}{2\left(3K_e + G_e\right)} \tag{1. 3b}$$

1.2.1.2 Types of FG and FG-sandwich structures

In this thesis, major attentions are paid for the through-the-thickness FG and FG-sandwich structures including the FG-skins homogeneous-core (ceramic and metal cores), and FG-core homogeneous-skins. In addition, the bidirectional FG beams, in which the material properties can be tailored in both the longitudinal and thickness directions, is also considered in Chapter Four.

a. FG structures

The structures are made of metal-ceramic material (Fig.1b) with the volume fraction of ceramic through thickness $V_c\left(z\right)$ being given by:

$$V_c(z) = \left(\frac{z}{h} + \frac{1}{2}\right)^p \tag{1. 4}$$

where p is the power-law index.

b. Sandwich structures with FG core and homogeneous skins

In these structures, metal and ceramic are placed on the metal-rich and ceramic-rich faces of the FG core (Fig.1c) with $V_c\left(z\right)$ being given by:

$$V_c(z)=\begin{cases}0 & if\ z\in[h_0,h_1]\\ \left(\dfrac{z-h_1}{h_2-h_1}\right)^p & if\ z\in[h_1,h_2]\\ 1 & if\ z\in[h_2,h_3]\end{cases} \quad (1.5)$$

c. Sandwich structures with FG skins and homogeneous core

Ceramic or metal cores are attached into two layers of FG skins in these structures. The expression of $V_c(z)$ for these two types of sandwich structures are described as follow:

- Ceramic core (Fig.1d):

$$V_c(z)=\begin{cases}\left(\dfrac{z-h_0}{h_1-h_0}\right)^p & if\ z\in[h_0,h_1]\\ 1 & if\ z\in[h_1,h_2]\\ \left(\dfrac{z-h_3}{h_2-h_3}\right)^p & if\ z\in[h_2,h_3]\end{cases} \quad (1.6)$$

- Metal core (Fig.1e):

$$V_c(z)=\begin{cases}1-\left(\dfrac{z-h_0}{h_1-h_0}\right)^p & \text{if } z\in[h_0,h_1]\\ 0 & \text{if } z\in[h_1,h_2]\\ 1-\left(\dfrac{z-h_3}{h_2-h_3}\right)^p & \text{if } z\in[h_2,h_3]\end{cases} \quad (1.7)$$

1.2.2 Thermal effect on the behaviours of FG-sandwich structures

1.2.2.1 Temperature distribution

In some examples of this thesis, the FG-sandwich structures are considered working in thermal environment, which is created by the elevated temperature on their top and bottom. The temperature profiles investigated are listed below:

a. Uniform Temperature Rise (UTR)

The temperature of the whole beams/plates is assumed uniform and increased from T_0=*300K* to the reference value. It means that the temperature at a point is $T(z)=T_0+\Delta T$, where ΔT is the temperature rise.

b. Linear Temperature Rise (LTR)

The temperature in the ceramic and metal faces of FG structures is assumed to be T_c and T_m. In this case, the temperature on the metal surface is supposed to be $T_m = 305K$, whereas on the ceramic surface it is surged to $T_c = T_0 + \Delta T$. With the assumption of linear distribution, the temperature through the thickness can be determined as:

$$T(z) = T_m + \Delta T\left(\frac{1}{2} + \frac{z}{h}\right) \tag{1. 8}$$

c. Non-linear Temperature Rise (NLTR)

The applied temperature is similar to the case of LTR; however, the temperature distribution is set to follow the heat conduction rule and obtained by solving the steady state equation [13] as:

$$T(z) = T_m + \frac{T_c - T_m}{C}\left(\begin{array}{l} V_f - \frac{K_{cm}}{(p+1)K_{cm}}V_f^{p+1} + \frac{K_{cm}^2}{(2p+1)K_m^2}V_f^{2p+1} - \frac{K_{cm}^3}{(3p+1)K_m^3}V_f^{3p+1} \\ + \frac{K_{cm}^4}{(4p+1)K_m^4}V_f^{4p+1} - \frac{K_{cm}^5}{(5p+1)K_m^5}V_f^{5p+1} \end{array}\right) \tag{1. 9}$$

where $C = 1 - \frac{K_{cm}}{(p+1)K_{cm}} + \frac{K_{cm}^2}{(2p+1)K_m^2} - \frac{K_{cm}^3}{(3p+1)K_m^3} + \frac{K_{cm}^4}{(4p+1)K_m^4} - \frac{K_{cm}^5}{(5p+1)K_m^5}$; $K_{cm} = K_c - K_m$; $V_f = \left(\frac{z}{h} + \frac{1}{2}\right)$, with K_c and K_m being the thermal conductivity of ceramic and metal calculated at the surfaces.

1.2.2.2 Temperature-dependent material properties

The thermo-elastic material properties are considered as a function of temperature *T* and can be calculated for ceramic and metal as described in [14]:

$$P(T) = P_0\left(P_{-1}T^{-1} + 1 + P_1T + P_2T^2 + P_3T^3\right) \tag{1. 10}$$

where P denotes Young's modulus E, mass density ρ and thermal expansion coefficient α, respectively. P_{-1}, P_1, P_2 and P_3 are the temperature dependent coefficients, which are provided for each material in the numerical examples.

1.2.3 Size effect in analysing the structural behaviours

In order to study the behaviours of small-scale structures, the higher-order continuum theories, which are widely known as the non-classical continua, were firstly presented in the work of Cosserat and Cosserat [15] in 1909. There have been significant developments of this idea since 1960s, which can be summarised into three major categories including the microcontinua,

nonlocal elasticity and the strain gradient family [16]. The microcontinua were developed by Eringen [17-20] for 3M theories including micropolar, microstretch and micromorphic. Among them, micropolar is the simplest theory, which was initiated by Cosserat and Cosserat [15], whilst the micromorphic is the most general one. Interested readers can refer to [21-25] for more details about these theories and their applications. The nonlocal elasticity was firstly proposed by Kroner in [26] and further developed by Eringen [27-29]. In these theories, the stress at a reference point is measured through the constitutive law by the strains at all points of the body. Therefore, the size effects are captured by introducing a nonlocal parameter to the constitutive equations. The third class of higher-order continua is the strain gradient family, which are composed of the couple stress theory, the strain gradient theory and their modified versions. In the strain gradient family, the strain energy is considered as a function of both strains and strain gradients, which requires additional material constants, i.e. material length scale parameters, compared to the classical continuum. The original strain gradient theory considering the first gradient of strains only was proposed by Mindlin [30]. He later developed another version including both the first and second gradients of strains [31]. A modified strain gradient theory was developed recently by Lam et al. [7] which requires only three material length scale parameters. These theories have drawn much attentions in applying for different behaviours of microstructures. Another member of the strain gradient family is the classical couple stress theory, which was proposed by Toupin [32, 33], Mindlin and Tiersten [34] and Koiter [35]. In these theories, only two additional material length scale parameters are required as only the gradients of rotation vectors are included. Yang et al. [36] developed a modified couple stress theory by introducing an equilibrium condition of moments of couples. This higher-order equilibrium results in a symmetricity of the couple stress tensor, hence only one material length scale parameter is required. This modified theory has been employed widely recently to investigate the size effects in microstructures, which is also the motivation of this study. The research using this theory for microbeams/plates is reviewed in detail at the beginning of the relevant chapters. A perceptive review of higher-order continua for size-dependent analysis of microstructures can also be found in the recent work of Thai et al. [16].

1.3 Organisation

There are six chapters in this thesis. Chapter One describes the purpose and scope as well as the background and organisation of the thesis. Based on the unified higher-order beam theories, Chapter Two deals with the vibration and buckling behaviours of axially loaded FG-sandwich beams. The governing equations of motion are derived from Hamilton's principle for the beams with arbitrary classical boundary conditions and several cases of elastic supports. Numerical

examples are presented to examine the effects of boundary conditions, material properties, and slenderness ratios on the fundamental natural frequencies of these sandwich beams. A number of possible modal frequencies, the buckling loads and temperatures as well as the load-frequency curves are also considered for the FG beams. Both temperature independent and dependent material properties are investigated to prove the necessity of considering the change of material properties under the elevated temperature gradients. The modified couple stress theory is employed in Chapter Three for FG-sandwich beams using the classical beam theory, first-order beam theory, different higher-order and quasi-3D theories. The Navier solutions are applied to solve analytically the deflection and stress, natural frequencies and critical buckling loads. Two homogenisation techniques to approximate the material properties including the rule of mixture and Mori-Tanaka scheme are considered. The comparison of various shear deformation theories, effects of Poisson's ratio and the size-dependent behaviours of FG beams are discussed in this chapter. The theoretical formulation in Chapter Three are extended in Chapter Four for the size-dependent vibration behaviours of bidirectional FG (BDFG) beams, in which the material properties vary exponentially in both the thickness and axial directions. This chapter also covers the behaviours of through-the-thickness FG beams by neglecting the axial exponential index. The state space approach is employed to analyse the free vibration of BDFG beams with arbitrary boundary conditions including the essential of clarifying the left and right end conditions. Chapter Five is devoted to the analysis of FG-sandwich microplates. Based on the framework of the modified coupe stress theory, the theoretical formulation for static bending, vibration and buckling of FG-sandwich microplates are presented. The simply supported plates are analysed applying the Navier solution, while other boundary conditions in combination with the two opposite simply supported edges are considered using the state space based solutions. In the last chapter, the main conclusions and recommendations for future research are presented. Finally, the coefficients for state space based solutions and stress resultants adopted for the analysis of beams/plates are given in the Appendices.

CHAPTER 2

FREE VIBRATION AND BUCKLING BEHAVIOURS OF FG-SANDWICH BEAMS

2.1 Introduction

In this section, a brief review of various shear deformation theories and analysis techniques applied to the vibration and buckling analysis of FG and FG-sandwich beams is carried out. The earliest beam model is due to the Euler-Bernoulli theory, which widely known as Classical Beam Theory (CBT). The ignorance of the shear effect in this theory provides acceptable results for thin beams only. This theory was applied to study the dynamic behaviour of FG beams by Alshorbagy et al. [37], Simsek and Kocaturk [38] and Jin and Wang [39]. It is worth noting that solutions based on the CBT overestimate natural frequencies/buckling loads of moderately thick beams. To overcome the limitation of the CBT, many shear deformation theories have been proposed. The Timoshenko beam theory known as the first-order beam theory (FOBT), which is the simplest model considering shear effect, attracts much attention of researchers. Aydogdu et al. [40] presented Navier solution of natural frequencies for FG beams. Su and Banerjee [41, 42] developed dynamic stiffness method for free vibration analysis of FG beams using the CBT and FOBT. Nguyen et al. [43] proposed an improvement on FOBT to present Navier solution for static and vibration responses of FG beams under axial load. Sina et al. [44] also applied FOBT to analyse free vibration of FG beams. However, the FOBT needs a shear correction factor to modify the results due to the dissatisfaction of free stress at the free surfaces. This factor is difficult to determine exactly since it depends on many parameters. To overcome this problem, the higher-order beam theory (HOBT) was developed to analyse beam's behaviours more accurately without using shear correction factor. Thai and Vo [45] investigated static and free vibration behaviour of FG beams using various HOBTs. Wattanasakulpong [46] and Pradhan and Chakraverty [47, 48] employed Rayleigh-Ritz method using the CBT, FOBT and HOBT to analyse natural vibration of FG beams. Simsek [49] obtained fundamental frequencies of FG beams with varying boundary conditions based on Lagrange approach. Mashat et al. [50] applied Carrera Unified Formulation to investigate free vibration of FG layered beams. Vo et al. [51] and Nguyen et al. [52] also employed different HOBTs with finite element and Rayleigh-Ritz methods to analyse the vibration and buckling behaviour of FG-sandwich beams. The investigation into free vibration behaviour of FG beams was also carried out by mesh-free techniques in [53-55] and also by homogenization approach [56].

One of the key parameters in the analysis of the vibration behaviour of structures is the boundary conditions. For the real structures, the imperfect boundary conditions known as non-

classical conditions consisting of rotational and translational displacements are essential and need to be considered. There are many publications relating to the investigation of free vibration under imperfect support, which mostly focus on isotropic beams such as the work of Hsu et al. [57] with Adomian modified decomposition method using FOBT; Sari [58, 59] with Chebyshev collocation method based on CBT and FOBT. Simsek and Cansiz [60] analysed dynamic behaviour of elastically connected double-FG beam with elastic supports under moving harmonic load. Shahba et al. [61] studied free vibration response of Timoshenko axially FG beams. Wattanasakulpong and Mao [62] also applied Chebyshev collocation to consider the free vibration of FG beams using FOBT.

Regarding the thermal environment, FG beams can be designed in a smart way to adapt the environment changes, which receive considerable attention in recent years. Sankar and Tzeng [63] used CBT to study the thermal stresses of simply supported FG beams. The FOBT was employed to investigate various behaviours of FG beams such as dynamic responses under a moving load [13], thermal stability with non-linear hardening elastic foundations [64], thermal dynamic buckling [65], and thermal buckling and post-buckling with non-linear elastic foundation [66]. Wattanasakulpong et al. [67] employed the HOBT to study the buckling and vibration of FG beams under the thermal loading for only uniform temperature distribution.

In this chapter, an analytical analysis [68-70] for vibration and buckling analysis of FG beams using HOBT under mechanical/thermal loads is proposed. Equations of motion are derived from Hamilton's principle. Three cases of the temperature rise through the thickness are considered. These are uniform, linear and nonlinear variations. State space based analytical approach is used to obtain closed-form solutions for the critical loads/temperatures and natural frequency of FG beams with various boundary conditions. The effects of boundary conditions, temperature distributions, power-law indices and slenderness ratios on the critical temperatures, critical buckling loads, and natural frequencies as well as load-frequencies curves, temperature-frequencies curves of FG beams under thermal/mechanical loads are investigated.

2.2 Kinematics

Consider a FG-sandwich beam with the geometry and co-ordinates described in Fig. 2.1. Assume that the deformation of FG-sandwich beam is confined only to $x-z$ plane and let $u(x,z,t)$ and $w(x,z,t)$ be the axial and transverse displacement components at an arbitrary point (x,z).

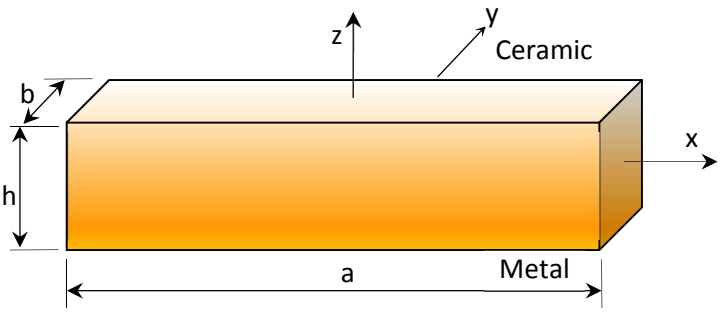

Fig. 2. 1: Geometry of FG beams.

These components can be expressed as shown in Eq. (2.1) using higher-order shear deformation:

$$u(x,z,t)=U(x,t)-zW^{'}(x,t)+f(z)\varphi(x,t) \tag{2. 1a}$$

$$w(x,z,t)=W(x,t) \tag{2. 1b}$$

where $U=U(x,t)$ and $W=W(x,t)$ represent the displacement components of a point on the beam's mid-line along x and z directions while $\varphi=\varphi(x,t)$ is the rotational angle of the cross-section about $y-$axis. The shape function $f(z)=z-\frac{4z^2}{3h^3}$, which is proposed by Reddy [71], is employed in this section. The prime (') represents the partial differentiation of the quantities with respect to *x*.

For the FOBT and CBT, the axial displacement is described respectively as follow:

$$u(x,z,t)=U(x,t)+z\varphi(x,t) \tag{2. 2a}$$

$$u(x,z,t)=U(x,t)-zW^{'}(x,t) \tag{2. 2b}$$

The strains related to the displacement field in Eq. (2.1) are:

$$\varepsilon_x=\frac{\partial u}{\partial x}=U^{'}-zW^{''}+f(z)\varphi^{'} \tag{2. 3a}$$

$$\gamma_{xz}=\frac{\partial u}{\partial z}+\frac{\partial w}{\partial x}=\left[1-\frac{\partial f(z)}{\partial z}\right]\varphi=g(z)\varphi \tag{2. 3b}$$

2.3 Variational formulation

To derive the governing equations of motions and boundary conditions, Hamilton's principle is employed to give

$$\int_{t_1}^{t_2}(\delta K-\delta U-\delta \mathrm{V})dt=0 \tag{2. 4}$$

where δU , $\delta \mathrm{V}$ denote the virtual variation of the strain energy, external work by axial load or thermal expansion and δK is the kinetic energy.

The virtual variation of the strain energy is given by:

$$\delta \mathrm{U} = \int_{-a/2}^{a/2}\int_{0}^{b}\int_{-h/2}^{h/2} \left(\sigma_x \delta\varepsilon_x + \sigma_{xz}\delta\gamma_{xz}\right) dz dy dx$$

$$= \int_{-a/2}^{a/2} \left(N_x \delta U^{'} - M_x \delta U^{''} + P_x \delta\varphi^{'} + Q_{xz} g(z)\delta\varphi\right) dx \tag{2. 5}$$

where the stress resultants N_x, M_x, P_x and Q_{xz} can be defined as:

$$\left(N_x, M_x, P_x\right) = \int_{-h/2}^{h/2} \sigma_x \left(1, z, f\right) b dz \tag{2. 6a}$$

$$Q_{xz} = \int_{-h/2}^{h/2} \sigma_{xz} b dz \tag{2. 6b}$$

The virtual variation of the external work can be determined as:

$$\delta V = -\int_{-a/2}^{a/2} P_0 W^{'} \delta W^{'} dx \tag{2. 7}$$

where P_0 is the mechanical load/thermal stress resultant, which is discussed in section 2.4.

It is noticeable that the integration is written for FG beams only, for sandwich beam a cumulative formulation is applied, i.e. $\int_{-h/2}^{h/2} \mathbb{F}\left(z\right) dz = \int_{h_0}^{h_1} \mathbb{F}\left(z\right) dz + \int_{h_1}^{h_2} \mathbb{F}\left(z\right) dz + \int_{h_2}^{h_3} \mathbb{F}\left(z\right) dz$ where $\mathbb{F}\left(z\right)$ is an arbitrary function of *z*.

The virtual variation of the kinetic energy can be determined as:

$$\delta K = \int_{-a/2}^{a/2} \left(\dot{u}\delta\dot{u} + \dot{w}\delta\dot{w}\right) \rho\left(z\right) b dx$$

$$= \int_{-a/2}^{a/2} \Big[I_0 \left(\dot{U}\delta\dot{U} + \dot{W}\delta\dot{W}\right) - I_1 \left(\dot{W}^{'}\delta\dot{U} + \dot{U}\delta\dot{W}^{'}\right) + I_2 \dot{W}^{'}\delta\dot{W}^{'}$$

$$+ I_f \left(\dot{\varphi}\delta\dot{U} + \dot{U}\delta\dot{\varphi}\right) - I_{fz} \left(\dot{\varphi}\delta\dot{W}^{'} + \dot{W}^{'}\delta\dot{\varphi}\right) + I_{f^2}\dot{\varphi}\delta\dot{\varphi} \Big] dx \tag{2. 8}$$

where (.) denotes the time derivative, and

$$\left(I_0, I_1, I_2, I_f, I_{fz}, I_{f^2}\right) = \int_{-a/2}^{a/2} \left(1, z, z^2, f, zf, f^2\right) \rho\left(z\right) b dz \tag{2. 9}$$

2.4 Constitutive equations

$$\sigma_x = E(z)\left[\varepsilon_x - \alpha(z)(T - T_0)\right] = Q_{11}\varepsilon_x + \sigma_x^T \tag{2. 10a}$$

$$\sigma_{xz} = \frac{E}{2(1+\nu)}\gamma_{xz} = Q_{55}\gamma_{xz} \tag{2. 10b}$$

$$\text{in which } Q_{11} = E(z),\ Q_{55} = \frac{E(z)}{2(1+\nu)} \text{ and } \sigma_x^T = E(z)\alpha(z)(T - T_0) \tag{2. 11}$$

where T and T_0 are the observed and referenced temperatures, respectively.

By substituting Eqs. (2.3) and (2.10) into Eq. (2.6), the stress resultants are obtained as:

$$\begin{Bmatrix} N_x \\ M_x \\ P_x \\ Q_{xz} \end{Bmatrix} = \begin{bmatrix} A & B & B & 0 \\ B & D & F & 0 \\ C & F & H & 0 \\ 0 & 0 & 0 & A_s \end{bmatrix} \begin{Bmatrix} U' \\ -W'' \\ \varphi' \\ g(z)\varphi \end{Bmatrix} - \begin{Bmatrix} N_x^T \\ M_x^T \\ P_x^T \\ Q_x^T \end{Bmatrix} \tag{2. 12}$$

where

$$(A, B, D, C, F, H) = \int_{-h/2}^{h/2} Q_{11}\left(1, z, z^2, f, zf, f^2\right) b dz \tag{2. 13a}$$

$$A_S = K_s \int_{-h/2}^{h/2} Q_{55} b dz\,. \tag{2. 13b}$$

$$\begin{Bmatrix} N_x^T \\ M_x^T \\ P_x^T \end{Bmatrix} = \int_{-h/2}^{h/2} Q_{11}\alpha(z)\left[T(z) - T_0\right] \begin{Bmatrix} 1 \\ z \\ z^3 \end{Bmatrix} dz \tag{2. 13c}$$

$$Q_x^T = 0 \tag{2. 13d}$$

in which K_s is the shear modified correction factor. K_s=5/6 in the FOBT model and K_s=1 for other models. In this section, M_x^T and P_x^T are neglected and the thermal load $P_0 = N_x^T$ is the load to cause the buckling response in the beams.

2.5 Governing equations of motion

By substituting Eqs. (2.5) and (2.7) into Eq. (2.4), integrating the equation by part, and collecting the coefficients of δU, $\delta\varphi$ and δW, the governing equations of motion are obtained as:

$$N_x' = I_0\ddot{U} - I_1\ddot{W}' + I_f\ddot{\varphi} \tag{2. 14a}$$

$$M_x'' - P_0 W'' = I_0 \ddot{W} + I_1 \ddot{U}' - I_2 \ddot{W}'' + I_{fz} \ddot{\varphi}' \quad \text{(2. 14b)}$$

$$P_x' - Q_{xz} g(z) = I_f \ddot{U} - I_{fz} \ddot{W}' + I_{f^2} \ddot{\varphi} \quad \text{(2. 14c)}$$

2.6 Boundary conditions (BCs)

In this section, both classical and non-classical BCs are investigated. Regarding the non-classical BCs, the elastic supports (E) including the translational (T) and rotational (R) springs, which are described in Fig. 2.2 are considered.

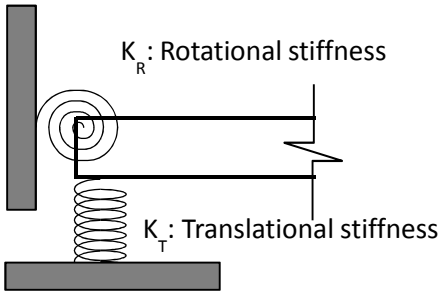

Fig. 2. 2: Model of elastic support.

Apart from the classical BCs, such as clamped, free, hinged, and simply supported, which can be observed in the perfect structures, this section examines the effect of elastic supported boundary, which occurs in the imperfect supports. These BCs are described in Tables 2.1 and 2.2, where k_T and k_R are the translational and rotational spring stiffness; '+' for the left end and '-' for the right end. For simplicity, the dimensionless spring factors for translational and rotational support are defined as $\beta_T = \frac{k_T L}{E_m h}$ and $\beta_R = \frac{12 k_R L}{E_m h^3}$, respectively.

Table 2. 1: The essential and natural BCs of FG-sandwich beams.

Type of BCs	Essential BCs	Natural BCs		
		CBT	FOBT	HOBT
Classical	U	N_x	N_x	N_x
	φ	n/a	M_x	P_x
	W	$M_x^{'}$	$M_x^{'}+Q_{xz}$	$M_x^{'}+Q_{xz}$
	W'	M_x	n/a	M_x
Non-classical	Rotational	$M_x \pm k_R W^{'}$	$M_x \pm k_R \varphi$	$M_x \pm k_R W^{'}$
		-	-	$P_x \pm k_R \varphi$
	Translational	$M_x^{'} \pm k_T W$	$M_x^{'}+Q_{xz} \pm k_T W$	$M_x^{'}+Q_{xz} \pm k_T W$

Table 2. 2: The essential and natural BCs of FG-sandwich beams expressed by the displacement.

BCs	Theory		
	CBT	FOBT	HOBT
C	$U=W=W'=0$	$U=\varphi=W=0$	$U=\varphi=W=W'=0$
H	$U=W=BU'-DW''=0$	$U=W=BU'+D\varphi'=0$	$U=W=AU'-FW''+H\varphi'$ $=BU'-DW''+F\varphi'=0$
S	$AU'-BW''=W$ $=BU'-DW''=0$	$AU'+B\varphi'=W$ $=BU'+D\varphi'=0$	$AU'-BW''+C\varphi'=W$ $=AU'-FW''+H\varphi'$ $=BU'-DW''+F\varphi'=0$
F	$AU'-BW''=BU'-DW''$ $=BU''-DW'''+\omega^2\left(I_1U-I_2W'\right)=0$	$AU'+B\varphi'=BU'+D\varphi'$ $=A_s\left(\varphi+W'\right)=0$	$AU'-BW''+C\varphi'$ $=BU'-DW''+F\varphi'$ $=BU''-DW'''+F\varphi''$ $+\omega^2\left(I_1U+J_2\varphi-I_2W'\right)$ $=AU'-FW''+H\varphi'=0$
E	$U=BU'-DW''\pm k_RW'$ $=BU''-DW'''$ $+\omega^2\left(I_1U-I_2W'\right)\pm k_TW=0$	$U=A_s\left(\varphi+W'\right)\pm k_TW$ $=BU'+D\varphi'\pm k_R\varphi=0$	$U=BU'-DW''+F\varphi'\pm k_R\varphi$ $=BU''-DW'''+F\varphi''$ $+\omega^2\left(I_1U+J_2\varphi-I_2W'\right)\pm k_TW$ $=AU'-FW''+H\varphi'\pm k_RW'=0$

2.7 State space based solution

2.7.1 Vibration analysis

By using the state space approach [68], the displacement components can be expressed as:

$$\begin{Bmatrix} U(x,t) \\ \varphi(x,t) \\ W(x,t) \end{Bmatrix} = \begin{Bmatrix} U(x) \\ \varphi(x) \\ W(x) \end{Bmatrix} e^{i\omega t} \tag{2. 15}$$

where ω is the natural frequency.

By substituting Eq. (2.15) into Eq. (2.14), a system of ordinary differential equations is obtained:

$$U'' = a_1 U + a_2 \varphi + a_3 W' + a_4 W''' \tag{2. 16a}$$

$$\varphi_x'' = a_5 U + a_6 \varphi + a_7 W' + a_8 W''' \tag{2. 16b}$$

$$W^{(iv)} = a_9 U' + a_{10} \varphi' + a_{11} W + a_{12} W'' \tag{2. 16c}$$

where the coefficients a_n are described as:

$$a_1 = \frac{e_1 e_8 - e_3 e_4}{e_2 e_8 - e_4^2},\ a_2 = \frac{e_3 e_8 - e_4 e_7}{e_2 e_8 - e_4^2},\ a_3 = \frac{e_5 e_8 - e_4 e_9}{e_2 e_8 - e_4^2},\ a_4 = \frac{-e_6 e_8 + e_4 e_{10}}{e_2 e_8 - e_4^2}, a_5 = \frac{e_2 e_3 - e_1 e_4}{e_2 e_8 - e_4^2},$$

$$a_6 = \frac{e_2 e_7 - e_3 e_4}{e_2 e_8 - e_4^2},\ a_7 = \frac{e_2 e_9 - e_4 e_5}{e_2 e_8 - e_4^2},\ a_8 = \frac{-e_2 e_{10} + e_4 e_6}{e_2 e_8 - e_4^2}, a_9 = \frac{a_1 e_6 + a_5 e_{10} - e_5}{e_{12} - a_4 e_6 - a_8 e_{10}},$$

$$a_{10} = \frac{a_2 e_6 + a_6 e_{10} - e_9}{e_{12} - a_4 e_6 - a_8 e_{10}},\ a_{11} = \frac{e_1}{e_{12} - a_4 e_6 - a_8 e_{10}},\ a_{12} = \frac{a_3 e_6 + a_7 e_{10} + e_{11} + P_0}{e_{12} - a_4 e_6 - a_8 e_{10}}, \tag{2. 17}$$

in which

$$e_1 = -I_0 \omega^2\ ,\ e_2 = A\ ,\ e_3 = -I_f \omega^2\ ,\ e_4 = C\ ,\ e_5 = I_1 \omega^2\ ,\ e_6 = -B\ ,$$

$$e_7 = -I_{f^2} \omega^2 + A_s\ ,\ e_8 = H\ ,\ e_9 = I_{fz} \omega^2\ ,\ e_{10} = -F\ ,\ e_{11} = I_2 \omega^2\ ,\ e_{12} = -D\ . \tag{2. 18}$$

The system of Eq. (2.16) can be converted into a matrix form as:

$$\mathbf{Z}'(x) = \mathbf{T}\mathbf{Z}(x) \tag{2. 19}$$

where

$$Z(x) = \left\{U, U', \varphi, \varphi', W, W', W'', W'''\right\} \text{ is the vector of unknowns,} \tag{2. 20}$$

and matrix of coefficients **T** is defined as:

$$\mathbf{T}=\begin{bmatrix} 0 & 1 & 0 & 0 & 0 & 0 & 0 & 0 \\ a_1 & 0 & a_2 & 0 & 0 & a_3 & 0 & a_4 \\ 0 & 0 & 0 & 1 & 0 & 0 & 0 & 0 \\ a_5 & 0 & a_6 & 0 & 0 & a_7 & 0 & a_8 \\ 0 & 0 & 0 & 0 & 0 & 1 & 0 & 0 \\ 0 & 0 & 0 & 0 & 0 & 0 & 1 & 0 \\ 0 & 0 & 0 & 0 & 0 & 0 & 0 & 1 \\ 0 & a_9 & 0 & a_{10} & a_{11} & 0 & a_{12} & 0 \end{bmatrix} \tag{2. 21}$$

Similarly, the vectors of unknowns for FOBT and CBT are described by:

$$\mathbf{Z}(x)=\left\{U,U',\varphi,\varphi',W,W'\right\} \text{ for the FOBT,} \tag{2. 22a}$$

$$\mathbf{Z}(x)=\left\{U,U',W,W',W'',W'''\right\} \text{ for the CBT} \tag{2. 22b}$$

and matrices of coefficients **T** are defined as:

$$\mathbf{T}=\begin{bmatrix} 0 & 1 & 0 & 0 & 0 & 0 \\ b_1 & 0 & b_2 & 0 & 0 & b_3 \\ 0 & 0 & 0 & 1 & 0 & 0 \\ b_4 & 0 & b_5 & 0 & 0 & b_6 \\ 0 & 0 & 0 & 0 & 0 & 1 \\ 0 & 0 & 0 & b_7 & b_8 & 0 \end{bmatrix} \text{ for the FOBT} \tag{2. 23}$$

where

$$b_1=\frac{e_{2a}e_3-e_2e_{3a}}{C_0},\ b_2=\frac{e_{2a}e_4-e_2e_{4a}}{C_0},\ b_3=\frac{-e_{5a}e_2}{C_0},\ b_4=\frac{e_{3a}e_1-e_3e_{1a}}{C_0},$$

$$b_5=\frac{e_{4a}e_1-e_{1a}e_4}{C_0},\ b_6=\frac{e_{5a}e_1}{C_0},\ b_7=\frac{-A_s}{A_s}=-1,\ b_8=\frac{-I_0\omega^2}{A_s},$$

$$e_1=A,\ e_2=B,\ e_3=-I_0\omega^2,\ e_4=-I_1\omega^2,\ e_{1a}=B,e_{2a}=D,e_{3a}=-I_1\omega^2,e_{4a}=A_s-I_2\omega^2,e_{5a}=A_s,$$

$$C_0=e_{2a}e_1-e_{1a}e_2. \tag{2. 24}$$

$$\mathbf{T}=\begin{bmatrix} 0 & 1 & 0 & 0 & 0 & 0 \\ c_1 & 0 & 0 & c_2 & 0 & c_3 \\ 0 & 0 & 0 & 1 & 0 & 0 \\ 0 & 0 & 0 & 0 & 1 & 0 \\ 0 & 0 & 0 & 0 & 0 & 1 \\ 0 & c_4 & c_5 & 0 & c_6 & 0 \end{bmatrix} \text{ for the CBT} \tag{2. 25}$$

where $c_1 = \frac{-I_0\omega^2}{A}$, $c_2 = \frac{I_1\omega^2}{A}$, $c_3 = \frac{B}{A}$, $c_4 = \frac{-\left(Bc_1 + I_1\omega^2\right)}{Bc_3 - D}$, $c_5 = \frac{-I_0\omega^2}{Bc_3 - D}$, $c_6 = \frac{-Bc_2 + I_2\omega^2}{Bc_3 - D}$ (2. 26)

The formal solutions of Eq. (2.19) are of the form:

$$\mathbf{Z}(x) = \mathbf{e}^{\mathbf{T}x}\mathbf{K} \tag{2. 27}$$

where **K** is a constant column vector determined from the boundary conditions at $x = \pm a/2$; and $\mathbf{e}^{\mathbf{T}x}$ is the general matrix solution of Eq. (2.19) which is given as:

$$\mathbf{e}^{\mathbf{T}x} = \mathbf{E}\begin{bmatrix} e^{\lambda_1 x} & & 0 \\ & \ddots & \\ 0 & & e^{\lambda_n x} \end{bmatrix}\mathbf{E}^{-1} \tag{2. 28}$$

where $\lambda_i \left(i = \overline{1,n} = \overline{1,8}\right)$ for the HOBT and $\lambda_i \left(i = \overline{1,n} = \overline{1,6}\right)$ for the FOBT/CBT are the eigenvalues whilst **E** is the corresponding matrix of eigenvectors, respectively, associated with the matrix **T**.

2.7.2 Buckling analysis

Similar to the above section for vibration analysis, by neglecting time derivatives and frequencies in Eq. (2.16), the system of equations can be obtained:

$$U'' = a_2\varphi + a_4 W''' \tag{2. 29a}$$

$$\varphi'' = a_6\varphi + a_8 W''' \tag{2. 29b}$$

$$W^{(iv)} = a_{10}\varphi' + a_{12}W'' \tag{2. 29c}$$

Since Eq. (2.29a) is an induced equation, the primary variables are reduced to $\mathbf{Z}(x) = \left\{\varphi, \varphi', W, W', W'', W'''\right\}$. As a result, matrix **T** in this case is assembled by neglecting the first 2 rows and 2 columns of **T** in Eq. (2.21). The coefficients in **T** are taken from those of Eq. (2.17) with the elimination of ω.

In addition, because of the multiplicity in eigenvalues ($\lambda_1 = \lambda_2 = 0$), Jordan canonical form is applied for the general matrix solution:

$$\mathbf{e}^{\mathbf{T}x} = \mathbf{E}\begin{bmatrix} 1 & x & 0 & 0 & 0 & 0 \\ 0 & 1 & 0 & 0 & 0 & 0 \\ 0 & 0 & e^{\lambda_3 x} & 0 & 0 & 0 \\ 0 & 0 & 0 & e^{\lambda_4 x} & 0 & 0 \\ 0 & 0 & 0 & 0 & e^{\lambda_5 x} & 0 \\ 0 & 0 & 0 & 0 & 0 & e^{\lambda_6 x} \end{bmatrix}\mathbf{E}^{-1} \tag{2. 30}$$

For the vibration and buckling analysis, the substitution of general solution in Eq. (2.27) to the appropriate BCs in Table 2.2 results in a homogeneous system of equations as follow:

$$\boldsymbol{\alpha}\mathbf{e}^{\mathsf{T}x}\mathbf{K}=\mathbf{0} \tag{2. 31}$$

where $\boldsymbol{\alpha}$ comes from the coefficients in Eq. (2.31) for the appropriate BCs at x=±a/2. The natural frequencies ω_n of the n^{th} mode of vibration can be obtained by setting $|\mathbf{G}|=|\boldsymbol{\alpha}\mathbf{e}^{\mathsf{T}x}|=0$. The flowcharts of iterative procedure [72] is presented in Figs. 2.3 and 2.4 for the natural frequencies and buckling loads/temperature.

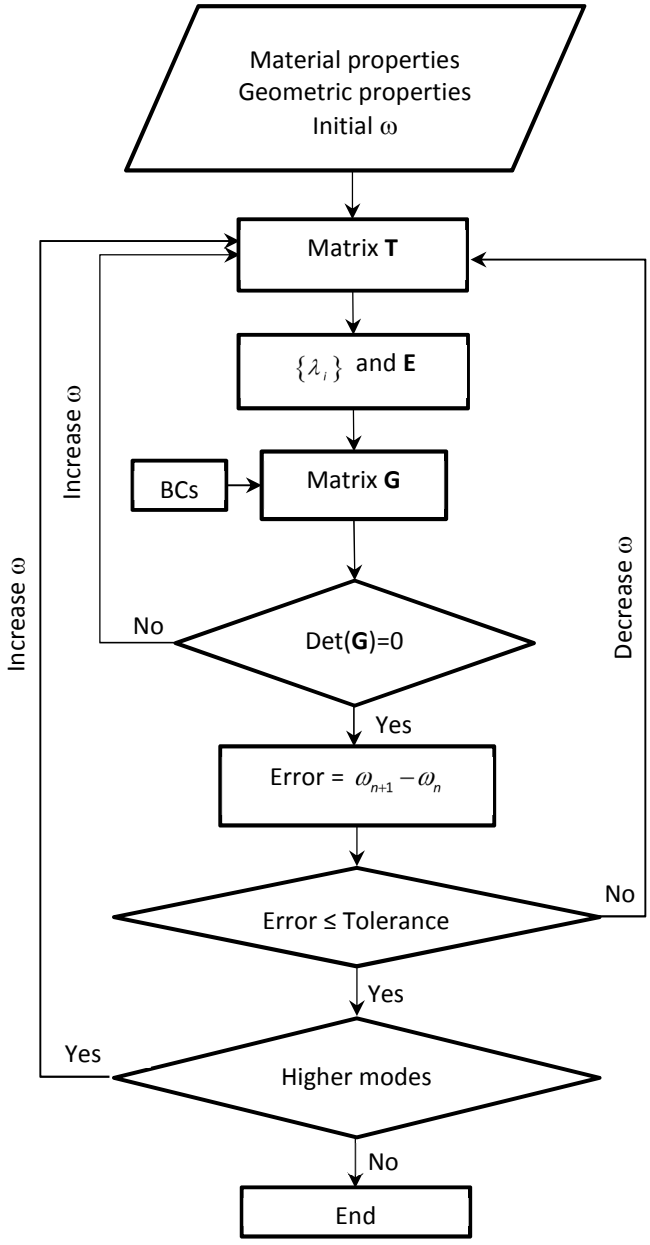

Fig. 2. 3: Iterative process of solving the natural frequencies using the state space based approach.

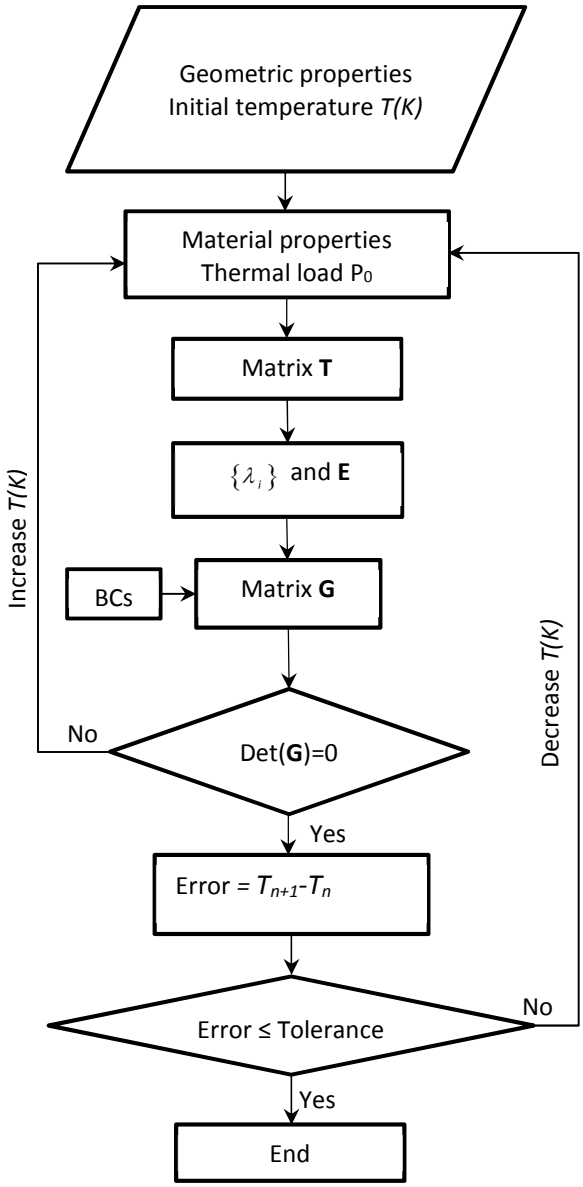

Fig. 2. 4: Iterative process of solving the critical temperatures using the state space based approach.

2.8 Numerical examples

2.8.1 Fundamental frequency of FG-sandwich beams

It should be noted that a slightly different version of the material presented in this section has been published in Composite structures [73].

The state space based approach is applied to investigate the fundamental natural frequencies of FG beams and FG-sandwich beams using various theories (CBT, FOBT and HOBT). Nine combinations of classical BCs from Clamped (C), Hinged (H), Simply-supported (S) and Free (F) and three combinations of non-classical BCs created from Elastic Supports (E) with translational and rotational springs are considered. The base materials of these beams are ceramic (Al_2O_3) and metal (Al) with material properties of E_c=380GPa, ρ_c=3960kg/m^3, ν_c=0.3 and E_m=70GPa, ρ_m=2702kg/m^3, ν_m=0.3, respectively. The power-law index *p* varies from 0 to 10 while the slenderness ratios a/h are 5 and 20 representing the thick and thin beams. The Young's modulus through the thickness are plotted in Fig. 2.5 for three types of beams considered. In order to verify with the reported results in the literature, the non-dimensional natural frequencies are defined as $\bar{\omega} = \frac{\omega a^2}{h}\sqrt{\rho_m / E_m}$ for classical BCs and $\hat{\omega} = \omega a\sqrt{\rho_m / E_m}$ for non-classical BCs.

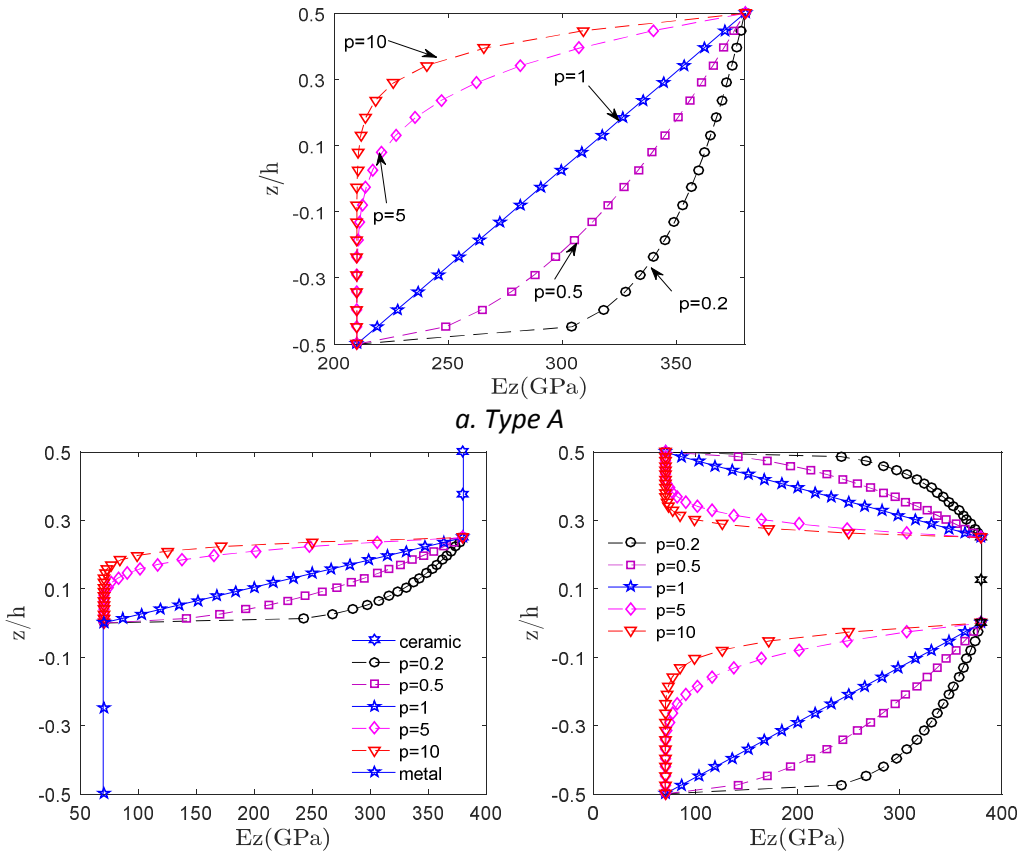

a. Type A

b. Type B (2-1-1)

c. Type C (2-1-1)

Fig. 2. 5: Variation of Young's modulus E(z) through the thickness.

2.8.1.1 Classical boundary conditions

For verification purpose, Tables 2.3-2.6 show the non-dimensional natural frequency of FG beams (Type A) and FG-sandwich beams (Types B and C) with various BCs. The material power-law indices are 0, 1 and 10. All the results relating to thin and thick beams under C-C, S-S and C-F boundary conditions agree well with Simsek's [49] for FG beams, Vo et al. [51] and Nguyen et al. [52] for FG-sandwich beams. Furthermore, for thin beams (a/h=20), the present results are in line with Jin and Wang's [39], which applied Quadrature Element Method using CBT, under nine classical BCs.

Table 2. 3: Non-dimensional fundamental frequency of FG beams (Type A) with various BCs (a/h=20, $\bar{\omega} = \frac{\omega a^2}{h}\sqrt{\rho_m / E_m}$).

p	Theory		BCs								
			C-C	F-F	H-C	S-C	S-F	H-F	H-H	S-S	C-F
0	CBT	Present	12.4143	12.3666	8.5559	8.5559	8.5420	8.5420	5.4778	5.4778	1.9528
		[39]	12.4143	12.3666	8.5558	8.5558	8.5419	8.5419	5.4777	5.4777	1.9525
		[49]	12.4142	-	-	-	-	-	-	5.4777	1.9525
	FOBT	Present	12.2205	12.3184	8.4818	8.4818	8.5107	8.5107	5.4604	5.4604	1.9499
		[51]	12.2202	-	-	-	-	-	-	5.4603	1.9496
		[49]	12.2235	-	-	-	-	-	-	5.4603	1.9496
	HOBT	Present	12.2222	12.3187	8.4818	8.4818	8.5104	8.5104	5.4604	5.4604	1.9496
		[51]	12.2228	-	-	-	-	-	-	5.4603	1.9496
		[49]	12.2238	-	-	-	-	-	-	5.4603	1.9495
1	CBT	Present	9.5554	9.5162	6.6682	6.5857	6.5747	6.5747	4.2168	4.2168	1.5030
		[39]	9.5554	9.5160	6.6677	6.5855	6.5743	6.5691	4.5161	4.2163	1.5029
		[49]	9.5554	-	-	-	-	-	-	4.2163	1.5029
	FOBT	Present	9.4297	9.4853	6.6185	6.5375	6.5544	6.5489	4.2039	4.2054	1.5010
		[51]	9.4311	-	-	-	-	-	-	4.2039	1.5011
		[49]	9.4314	-	-	-	-	-	-	4.2051	1.5010
	HOBT	Present	9.4304	9.4851	6.6187	6.5377	6.5541	6.5489	4.5024	4.2051	1.5013
		[51]	9.4328	-	-	-	-	-	-	4.2039	1.5011
		[49]	9.4316	-	-	-	-	-	-	4.2050	1.5011
10	CBT	Present	8.0559	8.0196	5.6070	5.5523	5.5419	5.5419	3.5548	3.5548	1.2674
		[39]	8.0556	8.0194	5.6069	5.5519	5.5416	5.5365	3.7568	3.5547	1.2671
		[49]	8.0556	-	-	-	-	-	-	3.5547	1.2671
	FOBT	Present	7.9103	7.9838	5.5503	5.4962	5.5180	5.5131	3.5404	3.5418	1.2649
		[51]	7.9128	-	-	-	-	-	-	3.5405	1.2650
		[49]	7.9128	-	-	-	-	-	-	3.5416	1.2650
	HOBT	Present	7.8844	7.9764	5.5394	5.4857	5.5136	5.5086	3.7387	3.5391	1.2647
		[51]	7.8862	-	-	-	-	-	-	3.5379	1.2645
		[49]	7.8859	-	-	-	-	-	-	3.5390	1.2645

Table 2. 4: Non-dimensional fundamental frequency of FG beams (Type A) with various BCs (a/h=5, $\bar{\omega} = \frac{\omega a^2}{h}\sqrt{\rho_m / E_m}$).

p	Theory		BCs								
			C-C	F-F	H-C	S-C	S-F	H-F	H-H	S-S	C-F
0	CBT	Present	12.4143	12.3666	8.5559	8.5559	8.5420	8.5420	5.4778	5.4778	1.9528
		[39]	12.4143	12.3666	8.5558	8.5558	8.5419	8.5419	5.4777	5.4777	1.9525
		[49]	12.4142	-	-	-	-	-	-	5.4777	1.9525
	FOBT	Present	12.2205	12.3184	8.4818	8.4818	8.5107	8.5107	5.4604	5.4604	1.9499
		[51]	12.2202	-	-	-	-	-	-	5.4603	1.9496
		[49]	12.2235	-	-	-	-	-	-	5.4603	1.9496
	HOBT	Present	12.2222	12.3187	8.4818	8.4818	8.5104	8.5104	5.4604	5.4604	1.9496
		[51]	12.2228	-	-	-	-	-	-	5.4603	1.9496
		[49]	12.2238	-	-	-	-	-	-	5.4603	1.9495
1	CBT	Present	9.5554	9.5162	6.6682	6.5857	6.5747	6.5747	4.2168	4.2168	1.5030
		[39]	9.5554	9.5160	6.6677	6.5855	6.5743	6.5691	4.5161	4.2163	1.5029
		[49]	9.5554	-	-	-	-	-	-	4.2163	1.5029
	FOBT	Present	9.4297	9.4853	6.6185	6.5375	6.5544	6.5489	4.2039	4.2054	1.5010
		[51]	9.4311	-	-	-	-	-	-	4.2039	1.5011
		[49]	9.4314	-	-	-	-	-	-	4.2051	1.5010
	HOBT	Present	9.4304	9.4851	6.6187	6.5377	6.5541	6.5489	4.5024	4.2051	1.5013
		[51]	9.4328	-	-	-	-	-	-	4.2039	1.5011
		[49]	9.4316	-	-	-	-	-	-	4.2050	1.5011
10	CBT	Present	8.0559	8.0196	5.6070	5.5523	5.5419	5.5419	3.5548	3.5548	1.2674
		[39]	8.0556	8.0194	5.6069	5.5519	5.5416	5.5365	3.7568	3.5547	1.2671
		[49]	8.0556	-	-	-	-	-	-	3.5547	1.2671
	FOBT	Present	7.9103	7.9838	5.5503	5.4962	5.5180	5.5131	3.5404	3.5418	1.2649
		[51]	7.9128	-	-	-	-	-	-	3.5405	1.2650
		[49]	7.9128	-	-	-	-	-	-	3.5416	1.2650
	HOBT	Present	7.8844	7.9764	5.5394	5.4857	5.5136	5.5086	3.7387	3.5391	1.2647
		[51]	7.8862	-	-	-	-	-	-	3.5379	1.2645
		[49]	7.8859	-	-	-	-	-	-	3.5390	1.2645

Table 2. 5: Non-dimensional fundamental frequency of FG-sandwich beams with ceramic core (Type C) for various BCs (a/h=5, $\bar{\omega} = \frac{\omega a^2}{h}\sqrt{\rho_m / E_m}$).

Scheme	p	Theory	BCs								
			C-C	F-F	H-C	S-C	S-F	H-F	H-H	S-S	C-F
1-1-1	0	CBT	12.1827	11.5140	8.4062	8.4062	8.2012	8.2012	5.3955	5.3955	1.9385
		FOBT	9.9977	11.0000	7.4652	7.4652	7.8070	7.8070	5.1525	5.1525	1.8945
		HOBT	10.0670	11.0020	7.4872	7.4872	7.8080	7.8080	5.1528	5.1528	1.8953
		HOBT [51]	10.0678	-	-	-	-	-	-	5.1528	1.8952
	1	CBT	9.0040	8.5565	6.2120	6.2120	6.0755	6.0755	3.9860	3.9860	1.4310
		FOBT	7.8235	8.2892	5.7197	5.7197	5.8735	5.8735	3.8628	3.8628	1.4090
		HOBT	7.9572	8.3162	5.7755	5.7755	5.8942	5.8942	3.8758	3.8758	1.4115
		HOBT [51]	7.9580	-	-	-	-	-	-	3.8755	1.4115
	10	CBT	6.6205	6.2995	4.5675	4.5675	4.4698	4.4698	2.9308	2.9308	1.0520
		FOBT	5.9755	6.1590	4.3043	4.3043	4.3635	4.3635	2.8660	2.8660	1.0405
		HOBT	6.1237	6.1907	4.3658	4.3658	4.3878	4.3878	2.8810	2.8810	1.0433
		HOBT [51]	6.1240	-	-	-	-	-	-	2.8808	1.0431
1-2-1	0	CBT	12.1827	11.5140	8.4062	8.4062	8.2012	8.2012	5.3955	5.3955	1.9385
		FOBT	9.9977	11.0000	7.4652	7.4652	7.8070	7.8070	5.1525	5.1525	1.8945
		HOBT	10.0670	11.0020	7.4872	7.4872	7.8080	7.8080	5.1528	5.1528	1.8953
		HOBT [51]	10.0678	-	-	-	-	-	-	5.1528	1.8952
	1	CBT	9.5762	9.0962	6.6070	6.6070	6.4605	6.4605	4.2395	4.2395	1.5220
		FOBT	8.2545	8.7952	6.0532	6.0532	6.2325	6.2325	4.1003	4.1003	1.4973
		HOBT	8.3697	8.8165	6.1005	6.1005	6.2490	6.2490	4.1108	4.1108	1.4993
		HOBT [51]	8.3705	-	-	-	-	-	-	4.1105	1.4992
	10	CBT	7.4595	7.1022	5.1463	5.1463	5.0375	5.0375	3.3020	3.3020	1.1850
		FOBT	6.6820	6.9307	4.8278	4.8278	4.9083	4.9083	3.2235	3.2235	1.1710
		HOBT	6.8082	6.9567	4.8800	4.8800	4.9283	4.9283	3.2358	3.2358	1.1735
		HOBT [51]	6.8087	-	-	-	-	-	-	3.2356	1.1734
2-2-1	0	CBT	12.1827	11.5140	8.4062	8.4062	8.2012	8.2012	5.3955	5.3955	1.9385
		FOBT	9.9977	11.0000	7.4652	7.4652	7.8070	7.8070	5.1525	5.1525	1.8945
		HOBT	10.0670	11.0020	7.4872	7.4872	7.8080	7.8080	5.1528	5.1528	1.8953
		HOBT [51]	10.0678	-	-	-	-	-	-	5.1528	1.8952
	1	CBT	9.2870	8.8185	6.4150	6.4075	6.2647	6.2647	4.1118	4.1118	1.4763
		FOBT	8.0325	8.5342	5.8892	5.8827	6.0492	6.0432	3.9785	3.9800	1.4528
		HOBT	8.1542	8.5577	5.9397	5.9332	6.0675	6.0615	4.0190	3.9913	1.4550
		HOBT [51]	8.1554	-	-	-	-	-	-	3.9896	1.4549
	10	CBT	7.0537	6.7002	4.8940	4.8665	4.7595	4.7595	3.1228	3.1228	1.1210
		FOBT	6.3322	6.5432	4.5960	4.5713	4.6405	4.6248	3.0460	3.0500	1.1083
		HOBT	6.4627	6.5707	4.6503	4.6253	4.6615	4.6455	3.1638	3.0630	1.1108
		HOBT [51]	6.4641	-	-	-	-	-	-	3.0588	1.1106

Table 2. 6: Non-dimensional fundamental natural frequency of FG-sandwich beams with FG core (Type B) for various BCs (a/h=5, $\bar{\omega} = \frac{\omega a^2}{h}\sqrt{\rho_m / E_m}$).

Scheme	p	Theory	BCs								
			C-C	F-F	H-C	S-C	S-F	H-F	H-H	S-S	C-F
1-1-1	0	CBT	8.8465	8.3495	6.2125	6.1042	5.9560	5.9560	3.9183	3.9183	1.4080
		FOBT	7.7235	8.1055	5.7315	5.6365	5.7667	5.6860	3.7795	3.8015	1.3870
		HOBT	7.8667	8.1342	5.7920	5.6957	5.7885	5.7062	4.1948	3.8148	1.3898
	1	CBT	8.3410	7.8145	5.9277	5.7560	5.6015	5.6015	3.6963	3.6963	1.3298
		FOBT	7.2607	7.5875	5.4547	5.3050	5.4210	5.2848	3.5470	3.5835	1.3095
		HOBT	7.3270	7.5972	5.4785	5.3295	5.4278	5.2915	4.1513	3.5873	1.3105
	10	CBT	8.1582	7.5827	5.8360	5.6307	5.4640	5.4640	3.6173	3.6173	1.3030
		FOBT	7.0057	7.3465	5.3218	5.1453	5.2713	5.0835	3.4458	3.4950	1.2808
		HOBT	6.9060	7.3125	5.2623	5.0915	5.2423	5.0618	4.1120	3.4763	1.2778
1-2-1	0	CBT	9.4637	8.9542	6.5945	6.5297	6.3765	6.3765	4.1908	4.1908	1.5055
		FOBT	8.1847	8.6695	6.0510	5.9945	6.1577	6.1065	4.0428	4.0565	1.4813
		HOBT	8.3232	8.6965	6.1090	6.0515	6.1782	6.1255	4.3043	4.0690	1.4840
		HOBT [52]	8.3282	-	-	-	-	-	-	4.0691	1.4840
	1	CBT	8.5340	8.0012	6.0422	5.8892	5.7322	5.7322	3.7815	3.7815	1.3603
		FOBT	7.3862	7.7575	5.5415	5.4085	5.5392	5.4120	3.6273	3.6610	1.3385
		HOBT	7.4452	7.7647	5.5620	5.4293	5.5440	5.4170	4.1733	3.6638	1.3395
		HOBT [52]	7.4487	-	-	-	-	-	-	3.6636	1.3393
	10	CBT	8.2517	7.6497	5.8847	5.6955	5.5217	5.5217	3.6595	3.6595	1.3188
		FOBT	6.9715	7.3857	5.3123	5.1513	5.3048	5.1068	3.4705	3.5210	1.2933
		HOBT	6.7540	7.3165	5.1918	5.0383	5.2470	5.0615	4.0640	3.4840	1.2870
		HOBT [52]	6.7543	-	-	-	-	-	-	3.4830	1.2867
2-2-1	0	CBT	8.4857	7.9865	5.9995	5.8555	5.7077	5.7077	3.7593	3.7593	1.3515
		FOBT	7.4360	7.7625	5.5455	5.4190	5.5322	5.4268	3.6218	3.6503	1.3320
		HOBT	7.5655	7.7882	5.5997	5.4722	5.5517	5.4448	4.1515	3.6623	1.3343
		HOBT [52]	7.5709	-	-	-	-	-	-	3.6624	1.3344
	1	CBT	8.2522	7.6962	5.8790	5.6952	5.5332	5.5332	3.6580	3.6580	1.3170
		FOBT	7.1057	7.4577	5.3723	5.2133	5.3410	5.1780	3.4940	3.5368	1.2950
		HOBT	7.0882	7.4455	5.3548	5.1988	5.3300	5.1700	4.1170	3.5295	1.2940
		HOBT [52]	7.0901	-	-	-	-	-	-	3.5292	1.2939
	10	CBT	8.3300	7.7132	5.9142	5.7492	5.5717	5.5717	3.6945	3.6945	1.3315
		FOBT	6.9167	7.4175	5.2818	5.1433	5.3280	5.1315	3.4903	3.5388	1.3030
		HOBT	6.5982	7.3140	5.1075	4.9768	5.2430	5.0635	3.9873	3.4843	1.2933
		HOBT [52]	8.8465	8.3495	6.2125	6.1042	5.9560	5.9560	3.9183	3.9183	1.4080

In addition, it is seen that natural frequencies reduce significantly along with the increase of material parameter p. Regarding the relation between frequencies and boundary conditions, the downtrend of natural frequencies for these beams is $\omega_{F\text{-}F} > \omega_{C\text{-}C} > \omega_{C\text{-}H} > \omega_{C\text{-}S} > \omega_{S\text{-}F} > \omega_{H\text{-}F} > \omega_{H\text{-}H} > \omega_{S\text{-}S} > \omega_{C\text{-}F}$. It is also worth noting that, $\omega_{C\text{-}C} > \omega_{F\text{-}F}$ for the CBT but $\omega_{C\text{-}C} < \omega_{F\text{-}F}$ when the FOBT and HOBT are considered. In addition, the natural frequencies under which combined of H and S for p=0 (isotropic material) are the same but for FG and FG-sandwich beams, there is a slight difference. For FG beams, the difference in the natural frequencies due to shear deformation effect is minor for all BCs with a maximum of 1.8% (Table 2.4). However, a large difference can be seen between the results from CBT and FOBT/HOBT for FG-sandwich thick beams: the highest

errors are observed for C-C (11- 22%); H-C and S-C (8-12%); F-F, S-F, H-F, H-H, S-S (2-5%) and the lowest errors are for C-F (1-2%) (Tables 2.5 and 2.6).

2.8.1.2 Non-classical boundary conditions

In order to verify the present theory further, Tables 2.7 and 2.8 present the fundamental frequency of FG beams (a/h=10) with elastic support at both ends (E-E), C-E and H-E with various power-law indices while the spring stiffness varies from 10^{-4} to 10^{6} ($\beta_T=\beta_R$). It can be seen that the results of FG beams with FOBT have excellent agreement with Wattanasakulpong and Mao [62], while the HOBT provides slightly higher values in comparison with FOBT. The frequencies increase with an increase in the spring stiffness, and similar to the case of classical BCs, they decrease consistent with the values of power-law index as expected. It is also seen that the frequency for C-E boundary condition is the highest, followed by E-E and H-E conditions.

Table 2. 7: Non-dimensional fundamental frequency of FG beams with E-E boundary condition and various spring factors ($\beta_R=\beta_T$, a/h=10, $\bar{\omega}=\omega a\sqrt{\rho_m/E_m}$).

p	Theory	Spring stiffness								
		$\beta_R=\beta_T$	10^{-4}	10^{-3}	10^{-2}	10^{-1}	1	10	10^{2}	10^{4}	10^{6}
0	FOBT		0.0117	0.0369	0.1147	0.3121	0.5116	0.6751	0.9993	1.1629	1.1652
	HOBT		0.0117	0.0369	0.1147	0.3122	0.5129	0.7063	1.0550	1.1653	1.1665
0.5	FOBT	Present	0.0124	0.0390	0.1203	0.3097	0.4663	0.6279	0.8957	0.9970	0.9982
		[62]	0.0123	0.0390	0.1202	0.3097	0.4663	0.6279	0.8957	0.9970	0.9983
	HOBT		0.0124	0.0390	0.1203	0.3098	0.4681	0.6631	0.9331	0.9993	1.0000
1	FOBT	Present	0.0127	0.0401	0.1233	0.3074	0.4455	0.6023	0.8299	0.9039	0.9048
		[62]	0.0127	0.0401	0.1233	0.3074	0.4455	0.6023	0.8299	0.9039	0.9048
	HOBT		0.0127	0.0402	0.1233	0.3075	0.4477	0.6390	0.8587	0.9052	0.9057
5	FOBT	Present	0.0136	0.0429	0.1301	0.3005	0.4090	0.5624	0.7334	0.7769	0.7774
		[62]	0.0136	0.0429	0.1301	0.3005	0.4090	0.5624	0.7334	0.7769	0.7774
	HOBT		0.0137	0.0429	0.1301	0.3001	0.4125	0.6037	0.7458	0.7696	0.7698
10	FOBT		0.0138	0.0436	0.1311	0.2912	0.3893	0.5486	0.7103	0.7486	0.7490
	HOBT		0.0139	0.0436	0.1311	0.2908	0.3939	0.5920	0.7205	0.7409	0.7411

Table 2. 8: Non-dimensional fundamental frequency of FG and FG-sandwich beams with various boundary conditions ($\beta_R=\beta_T=10^2$ for Elastic support, $\hat{\omega}=\omega a\sqrt{\rho_m/E_m}$).

Type	Scheme	P	Theory	a/h=5			a/h=20		
				C-E	E-E	H-E	C-E	E-E	H-E
Type A		0	FOBT	1.8768	1.7619	1.3909	0.5626	0.5189	0.3891
			HOBT	1.9816	1.8600	1.4331	0.5925	0.5455	0.3997
		0.5	FOBT	1.6571	1.5842	1.2309	0.4917	0.4646	0.3428
			FOBT [62]	1.6571	1.5842	1.2309	0.4917	0.4646	0.3428
			HOBT	1.7317	1.6537	1.2522	0.5136	0.4827	0.3474
		1	FOBT	1.5234	1.4697	1.1384	0.4501	0.4303	0.3167
			HOBT	1.5783	1.5225	1.1435	0.4671	0.4445	0.3171
		10	FOBT	1.2370	1.2117	0.9388	0.3842	0.3734	0.2699
			HOBT	1.2288	1.2077	0.9229	0.3933	0.3817	0.2699
Type C	1-1-1	0	FOBT	1.8768	1.7619	1.3909	0.5626	0.5189	0.3891
			HOBT	1.9816	1.8600	1.4331	0.5925	0.5455	0.3997
		1	FOBT	1.5062	1.4504	1.0978	0.4328	0.4138	0.2994
			HOBT	1.5791	1.5106	1.1233	0.4489	0.4251	0.3036
		10	FOBT	1.1701	1.1459	0.8419	0.3261	0.3185	0.2254
			HOBT	1.2200	1.1902	0.8603	0.3334	0.3239	0.2275
Type B	1-1-1	0	FOBT	1.4887	1.4359	1.1068	0.4270	0.4090	0.3023
			HOBT	1.5612	1.5035	1.1114	0.4420	0.4218	0.3001
		1	FOBT	1.4077	1.3657	1.0618	0.4061	0.3915	0.2917
			HOBT	1.4567	1.4144	1.0453	0.4188	0.4029	0.2853
		10	FOBT	1.3628	1.3267	1.0402	0.3990	0.3859	0.2889
			HOBT	1.3745	1.3416	1.0017	0.4101	0.3958	0.2800

Tables 2.9 and 2.10 provide the frequency of non-rotational and non-translational FG-sandwich beams, respectively. For the non-rotational beams, the rotational spring stiffness is set as ($\beta_R=10^6$) (considered as clamped), whereas the translational spring factor β_T varies from 10^{-4} to 10^6. Similarly, $\beta_T=10^6$ (considered as supported) and $\beta_R=10^{-4}\rightarrow 10^6$ are adopted for non-translational case. The trend of variation of the frequencies in these cases is comparable to the response of FG beams (a/h=10) in Fig. 2.6.

Table 2. 9: Non-dimensional fundamental frequency of non-rotational FG-sandwich beams (1-1-1) with different translational spring factors ($\hat{\omega} = \omega a\sqrt{\rho_m / E_m}$).

Type	p	Theory	a/h=5				a/h=20			
			$\beta_T=10^{-4}$	1	10^2	10^6	$\beta_T=10^{-4}$	1	10^2	10^6
Type A	0	CBT	0.0117	1.0827	2.4017	2.4366	0.0117	0.5643	0.6201	0.6207
		FOBT	0.0117	1.0374	1.9786	1.9995	0.0117	0.5569	0.6104	0.6110
		HOBT	0.0117	1.0400	1.9923	2.0134	0.0118	0.5570	0.6106	0.6111
	1	CBT	0.0127	1.0974	1.8595	1.8729	0.0127	0.4553	0.4775	0.4778
		FOBT	0.0127	1.0297	1.5713	1.5799	0.0127	0.4498	0.4712	0.4715
		HOBT	0.0128	1.0332	1.5809	1.5896	0.0128	0.4500	0.4714	0.4715
	10	CBT	0.0139	1.0918	1.5693	1.5759	0.0138	0.3913	0.4027	0.4028
		FOBT	0.0139	0.9693	1.2592	1.2630	0.0138	0.3845	0.3954	0.3955
		HOBT	0.0139	0.9568	1.2293	1.2328	0.0139	0.3834	0.3942	0.3943
Type C	0	CBT	0.0117	1.0827	2.4017	2.4366	0.0117	0.5643	0.6201	0.6207
		FOBT	0.0117	1.0374	1.9786	1.9995	0.0117	0.5569	0.6104	0.6110
		HOBT	0.0117	1.0400	1.9923	2.0134	0.0118	0.5570	0.6106	0.6111
	1	CBT	0.0124	1.0611	1.7881	1.8008	0.0124	0.4369	0.4576	0.4579
		FOBT	0.0124	1.0072	1.5558	1.5647	0.0124	0.4326	0.4528	0.4530
		HOBT	0.0124	1.0146	1.5822	1.5914	0.0125	0.4332	0.4535	0.4536
	10	CBT	0.0130	0.9731	1.3195	1.3241	0.0130	0.3289	0.3364	0.3365
		FOBT	0.0130	0.9176	1.1916	1.1951	0.0130	0.3265	0.3339	0.3340
		HOBT	0.0130	0.9313	1.2210	1.2247	0.0130	0.3271	0.3346	0.3347
Type B	0	CBT	0.0124	1.0561	1.7573	1.7693	0.0124	0.4308	0.4507	0.4509
		FOBT	0.0124	1.0029	1.5362	1.5446	0.0124	0.4267	0.4461	0.4463
		HOBT	0.0124	1.0111	1.5645	1.5734	0.0125	0.4274	0.4468	0.4470
	1	CBT	0.0127	1.0590	1.6588	1.6682	0.0127	0.4102	0.4260	0.4262
		FOBT	0.0127	0.9971	1.4455	1.4521	0.0127	0.4061	0.4215	0.4217
		HOBT	0.0128	1.0020	1.4587	1.4654	0.0128	0.4063	0.4218	0.4220
	10	CBT	0.0131	1.0695	1.6234	1.6317	0.0131	0.4036	0.4178	0.4180
		FOBT	0.0131	0.9959	1.3955	1.4011	0.0131	0.3991	0.4129	0.4130
		HOBT	0.0131	0.9897	1.3758	1.3812	0.0132	0.3985	0.4123	0.4124

Table 2. 10: Non-dimensional fundamental frequency of non-translational FG-sandwich beams (1-1-1) with different rotational spring factors ($\hat{\omega} = \omega a\sqrt{\rho_m / E_m}$).

Type	p	Theory	a/h=5				a/h=20			
			$\beta_T=10^{-4}$	1	10^2	10^6	$\beta_T=10^{-4}$	1	10^2	10^6
Type A	0	FOBT	1.0305	1.0642	1.7770	1.9995	0.2730	0.2828	0.5193	0.6110
		HOBT	1.0306	1.0723	1.8774	2.0134	0.2730	0.2832	0.5458	0.6111
	1	FOBT	0.8510	0.8952	1.4769	1.5799	0.2251	0.2379	0.4305	0.4715
		HOBT	0.8511	0.9071	1.5304	1.5896	0.2251	0.2385	0.4447	0.4715
	10	FOBT	0.6974	0.7554	1.2151	1.2630	0.1871	0.2047	0.3735	0.3955
		HOBT	0.6903	0.7712	1.2110	1.2328	0.1870	0.2062	0.3818	0.3943
Type C	0	FOBT	1.0305	1.0642	1.7770	1.9995	0.2730	0.2828	0.5193	0.6110
		HOBT	1.0306	1.0723	1.8774	2.0134	0.2730	0.2832	0.5458	0.6111
	1	FOBT	0.7725	0.8241	1.4577	1.5647	0.2016	0.2159	0.4139	0.4530
		HOBT	0.7751	0.8364	1.5187	1.5914	0.2018	0.2165	0.4253	0.4536
	10	FOBT	0.5732	0.6476	1.1490	1.1951	0.1483	0.1685	0.3186	0.3340
		HOBT	0.5762	0.6637	1.1937	1.2247	0.1484	0.1693	0.3240	0.3347
Type B	0	FOBT	0.8355	0.8777	1.4429	1.5446	0.2193	0.2312	0.4092	0.4463
		HOBT	0.8389	0.8911	1.5114	1.5734	0.2195	0.2318	0.4221	0.4470
	1	FOBT	0.8301	0.8709	1.3714	1.4521	0.2191	0.2308	0.3916	0.4217
		HOBT	0.8303	0.8842	1.4206	1.4654	0.2192	0.2315	0.4030	0.4220
	10	FOBT	0.8303	0.8701	1.3316	1.4011	0.2208	0.2326	0.3860	0.4130
		HOBT	0.8224	0.8777	1.3467	1.3812	0.2208	0.2333	0.3959	0.4124

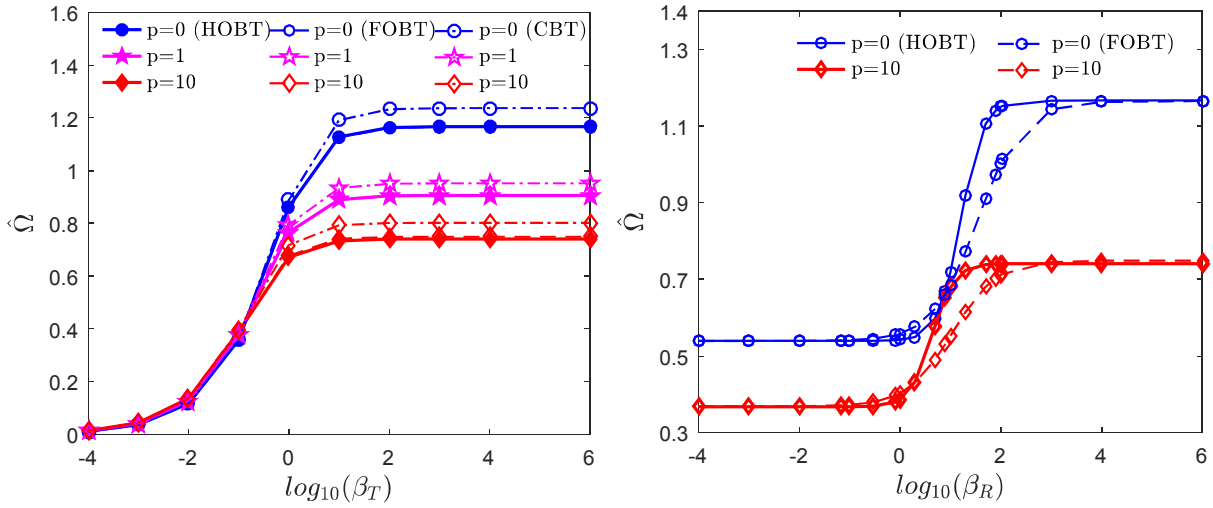

a. Non-rotational (β_R=10^6) *b. Non-translational (β_T=10^6)*

Fig. 2. 6: Non-dimensional fundamental frequency of FG beams (a/h=10, $\hat{\omega} = \omega a\sqrt{\rho_m / E_m}$).

It is seen that for the non-rotational beams, the frequencies increase rapidly when β_T changes from 10^{-4} to 10, and plateau for higher values of β_T; however, for the non-translational ones, they only change for the interval $\beta_T \in [10^{-1};10^3]$ using the FOBT or $\beta_T \in [10;10^2]$ using the HOBT. In addition, the variation of translational spring stiffness results in a larger range of the frequencies compared to the change of rotational spring stiffness. This tendency can be seen more clearly in Fig. 2.7, which presents the frequencies of C-E FG beams (a/h=10, p=1 and p=10) according to various rotational and translational spring factors (both β_T and β_R range from 10^{-4} to 10^6).

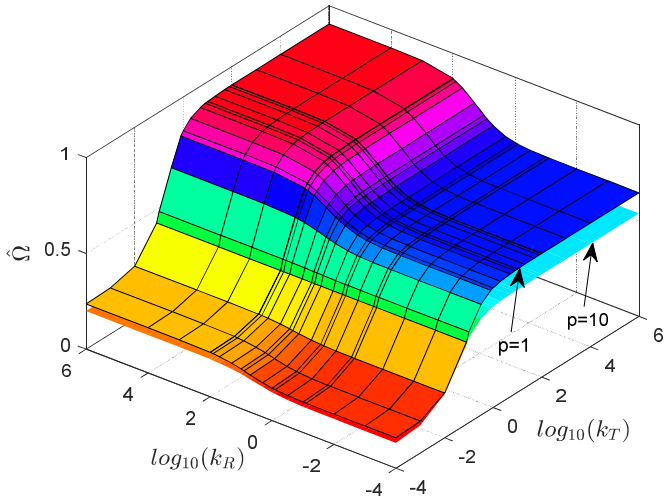

Fig. 2. 7: Non-dimensional fundamental frequency of FG beams with various rotational and translational spring factors (a/h=10, $\hat{\omega} = \omega a\sqrt{\rho_m / E_m}$).

It is seen that the frequencies increase slightly in accordance with the rotational stiffness and sharply with respect to the translational spring stiffness.

2.8.2 Vibration and buckling of FG beams under mechanical loads

A slightly different version of sections 2.8.2 and 2.8.3 has been published in Composites Part B: Engineering [74].

This section presents the numerical examples of vibration and buckling analysis of Al_2O_3/Fe and Al_2O_3/Al beams under axial load. The ceramic component is Al_2O_3 (E_c=380GPa, ρ_c=3800kg/m^3) and the metal is either Fe (E_m=210GPa, ρ_m=7800kg/m^3) or Al (E_m=70GPa, ρ_m=2702kg/m^3). The Poisson's ratio is assumed to be constant and indicated in Tables 2.11-2.13. In these tables, the dimensionless natural frequencies and buckling loads are $\bar{\omega} = \omega \frac{a^2}{h}\sqrt{\rho_m / E_m}$ and $\bar{P} = P\frac{12a^2}{E_m h^3}$. The first five natural frequencies and critical buckling loads of Al_2O_3/Fe and Al_2O_3/Al beams with various boundary conditions are displayed in Tables 2.11-2.13. The first three mode shapes and the buckling shape for Al_2O_3/Al beams under different BCs are also plotted in Figs. 2.8-2.10.

Table 2. 11: The first five natural frequencies of Al_2O_3/Fe beam (a/h=5, ν=0.23).

BCs	Mode	HOBT [75]			Present		
		p = 0	1	5	p = 0	1	5
C–C	1	10.1083	7.1931	5.9855	10.0900	7.1792	5.9733
	2	23.4657	16.6790	13.7711	23.3851	16.6227	13.7217
	3	30.1621	21.6365	17.5660	30.0429	21.5514	17.4969
	4	39.5482	28.1168	23.1248	39.3343	27.9666	22.9966
	5	56.9319	40.5008	33.2252	56.6051	40.2698	33.0330
C–H	1	7.4965	5.3367	4.4732	7.4820	5.3258	4.4630
	2	20.8194	14.7529	12.2782	20.7202	14.6850	12.2137
	3	30.1051	21.5866	17.5253	30.0429	21.5411	17.4888
	4	37.1746	26.3968	21.8323	36.9144	26.2154	21.6648
	5	55.0385	39.1297	32.2220	54.5653	38.7958	31.9196
H-H	1	5.1421	3.6904	3.1102	5.1328	3.6838	3.1036
	2	17.9856	12.6934	10.6599	17.8919	12.6305	10.5962
	3	30.0429	21.5385	17.4859	30.0429	21.5363	17.4851
	4	34.6496	24.5556	20.4458	34.3664	24.3597	20.2538
	5	52.9685	37.6354	31.1266	52.4237	37.2521	30.7598
C-F	1	1.8859	1.3370	1.1330	1.8856	1.3366	1.1328
	2	10.2557	7.2519	6.0953	10.2424	7.2424	6.0869
	3	15.0556	10.8759	8.8021	15.0215	10.8509	8.7820
	4	24.6380	17.4526	14.5612	24.5760	17.4088	14.5232
	5	41.2404	29.2206	24.2486	41.0964	29.1177	24.1625

Table 2. 12: The first five natural frequencies of Al_2O_3/Al beams (a/h=5, ν=0.3).

BCs	Mode	Theory	p					
			0	0.2	1	2	5	10
C-C	1	Present	10.0670	9.4610	7.9479	7.1749	6.4920	6.1637
		HOBT [75]	10.0858	9.4789	7.9680	7.1963	6.5120	6.1809
		HOBT [51]	9.9984	9.3834	7.1905	7.1901	6.6447	6.3161
	2	Present	23.2348	21.9426	18.5535	16.6326	14.6873	13.8331
		HOBT [75]	23.1004	21.7700	18.4654	16.7457	15.2301	14.3617
		HOBT [51]	23.8754	22.4840	19.0494	17.2924	15.7868	14.9035
	3	Present	30.2314	28.8710	25.2965	22.8618	19.7959	18.1426
		HOBT [75]	30.3513	28.9837	25.3859	22.9576	19.9122	18.2304
		HOBT [51]	30.2391	28.8837	25.3746	23.0112	19.9634	18.2321
	4	Present	38.9966	36.9209	31.3450	28.0113	24.4518	22.9386
		HOBT [75]	38.6867	36.5446	31.1243	28.1712	25.4176	23.8724
		HOBT [51]	38.1841	36.0793	30.7500	27.8331	25.0901	23.5501
	5	Present	56.0388	53.1438	45.2610	40.3898	34.9988	32.7237
C-H	1	Present	7.4872	7.0190	5.9194	5.3973	4.9555	4.7096
	2	Present	20.6436	19.4245	16.2594	14.5784	13.0744	12.4237
	3	Present	30.2314	28.8346	24.9211	22.3225	19.4312	17.9731
	4	Present	36.6649	34.6508	29.4057	26.3838	23.2037	21.8094
	5	Present	54.0805	51.2108	43.4538	38.8345	33.8788	31.7447
H-H	1	Present	5.1528	4.8373	4.2551	4.0060	3.7055	3.4513
		HOBT [75]	5.1629	4.8459	4.2632	4.0165	3.7178	3.4617
		HOBT [49]	5.1527	4.8092	3.9904	3.6264	3.4012	3.2816
	2	Present	17.8812	16.7457	13.7721	12.2950	11.2435	10.8417
		HOBT [75]	17.8908	16.7317	13.7778	12.3619	11.4822	11.1126
		HOBT [45]	17.8812	–	14.0100	12.6405	11.5431	11.0240
	3	Present	30.2314	28.8216	24.8044	22.1397	19.2751	17.8986
		HOBT [75]	30.2314	28.8311	24.9042	22.3517	19.5600	18.0553
	4	Present	34.2097	32.2316	27.0642	24.2724	21.6679	20.5189
		HOBT [75]	34.2103	32.1672	27.0657	24.4881	22.4290	21.3110
	(3^{rd})	HOBT [45]	34.2097	–	27.0979	24.3152	21.7158	20.5561
	5	Present	52.0266	49.2114	41.7866	37.4666	32.8483	30.8097
C-F	1	Present	1.8952	1.7659	1.4633	1.3325	1.2592	1.2183
		HOBT [75]	1.8955	1.7663	1.4645	1.3341	1.2605	1.2192
		HOBT [49]	1.8952	1.7664	1.4633	1.3325	1.2592	1.2183
	2	Present	10.2449	9.6009	8.0000	7.2165	6.6126	6.3329
	3	Present	15.1157	14.4405	12.7064	11.5380	10.0175	9.1418
	4	Present	24.4943	23.0540	19.3344	17.3571	15.5929	14.8146
	5	Present	40.8428	38.5697	32.5036	29.0633	25.7015	24.2665

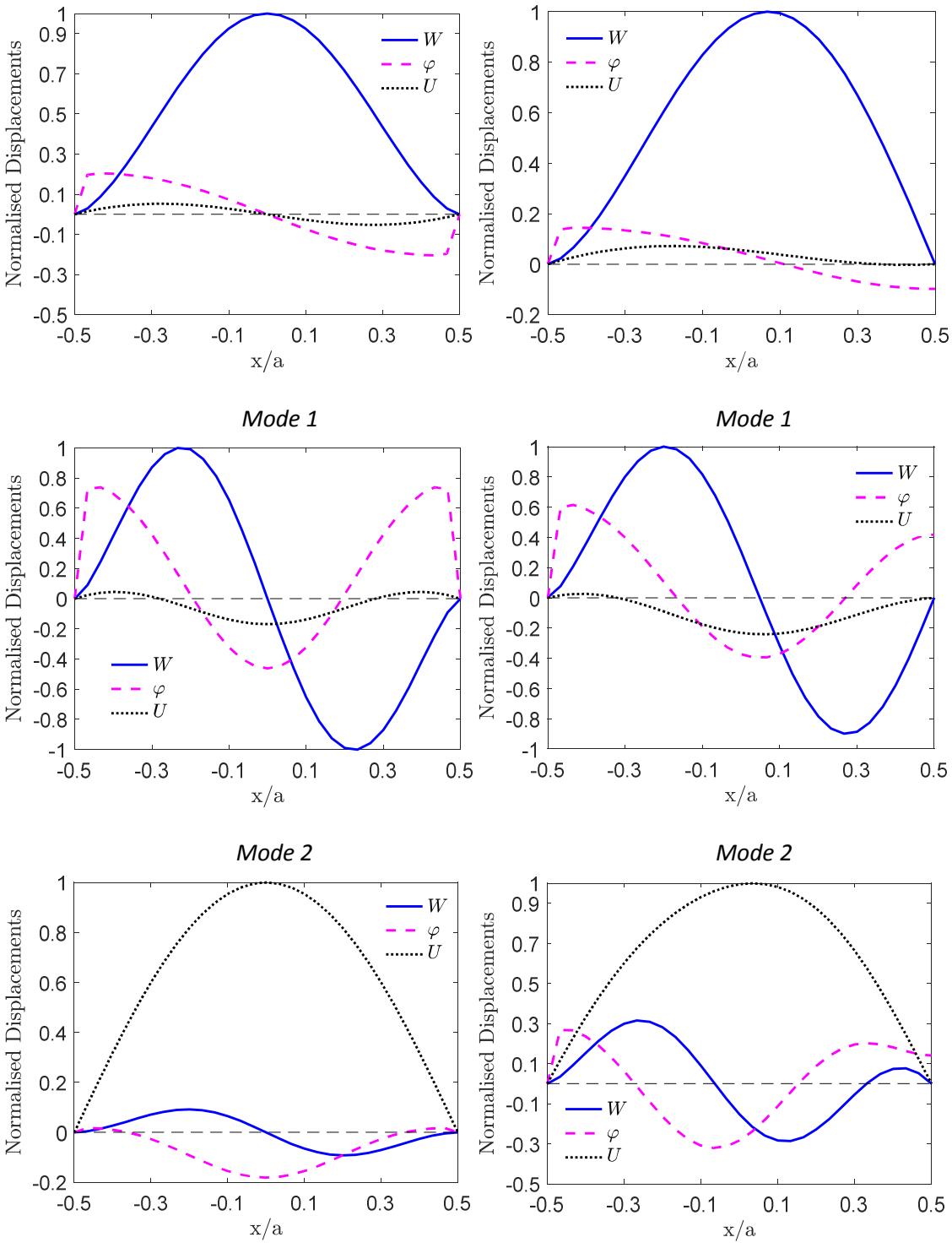

Fig. 2. 8: The first three mode shapes of Al_2O_3/Al beams (a/h=5, p=1, ν=0.3).

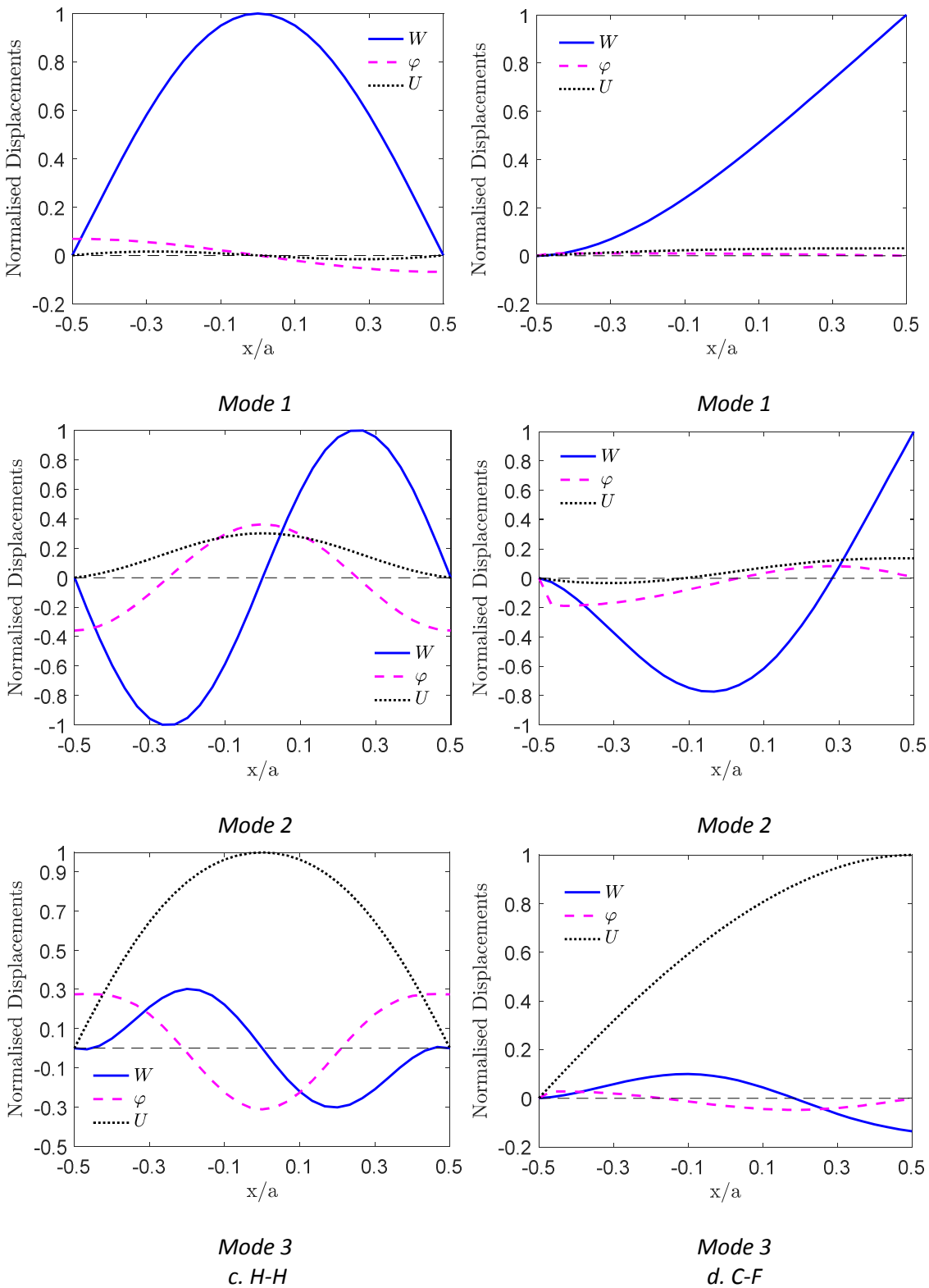

Fig. 2. 9: The first three mode shapes of Al_2O_3/Al beams (a/h=5, p=1, ν=0.3) (cont.).

Table 2. 13: Dimensionless critical buckling loads of Al_2O_3/Al beams (ν=0.23).

a/h	BCs	Theory	p					
			0	0.5	1	2	5	10
5	C-C	Present	154.534	103.732	80.566	61.733	47.468	41.759
		HOBT [51]	154.550	103.732	80.609	61.793	47.756	41.804
		FOBT [76]	154.350	103.220	80.498	62.614	50.384	44.267
	C-H	Present	90.022	59.500	46.107	35.568	28.387	25.203
		FOBT [76]	97.580	64.052	49.497	38.576	32.000	28.731
	H-H	Present	48.648	31.987	24.648	19.109	15.664	14.098
		HOBT [51]	48.840	32.009	24.691	19.161	15.740	14.147
		FOBT [76]	48.835	31.967	24.687	19.245	16.024	14.427
	C-F	Present	13.043	8.293	6.500	4.931	4.270	3.848
		HOBT [51]	13.077	8.502	6.543	5.098	4.278	3.882
		FOBT [76]	13.213	8.578	6.600	5.150	4.345	3.950
10	C-C	Present	195.179	127.876	98.625	76.622	62.902	56.431
		HOBT [51]	195.361	128.050	98.787	76.668	62.979	56.597
		FOBT [76]	195.340	127.870	98.749	76.980	61.062	57.708
	C-H	Present	103.596	67.284	51.264	40.584	33.108	29.904
		FOBT [76]	106.330	69.154	52.251	41.535	33.436	31.705
	H-H	Present	52.204	33.478	26.102	19.860	17.023	15.321
		HOBT [51]	52.308	34.009	26.173	20.394	17.112	15.529
		FOBT [76]	52.309	33.996	26.171	20.416	17.192	15.612
	C-F	Present	13.173	8.523	6.586	5.037	4.262	3.874
		HOBT [51]	13.374	8.671	6.668	5.203	4.398	4.005
		FOBT [76]	13.349	8.657	6.657	5.194	4.209	3.997

It can be seen that the current solutions are in excellent agreement with previous studies for both vibration ([49, 51, 75, 77]) and buckling problems ([14, 51]). It is clear that the critical buckling loads are calculated directly in section 2.7.2. However, they can also be determined by increasing the axial force until the lowest natural frequency vanishes. By using this way, load-frequency curves can be plotted and used to explain the duality between the buckling load and natural frequency. The first load-frequency curves with various power-law indices and the first five load – frequency curves with p=0.5 of C-C Al_2O_3/Al beams are plotted in Figs. 2.11 and 2.12, respectively.

It can be seen that an increase of p leads to the reduction of frequencies in any axial load values. As expected, the bending natural frequencies decrease as the axial force changes from tension to compression, while the axial modes (mode 3 for a/h=5 and mode 5 for a/h=20) are almost constant. It is from load-frequency curves that for (a/h=5, p=0.5) (Fig. 2.12), the first, second, third and fourth buckling occurs at $\bar{P}$ = 103.732, 161.925, 237.383 and 274.285, respectively.

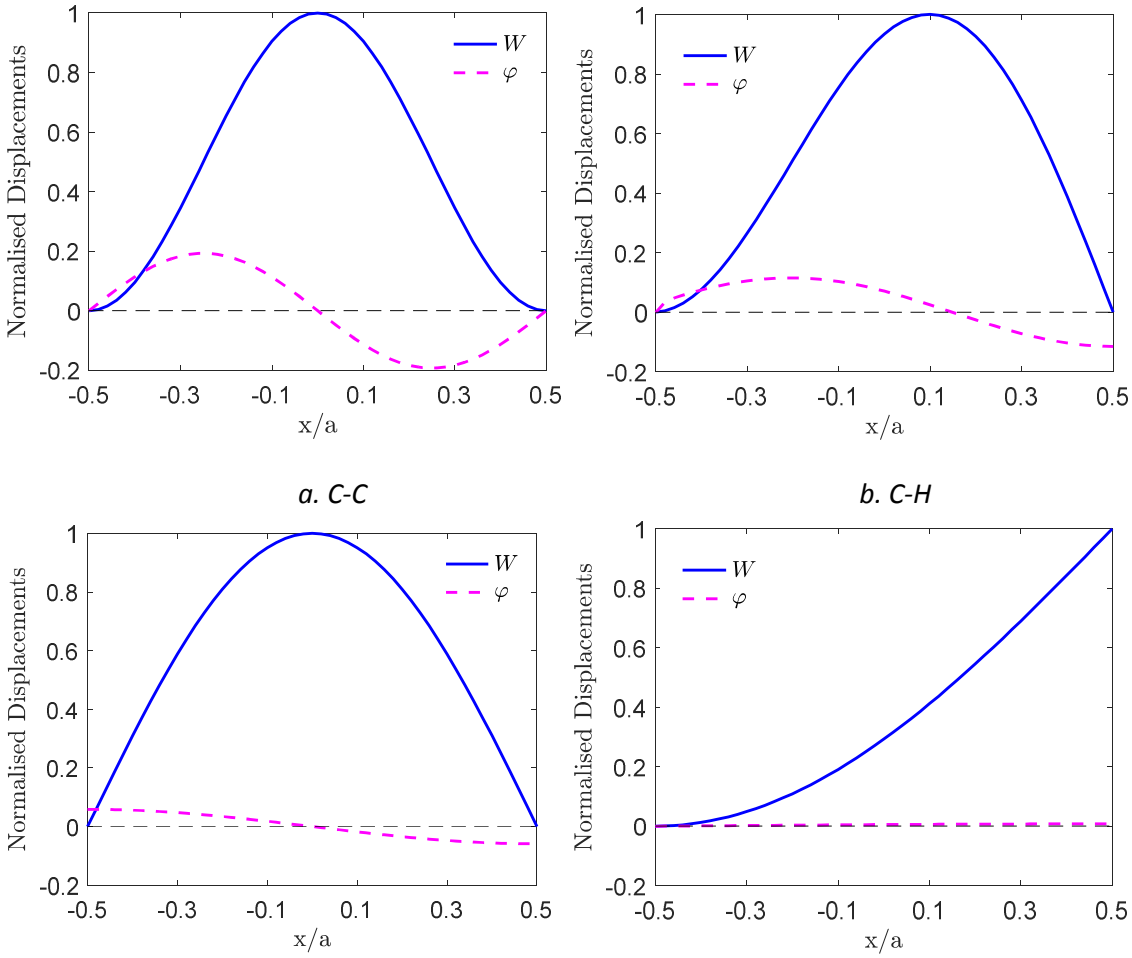

a. C-C *b. C-H*

c. H-H *d. C-F*

Fig. 2. 10: The first buckling shapes of Al_2O_3/Al beams (a/h=5, p=1, ν=0.23).

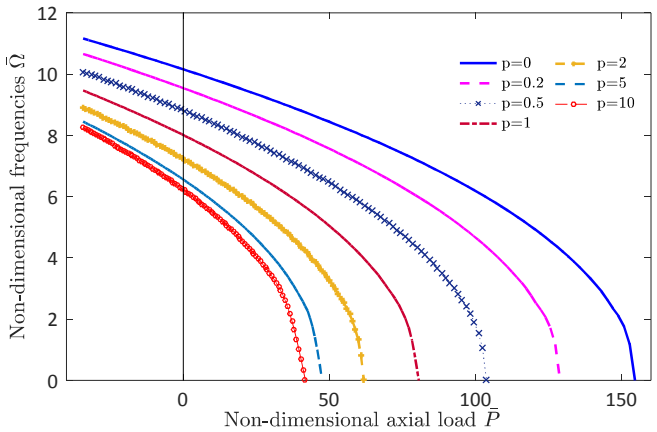

Fig. 2. 11: The effect of power-law index on the first load - frequency curves of C-C Al_2O_3/Al beams (a/h=5).

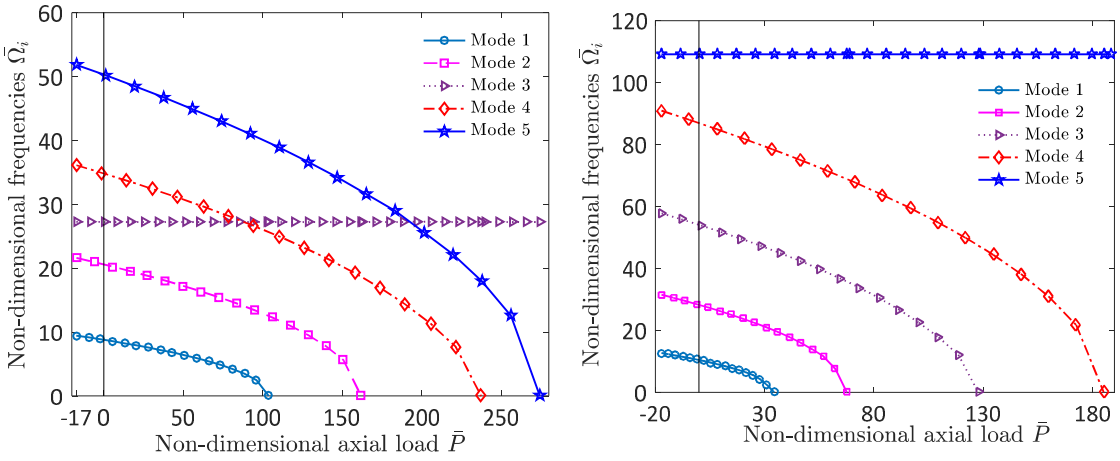

a. a/h=5 *b. a/h=20*

Fig. 2. 12: The first five load - frequency curves of C-C Al_2O_3/Al beams (p=0.5).

2.8.3 Vibration and buckling of FG beams under thermal loads

The following section aims to present the results derived from thermal vibration and buckling analysis of various FG beams including Si_3N_4/SUS304, Al_2O_3/SUS304, ZrO_2/SUS304 and ZrO_2/Ti-6Al-4V. The temperature-dependent properties of these materials are given in Table 2.14.

Table 2. 14: Temperature-dependent coefficients for ceramics and metals [14, 78].

Materials	Proprieties	P_0	P_{-1}	P_1	P_2	P_3
ZrO_2	*E(Pa)*	244.27e+9	0.0	−1.371e−3	1.214e−6	−3.681e−10
	α (1/K)	12.766e−6	0.0	−1.491e−3	1.006e−5	−6.778e−11
	κ (W/mK)	1.7	0.0	1.276e−4	6.648e−8	0.0
	ν	0.2882	0.0	1.133e−4	0.0	0.0
	ρ (kg/m³)	3000	0.0	0.0	0.0	0.0
Ti–6Al–4V	*E(Pa)*	122.56e+9	0.0	−4.586e−4	0.0	0.0
	α (1/K)	7.5788e−6	0.0	6.638e−4	−3.147e−6	0.0
	κ (W/mK)	1	0.0	1.704e−2	0.0	0.0
	ν	0.2884	0.0	1.121e−4	0.0	0.0
	ρ (kg/m³)	4429	0.0	0.0	0.0	0.0
Al_2O_3	*E(Pa)*	349.55e+9	0.0	−3.853e−4	4.027e−7	−1.673e−10
	α (1/K)	6.8269e−6	0.0	1.838e−4	0.0	0.0
	ν	0.26	0.0	0.0	0.0	0.0
	ρ (kg/m³)	3800	0.0	0.0	0.0	0.0
Si_3N_4	*E(Pa)*	348.43e+9	0.0	−3.070e−4	2.160e−7	−8.946e−11
	α (1/K)	5.8723e−6	0.0	9.095e−4	0.0	0.0
	κ (W/mK)	13.723	0.0	−1.032e−3	5.466e−7	−7.876e−11
	ν	0.24	0.0	0.0	0.0	0.0
	ρ (kg/m³)	2370	0.0	0.0	0.0	0.0
SUS304	*E(Pa)*	201.04e+9	0.0	3.079e−4	−6.534e−7	0.0
	α (1/K)	12.330e−6	0.0	8.086e−4	0.0	0.0
	κ (W/mK)	15.379	0.0	−1.264e−3	2.092e−6	−7.223e−10
	ν	0.3262	0.0	−2.002e−4	3.797e−7	0.0
	ρ (kg/m³)	8166	0.0	0.0	0.0	0.0

Three types of temperature distribution through the thickness, which are uniform temperature rise (UTR), linear temperature rise (LNR) and non-linear temperature rise (NLNR), are considered. Accordingly, the temperature and the Young's modulus along the thickness direction for Si_3N_4/SUS304 beam at $\Delta T = 0$ and 900K are plotted in Fig. 2.13. Besides, the temperature-dependent properties are illustrated in Fig. 2.14 for different materials under a range of temperature.

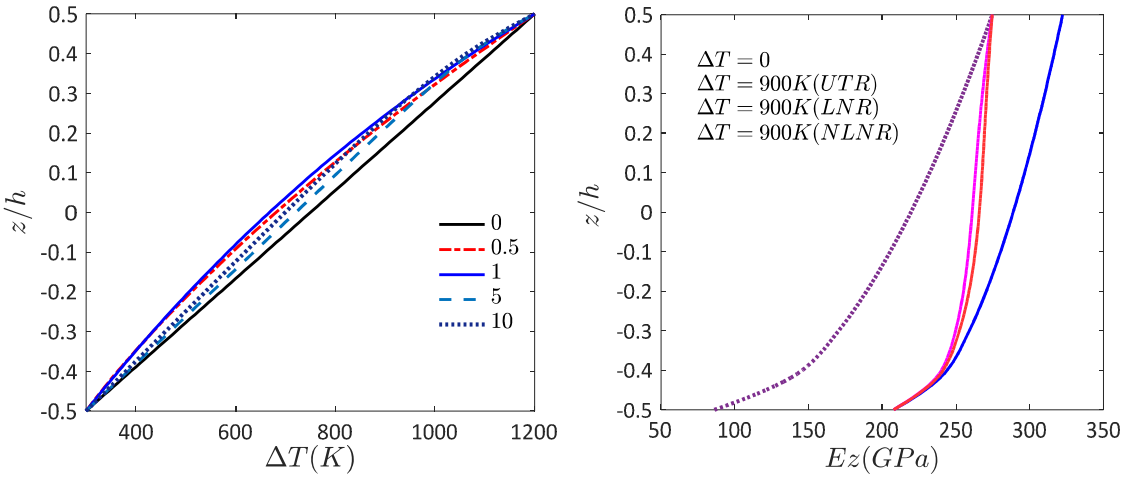

a. Temperature distributions *b. Young's modulus (Si_3N_4/SUS304, p=0.5)*

Fig. 2. 13: Temperature distributions and Young's modulus of Si_3N_4/SUS304 beams through the thickness with ΔT=0 and 900 K.

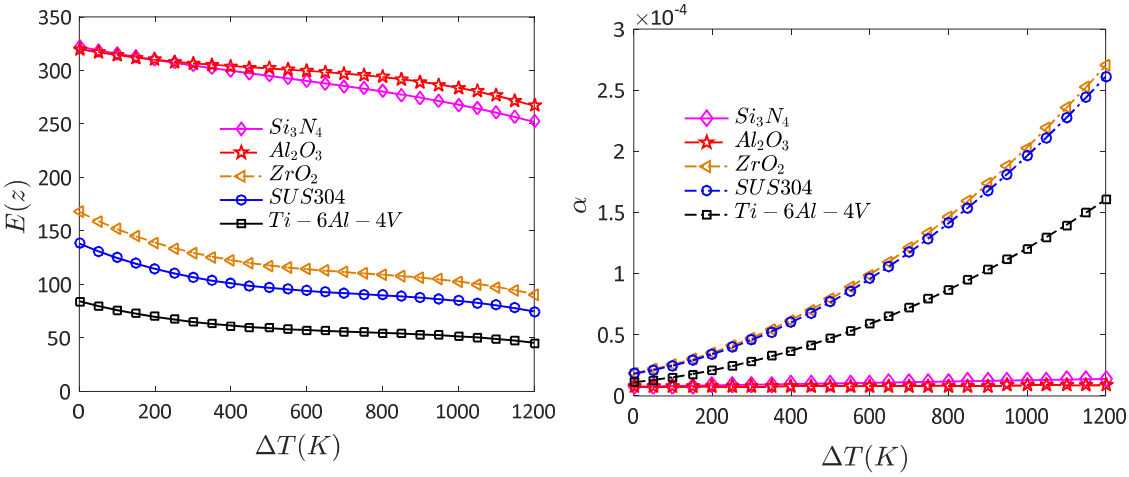

a. Young's modulus *b. Thermal expansion*

Fig. 2. 14: Young's modulus and thermal expansion of ceramics and metals with respect to the temperature change.

2.8.3.1 Uniform Temperature Rise (UTR)

This example aims to verify the accuracy further in thermal vibration and buckling behaviours and to investigate the thermal effect of temperature independent (TID) and temperature dependence (TD) material properties. The temperature is assumed to be uniform through the

thickness. In order to verify with Wattanasakulpong et al. [67], the elastic constants of FG beams in this example are taken as $Q_{11}=\frac{E(z)}{1-\nu^2}$ and $Q_{55}=\frac{E(z)}{2(1+\nu)}$; and the thermal stresses are calculated as $\sigma_x^T=-\frac{E(z)\alpha(z)\Delta T}{1-\nu}$. The following dimensionless critical temperature and natural frequency are used: $\lambda=\Delta T_{cr}\left(\frac{a}{h}\right)^2\alpha_m$ and $\Omega=\omega\frac{a^2}{h}\sqrt{\frac{I_0}{\int_{-h/2}^{h/2}E(z)dz}}$ with α_m being thermal expansion of metals at T_m=300 K.

Tables 2.15-2.17 present the critical temperatures and fundamental frequencies of various FG beams under the UTR. The present TID and TD solutions are in good agreement with those from [67] for all boundary conditions and slenderness ratios. These tables also reveal that the TD solution gives significantly lower values compared to TID one, which highlights the importance of considering the variation of material properties along with respect to the temperature. Due to this reason, only TD solution is used in the rest of this chapter. It can be seen from Table 2.16 the difference in buckling behaviour of Si_3N_4 and Al_2O_3 in combination with SUS304 is significant inspite of a slight difference of properties between these two ceramics, whose properties are shown in Fig. 2.14. In addition, Ti-6Al-4V presents a much higher buckling temperature over SUS304 in the mixture with the ceramic ZrO_2, especially with a high volume of metal.

Table 2. 15: Dimensionless critical temperatures of Al_2O_3/SUS304 beams under UTR (p=0.3).

	a/h	20			40		
	BCs	C-C	C-H	H-H	C-C	C-H	H-H
TID	HOBT [67]	4.1231	2.1418	1.0650	4.2251	2.1740	1.0685
	Present	4.1545	2.4206	1.1319	4.2349	2.2709	1.0861
TD	HOBT [67]	3.4279	1.9274	1.0036	3.9992	2.1081	1.0527
	Present	3.4246	1.9165	0.9924	3.9695	2.0902	1.0353

Table 2. 16: The critical temperatures of various FG beams under UTR (a/h=20).

BCs	Materials	Theory	TID				TD			
			p = 0	1	5	10	p = 0	1	5	10
H-H	Si_3N_4/SUS304	HOBT [67]	1.348	0.876	0.750	0.712	1.185	0.805	0.697	0.664
		Present	1.307	0.866	0.744	0.710	1.151	0.796	0.693	0.663
	Al_2O_3/SUS304	HOBT [67]	1.376	0.880	0.747	0.708	1.326	0.827	0.698	0.662
		Present	1.347	0.870	0.740	0.705	1.296	0.817	0.694	0.661
	ZrO_2/SUS304	HOBT [67]	0.518	0.565	0.589	0.600	0.416	0.481	0.530	0.549
		Present	0.514	0.562	0.588	0.600	0.414	0.479	0.529	0.549
	ZrO_2/Ti-6Al-4V	Present	0.514	0.715	1.091	1.227	0.414	0.583	1.003	8.104
C-H	Si_3N_4/SUS304	Present	2.654	1.758	1.510	1.440	2.115	1.503	1.321	1.267
	Al_2O_3/SUS304	Present	2.732	1.767	1.502	1.430	2.526	1.567	1.329	1.267
	ZrO_2/SUS304	Present	1.042	1.143	1.194	1.217	0.715	0.850	0.977	1.029
	ZrO_2/Ti-6Al-4V	Present	1.042	1.453	2.212	2.489	0.715	1.009	1.865	9.285
C-C	Si_3N_4/SUS304	Present	5.130	3.398	2.917	2.782	3.559	2.609	2.333	2.244
	Al_2O_3/SUS304	Present	5.280	3.415	2.902	2.763	4.540	2.769	2.364	2.254
	ZrO_2/SUS304	Present	2.013	2.207	2.309	2.352	1.117	1.363	1.642	1.762
	ZrO_2/Ti-6Al-4V	Present	2.013	2.809	4.269	4.806	1.117	1.570	3.070	8.104

Table 2. 17: Fundamental frequency with respect to the temperature rise of Al_2O_3/SUS304 beams under UTR (a/h=30).

			p = 0.2			p = 0.2		
	BCs	Theory	ΔT = 0	50	100	ΔT = 0	50	100
TID	C-C	HOBT [67]	6.6394	6.1189	5.5452	6.7355	5.9802	5.1028
		Present	6.6371	6.1209	5.5489	6.7366	5.9834	5.1125
	C-H	Present	4.5898	3.8574	2.9297	4.6653	3.5731	1.8925
	H-H	Present	2.9506	1.8450	-	3.0129	1.1816	-
TD	C-C	HOBT [67]	6.6394	6.1109	5.5081	6.7335	5.9581	4.9965
		Present	6.6371	6.1142	5.5141	6.7366	5.9631	5.0068
	C-H	Present	4.5898	3.8437	2.8608	4.6653	3.5391	1.5946
	H-H	Present	2.9506	1.8220	-	3.0129	1.0868	-

The effect of temperature on the fundamental frequencies of various FG beams with p=0.2 and 2 are illustrated in Fig. 2.15.

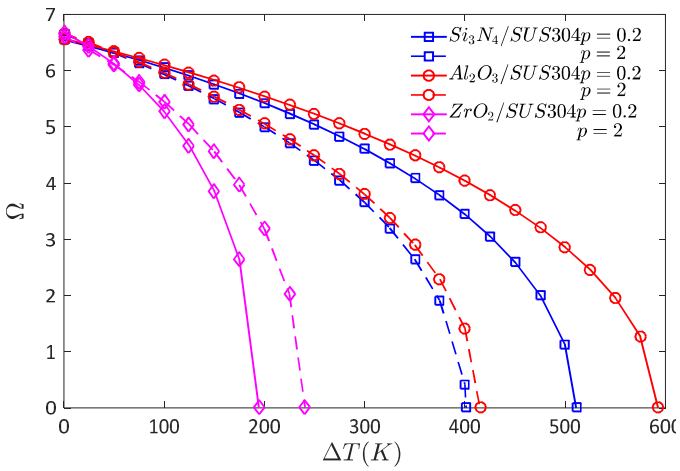

Fig. 2. 15: The temperature - frequency curves of C-C FG beams (a/h=20).

As the temperature increases, the fundamental frequencies decrease and finally vanish at critical temperature point. That is the characteristic of frequency-temperature curves, which can be used to determine the critical temperature of FG beams. For example, with p=2, the critical temperatures of Si_3N_4/SUS304, Al_2O_3/SUS304 and ZrO_2/SUS304 beams are 401.25, 415.14 and 240.65 (K), respectively.

2.8.3.2 Linear temperature rise (LNR) and Nonlinear temperature rise (NLNR)

The comparison between UTR and LNR solutions as well as LNR and NLNR solutions for the critical temperatures and natural frequencies of FG beams is given in Tables 2.18-2.21. The following dimensionless natural frequency is used: $\bar{\Omega} = \omega a^2 \sqrt{\frac{\rho_c A}{E_c I}}$. The results reported by Ebrahimi and Salari [79] for the case of H-H beams using the FOBT are also given for the verification purpose.

Table 2. 18: The critical temperatures of Si_3N_4/SUS304 beams under UTR and LNR.

a/h	BCs	Theory	UTR			LNR		
			p = 0	1	5	p = 0	1	5
40	H-H	Present	51.72	34.69	29.95	125.00	85.94	71.88
		FOBT [79]	–	–	–	127.33	84.62	69.43
	C-H	Present	102.02	69.26	59.96	246.88	175.00	146.88
	C-C	Present	187.87	129.87	113.01	451.56	328.13	279.69
20	H-H	Present	187.88	129.87	113.01	451.56	328.13	279.69
	C-H	Present	345.14	245.24	215.51	814.06	612.50	531.25
	C-C	Present	580.66	425.69	380.61	–*	1062.50	957.81

(–*) This value does not exist since the critical temperature of FG beams is higher than the melting point E_m=0.

Table 2. 19: Dimensionless natural frequencies of H-H Si_3N_4/SUS304 beams under UTR and LNR (a/h=20).

ΔT	Mode	Theory	UTR			LNR		
			p=0	1	5	p=0	1	5
10	1	FOBT [79]	–	–	–	9.6461	5.7717	4.6925
		Present	2.8842	2.7347	2.4845	9.6843	5.8432	4.7454
	2	FOBT [79]	–	–	–	38.6688	23.2890	19.0001
		Present	11.5991	11.4594	11.2261	38.6698	23.2942	19.0058
	3	FOBT [79]	–	–	–	85.5816	51.5787	42.0838
		Present	25.6350	25.5020	25.2740	85.4928	51.5782	42.0626
30	1	FOBT [79]	–	–	–	9.4538	5.6105	4.5363
		Present	2.8450	2.6157	2.2158	9.4864	5.6727	4.5792
	2	FOBT [79]	–	–	–	38.4794	23.1492	18.8693
		Present	11.4678	11.2543	10.9045	38.4431	23.1103	18.8315
	3	FOBT [79]	–	–	–	85.3911	51.4659	41.9855
		Present	25.4240	25.2178	24.8745	85.2146	51.3662	41.8680
60	1	FOBT [79]	–	–	–	9.1475	5.3537	4.2875
		Present	2.9109	2.6325	2.1295	9.1774	5.4030	4.3136
	2	FOBT [79]	–	–	–	38.1838	22.9319	18.6672
		Present	11.8148	11.5484	11.1378	38.0975	22.8282	18.5625
	3	FOBT [79]	–	–	–	85.0946	51.2893	41.8321
		Present	26.1669	25.9057	25.4947	84.7945	51.0434	41.5692

Table 2. 20: Fundamental frequency of Si_3N_4/SUS304 beams under LNR and NLNR (a/h=20).

BCs	Temperature distribution	ΔT(K) = 20			80		
		p=0.1	0.5	1	p=0.1	0.5	1
C-C	LNR [80]	19.6398	15.2580	13.3671	19.3420	15.0040	13.1304
	Present	19.3371	15.0222	13.1554	18.9778	14.6972	12.8431
	NLNR [80]	19.6390	15.2501	13.3558	19.3552	14.9886	13.1011
	Present	19.3379	15.0244	13.1579	18.9832	14.7115	12.8600
C-H	LNR [80]	13.4380	10.4238	9.1227	13.0201	10.0515	8.7674
	Present	13.3373	10.3526	9.0635	12.8837	9.9342	8.6571
	NLNR [80]	13.4395	10.4211	9.1178	13.0483	10.0594	8.7648
	Present	13.3382	10.3553	9.0669	12.8907	9.9533	8.6801
H-H	LNR [80]	8.4634	6.5415	5.7114	7.8795	6.0063	5.1927
	Present	8.4716	6.5742	5.7588	7.8766	6.0166	5.2128
	NLNR [80]	8.4675	6.5437	5.7124	7.9265	6.0402	5.2186
	Present	8.4730	6.5779	5.7632	7.8861	6.0431	5.2448

A good agreement between the present results with previous ones can be observed for various p values. For all boundary conditions and power-law indices, the LNR results are significantly greater than those from the UTR. It should be noted that there are some limitations for thermal buckling of moderate thick beams since their critical temperatures are greater than the melting point of the metals, for example with Si_3N_4/SUS304 C-C beam (a/h=20, p=0) in Table 2.21. As expected, the critical temperatures obtained from LNR and NLNR are the same for isotropic beams. As *p* increases, difference becomes more pronounced with higher values for NLNR solution.

Table 2. 21: The critical temperatures of various FG beams under LNR and NLTR with various power-law indices (a/h=20).

BCs	Materials	Temp. profile	p				
			0	1	2	5	10
C-C	Si_3N_4/SUS304	LNR	-	1062.50	1004.69	957.81	921.88
		NLNR	-	-	1132.50	1042.50	972.50
	ZrO_2/SUS304	LNR	390.74	438.14	465.66	521.28	583.24
		NLNR	390.74	532.42	565.64	605.16	642.05
	ZrO_2/Ti-6Al-4V	LNR	390.40	431.43	484.90	625.60	828.12
		NLNR	390.40	484.92	539.57	668.54	853.83
C-H	Si_3N_4/SUS304	LNR	814.06	612.50	570.31	531.25	507.81
		NLNR	814.06	688.75	637.50	572.50	531.25
	ZrO_2/SUS304	LNR	258.41	289.76	305.47	336.40	365.50
		NLNR	258.41	357.72	377.09	393.99	406.30
	ZrO_2/Ti-6Al-4V	LNR	259.23	286.47	325.85	428.52	565.48
		NLNR	259.23	325.87	366.91	461.02	587.44
H-H	Si_3N_4/SUS304	LNR	451.56	328.13	301.56	279.69	265.63
		NLNR	451.56	357.50	327.50	293.75	273.75
	ZrO_2/SUS304	LNR	155.05	173.86	179.21	192.87	204.68
		NLNR	155.05	216.12	227.83	230.85	231.72
	ZrO_2/Ti-6Al-4V	LNR	155.54	174.17	200.72	263.97	343.81
		NLNR	155.54	200.73	228.95	287.68	361.86

(-) These values do not exist since the critical temperature of FG beams is higher than the melting point (E_m=0)

Fig. 2.16 illustrates the critical temperatures of C-H FG beams under LNR with the variation of power-law indices and slenderness ratios. It is clear that with an increase of p, the critical temperatures of Si_3N_4/SUS304 and Al_2O_3/SUS304 beams decrease, whereas those of ZrO_2/SUS304 and ZrO_2/Ti-6Al-4V beams increase. Comparing the buckling temperature of ZrO_2/SUS304 and ZrO_2/Ti-6Al-4V beams, values for the latter is lower for $0 \le p \le 1.2$ but higher for $p > 1.2$ (Fig. 2.16a). As expected, low critical buckling temperatures are observed in the slender beams (Fig. 2.16b).

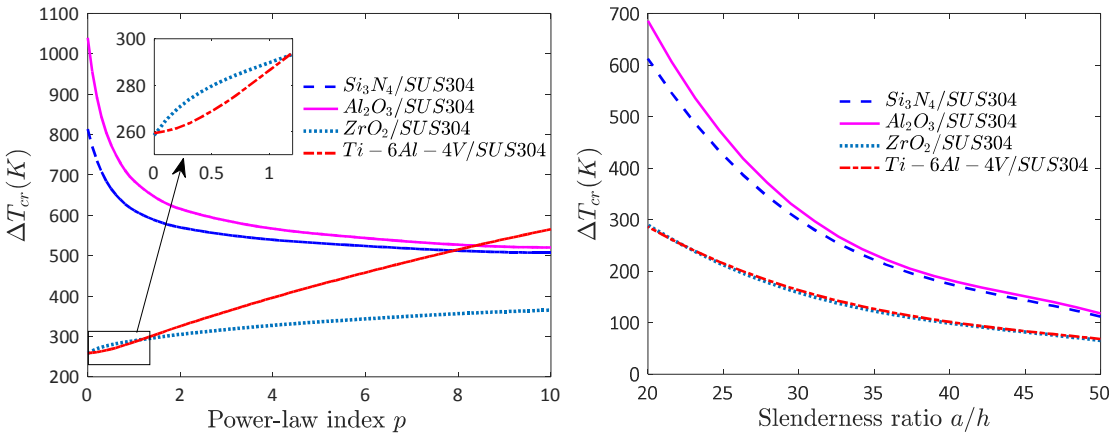

a. a/h=20 *b. p=0.5*

Fig. 2. 16: The critical temperatures of C-H FG beams under LNR.

Finally, a comprehensive 3D interaction diagram of the natural frequencies, temperature and power-law indices is plotted in Fig. 2.17. With a specific value of *p*, the natural frequencies of ZrO_2/SUS304 beams are smaller than those of Si_3N_4/SUS304 beams at the same temperature.

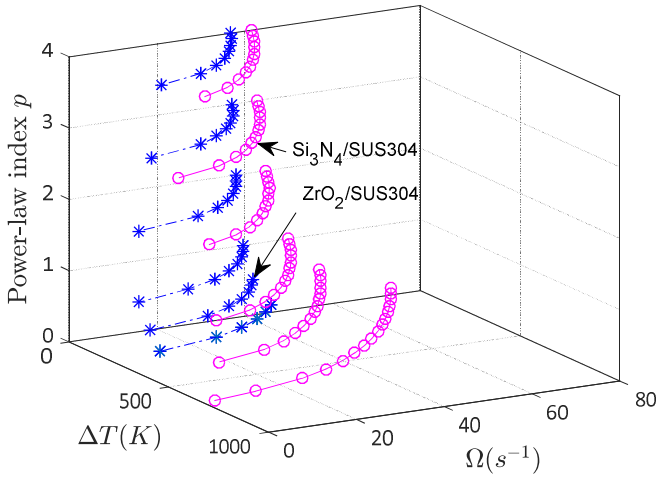

Fig. 2. 17: Frequency – temperature – power-law index interaction curves of Si_3N_4/SUS304 and ZrO_2/SUS304 beams under NLNR.

2.9 Concluding remarks

In this chapter, the state space approach is applied to analyse free vibration and buckling behaviours of FG beams with various shear deformation theories (CBT, FOBT and HOBT). Hamilton's principle is applied to derive the governing equations of motion and boundary conditions. Numerical results are presented firstly for the fundamental frequencies of FG sandwich beams under nine combinations of classical BCs and three combinations of non-classical BCs. The effects of geometric, material parameters, graded sandwich schemes as well as the rotational and translational stiffness at the ends to the free vibration of FG sandwich beams are examined. The free vibration and buckling of FG beams under mechanical load and thermal environment are investigated in the second part. The natural frequencies and corresponding mode shapes together with the buckling loads and buckling shapes are presented under the mechanical loads. The effects of thermal environment considering the material temperature dependence to the free vibration and buckling behaviours are investigated, showing the necessity of evaluating the change of material properties under the elevated temperature. The present model is found to be appropriate and efficient in analysing the vibration and buckling of FG beams under mechanical/thermal loads.

CHAPTER 3

MODIFIED COUPLE STRESS THEORY FOR FG MICROBEAMS

3.1 Introduction

In this section, a brief review of the publications investigating the size-dependent behaviours of FG microbeams based on the modified couple stress theory (MCST) is carried out. One of the earliest work on the application of MCST was to analyse the bending behaviour of an epoxy cantilever beam by Park and Gao [81] based on the CBT. Kong et al. [82] compared the variation of natural frequencies of the cantilever and simply supported homogeneous beams. Xia et al. [83] studied the static, post-buckling and free vibration behaviours of an epoxy beams considering geometric nonlinearity. It is worth noting that in the CBT, the cross-section is assumed to be flat and perpendicular to the neutral axis as deformed, which actually neglects the shear deformation effect. This results in the stiffer behaviours compared to the real working order of structures. The FOBT was then developed to include the shear effect in analysing the structural behaviours. Using the FOBT, Ma et al. [84] examined the static and free vibration behaviours of simply supported epoxy beams. Asghari et al. [85] obtained the Navier solution for static and vibration behaviours of cantilever FG beams by the CBT and then developed this model to the FOBT and von-Karman strain formulation for a simply supported homogeneous beams. Using the differential quadrature method, Ke and Wang [86] studied the dynamic stability of FG beams under the hinged and clamped supports. Ke et al. [87] also incorporated the geometric nonlinearity effects in the free vibration of FG beams. Dehrouyeh-Semnani et al. [88] investigated the free vibration of geometrically imperfect FG beams under various BCs based on the Rayleigh-Ritz's method. Reddy [89] examined the static bending, vibration and buckling behaviours of simply supported FG beams using both CBT and FOBT, which included the geometric nonlinearity effect. Using Navier solution, Simsek et al. [90] studied static bending behaviours of FG beams. Kahrobaiyan et al. [91] developed a FOBT beam element and applied to the cantilever FG beams under a concentrated load and a pull-in voltage. Thai et al. [92] studied the static, vibration and buckling behaviours of FG-sandwich beams without a shear correction factor. They computed the transverse shear force and shear stress by using the equilibrium equations. Nateghi and Salamat-talab [93] included the thermal effect in analysing the free vibration and buckling behaviours of FG beams using both CBT and FOBT. Akgoz and Civalek [94] utilised the Rayleigh-Ritz solution to study the free vibration of axially graded tapered beams. In the FOBT, the cross-section is still assumed to be flat while loaded, which violates the free shear stress conditions at the top and bottom surfaces, and hence a shear

correction factor is needed. This leads to the proposition of the third-order beam theory (TBT) and HOBT. Nateghi et al. [95] applied the generalized differential quadrature method (GDQM) to examine the size-dependent buckling behaviour of FG beams using the CBT, FOBT and TBT. Salamat-talab et al. [96] also developed an analytical solution to analyse the static and free vibration of simply supported beams. Ansari et al. [97] developed a general strain gradient theory using the FOBT, which comprises the MCST, in analysing the bending, vibration and buckling of FG beams by applying the GDQM. Sahmani and Ansari [98] also extended the solutions of buckling behaviour for the TBT with the inclusion of the thermal environment effect. Mohammad-Abadi and Daneshmehr [99] considered the buckling of FG beams under the CBT, FOBT and TBT. Simsek and Reddy [100] analysed bending and vibration behaviours, as well as buckling responses of FG beams with the inclusion of elastic Pasternak medium based on various HOBTs. Akgoz and Civalek [101, 102] employed a sinusoidal shear deformation to study the static and buckling behaviours, and the thermo-mechanical buckling of FG beams embedded in Winkler elastic medium under the framework of general strain gradient theory. Darijani and Mohammadabadi [103] employed the refined fifth-order shear deformation model for static, vibration and buckling behaviours of FG beams. Al-Basyouni et al. [104] studied the bending and vibration of FG beams based on the neutral surface position and unified HOBTs. Arbind and Reddy [105] proposed nonlinear finite element models based on the CBT and FOBT to analyse the bending behaviour of FG beams. Arbind et al. [106] later expanded these models to TBT and included the analytical solution to verify the finite element models. Al-Basyouni et al. [104] utilised the neutral surface concept to analyse the bending and vibration behaviours of simply supported FG microbeams using the CBT, FOBT and sinusoidal beam theory. Trinh et al. [107] analysed static bending, vibration and buckling of simply supported microbeams using various shear deformation theories. A comprehensive review on the development of MCST models and other non-classical continua, such as non-local elasticity [108-116] and strain gradient [7, 31, 117] can be found in the recent works by Thai et al. [16] and Romano et al. [113].

In this chapter, a unified framework for various beam theories are proposed to investigate the size-dependent bending, vibration and buckling behaviours of FG microbeams based on the MCST. The material properties of these beams are varied through beam's depth and calculated by using the rule of mixture and Mori-Tanaka scheme. The beam theories which includes the CBT, FOBT, TBT, Sinusoidal beam theory (SBT) and quasi-3D theories are presented systematically under one unified formula. The size-dependent behaviours are then solved using the analytical Navier approach in which the problems with simply-supported boundary conditions are considered. Effects of Poisson's ratio, length scale parameter, power-law index,

estimation methods of material properties and slenderness ratio on deflections, stresses, natural frequencies and critical buckling loads of FG microbeams are examined.

3.2 Constitutive Equations

The linear constitutive relations are given as:

$$\begin{Bmatrix} \sigma_x \\ \sigma_z \\ \sigma_{xz} \end{Bmatrix} = \begin{bmatrix} Q_{11} & Q_{13} & 0 \\ Q_{13} & Q_{11} & 0 \\ 0 & 0 & Q_{55} \end{bmatrix} \begin{Bmatrix} \varepsilon_x \\ \varepsilon_z \\ \gamma_{xz} \end{Bmatrix} \tag{3. 1}$$

where

$$Q_{11} = \frac{E(z)}{1-\nu^2} \; ; \; Q_{13} = \frac{E(z)\nu}{1-\nu^2} \; ; \; Q_{55} = \frac{E(z)}{2(1+\nu)} \tag{3. 2}$$

If the thickness stretching effect is omitted ($\varepsilon_z = 0$), elastic constants Q_{ij} in Eq. (3.1) are reduced as follow:

$$Q_{11} = E(z) \; ; \; Q_{13} = 0 \; ; \; Q_{55} = \frac{E(z)}{2(1+\nu)} \tag{3. 3}$$

3.3 Governing Equations of Motion

Based on the MCST [36], the virtual strain energy can be written as:

$$\delta U = \int_v (\sigma_{ij}\delta\varepsilon_{ij} + m_{ij}\delta\chi_{ij}) dv \;\; i,j = x,y,z \tag{3. 4}$$

where m_{ij} and χ_{ij} denote deviatoric part of the couple stress tensor, and symmetric curvature tensor, which are defined by:

$$\chi_{ij} = \frac{1}{2}\left(\theta_{i,j} + \theta_{j,i}\right) \tag{3. 5}$$

$$m_{ij} = \frac{E(z)}{1+\nu}\chi_{ij}$$

where *l* is a material length scale parameter and θ_i is the components of the rotation vector given by:

$$\theta_x = \theta_1 = \frac{1}{2}\left(\frac{\partial u_3}{\partial x_2} - \frac{\partial u_2}{\partial x_3}\right) \tag{3. 6a}$$

$$\theta_y = \theta_2 = \frac{1}{2}\left(\frac{\partial u_1}{\partial x_3} - \frac{\partial u_3}{\partial x_1}\right) \tag{3. 6b}$$

$$\theta_z = \theta_3 = \frac{1}{2}\left(\frac{\partial u_2}{\partial x_1} - \frac{\partial u_1}{\partial x_2}\right) \tag{3. 6c}$$

The displacement fields for different beam theories can be obtained as:

$$u_1(x,z,t) = U(x,t) - zW_b'(x,t) - f(z)W_s'(x,t) \tag{3. 7a}$$

$$u_2(x,z,t) = 0 \tag{3. 7b}$$

$$u_3(x,z,t) = W_b(x,t) + W_s(x,t) + g(z)W_z(x,t) \tag{3. 7c}$$

where U, W_b and W_s are the axial displacement, the bending and shear components of vertical displacement along the mid-plane of the beam. The thickness stretching effect in quasi-3D theories is taken into account by adding the component $g(z)W_z(x,t)$ in Eq. (3.7c). $f(z)$ and $g(z)$ represents shape function determining the distribution of the transverse shear strains and stress through the beam depth, which can be chosen as follows:

CBT: $f(z) = z$ (3. 8a)

FOBT: $f(z) = 0$ (3. 8b)

TBT: $f(z) = \frac{4}{3}\frac{z^3}{h^2}$ (3. 8c)

SBT: $f(z) = z - \frac{h}{\pi}\sin\frac{\pi z}{h}$ (3. 8d)

Quasi-3D (TBT): $f(z) = \frac{4}{3}\frac{z^3}{h^2}; g(z) = 1 - \frac{df}{dz} = 1 - \frac{4}{3}\frac{z^3}{h^2}$ (3. 8e)

Quasi-3D (SBT): $f(z) = z - \frac{h}{\pi}\sin\frac{\pi z}{h}$; $g(z) = \cos\left(\frac{\pi z}{h}\right)$ (3. 8f)

The non-zero strains and symmetric curvature tensors are given by:

$$\varepsilon_{xx} = \frac{\partial u_1}{\partial x} = U' - zW_b'' - fW_s'' \tag{3. 9a}$$

$$\varepsilon_{zz} = \frac{\partial u_3}{\partial z} = \frac{\partial g}{\partial z}W_z \tag{3. 9b}$$

$$\gamma_{xz} = \frac{\partial u_3}{\partial x} + \frac{\partial u_1}{\partial z} = g\left(W_s' + W_z'\right) \tag{3. 9c}$$

$$\chi_{xy} = \frac{1}{2}\frac{\partial \theta}{\partial x} = -\frac{1}{2}\left(W_b'' + W_s''\right) + \frac{g}{4}\left(W_s'' - W_z''\right) \tag{3. 9d}$$

$$\chi_{yz} = \frac{1}{2}\frac{\partial \theta}{\partial z} = \frac{1}{4}\frac{\partial g}{\partial z}\left(W_s' - W_z'\right) \tag{3. 9e}$$

where prime (') indicates the differentiation with respect to the *x*-axis.

3.3.1 Quasi-3D shear deformation theories

In order to derive the equations of motion, Hamilton's principle is used:

$$\int_{t_1}^{t_2}\left(\delta K-\delta \mathrm{U}-\delta V\right)dt=0 \tag{3. 10}$$

where *U*, *K* and *V* denote the strain energy, kinetic energy and potential energy, respectively.

The variation of the strain energy can be stated as:

$$\delta U=\int_V\Big[\left(\sigma_{xx}\delta\varepsilon_{xx}+\sigma_{xz}\delta\gamma_{xz}+\sigma_{zz}\delta\varepsilon_{zz}+2m_{xy}\delta\chi_{xy}+2m_{yz}\delta\chi_{yz}\right)dV$$

$$=\int_0^a\Big[\left(N_x\delta U^{'}-M_x\delta W_b^{''}-P_xW_s^{''}\right)+Q_{xz}\left(W_s^{'}+W_z^{'}\right)+O_z\delta W_z$$

$$-R_{xy}\delta\left(W_b^{''}+W_s^{''}\right)+\frac{S_{xy}}{2}\delta\left(W_s^{''}-W_z^{''}\right)+\frac{T_{yz}}{2}\delta\left(W_s^{'}-W_z^{'}\right)\Big]dx \tag{3. 11}$$

where $N_x, M_x, P_x, Q_{xz}, O_z, R_{xy}, S_{xy}$ and T_{yz} are the stress resultants, respectively, defined as:

$$N_x=\int_A\sigma_x dA=AU^{'}-BW_b^{''}-B_sW_s^{''}+XW_z \tag{3. 12a}$$

$$M_x=\int_A z\sigma_x dA=BU^{'}-DW_b^{''}-D_sW_s^{''}+YW_z \tag{3. 12b}$$

$$P_x=\int_A f\sigma_x dA=B_sU^{'}-D_sW_b^{''}-HW_s^{''}+Y_sW_z \tag{3. 12c}$$

$$O_z=\int_A\sigma_z\frac{\partial g}{\partial z}dA=XU^{'}-YW_b^{''}-Y_sW_s^{''}+ZW_z \tag{3. 12d}$$

$$Q_{xz}=\int_A g\sigma_{xz}dA=A_s\left(W_s^{'}+W_z^{'}\right) \tag{3. 12e}$$

$$R_{xy}=\int_A m_{xy}dA=-A_n\left(W_b^{''}+W_s^{''}\right)+\frac{B_n}{2}\left(W_s^{''}-W_z^{''}\right) \tag{3. 12f}$$

$$S_{xy}=\int_A gm_{xy}dA=-B_n\left(W_b^{''}+W_s^{''}\right)+\frac{D_n}{2}\left(W_s^{''}-W_z^{''}\right) \tag{3. 12g}$$

$$T_{yz}=\int_A\frac{\partial g}{\partial z}m_{yz}dA=\frac{H_n}{2}\left(W_s^{'}-W_z^{'}\right) \tag{3. 12h}$$

where

$$\left(A,B,B_s,D,D_s,H,Z\right)=\int_{-h/2}^{h/2}\left[1,z,f,z^2,fz,f^2,\left(\frac{\partial g}{\partial z}\right)^2\right]Q_{11}bdz \tag{3. 13a}$$

$$A_s=\int_{-h/2}^{h/2}g^2Q_{55}bdz \tag{3. 13b}$$

$$\left(X,Y,Y_s\right)=\int_{-h/2}^{h/2}\left(1,z,f\right)\frac{\partial g\left(z\right)}{\partial z}Q_{13}bdz \tag{3. 13c}$$

$$\left(A_n,B_n,D_n,H_n\right)=\int_{-h/2}^{h/2}\left[1,g,g^2,\left(\frac{\partial g}{\partial z}\right)^2\right]l^2\frac{E\left(z\right)}{2\left(1+\nu\right)}dz \tag{3. 13d}$$

The variation of the potential energy by the axial force P_0 and a transverse load q can be written as:

$$\delta V=-\int_0^l[P_0[\delta w_b^{'}(w_b^{'}+w_s^{'})+\delta w_s^{'}(w_b^{'}+w_s^{'})]+q(\delta w_b+\delta w_s)]dx \tag{3. 14}$$

The variation of the kinetic energy is obtained as:

$$\delta K=\int_{t_1}^{t_2}\int_V\rho\left(z\right)\left(\dot{u}_1\delta\dot{u}_1+\dot{u}_2\delta\dot{u}_2+\dot{u}_3\delta\dot{u}_3\right)dVdt$$

$$=\int_0^l[\delta\dot{u}(I_0\dot{u}-I_1\dot{w}_b^{'}-I_f\dot{w}_s^{'})+\delta w_b[I_0(\dot{w}_b+\dot{w}_s)+I_g\dot{w}_z]$$

$$+\delta\dot{w}_b^{'}(-I_1\dot{u}+I_2\dot{w}_b^{'}+I_{fz}\dot{w}_s^{'})+\delta\dot{w}_s^{'}[I_0(\dot{w}_b+\dot{w}_s)+I_g\dot{w}_z]$$

$$+\delta\dot{w}_b^{'}(-I_f\dot{u}+I_{fz}\dot{w}_b^{'}+I_{f^2}\dot{w}_s^{'})+\delta\dot{w}_z^{'}[I_g(\dot{w}_b+\dot{w}_s)+I_{g^2}\dot{w}_z] \tag{3. 15}$$

where

$$\left(I_0,I_1,I_2\right)=\int_{-h/2}^{h/2}\rho\left(1,z,z^2\right)bdz \tag{3. 16a}$$

$$\left(I_f,I_{fz},I_{f^2}\right)=\int_{-h/2}^{h/2}\rho\left(f,zf,f^2\right)bdz \tag{3. 16b}$$

$$\left(I_g,I_{g^2}\right)=\int_{-h/2}^{h/2}\rho\left(g,g^2\right)bdz \tag{3. 16c}$$

By substituting Eqs. (3.11), (3.14) and (3.15) into Eq. (3.10), the following weak statement is obtained:

$$\int_{t_1}^{t_2}\int_{0}^{a}\Big\{\delta\dot{U}\left(I_0\dot{U}-I_1\dot{W}_b^{'}-I_f\dot{W}_s^{'}\right)+\delta\dot{W}_b\left[I_0\left(\dot{W}_b+\dot{W}_s\right)+I_g\dot{W}_z\right]+\delta\dot{W}_b^{'}\left(-I_1\dot{U}+I_2\dot{W}_b^{'}+I_{fz}\dot{W}_s^{'}\right)$$

$$+\delta\dot{W}_s\left[I_0\left(\dot{W}_b+\dot{W}_s\right)+I_g\dot{W}_z\right]+\delta\dot{W}_s^{'}\left(-I_f\dot{U}+I_{fz}\dot{W}_b^{'}+I_{f^2}\dot{W}_s^{'}\right)+\delta\dot{W}_z\left[I_g\left(\dot{W}_b+\dot{W}_s\right)+I_{g^2}\dot{W}_z\right]$$

$$-N_x\delta U^{'}+M_x\delta W_b^{''}+P_x\delta W_s^{''}-Q_{xz}\delta\left(W_s^{'}+W_z^{'}\right)-O_z\delta W_z+R_{xy}\delta\left(W_b^{''}+W_s^{''}\right)-\frac{S_{xy}}{2}\delta\left(W_s^{''}-W_z^{''}\right)$$

$$-\frac{T_{yz}}{2}\delta\left(W_s^{'}-W_z^{'}\right)+P_0\left[\delta W_b^{'}\left(W_b^{'}+W_s^{'}\right)+\delta W_s^{'}\left(W_b^{'}+W_s^{'}\right)\right]+q\left(\delta W_b+\delta W_s\right)\Big\}dxdt \tag{3. 17}$$

By integrating Eq. (3.17) by parts and collecting the coefficients of $\delta U,\delta W_b$ and δW_s, the governing equations of motion can be obtained:

$$N_{xx}^{'}=I_0\ddot{U}-I_1\ddot{W}_b^{'}-I_f\ddot{W}_s^{'} \tag{3. 18a}$$

$$M_x^{b''}+R_{xy}^{''}-P_0\left(W_b^{''}+W_s^{''}\right)+q=I_1\ddot{U}^{'}+I_0\left(\ddot{W}_b+\ddot{W}_s\right)-I_2\ddot{W}_b^{''}-I_{fz}\ddot{W}_s^{''}+I_g\ddot{W}_z \tag{3. 18b}$$

$$P_x^{''}+Q_{xz}^{'}+R_{xy}^{''}-\frac{S_{xy}^{''}}{2}-\frac{T_{yz}^{''}}{2}-P_0\left(W_b^{''}+W_s^{''}\right)+q=I_f\ddot{U}^{'}+I_0\left(\ddot{W}_b+\ddot{W}_s\right)-I_{fz}\ddot{W}_b^{''}-I_{f^2}\ddot{W}_s^{''}+I_g\ddot{W}_z \tag{3. 18c}$$

$$Q_{xz}^{'}-O_z+\frac{S_{xy}^{''}}{2}+\frac{T_{yz}^{'}}{2}=I_g\left(\ddot{W}_b+\ddot{W}_s\right)+I_{g^2}\ddot{W}_z \tag{3. 18d}$$

By substituting Eq. (3.12) into Eq. (3.18), the governing equations of motion can be expressed in term of displacements:

$$AU^{''}-BW_b^{'''}-B_sW_s^{'''}+XW_z^{'}=I_0\ddot{U}-I_1\ddot{W}_b^{'}-I_f\ddot{W}_s^{'} \tag{3. 19a}$$

$$BU^{'''}-\left(D+A_n\right)W_b^{(iv)}-\left(D_s+A_n-\frac{B_n}{2}\right)W_s^{(iv)}-\frac{B_n}{2}W_z^{(iv)}+YW_z^{''}-P_0\left(W_b^{''}+W_s^{''}\right)+q \tag{3. 19b}$$

$$=I_1\ddot{U}^{'}+I_0\left(\ddot{W}_b+\ddot{W}_s\right)-I_2\ddot{W}_b^{''}-I_{fz}\ddot{W}_s^{''}+I_g\ddot{W}_z \tag{3. 19c}$$

$$B_sU^{'''}-\left(D_s+A_n-\frac{B_n}{2}\right)W_b^{(iv)}-\left[H+A_n-B_n+\frac{D_n}{4}\right]W_s^{(iv)}+\left(A_s+\frac{H_n}{4}\right)W_s^{''}-\left(\frac{B_n}{2}-\frac{D_n}{4}\right)W_z^{(iv)}$$

$$+\left(A_s+Y_s-\frac{H_n}{4}\right)W_z^{''}-P_0\left(W_b^{''}+W_s^{''}\right)+q=I_f\ddot{U}^{'}+I_0\left(\ddot{W}_b+\ddot{W}_s\right)-I_{fz}\ddot{W}_b^{''}-I_{f^2}\ddot{W}_s^{''}+I_g\ddot{W}_z \tag{3. 19d}$$

$$-XU^{'}-\frac{B_n}{2}W_b^{(iv)}+YW_b^{''}+\left(\frac{B_n}{2}-\frac{D_n}{4}\right)W_s^{(iv)}+\left(A_s-\frac{H_n}{4}+Y_s\right)W_z^{''}-ZW_z+\left(A_{55}^{s}+\frac{H_n}{4}\right)W_z^{''}-\frac{D_n}{4}W_z^{(iv)}$$

$$=I_g\left(\ddot{W}_b+\ddot{W}_s\right)+I_{g^2}\ddot{W}_z \tag{3. 19e}$$

3.3.2 Third-order beam theory and Sinusoidal beam theory

By neglecting the shape function $g(z)$ in Eq. (3.17), the following weak statement is obtained:

$$\int_{t_1}^{t_2}\int_{0}^{a}\left\{\delta\dot{U}\left(I_0\dot{U}-I_1\dot{W}_b^{'}-I_f\dot{W}_s^{'}\right)+\delta\dot{W}_bI_0\left(\dot{W}_b+\dot{W}_s\right)+\delta\dot{W}_b^{'}\left(-I_1\dot{U}+I_2\dot{W}_b^{'}+I_{fz}\dot{W}_s^{'}\right)+\delta\dot{W}_sI_0\left(\dot{W}_b+\dot{W}_s\right)\right.$$

$$+\delta\dot{W}_s^{'}\left(-I_f\dot{U}+I_{fz}\dot{W}_b^{'}+I_{f^2}\dot{W}_s^{'}\right)-N_x\delta U^{'}+M_x\delta W_b^{''}+P_x\delta W_s^{''}-Q_{xz}\delta W_s^{'}+R_{xy}\delta\left(W_b^{''}+W_s^{''}\right)-\frac{S_{xy}}{2}\delta W_s^{''}$$

$$\left.-\frac{T_{yz}}{2}\delta W_s^{'}+P_0\left[\delta W_b^{'}\left(W_b^{'}+W_s^{'}\right)+\delta W_s^{'}\left(W_b^{'}+W_s^{'}\right)\right]+q\left(\delta W_b+\delta W_s\right)\right\}dxdt \tag{3. 20}$$

where $N_x, M_x^b, M_x^s, Q_{xz}, R_{xy}, S_{xy}$ and T_{yz} are defined as:

$$N_x=\int_A\sigma_xdA=AU^{'}-BW_b^{''}-B_sW_s^{''} \tag{3. 21a}$$

$$M_x=\int_A z\sigma_xdA=BU^{'}-DW_b^{''}-D_sW_s^{''} \tag{3. 21b}$$

$$P_x=\int_A f\sigma_xdA=B_sU^{'}-D_sW_b^{''}-HW_s^{''} \tag{3. 21c}$$

$$Q_{xz}=\int_A g\sigma_{xz}dA=A_sW_s^{'} \tag{3. 21d}$$

$$R_{xy}=\int_A m_{xy}dA=-A_n\left(W_b^{''}+W_s^{''}\right)+\frac{B_n}{2}W_s^{''} \tag{3. 21e}$$

$$S_{xy}=\int_A gm_{xy}dA=-B_n\left(W_b^{''}+W_s^{''}\right)+\frac{D_n}{2}W_s^{''} \tag{3. 21f}$$

$$T_{yz}=\int_A\frac{\partial g}{\partial z}m_{yz}dA=\frac{H_n}{2}W_s^{'} \tag{3. 21g}$$

Similarly, the equations of motion can be expressed:

$$N_{xx}^{'}=I_0\ddot{U}-I_1\ddot{W}_b^{'}-I_f\ddot{W}_s^{'} \tag{3. 22a}$$

$$M_x^{b''}+R_{xy}^{''}-P_0\left(W_b^{''}+W_s^{''}\right)+q=I_1\ddot{U}^{'}+I_0\left(\ddot{W}_b+\ddot{W}_s\right)-I_2\ddot{W}_b^{''}-I_{fz}\ddot{W}_s^{''} \tag{3. 22b}$$

$$P_x^{''}+Q_{xz}^{'}+R_{xy}^{''}-\frac{S_{xy}^{''}}{2}+\frac{T_{yz}^{''}}{2}-P_0\left(W_b^{''}+W_s^{''}\right)+q=I_f\ddot{U}^{'}+I_0\left(\ddot{W}_b+\ddot{W}_s\right)-I_{fz}\ddot{W}_b^{''}-I_{f^2}\ddot{W}_s^{''} \tag{3. 22c}$$

Eq. (3.22) is rewritten in term of displacements:

$$AU^{''}-BW_b^{'''}-B_sW_s^{'''}=I_0\ddot{U}-I_1\ddot{W}_b^{'}-I_f\ddot{W}_s^{'} \tag{3. 23a}$$

$$BU^{'''}-\left(D+A_n\right)W_b^{(iv)}-\left(D_s+A_n-\frac{B_n}{2}\right)W_s^{(iv)}-P_0\left(W_b^{''}+W_s^{''}\right)+q$$

$$=I_1\ddot{U}^{'}+I_0\left(\ddot{W}_b+\ddot{W}_s\right)-I_2\ddot{W}_b^{''}-I_{fz}\ddot{W}_s^{''} \tag{3. 23b}$$

$$B_s U''' - \left(D_s + A_n - \frac{B_n}{2} \right) W_b^{(iv)} - \left[H + A_n - B_n + \frac{D_n}{4} \right] W_s^{(iv)} + \left(A_s + \frac{H_n}{4} \right) W_s'' - P_0 \left(W_b'' + W_s'' \right) + q$$

$$= I_f \ddot{U}' + I_0 \left(\ddot{W}_b + \ddot{W}_s \right) - I_{fz} \ddot{W}_b'' - I_{f^2} \ddot{W}_s'' \tag{3. 23c}$$

3.3.3 First-order beam theory

By considering the shape functions $f = g = 0$, the following weak statement is obtained:

$$\int_{t_1}^{t_2} \int_0^a \left\{ \delta \dot{U} \left(I_0 \dot{U} - I_1 \dot{W}_b' \right) + \delta \dot{W}_b I_0 \left(\dot{W}_b + \dot{W}_s \right) + \delta \dot{W}_b' \left(-I_1 \dot{U} + I_2 \dot{W}_b' \right) + \delta \dot{W}_s I_0 \left(\dot{W}_b + \dot{W}_s \right) \right.$$

$$- N_x \delta U' + M_x \delta W_b'' - Q_{xz} \delta W_s' + R_{xy} \delta W_b'' - \frac{R_{xy}}{2} \delta W_s''$$

$$\left. + P_0 \left[\delta W_b' \left(W_b' + W_s' \right) + \delta W_s' \left(W_b' + W_s' \right) \right] + q \left(\delta W_b + \delta W_s \right) \right\} dx dt \tag{3. 24}$$

where N_x, M_x^b, Q_{xz} and R_{xy} are defined as:

$$N_x = \int_A \sigma_x dA = AU' - BW_b'' \tag{3. 25a}$$

$$M_x = \int_A z \sigma_x dA = BU' - DW_b'' \tag{3. 25b}$$

$$Q_{xz} = K_s \int_A g \sigma_{xz} dA = K_s A_s W_s' \tag{3. 25c}$$

$$R_{xy} = \int_A m_{xy} dA = -A_n W_b'' - \frac{A_n}{2} W_s'' \tag{3. 25d}$$

Similarly, the equations of motion can be expressed:

$$N_{xx}' = I_0 \ddot{U} - I_1 \ddot{W}_b' \tag{3. 26a}$$

$$M_x^{b''} + R_{xy}'' - P_0 \left(W_b'' + W_s'' \right) + q = I_1 \ddot{U}' + I_0 \left(\ddot{W}_b + \ddot{W}_s \right) - I_2 \ddot{W}_b'' \tag{3. 26b}$$

$$Q_{xz}' + \frac{R_{xy}''}{2} + \frac{T_{yz}''}{2} - P_0 \left(W_b'' + W_s'' \right) + q = I_0 \left(\ddot{W}_b + \ddot{W}_s \right) \tag{3. 26c}$$

Eq. (3.26) is rewritten in term of displacements:

$$AU'' - BW_b''' = I_0 \ddot{U} - I_1 \ddot{W}_b' \tag{3. 27a}$$

$$BU''' - \left(D + A_n \right) W_b^{(iv)} - \frac{A_n}{2} W_s^{(iv)} - P_0 \left(W_b'' + W_s'' \right) + q = I_1 \ddot{U}' + I_0 \left(\ddot{W}_b + \ddot{W}_s \right) - I_2 \ddot{W}_b'' \tag{3. 27b}$$

$$- \frac{A_n}{2} W_b^{(iv)} - \frac{A_n}{4} W_s^{(iv)} + A_s W_s'' - P_0 \left(W_b'' + W_s'' \right) + q = I_0 \left(\ddot{W}_b + \ddot{W}_s \right) \tag{3. 27c}$$

3.3.4 Classical beam theory

By neglecting shear component ($w_s = 0$), the following weak statement is obtained:

$$\int_{t_1}^{t_2}\int_0^a \left\{ \delta\dot{U}\left(I_0\ddot{U} - I_1\ddot{W}_b^{'}\right) + \delta\dot{W}_b I_0 \ddot{W}_b + \delta\dot{W}_b^{'}\left(-I_1\ddot{U} + I_2\ddot{W}_b^{'}\right) - N_x\delta U^{'} + M_x\delta W_b^{''} + R_{xy}\delta W_b^{''} \right.$$

$$\left. + P_0\delta W_b^{'}W_b^{'} + q\delta W \right\} dxdt \tag{3. 28}$$

By integrating Eq. (3.28) by parts and collecting the coefficients of δU and δW_b, the governing equations of motion can be obtained:

$$N_{xx}^{'} = I_0\ddot{U} - I_1\ddot{W}_b^{'} \tag{3. 29a}$$

$$M_x^{b''} + R_{xy}^{''} - P_0 W_b^{''} + q = I_1\ddot{U}^{'} + I_0\left(\ddot{W}_b + \ddot{W}_s\right) - I_2\ddot{W}_b^{''} \tag{3. 29b}$$

where N_x, M_x^b, Q_{xz} and R_{xy} are defined as:

$$N_x = \int_A \sigma_x dA = AU^{'} - BW_b^{''} \tag{3. 30a}$$

$$M_x^b = \int_A z\sigma_x dA = BU^{'} - DW_b^{''} \tag{3. 30b}$$

$$R_{xy} = \int_A m_{xy} dA = -A_n W_b^{''} \tag{3. 30c}$$

Eq. (3.29) can be expressed in term of displacements:

$$AU^{''} - BW_b^{'''} = I_0\ddot{U} - I_1\ddot{W}_b^{'} \tag{3. 31a}$$

$$BU^{'''} - \left(D + A_n\right)W_b^{(iv)} - P_0 W_b^{''} + q = I_1\ddot{U}^{'} + I_0\ddot{W}_b - I_2\ddot{W}_b^{''} \tag{3. 31b}$$

3.4 Navier's solutions

3.4.1 Quasi-3D shear theories, third-order and sinusoidal beam theories

The Navier solution procedure is used to determine the analytical solutions for a simply-supported sandwich beam. The solution is assumed to be of the form:

$$U\left(x,t\right) = \sum_{n=1}^{\infty} U_n \cos\alpha x e^{i\omega t} \tag{3. 32a}$$

$$W_b\left(x,t\right) = \sum_{n=1}^{\infty} W_{bn} \sin\alpha x e^{i\omega t} \tag{3. 32b}$$

$$W_s\left(x,t\right) = \sum_{n=1}^{\infty} W_{sn} \sin\alpha x e^{i\omega t} \tag{3. 32c}$$

$$W_z(x,t)=\sum_{n=1}^{\infty}W_{zn}\sin\alpha x e^{i\omega t} \tag{3. 32d}$$

where $\alpha=n\pi/a$ and U_n, W_{bn}, W_{sn} and W_{zn} are the coefficients. The transverse load q is also expanded in Fourier series for a uniform load (q_o) as:

$$q(x)=\sum_{n=1}^{\infty}Q_n\sin\alpha x=\sum_{n=1}^{\infty}\frac{4q_o}{n\pi}\sin\alpha x \text{ with } n=1,3,5,.... \tag{3. 33}$$

By substituting Eq. (3.32) into Eq. (3.19), the analytical solution can be obtained from the following equations:

$$\begin{bmatrix} K_{11} & K_{12} & K_{13} & K_{14} \\ & K_{22}-P_0\alpha^2 & K_{23}-P_0\alpha^2 & K_{24} \\ & & K_{33}-P_0\alpha^2 & K_{34} \\ sym. & & & K_{44} \end{bmatrix} - \omega^2 \begin{bmatrix} M_{11} & M_{12} & M_{13} & 0 \\ & M_{22} & M_{23} & M_{24} \\ & & M_{33} & M_{34} \\ sym. & & & M_{44} \end{bmatrix} \begin{Bmatrix} U_n \\ W_{bn} \\ W_{sn} \\ W_{zn} \end{Bmatrix} = \begin{Bmatrix} 0 \\ Q_n \\ Q_n \\ 0 \end{Bmatrix} \tag{3. 34}$$

where

$$K_{11}=A\alpha^2;\ K_{12}=-B\alpha^3;K_{13}=-B_s\alpha^3;\ K_{14}=-X\alpha;\ K_{22}=(D+A_n)\alpha^4;\ K_{23}=\left(A_n-\frac{B_n}{2}+D_s\right)\alpha^4;$$

$$K_{24}=\frac{B_n}{2}\alpha^4+Y\alpha^2;\ K_{33}=-\left(H+A_n-B_n+\frac{D_n}{4}\right)\alpha^4+\left(A_s+\frac{H_n}{4}\right)\alpha^2;$$

$$K_{34}=\left(\frac{B_n}{2}-\frac{D_n}{4}\right)\alpha^4+\left(A_s-\frac{H_n}{4}+Y_s\right)\alpha^2;\ K_{44}=\frac{D_n}{4}\alpha^4+\left(A_s+\frac{H_n}{4}\right)\alpha^2+Z \tag{3. 35a}$$

$$M_{11}=I_0;\ M_{12}=-I_1\alpha;\ M_{13}=-I_f\alpha;M_{22}=I_0+I_2\alpha^2;\ M_{23}=I_0+I_{fz}\alpha^2;\ M_{24}=I_g;$$

$$M_{33}=I_0+I_{f^2}\alpha^2;\ M_{34}=I_g;\ M_{44}=I_{g^2} \tag{3. 35b}$$

It should be noted that TBT and SBT's solution can be obtained by neglecting the last row and column in Eq. (3.34).

3.4.2 First-order and classical beam theories

Similarly, deflections, natural frequencies and buckling loads are calculated from the following equations:

$$\begin{bmatrix} K_{11} & K_{12} & K_{13} \\ & K_{22}-P_0\alpha^2 & K_{23}-P_0\alpha^2 \\ sym. & & K_{33}-P_0\alpha^2 \end{bmatrix} - \omega^2 \begin{bmatrix} M_{11} & M_{12} & M_{13} \\ & M_{22} & M_{23} \\ sym. & & M_{33} \end{bmatrix} = \begin{Bmatrix} 0 \\ Q_n \\ Q_n \end{Bmatrix} \tag{3. 36}$$

where

$$K_{11}=A\alpha^2;\ K_{12}=-B\alpha^3;\ K_{13}=0;\ K_{22}=(D+A_n)\alpha^4;\ K_{23}=\frac{A_n}{2}\alpha^4;\ K_{33}=\frac{A_n}{4}\alpha^4+A_s\alpha^2 \tag{3. 37a}$$

$$M_{11}=I_0;\ M_{12}=-I_1\alpha;M_{22}=I_0+I_2\alpha^2;\ M_{23}=I_0;M_{33}=I_0 \tag{3. 37b}$$

Again, CBT's solution can be obtained by neglecting the last row and column in Eq. (3.36).

3.5 Numerical examples

A slightly different version of this section has been published in Composite Structures [107].

In this section, a number of numerical examples are conducted to show the validity and accuracy of the proposed approaches. Unless stated otherwise, simply-supported FG microbeams with two slenderness ratios (a/h=5,10) composed of SiC (E_c=427GPa, ρ_c=3100kg/m^3, ν_c=0.17) and Al (E_m=70GPa, ρ_m=2702kg/m^3, ν_m=0.3) are considered. The material properties are estimated by Mori-Tanaka scheme and the rule of mixture. The material length scale parameter is assumed to be l=15μm ([86, 118]). The shear correction factor is taken as 5/6 for the FOBT. The dimensionless terms are defined in this chapter as:

$$\bar{u}_3(z)=\frac{100E_mh^3}{12q_0a^4}u_3\left(\frac{a}{2},0\right); \tag{3. 38a}$$

$$\bar{\sigma}_x=\frac{h}{aq_0}\sigma_x\left(\frac{a}{2},z\right);\bar{\sigma}_{xz}=\frac{h}{aq_0}\sigma_{xz}(0,z);\bar{\sigma}_z=\frac{h}{aq_0}\sigma_z\left(\frac{a}{2},z\right) \tag{3. 38b}$$

$$\bar{\omega}=\frac{\omega a^2}{h}\sqrt{\frac{\rho_m}{E_m}} \tag{3. 38c}$$

$$\bar{P}_{cr}=P_{cr}\frac{12a^2}{E_mh^3}\sqrt{\frac{\rho_m}{E_m}} \tag{3. 38d}$$

3.5.1 Verification

Since there is no published data using quasi-3D theories for FG microbeams, the verification is firstly carried out for Al/Al_2O_3 beams (a/h=5) without size effect (Al: E_m=70GPa, ρ_m=2702kg/m^3, ν_m=0.3 and Al_2O_3: E_c=380GPa, ρ_c=3960kg/m^3, ν_c=0.3). The deflections, fundamental frequencies and critical buckling loads are computed for FG beams and given in Table 3.1 along with previous results. It can be seen that the obtained results are very close with those from ([119, 120]), which demonstrates the validation of the present theory.

In order to verify further, Tables 3.2-3.4 show the deflections, fundamental frequencies of SiC/Al microbeams and critical buckling loads of Al_2O_3/SUS304 microbeams (Al_2O_3: E_c=390GPa, ρ_c=3960kg/m^3, ν_c=0.3; SUS304: E_m=210GPa, ρ_m=8166kg/m^3, ν_m=0.3177), respectively. The results are calculated with four dimensionless material length scale parameters (h/l=1,2,4,8) from two types of constitute relations to verify and investigate the Poisson's effect. The first one includes this effect by using elastic constants extracted from 3D model ([100, 121])

($Q_{11}=\frac{E(z)\left[1-\nu(z)\right]}{\left[1+\nu(z)\right]\left[1-2\nu(z)\right]}$ and $Q_{13}=\frac{E(z)\nu(z)}{\left[1+\nu(z)\right]\left[1-2\nu(z)\right]}$ for all theories), whereas, the second one ignores it by using those from 1D model (Eq. (3.2) for quasi-3D theories and Eq. (3.3) for the others).

Table 3. 1: Dimensionless deflections, fundamental frequencies and critical buckling loads of Al_2O_3/Al beams (a/h=5).

Behaviour	Theory	p					
		0	0.5	1	2	5	10
Deflection	Quasi-3D TBT - Navier [5]	3.1397	-	6.1338	7.8606	9.6037	10.7578
($\nu_c=\nu_m=0.3$)	Quasi-3D TBT - FEM [5]	3.1397	-	6.1334	7.8598	9.6030	10.7572
	Quasi-3D TBT	3.1397	4.7631	6.1338	7.8606	9.6037	10.7578
	Quasi-3D SBT	3.1342	4.7559	6.1237	7.8457	9.5982	10.7513
Vibration	Quasi-3D TBT [4]	5.1618	4.4240	4.0079	3.6442	3.4133	3.2903
($\nu_c=\nu_m=0.3$)	Quasi-3D TBT	5.1616	4.4312	4.0238	3.6689	3.4364	3.3039
	Quasi-3D SBT	5.1665	4.8238	4.4347	4.0271	3.6723	3.4374
Buckling load	Quasi-3D TBT [4]	49.5901	32.5867	25.2116	19.6124	16.0842	14.4116
($\nu_c=\nu_m=0.23$)	Quasi-3D TBT	49.6154	32.6041	25.2248	19.6219	16.0910	14.4177
	Quasi-3D SBT	49.6378	32.6097	25.2306	19.6284	16.0833	14.4172

Table 3. 2: Dimensionless deflections of SiC/Al microbeams under uniform load (a/h=10).

h/l	Beam theory	With Poisson effect				Without Poisson effect			
		p = 0.3	1	3	10	p = 0.3	1	3	10
1	CBT	0.0566	0.0860	0.1263	0.1699	0.0578	0.0888	0.1320	0.1791
	CBT [100]	0.0565	0.0859	0.1262	0.1698	-	-	-	-
	FOBT	0.0592	0.0902	0.1331	0.1798	0.0604	0.0928	0.1384	0.1884
	FOBT [100]	0.0592	0.0902	0.1330	0.1797	-	-	-	-
	TBT	0.0571	0.0868	0.1273	0.1715	0.0584	0.0895	0.1330	0.1806
	TBT [100]	0.0571	0.0867	0.1273	0.1715	-	-	-	-
	SBT	0.0571	0.0868	0.1274	0.1716	0.0584	0.0895	0.1330	0.1807
	SBT [100]	0.0571	0.0867	0.1273	0.1716	-	-	-	-
	Quasi-3D TBT	0.0579	0.0882	0.1304	0.1776	0.0584	0.0894	0.1328	0.1807
	Quasi-3D SBT	0.0579	0.0884	0.1309	0.1787	0.0584	0.0894	0.1328	0.1809
2	CBT	0.1496	0.2228	0.3069	0.3939	0.1587	0.2426	0.3431	0.4473
	CBT [100]	0.1496	0.2227	0.3068	0.3939	-	-	-	-
	FOBT	0.1538	0.2293	0.3176	0.4095	0.1627	0.2488	0.3530	0.4618
	FOBT [100]	0.1537	0.2292	0.3175	0.4095	-	-	-	-
	TBT	0.1519	0.2261	0.3121	0.4017	0.1608	0.2457	0.3478	0.4543
	TBT [100]	0.1518	0.2261	0.3121	0.4017				
	SBT	0.1519	0.2261	0.3123	0.4020	0.1608	0.2457	0.3479	0.4545
	SBT [100]	0.1518	0.2261	0.3123	0.4019	-	-	-	-
	Quasi-3D TBT	0.1565	0.2347	0.3291	0.4333	0.1603	0.2437	0.3447	0.4530
	Quasi-3D SBT	0.1569	0.2357	0.3318	0.4387	0.1603	0.2437	0.3450	0.4535
4	CBT	0.2543	0.3698	0.4777	0.5876	0.2817	0.4280	0.5715	0.7150
	CBT [100]	0.2542	0.3698	0.4776	0.5876	-	-	-	-
	FOBT	0.2604	0.3794	0.4929	0.6093	0.2877	0.4372	0.5861	0.7359
	FOBT [100]	0.2603	0.3794	0.4928	0.6093	-	-	-	-
	TBT	0.2594	0.3781	0.4914	0.6067	0.2866	0.4358	0.5844	0.7330
	TBT [100]	0.2593	0.3780	0.4913	0.6067	-	-	-	-
	SBT	0.2594	0.3781	0.4916	0.6069	0.2866	0.4359	0.5846	0.7332
	SBT [100]	0.2593	0.3781	0.4916	0.6069	-	-	-	-
	Quasi-3D TBT	0.2726	0.4014	0.5322	0.6777	0.2845	0.4287	0.5745	0.7275
	Quasi-3D SBT	0.2737	0.4042	0.5390	0.6904	0.2845	0.4287	0.5751	0.7284
8	CBT	0.3082	0.4429	0.5548	0.6700	0.3494	0.5291	0.6856	0.8408
	CBT [100]	0.3081	0.4429	0.5548	0.6700	-	-	-	-
	FOBT	0.3155	0.4543	0.5724	0.6946	0.3566	0.5402	0.7029	0.8651
	FOBT [100]	0.3154	0.4542	0.5723	0.6946	-	-	-	-
	TBT	0.3152	0.4545	0.5744	0.6962	0.3563	0.5404	0.7046	0.8664
	TBT [100]	0.3150	0.4545	0.5743	0.6962	-	-	-	-
	SBT	0.3152	0.4546	0.5746	0.6963	0.3563	0.5404	0.7048	0.8665
	SBT [100]	0.3150	0.4545	0.5745	0.6963	-	-	-	-
	Quasi-3D TBT	0.3346	0.4882	0.6297	0.7894	0.3529	0.5291	0.6897	0.8578
	Quasi-3D SBT	0.3363	0.4923	0.6389	0.8062	0.3528	0.5292	0.6904	0.8587
∞	CBT	0.3316	0.4742	0.5864	0.7028	0.3796	0.5739	0.7341	0.8929
	CBT [100]	0.3315	0.4741	0.5864	0.7028	-	-	-	-
	FOBT	0.3394	0.4863	0.6050	0.7286	0.3875	0.5860	0.7527	0.9187
	FOBT [100]	0.3393	0.4862	0.6049	0.7286	-	-	-	-
	TBT	0.3395	0.4874	0.6088	0.7324	0.3875	0.5871	0.7563	0.9221
	TBT [100]	0.3394	0.4874	0.6087	0.7324	-	-	-	-
	SBT	0.3395	0.4874	0.6089	0.7323	0.3875	0.5871	0.7564	0.9220
	SBT [100]	0.3394	0.4874	0.6089	0.7323	-	-	-	-
	Quasi-3D TBT	0.3619	0.5258	0.6704	0.8350	0.3833	0.5736	0.7389	0.9119
	Quasi-3D SBT	0.3638	0.5305	0.6807	0.8537	0.3833	0.5737	0.7395	0.9129

Table 3. 3: Dimensionless fundamental frequencies of SiC/Al microbeams (a/h=10).

h/l	Theory	With Poisson effect				Without Poisson effect			
		p = 0.3	1	3	10	p = 0.3	1	3	10
1	CBT	12.9001	10.6483	8.9420	7.8015	12.7586	10.4765	8.7436	7.5970
	CBT [100]	12.9004	10.6483	8.9420	7.8011	-	-	-	-
	FOBT	12.6055	10.3983	8.7111	7.5840	12.4821	10.2486	8.5396	7.4084
	FOBT [100]	12.6058	10.3982	8.7110	7.5835	-	-	-	-
	TBT	12.8333	10.6010	8.9049	7.7644	12.6967	10.4344	8.7121	7.5663
	TBT [100]	12.8337	10.6009	8.9048	7.7640	-	-	-	-
	SBT	12.8394	10.6099	8.9109	7.7649	12.6974	10.4340	8.7110	7.5647
	SBT [100]	12.8344	10.6004	8.9034	7.7620	-	-	-	-
	Quasi-3D TBT	12.7422	10.5093	8.7936	7.6236	12.6894	10.4388	8.7161	7.5587
	Quasi-3D SBT	12.7371	10.5001	8.7775	7.6019	12.6906	10.4383	8.7140	7.5559
2	CBT	7.9303	6.6160	5.7362	5.1234	7.6991	6.3380	5.4239	4.8071
	CBT [100]	7.9307	6.6159	5.7362	5.1231	-	-	-	-
	FOBT	7.8229	6.5211	5.6383	5.0240	7.6052	6.2598	5.3470	4.7308
	FOBT [100]	7.8233	6.5211	5.6383	5.0237	-	-	-	-
	TBT	7.8718	6.5671	5.6877	5.0734	7.6486	6.2988	5.3872	4.7702
	TBT [100]	7.8722	6.5670	5.6876	5.0731	-	-	-	-
	SBT	7.8811	6.5838	5.7017	5.0768	7.6489	6.2985	5.3862	4.7690
	SBT [100]	7.8725	6.5666	5.6861	5.0713	-	-	-	-
	Quasi-3D TBT	7.7504	6.4429	5.5363	4.8816	7.6582	6.3231	5.4091	4.7749
	Quasi-3D SBT	7.7418	6.4294	5.5137	4.8513	7.6590	6.3227	5.4072	4.7724
4	CBT	6.0835	5.1348	4.5978	4.1947	5.7793	4.7722	4.2025	3.8022
	CBT [100]	6.0840	5.1348	4.5978	4.1945	-	-	-	-
	FOBT	6.0110	5.0692	4.5257	4.1186	5.7188	4.7214	4.1494	3.7474
	FOBT [100]	6.0115	5.0692	4.5256	4.1184	-	-	-	-
	TBT	6.0231	5.0784	4.5327	4.1278	5.7292	4.7292	4.1556	3.7550
	TBT [100]	6.0236	5.0783	4.5327	4.1276	-	-	-	-
	SBT	6.0354	5.1025	4.5559	4.1349	5.7293	4.7290	4.1548	3.7544
	SBT [100]	6.0237	5.0780	4.5316	4.1267	-	-	-	-
	Quasi-3D TBT	5.8726	4.9262	4.3533	3.9029	5.7486	4.7672	4.1898	3.7676
	Quasi-3D SBT	5.8612	4.9093	4.3262	3.8672	5.7494	4.7669	4.1881	3.7655
8	CBT	5.5262	4.6920	4.2660	3.9284	5.1895	4.2923	3.8368	3.5063
	CBT [100]	5.5267	4.6920	4.2659	3.9282	-	-	-	-
	FOBT	5.4612	4.6328	4.1996	3.8575	5.1361	4.2474	3.7889	3.4562
	FOBT [100]	5.4617	4.6327	4.1995	3.8573	-	-	-	-
	TBT	5.4640	4.6314	4.1922	3.8531	5.1385	4.2468	3.7842	3.4537
	TBT [100]	5.4646	4.6313	4.1922	3.8528	-	-	-	-
	SBT	5.4776	4.6591	4.2201	3.8622	5.1386	4.2466	3.7838	3.4536
	SBT [100]	5.4645	4.6311	4.1915	3.8526	-	-	-	-
	Quasi-3D TBT	5.3001	4.4671	4.0022	3.6163	5.1619	4.2908	3.8238	3.4696
	Quasi-3D SBT	5.2875	4.4487	3.9734	3.5785	5.1627	4.2906	3.8223	3.4678
∞	CBT	5.3275	4.5348	4.1495	3.8355	4.9788	4.1211	3.7078	3.4026
	CBT [100]	5.3280	4.5348	4.1494	3.8353	-	-	-	-
	FOBT	5.2648	4.4776	4.0849	3.7663	4.9276	4.0780	3.6615	3.3540
	FOBT [100]	5.2654	4.4775	4.0848	3.7661	-	-	-	-
	TBT	5.2644	4.4724	4.0720	3.7566	4.9273	4.0744	3.6527	3.3477
	TBT [100]	5.2649	4.4723	4.0719	3.7564	-	-	-	-
	SBT	5.2786	4.5016	4.1019	3.7666	4.9273	4.0743	3.6524	3.3478
	SBT [100]	5.2650	4.4722	4.0715	3.7565	-	-	-	-
	Quasi-3D TBT	5.0964	4.3042	3.8787	3.5160	4.9523	4.1209	3.6944	3.3649
	Quasi-3D SBT	5.0832	4.2852	3.8493	3.4775	4.9531	4.1207	3.6930	3.3633

Table 3. 4: Dimensionless critical buckling loads of Al_2O_3/SUS304 microbeams (a/h=10).

h/l	Theory	With Poisson effect				Without Poisson effect			
		p=0	0.5	1	10	p=0	0.5	1	10
1	CBT	109.2706	88.8923	80.9467	63.6997	102.9259	83.5272	75.8559	59.1987
	CBT [122]	-	-	-	-	102.9258	83.5292	75.8558	59.1987
	FOBT	107.7255	90.5034	82.4063	63.5569	101.6569	82.5099	74.9253	58.4445
	FOBT [122]	-	-	-	-	101.7143	82.5580	74.9674	58.4786
	TBT	108.9131	91.4867	83.3159	64.3237	102.6399	83.2946	75.6501	59.0435
	TBT [122]	-	-	-	-	102.6398	83.2967	75.6500	59.0434
	SBT	108.9158	91.4901	83.3179	64.3218	102.6425	83.2973	75.6516	59.0425
	SBT [122]	-	-	-	-	102.6425	83.2994	75.6516	59.0424
	Quasi-3D TBT	104.4661	87.6181	79.7097	61.0582	102.6622	86.0353	78.2045	59.7993
	Quasi-3D SBT	104.1111	87.3333	79.4222	60.7151	102.6911	86.0600	78.2260	59.8125
2	CBT	45.8232	37.1353	34.0872	27.7156	39.4784	31.7701	28.9964	23.2146
	CBT [122]	-	-	-	-	39.4784	31.7713	28.9963	23.2146
	FOBT	45.3928	37.9704	34.7503	27.8442	39.1884	31.5421	28.7854	23.0333
	FOBT [122]	-	-	-	-	39.2016	31.5537	28.7950	23.0415
	TBT	45.5832	38.1262	34.8962	27.9781	39.3205	31.6455	28.8823	23.1189
	TBT [122]	-	-	-	-	39.3205	31.6467	28.8823	23.1188
	SBT	45.5840	38.1273	34.8968	27.9770	39.3213	31.6463	28.8828	23.1185
	SBT [122]	-	-	-	-	39.3213	31.6475	28.8276	23.1184
	Quasi-3D TBT	41.1488	34.2661	31.2999	24.7285	39.3449	32.6832	29.7946	23.4698
	Quasi-3D SBT	40.7918	33.9789	31.0108	24.3864	39.3719	32.7058	29.8147	23.4835
4	CBT	29.9613	24.1960	22.3724	18.7196	23.6166	18.8309	17.2815	14.2186
	CBT [122]	-	-	-	-	23.6165	18.8318	17.2815	14.2185
	FOBT	29.7025	24.7468	22.7544	18.8547	23.4637	18.7124	17.1709	14.1195
	FOBT [122]	-	-	-	-	23.4706	18.7187	17.1759	14.1239
	TBT	29.7443	24.7818	22.7864	18.8821	23.4897	18.7328	17.1896	14.1356
	TBT [122]	-	-	-	-	23.4896	18.7337	17.1895	14.1355
	SBT	29.7447	24.7822	22.7867	18.8817	23.4900	18.7331	17.1897	14.1355
	SBT [122]	-	-	-	-	23.4900	18.7340	17.1897	14.1354
	Quasi-3D TBT	25.3195	20.9280	19.1974	15.6454	23.5156	19.3452	17.6922	14.3868
	Quasi-3D SBT	24.9619	20.6401	18.9079	15.3040	23.5421	19.3672	17.7119	14.4008
8	CBT	25.9958	20.9612	19.4436	16.4706	19.6511	15.5960	14.3528	11.9696
	CBT [122]	-	-	-	-	19.6510	15.5969	14.3528	11.9695
	FOBT	25.7731	21.4352	19.7502	16.6035	19.5257	15.4994	14.2623	11.8872
	FOBT [122]	-	-	-	-	19.5314	15.5047	14.2664	11.8909
	TBT	25.7833	21.4448	19.7579	16.6058	19.5318	15.5045	14.2662	11.8892
	TBT [122]	-	-	-	-	19.5317	15.5053	14.2661	11.8892
	SBT	25.7836	21.4451	19.7582	16.6059	19.5320	15.5046	14.2663	11.8893
	SBT [122]	-	-	-	-	19.5319	15.5055	14.2662	11.8892
	Quasi-3D TBT	21.3621	17.5935	16.1718	13.3745	19.5583	16.0106	14.6665	12.1160
	Quasi-3D SBT	21.0045	17.3053	15.8822	13.0333	19.5847	16.0325	14.6862	12.1300
∞	CBT	24.6825	19.8898	18.4736	15.7257	18.3293	14.5178	13.3766	11.2199
	CBT [122]	-	-	-	-	18.3292	14.5186	13.3765	11.2198
	FOBT	24.4711	20.3379	18.7548	15.8575	18.2208	14.4348	13.2985	11.1475
	FOBT [122]	-	-	-	-	18.2177	14.4329	13.2961	11.1462
	TBT	24.4712	20.3395	18.7547	15.8516	18.2209	14.4352	13.2979	11.1452
	TBT [122]	-	-	-	-	18.2124	14.4292	13.2916	11.1403
	SBT	24.4715	20.3397	18.7550	15.8518	18.2211	14.4354	13.2980	11.1453
	SBT [122]	-	-	-	-	18.2126	14.4293	13.2917	11.1405
	Quasi-3D TBT	20.0515	16.4891	15.1697	12.6223	18.2476	14.9062	13.6645	11.3638
	Quasi-3D SBT	19.6937	16.2009	14.8801	12.2813	18.2739	14.9281	13.6841	11.3779

It can be seen that the results are in excellent agreement with those from previous papers ([100], [122]) for CBT, FOBT, TBT and SBT with two sets of constitute relations. As expected, the results from TBT, SBT and quasi-3D theories lie between those from CBT and FOBT. Due to decrement of beam's stiffness, the inclusion of Poisson's effect leads to decrease deflections and increase natural frequencies and buckling loads. This effect increases with the increase of power-law index and decrease of material length scale parameter. Besides, due to thickness stretching effect, it is less pronounced for quasi-3D theories than others. For example, with p=10, the relative difference between the deflections of two constitute relations using TBT is 5.28%, 24.45%, 25.90%, whereas, it is 1.75%, 8.66%, 9.21% using quasi-3D TBT for h/l=1,8 and l=0, respectively (Table 3.2). It is worth noting that, the exclusion of Poisson's effect provides better agreement with those from experiments [123]. Therefore, in the following examples, the numerical results are computed without this effect.

3.5.2 Parameter study

In this section, effects of length scale parameter, power-law index and slenderness ratio on bending, vibration and buckling responses of FG microbeams are investigated. Tables 3.5-3.7 present the deflections and stresses of SiC/Al microbeams under uniform loads. Since the results between TBT and SBT as well as between quasi-3D (TBT) and quasi-3D (SBT) theory are nearly similar, all figures are presented for TBT and quasi-3D (TBT) only. The variation of deflection versus material length scale parameter and distribution of stresses through the depth for p=1 and p=10 are plotted in Figs. 3.1-3.4.

It is clear that the results by classical model (l=0) are always higher than those obtained by size-dependent one ($l\neq0$). For the same power-law index, Mori-Tanaka scheme always provides higher results than the rule of mixture does. Due to very strong size effect (h/l = 1), very small deflections and stresses are obtained. As the size effect decreases, deflections increase with the increase power-law index and finally approach those from classical model as h/l = 20 (Fig. 3.1). Although TBT and quasi-3D (TBT) give the same axial stress, there is slightly difference in shear stress (Fig. 3.3). It is due to the fact that quasi-3D theory includes the thickness stretching effect. This effect is highlighted in Fig. 3.4. Significant difference in these two material models can be seen in both numerical results and even in stress distribution.

Table 3. 5: Dimensionless deflections of SiC/Al microbeams under uniform load (a/h=5).

h/l	Theory	Mori-Tanaka Scheme				Rule of mixture			
		p=0	0.5	1	10	p=0	0.5	1	10
1	CBT	0.0348	0.0685	0.0888	0.1791	0.0348	0.0504	0.0638	0.1512
	FOBT	0.0412	0.0806	0.1047	0.2156	0.0412	0.0594	0.0748	0.1816
	TBT	0.0363	0.0710	0.0917	0.1849	0.0363	0.0525	0.0662	0.1555
	SBT	0.0362	0.0710	0.0917	0.1852	0.0362	0.0525	0.0661	0.1557
	Quasi-3D TBT	0.0364	0.0712	0.0920	0.1865	0.0364	0.0527	0.0663	0.1565
	Quasi-3D SBT	0.0364	0.0713	0.0920	0.1870	0.0364	0.0527	0.0663	0.1569
2	CBT	0.0935	0.1886	0.2426	0.4473	0.0935	0.1390	0.1781	0.3804
	FOBT	0.1034	0.2070	0.2669	0.5048	0.1034	0.1525	0.1948	0.4283
	TBT	0.0988	0.1982	0.2547	0.4748	0.0988	0.1464	0.1870	0.4026
	SBT	0.0988	0.1981	0.2548	0.4757	0.0988	0.1463	0.1869	0.4035
	Quasi-3D TBT	0.0990	0.1975	0.2534	0.4759	0.0990	0.1461	0.1861	0.4021
	Quasi-3D SBT	0.0989	0.1975	0.2535	0.4771	0.0989	0.1461	0.1861	0.4034
4	CBT	0.1616	0.3356	0.4280	0.7150	0.1616	0.2475	0.3229	0.6127
	FOBT	0.1764	0.3636	0.4647	0.7983	0.1764	0.2681	0.3485	0.6823
	TBT	0.1738	0.3588	0.4590	0.7864	0.1738	0.2644	0.3439	0.6753
	SBT	0.1737	0.3588	0.4591	0.7873	0.1737	0.2643	0.3439	0.6766
	Quasi-3D TBT	0.1734	0.3546	0.4516	0.7809	0.1734	0.2623	0.3391	0.6670
	Quasi-3D SBT	0.1734	0.3546	0.4518	0.7822	0.1734	0.2622	0.3391	0.6689
8	CBT	0.1976	0.4169	0.5291	0.8408	0.1976	0.3076	0.4053	0.7231
	FOBT	0.2154	0.4511	0.5737	0.9380	0.2154	0.3328	0.4367	0.8045
	TBT	0.2145	0.4501	0.5743	0.9428	0.2145	0.3312	0.4353	0.8161
	SBT	0.2144	0.4501	0.5744	0.9430	0.2144	0.3312	0.4352	0.8170
	Quasi-3D TBT	0.2136	0.4426	0.5615	0.9313	0.2136	0.3274	0.4269	0.8010
	Quasi-3D SBT	0.2136	0.4426	0.5617	0.9322	0.2136	0.3274	0.4269	0.8026
∞	CBT	0.2133	0.4532	0.5739	0.8929	0.2133	0.3345	0.4427	0.7690
	FOBT	0.2325	0.4904	0.6223	0.9961	0.2325	0.3619	0.4770	0.8556
	TBT	0.2325	0.4915	0.6264	1.0097	0.2325	0.3615	0.4772	0.8773
	SBT	0.2325	0.4915	0.6265	1.0094	0.2325	0.3614	0.4772	0.8778
	Quasi-3D TBT	0.2314	0.4822	0.6108	0.9950	0.2314	0.3568	0.4669	0.8585
	Quasi-3D SBT	0.2313	0.4823	0.6109	0.9956	0.2313	0.3567	0.4670	0.8599

Table 3. 6: Dimensionless axial stress σ_x (a/2, h/2) of SiC/Al microbeams under uniform load (a/h=5).

h/l	Theory	Mori-Tanaka Scheme				Rule of mixture			
		p=0	0.5	1	10	p=0	0.5	1	10
1	CBT	0.6119	0.9204	1.1128	2.6143	0.6119	0.7493	0.8520	1.9549
	FOBT	0.5436	0.8187	0.9895	2.3130	0.5436	0.6665	0.7584	1.7304
	TBT	0.5987	0.9039	1.0941	2.5638	0.5987	0.7345	0.8367	1.9205
	SBT	0.5974	0.9014	1.0906	2.5539	0.5974	0.7328	0.8345	1.9127
	Quasi-3D TBT	0.6001	0.9082	1.1014	2.5431	0.6001	0.7367	0.8422	1.9205
	Quasi-3D SBT	0.6031	0.9145	1.1092	2.5593	0.6031	0.7417	0.8481	1.9326
2	CBT	1.6433	2.5336	3.0407	6.5295	1.6433	2.0639	2.3801	4.9192
	FOBT	1.5865	2.4475	2.9369	6.2943	1.5865	1.9938	2.3001	4.7428
	TBT	1.6245	2.5114	3.0142	6.4505	1.6245	2.0448	2.3601	4.8630
	SBT	1.6255	2.5130	3.0158	6.4506	1.6255	2.0463	2.3618	4.8625
	Quasi-3D TBT	1.6284	2.5137	3.0187	6.3948	1.6284	2.0447	2.3634	4.8485
	Quasi-3D SBT	1.6365	2.5314	3.0408	6.4414	1.6284	2.0447	2.3634	4.8485
4	CBT	2.8398	4.5094	5.3636	10.4371	2.8398	3.6764	4.3150	7.9226
	FOBT	2.8099	4.4623	5.3075	10.3243	2.8099	3.6381	4.2702	7.8372
	TBT	2.8450	4.5277	5.3876	10.4667	2.8450	3.6891	4.3319	7.9555
	SBT	2.8470	4.5315	5.3925	10.4753	2.8470	3.6919	4.3354	7.9630
	Quasi-3D TBT	2.8479	4.5034	5.3519	10.3383	2.8479	3.6718	4.3053	7.8851
	Quasi-3D SBT	2.8620	4.5354	5.3920	10.4199	2.8620	3.6970	4.3367	7.9491
8	CBT	3.4718	5.6014	6.6299	12.2733	3.4718	4.5689	5.4156	9.3497
	FOBT	3.4618	5.5853	6.6108	12.2376	3.4618	4.5557	5.4000	9.3225
	TBT	3.5037	5.6662	6.7142	12.4263	3.5037	4.6164	5.4752	9.4918
	SBT	3.5064	5.6714	6.7211	12.4384	3.5064	4.6202	5.4800	9.5034
	Quasi-3D TBT	3.5036	5.6138	6.6361	12.2402	3.5036	4.5821	5.4167	9.3708
	Quasi-3D SBT	3.5208	5.6540	6.6860	12.3379	3.5208	4.6135	5.4565	9.4487
∞	CBT	3.7481	6.0899	7.1922	13.0327	3.7481	4.9683	5.9153	9.9429
	FOBT	3.7480	6.0898	7.1921	13.0325	3.7480	4.9682	5.9151	9.9427
	TBT	3.7947	6.1811	7.3113	13.2534	3.7947	5.0354	5.9994	10.1470
	SBT	3.7868	6.1651	7.2887	13.1975	3.7868	5.0245	5.9852	10.0953
	Quasi-3D TBT	3.7926	6.1129	7.2093	13.0376	3.7926	4.9916	5.9227	9.9991
	Quasi-3D SBT	3.8112	6.1567	7.2637	13.1415	3.8112	5.0258	5.9665	10.0823

Table 3. 7: Dimensionless shear stress σ_{xz} (0,0) of SiC/Al microbeams under uniform load (a/h=5).

h/l	Theory	Mori-Tanaka Scheme				Rule of mixture			
		p=0	0.5	1	10	p=0	0.5	1	10
1	FOBT	0.3181	0.2948	0.2612	0.2583	0.3181	0.3296	0.3104	0.2173
	TBT	0.1019	0.0896	0.0727	0.0656	0.1019	0.1091	0.0977	0.0506
	SBT	0.1049	0.0929	0.0766	0.0719	0.1049	0.1114	0.1007	0.0559
	Quasi-3D TBT	0.1064	0.0959	0.0798	0.0773	0.1064	0.1146	0.1036	0.0602
	Quasi-3D SBT	0.1095	0.0995	0.0840	0.0840	0.1095	0.1173	0.1069	0.0660
2	FOBT	0.4002	0.3683	0.3271	0.3303	0.4002	0.4118	0.3862	0.2774
	TBT	0.2868	0.2600	0.2258	0.2225	0.2868	0.2972	0.2744	0.1842
	SBT	0.2955	0.2693	0.2365	0.2386	0.2955	0.3047	0.2829	0.1996
	Quasi-3D TBT	0.2926	0.2698	0.2370	0.2393	0.2926	0.3057	0.2840	0.1990
	Quasi-3D SBT	0.3014	0.2793	0.2479	0.2555	0.2926	0.3057	0.2840	0.1990
4	FOBT	0.5020	0.4641	0.4116	0.4085	0.5020	0.5190	0.4878	0.3436
	TBT	0.5242	0.4922	0.4500	0.4584	0.5242	0.5361	0.5098	0.4066
	SBT	0.5402	0.5088	0.4681	0.4808	0.5402	0.5512	0.5256	0.4304
	Quasi-3D TBT	0.5240	0.4959	0.4552	0.4664	0.5240	0.5383	0.5136	0.4143
	Quasi-3D SBT	0.5398	0.5123	0.4731	0.4881	0.5398	0.5534	0.5293	0.4377
8	FOBT	0.5625	0.5231	0.4631	0.4508	0.5625	0.5850	0.5519	0.3798
	TBT	0.6643	0.6357	0.5932	0.6060	0.6643	0.6790	0.6553	0.5562
	SBT	0.6845	0.6564	0.6151	0.6286	0.6845	0.6988	0.6755	0.5815
	Quasi-3D TBT	0.6582	0.6317	0.5906	0.6045	0.6582	0.6737	0.6513	0.5553
	Quasi-3D SBT	0.6779	0.6520	0.6120	0.6262	0.6779	0.6931	0.6710	0.5798
∞	FOBT	0.5971	0.5572	0.4927	0.4749	0.5971	0.6232	0.5891	0.4003
	TBT	0.7336	0.7079	0.6661	0.6797	0.7336	0.7503	0.7289	0.6337
	SBT	0.7553	0.7303	0.6893	0.7013	0.7553	0.7720	0.7508	0.6585
	Quasi-3D TBT	0.7235	0.6988	0.6584	0.6725	0.7235	0.7398	0.7194	0.6276
	Quasi-3D SBT	0.7446	0.7206	0.6809	0.6932	0.7446	0.7608	0.7407	0.6515

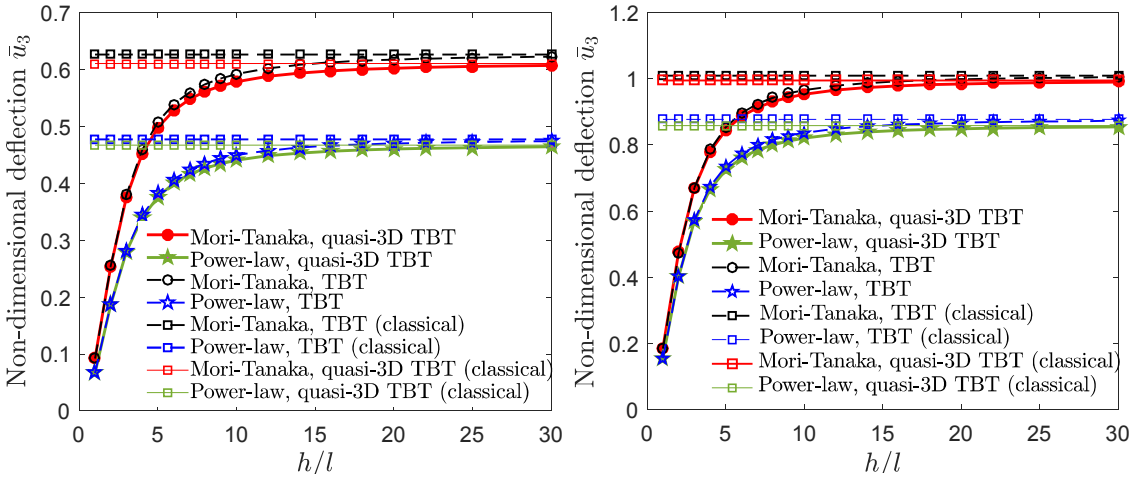

a. p=1 *b. p=10*

Fig. 3. 1: Dimensionless maximum deflections of SiC/Al microbeams under uniform loads using TBT and quasi-3D TBT.

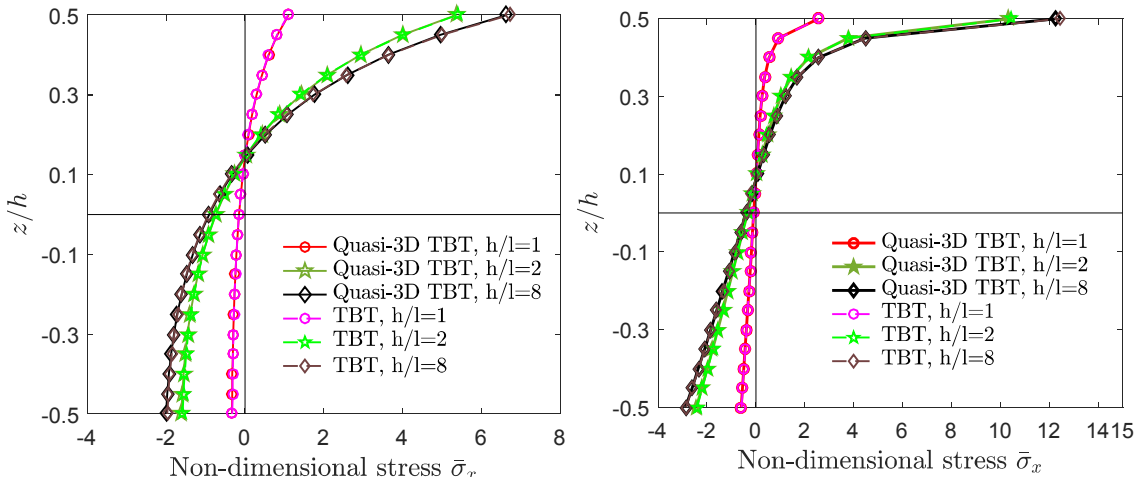

a. p=1 *b. p=10*

Fig. 3. 2: Variation of σ_x (a/2, z) through the depth using TBT and quasi-3D TBT (Mori–Tanaka scheme).

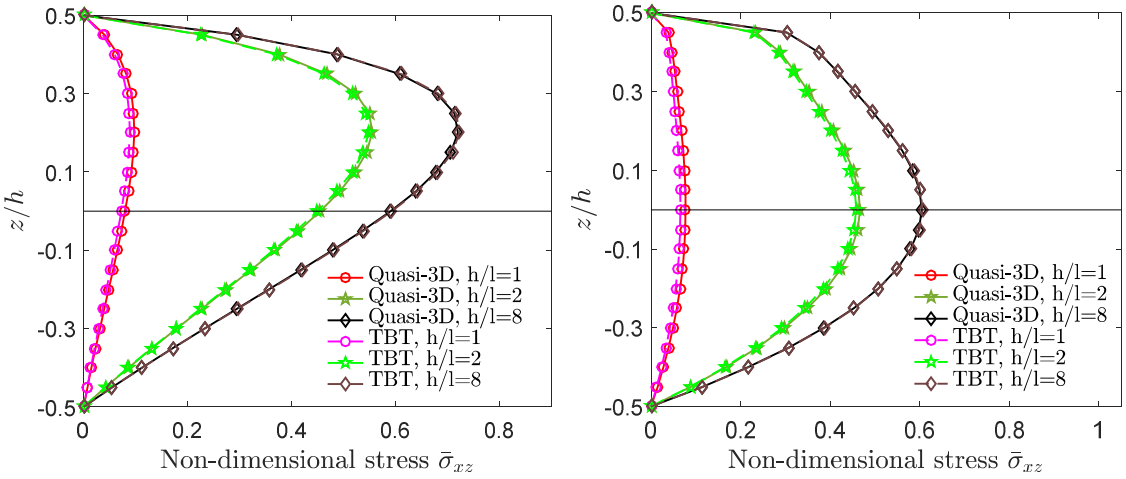

a. p=1 *b. p=10*

Fig. 3. 3: Variation of σ_{xz} (0, z) through the depth using TBT and quasi-3D TBT (Mori–Tanaka scheme).

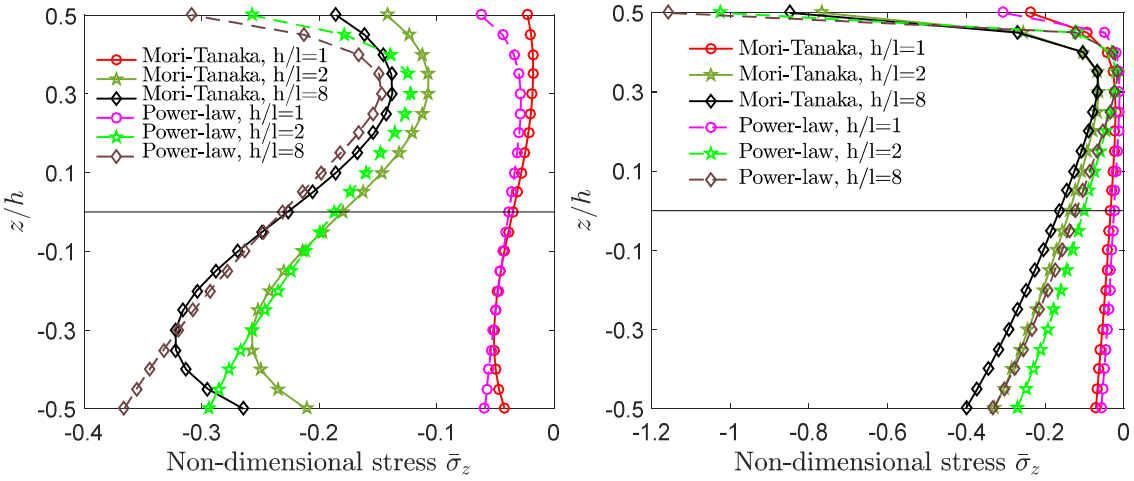

a. p=1 *b. p=10*

Fig. 3. 4: Variation of σ_z (a/2, z) through the depth using quasi-3D TBT.

Table 3. 8: Dimensionless fundamental frequencies of SiC/Al microbeams (a/h=5).

h/l	Theory	Mori-Tanaka Scheme				Rule of mixture			
		p=0	0.5	1	10	p=0	0.5	1	10
1	CBT	16.0020	11.6321	10.3181	7.4958	16.0020	13.5770	12.1927	8.1401
	FOBT	14.7917	10.7926	9.5724	6.8775	14.7917	12.5885	11.3293	7.4837
	TBT	15.7140	11.4489	10.1757	7.3899	15.7140	13.3318	11.9948	8.0425
	SBT	15.7174	11.4501	10.1748	7.3849	15.7174	13.3364	11.9971	8.0375
	Quasi-3D TBT	15.6249	11.3964	10.1345	7.3354	15.6249	13.2627	11.9444	7.9967
	Quasi-3D SBT	15.6304	11.3984	10.1336	7.3285	15.6304	13.2692	11.9477	7.9887
2	CBT	9.7649	7.0135	6.2452	4.7439	9.7649	8.1817	7.2974	5.1338
	FOBT	9.3153	6.7150	5.9757	4.4815	9.3153	7.8316	6.9992	4.8579
	TBT	9.5175	6.8550	6.1087	4.6144	9.5175	7.9867	7.1369	5.0026
	SBT	9.5191	6.8554	6.1078	4.6104	9.5191	7.9888	7.1380	4.9975
	Quasi-3D TBT	9.4917	6.8550	6.1160	4.5998	9.4917	7.9776	7.1420	4.9979
	Quasi-3D SBT	9.4950	6.8561	6.1154	4.5952	9.4950	7.9809	7.1435	4.9913
4	CBT	7.4281	5.2575	4.7027	3.7523	7.4281	6.1304	5.4202	4.0457
	FOBT	7.1237	5.0613	4.5236	3.5599	7.1237	5.9008	5.2281	3.8445
	TBT	7.1753	5.0937	4.5509	3.5864	7.1753	5.9407	5.2614	3.8645
	SBT	7.1761	5.0938	4.5503	3.5846	7.1761	5.9416	5.2619	3.8610
	Quasi-3D TBT	7.1713	5.1170	4.5826	3.5927	7.1713	5.9547	5.2913	3.8833
	Quasi-3D SBT	7.1738	5.1179	4.5823	3.5902	7.1738	5.9568	5.2922	3.8786
8	CBT	6.7181	4.7173	4.2300	3.4603	6.7181	5.4993	4.8382	3.7243
	FOBT	6.4448	4.5428	4.0701	3.2832	6.4448	5.2952	4.6687	3.5393
	TBT	6.4583	4.5477	4.0683	3.2755	6.4583	5.3073	4.6764	3.5157
	SBT	6.4588	4.5478	4.0680	3.2752	6.4588	5.3078	4.6767	3.5139
	Quasi-3D TBT	6.4615	4.5801	4.1098	3.2901	6.4615	5.3296	4.7159	3.5444
	Quasi-3D SBT	6.4638	4.5808	4.1097	3.2890	6.4638	5.3314	4.7166	3.5413
∞	CBT	6.4657	4.5242	4.0613	3.3580	6.4657	5.2736	4.6294	3.6115
	FOBT	6.2021	4.3564	3.9073	3.1857	6.2021	5.0775	4.4667	3.4317
	TBT	6.2025	4.3518	3.8952	3.1651	6.2025	5.0801	4.4657	3.3909
	SBT	6.2029	4.3518	3.8949	3.1655	6.2029	5.0804	4.4659	3.3900
	Quasi-3D TBT	6.2085	4.3877	3.9406	3.1830	6.2085	5.1057	4.5091	3.4237
	Quasi-3D SBT	6.2107	4.3884	3.9406	3.1825	6.2107	5.1073	4.5097	3.4200

Table 3. 9: Dimensionless fundamental frequencies of SiC/Al microbeams (a/h=10).

h/l	Theory	Mori-Tanaka Scheme				Rule of mixture			
		p=0	0.5	1	10	p=0	0.5	1	10
1	CBT	16.1966	11.7981	10.4765	7.5970	16.1966	13.7529	12.3671	8.2646
	FOBT	15.8337	11.5436	10.2486	7.4084	15.8337	13.4558	12.1057	8.0624
	TBT	16.1144	11.7447	10.4344	7.5663	16.1144	13.6824	12.3095	8.2357
	SBT	16.1152	11.7449	10.4340	7.5647	16.1152	13.6837	12.3100	8.2341
	Quasi-3D TBT	16.0945	11.7428	10.4388	7.5587	16.0945	13.6728	12.3100	8.2363
	Quasi-3D SBT	16.0963	11.7432	10.4383	7.5559	16.0963	13.6747	12.3107	8.2330
2	CBT	9.8837	7.1113	6.3381	4.8071	9.8837	8.2867	7.3994	5.2101
	FOBT	9.7550	7.0251	6.2598	4.7308	9.7550	8.1863	7.3134	5.1293
	TBT	9.8140	7.0661	6.2988	4.7702	9.8140	8.2316	7.3536	5.1723
	SBT	9.8144	7.0662	6.2985	4.7690	9.8144	8.2321	7.3539	5.1707
	Quasi-3D TBT	9.8072	7.0825	6.3231	4.7749	9.8072	8.2393	7.3747	5.1889
	Quasi-3D SBT	9.8087	7.0829	6.3227	4.7724	9.8087	8.2406	7.3751	5.1855
4	CBT	7.5185	5.3304	4.7722	3.8022	7.5185	6.2089	5.4955	4.1055
	FOBT	7.4332	5.2751	4.7214	3.7474	7.4332	6.1445	5.4415	4.0479
	TBT	7.4479	5.2843	4.7292	3.7550	7.4479	6.1559	5.4510	4.0534
	SBT	7.4481	5.2844	4.7290	3.7544	7.4481	6.1561	5.4511	4.0523
	Quasi-3D TBT	7.4468	5.3125	4.7672	3.7676	7.4468	6.1733	5.4856	4.0810
	Quasi-3D SBT	7.4484	5.3128	4.7669	3.7655	7.4484	6.1745	5.4857	4.0779
8	CBT	6.7998	4.7827	4.2923	3.5063	6.7998	5.5696	4.9054	3.7792
	FOBT	6.7238	4.7339	4.2474	3.4562	6.7238	5.5129	4.8581	3.7266
	TBT	6.7276	4.7352	4.2468	3.4537	6.7276	5.5163	4.8603	3.7192
	SBT	6.7277	4.7352	4.2466	3.4536	6.7277	5.5164	4.8604	3.7187
	Quasi-3D TBT	6.7285	4.7684	4.2908	3.4696	6.7285	5.5376	4.9007	3.7516
	Quasi-3D SBT	6.7301	4.7687	4.2906	3.4678	6.7301	5.5387	4.9008	3.7488
∞	CBT	6.5444	4.5869	4.1211	3.4026	6.5444	5.3410	4.6937	3.6647
	FOBT	6.4713	4.5401	4.0780	3.3540	6.4713	5.2867	4.6484	3.6138
	TBT	6.4713	4.5387	4.0744	3.3477	6.4713	5.2874	4.6481	3.6013
	SBT	6.4714	4.5387	4.0743	3.3478	6.4714	5.2875	4.6482	3.6010
	Quasi-3D TBT	6.4731	4.5740	4.1209	3.3649	6.4731	5.3102	4.6909	3.6356
	Quasi-3D SBT	6.4747	4.5743	4.1207	3.3633	6.4747	5.3113	4.6910	3.6330

Table 3. 10: Dimensionless critical buckling loads of SiC/Al microbeams (a/h=5).

h/l	Theory	Mori-Tanaka Scheme				Rule of mixture			
		p=0	0.5	1	10	p=0	0.5	1	10
1	CBT	368.9461	187.6062	144.7108	71.7514	368.9461	254.7402	201.5379	85.0019
	FOBT	310.5978	160.9292	124.6102	61.7351	310.5978	218.6399	174.4544	73.1689
	TBT	354.1249	180.8209	140.0364	69.4318	354.1249	244.3914	194.0359	82.6019
	SBT	354.2790	180.8531	139.9959	69.3196	354.2790	244.5700	194.1098	82.4758
	Quasi-3D TBT	354.6933	181.4854	140.6387	69.5886	354.6933	245.1900	194.8498	82.8707
	Quasi-3D SBT	354.8704	181.5266	140.6068	69.4809	354.8704	245.3746	194.9271	82.7386
2	CBT	137.3900	68.1560	52.9616	28.7283	137.3900	92.4829	72.1428	33.7797
	FOBT	124.0410	62.4722	48.6502	26.0529	124.0410	84.9125	66.7563	30.7010
	TBT	129.8802	64.7694	50.3920	27.0246	129.8802	87.6942	68.6522	31.8762
	SBT	129.9246	64.7767	50.3737	26.9727	129.9246	87.7416	68.6725	31.8019
	Quasi-3D TBT	130.4657	65.4449	51.0256	27.2470	130.4657	88.4632	69.4552	32.2157
	Quasi-3D SBT	130.5332	65.4602	51.0144	27.1995	130.5332	88.5192	69.4786	32.1388
4	CBT	79.5009	38.2935	30.0243	17.9726	79.5009	51.9186	39.7940	20.9741
	FOBT	72.6931	35.3507	27.7292	16.2486	72.6931	48.0757	37.0774	19.0300
	TBT	73.8107	35.7506	27.9480	16.3030	73.8107	48.5182	37.3062	18.9845
	SBT	73.8277	35.7525	27.9396	16.2849	73.8277	48.5334	37.3131	18.9470
	Quasi-3D TBT	74.4088	36.4348	28.6071	16.5816	74.4088	49.2648	38.1008	19.3890
	Quasi-3D SBT	74.4489	36.4437	28.6041	16.5650	74.4489	49.2907	38.1105	19.3483
8	CBT	65.0287	30.8279	24.2899	15.2836	65.0287	41.7775	31.7068	17.7727
	FOBT	59.5305	28.3968	22.3653	13.7366	59.5305	38.6308	29.4669	16.0395
	TBT	59.7916	28.4947	22.3291	13.5907	59.7916	38.7239	29.4697	15.6980
	SBT	59.8018	28.4953	22.3244	13.5877	59.8018	38.7311	29.4733	15.6806
	Quasi-3D TBT	60.3946	29.1822	22.9987	13.8927	60.3946	39.4618	30.2609	16.1306
	Quasi-3D SBT	60.4278	29.1895	22.9985	13.8894	60.4278	39.4804	30.2671	16.1090
∞	CBT	60.2355	28.3553	22.3907	14.3930	60.2355	38.4188	29.0283	16.7124
	FOBT	55.1416	26.0779	20.5767	12.8990	55.1416	35.4813	26.9291	15.0425
	TBT	55.1483	26.0913	20.4668	12.6871	55.1483	35.4799	26.8743	14.5981
	SBT	55.1562	26.0916	20.4636	12.6904	55.1562	35.4845	26.8767	14.5897
	Quasi-3D TBT	55.7531	26.7802	21.1405	12.9983	55.7531	36.2145	27.6641	15.0419
	Quasi-3D SBT	55.7841	26.7869	21.1415	13.0005	55.7841	36.2309	27.6692	15.0288

Table 3. 11: Dimensionless critical buckling loads of Al_2O_3/SUS304 microbeams (a/h=5).

h/l	Theory	Mori-Tanaka Scheme				Rule of mixture			
		p=0	0.5	1	10	p=0	0.5	1	10
1	CBT	102.9259	83.5272	75.8559	59.1987	102.9259	86.2293	78.3554	59.9323
	FOBT	86.0687	69.9834	63.4828	49.2406	86.0687	72.2650	65.6283	49.8307
	TBT	98.5842	79.9966	72.7288	56.8378	98.5842	82.5560	75.0903	57.5577
	SBT	98.6269	80.0392	72.7542	56.8261	98.6269	82.6046	75.1226	57.5446
	Quasi-3D TBT	98.8844	80.2800	72.9823	56.9828	98.8844	82.8519	75.3618	57.7019
	Quasi-3D SBT	98.9519	80.3415	73.0273	56.9914	98.9519	82.9189	75.4128	57.7094
2	CBT	39.4784	31.7701	28.9964	23.2146	39.4784	32.7631	29.8462	23.5407
	FOBT	35.3465	28.5139	25.9872	20.6480	35.3465	29.4140	26.7761	20.9276
	TBT	37.1259	29.9112	27.2953	21.7917	37.1259	30.8452	28.1034	22.0945
	SBT	37.1384	29.9236	27.3026	21.7872	37.1384	30.8593	28.1128	22.0891
	Quasi-3D TBT	37.4450	30.2020	27.5648	21.9705	37.4450	31.1459	28.3860	22.2751
	Quasi-3D SBT	37.4825	30.2338	27.5913	21.9847	37.4825	31.1792	28.4142	22.2887
4	CBT	23.6166	18.8309	17.2815	14.2186	23.6166	19.3965	17.7189	14.4429
	FOBT	21.3975	17.1068	15.6747	12.7900	21.3975	17.6265	16.0893	12.9847
	TBT	21.7522	17.3858	15.9291	13.0070	21.7522	17.9144	16.3512	13.2026
	SBT	21.7573	17.3905	15.9320	13.0066	21.7573	17.9196	16.3549	13.2017
	Quasi-3D TBT	22.0851	17.6820	16.2104	13.2116	22.0851	18.2184	16.6420	13.4112
	Quasi-3D SBT	22.1151	17.7064	16.2323	13.2282	22.1151	18.2434	16.6645	13.4275
8	CBT	19.6511	15.5960	14.3528	11.9696	19.6511	16.0549	14.6871	12.1684
	FOBT	17.8226	14.1831	13.0317	10.7765	17.8226	14.6054	13.3503	10.9494
	TBT	17.9069	14.2537	13.0859	10.8058	17.9069	14.6810	13.4120	10.9738
	SBT	17.9102	14.2565	13.0878	10.8071	17.9102	14.6841	13.4144	10.9747
	Quasi-3D TBT	18.2452	14.5519	13.3718	11.0206	18.2452	14.9863	13.7060	11.1935
	Quasi-3D SBT	18.2733	14.5745	13.3925	11.0381	18.2733	15.0093	13.7270	11.2109
∞	CBT	18.3377	14.5247	13.3828	11.2247	18.3377	14.9481	13.6829	11.4151
	FOBT	16.6307	13.2083	12.1505	10.1052	16.6307	13.5980	12.4371	10.2709
	TBT	16.6331	13.2162	12.1440	10.0760	16.6331	13.6101	12.4384	10.2348
	SBT	16.6358	13.2183	12.1456	10.0779	16.6358	13.6123	12.4403	10.2364
	Quasi-3D TBT	16.9734	13.5152	12.4316	10.2947	16.9734	13.9158	12.7335	10.4587
	Quasi-3D SBT	17.0009	13.5372	12.4520	10.3125	17.0009	13.9381	12.7542	10.4765

The fundamental natural frequencies and critical buckling loads of SiC/Al and Al_2O_3/SUS304 microbeams are presented in Tables 3.8-3.11. Since classical model cannot capture size effect, its results differ significantly with those from the proposed model. It is interesting to see that for classical model, due to ignoring the thickness stretching effect, the results from FOBT, TBT and SBT are slightly underestimate when comparing with those from quasi-3D theories. However, when size effect is incorporated, this tendency is different and depends on size effect. For example, when this effect is strong (h/l=1), fundamental frequencies from quasi-3D theories are slightly lower than those from TBT and SBT (Tables 3.8 and 3.9). The effect of length scale parameter on the frequencies and buckling loads of micro FG beams is sketched on Figs. 3.5 and 3.6. It can be seen again that when beam's depth is very small at micron scale, this effect is significant, but become negligible as beam's depth increases.

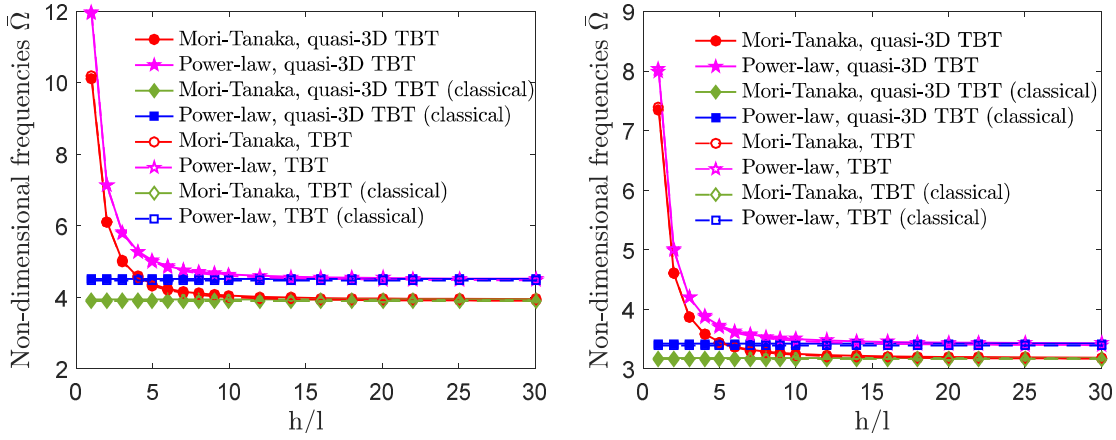

Fig. 3. 5: Dimensionless fundamental frequencies of SiC/Al microbeams using TBT and quasi-TBT.

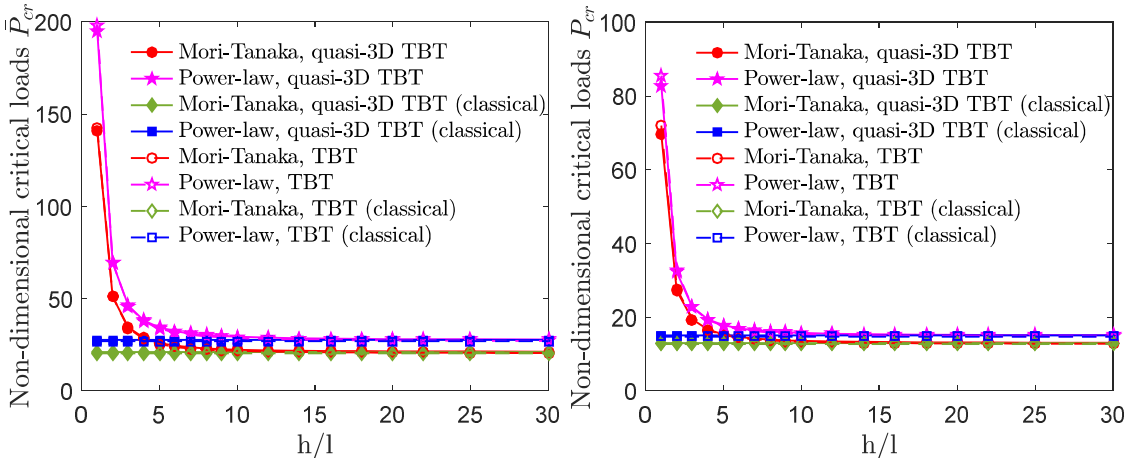

Fig. 3. 6: Dimensionless critical buckling loads of SiC/Al microbeams using TBT and quasi-TBT.

3.6 Concluding remarks

The mechanical behaviours of the simply supported functionally graded beams based on the modified couple stress theory is investigated in this chapter. While the displacement fields of beams are governed by the unified framework which covers various beam theories, the modified couple stress theory efficiently captures the size-dependent effects of the small-scale beams. The numerical examples of the bending, vibration and buckling behaviours of microbeams sufficiently prove the validity and accuracy of the proposed approach. These solutions also reveal that the increase of material length scale ratio leads to the growth in beams' stiffness. Consequently, there is a decrease in displacements, stresses as well as an increase in natural frequency and critical buckling load of microbeams.

CHAPTER 4

FREE VIBRATION OF BIDIRECTIONAL FUNCTIONALLY GRADED MICROBEAMS

4.1 Introduction

Following the introduction of the MCST in Chapter Three for the analysis of FG beams, this section briefly reviews the publications on the bidirectional functionally graded (BDFG) beams, in which the material properties can be tailored in both the longitudinal and thickness directions. Lu et al. [124] analysed the bending and thermal deformations of BDFG beams using a system of state space equations on the combination of stress and displacement variables. Lezgy-Nazargah [125] studied the fully coupled thermos-mechanical static behaviour of BDFG beams using NURBS isogeometric finite element method. Simsek analysed the free and force vibration [126] and buckling [127] of BDFG beams under various BCs. Hao and Wei [128] studied the dynamic characteristics of BDFG beams using a FOBT model. Utilising the NURBS-based isogeometric method, Huynh et al. [129] analysed the free vibration of various types of BDFG beams. Karamanlı [130] studied the bending behaviour of a BDFG beams using different shear deformation theories using the symmetric smoothed particle hydrodynamics method. He then expanded this solution for BDFG sandwich beams using a quasi-3D theory [131]. However, only few anthors investigated the small-scale analysis of BDFG beams. Nejad and Hadi [132, 133] analysed bending and vibration of BDFG nanobeams. Nejad et al. [134] also studied the buckling behaviour of these beams. In their papers, they developed the Eringen's nonlocal theory based on the CBT model with the GDQM. Shafiei and Kazemi [135] studied the buckling behaviour of BDFG porous tapered nano-/micro-scale beams using the CBT. Shafiei et al. [136] also investigated the vibration of imperfect BDFG porous nano-/micro-beams using the FOBT.

This chapter presents a quasi-3D theory which includes both the transverse shear and normal deformation effects for the free vibration of conventional FG and BDFG microbeams. The state space method is applied to analytically solve the governing equations for natural frequencies and vibration mode shapes of microbeams. The HOBT can be also deduced from the present quasi-3D theory as a special case by neglecting the normal stretching effect. The effect of material properties, geometric parameters and BCs on the free vibration behaviour of conventional and BDFG microbeams are discussed.

4.2 BDFG materials

Consider a BDFG microbeam with its dimensions and coordinate shown in Fig. 4.1a. The typical material properties of BDFG microbeams are expressed as:

$$P(x,z)=e^{V_x(x)}P(z) \tag{4. 1}$$

where $P(x,z)$ stands for Young's modulus $E(x,z)$ or mass density $\rho(x,z)$. Poisson's ratio is assumed to be constant [126, 129]. The material properties vary exponentially along the axial direction describing by $V_x(x)=n_x\left(\frac{x}{a}+\frac{1}{2}\right)$. $P(z)$ is the function governing the variation of material properties across the thickness. Three types of FG beams are considered in this chapter including:

Type A: $P(z)=(P_c-P_m)\left(\frac{1}{2}+\frac{z}{h}\right)^{n_z}+P_m$ (4. 2a)

Type BD1 [126]: $P(z)=P_0e^{V_z(z)}$, where $V_z(z)=n_z\left(\frac{z}{h}+\frac{1}{2}\right)$ (4. 2b)

Type BD2 [129]: $P(z)=P_0e^{V_z(z)}$, where $V_z(z)=\begin{cases}2n_z\frac{z}{h} \text{ if } z\in\left[-\frac{h}{2};0\right]\\ -2n_z\frac{z}{h} \text{if } z\in\left[0;\frac{h}{2}\right]\end{cases}$ (4. 2c)

where P_c and P_m are the material properties of ceramic and metal, and n_z is the power-law index in Type A. For Types BD1 and BD2, P_0 is the based material properties, whilst n_x and n_z are the exponential indices in x and z directions, respectively. The variation of Young's modulus is illustrated in Fig. 4.1 for conventional FG microbeams (n_x=0, n_z=2) and BDFG microbeams (n_x=n_z=2).

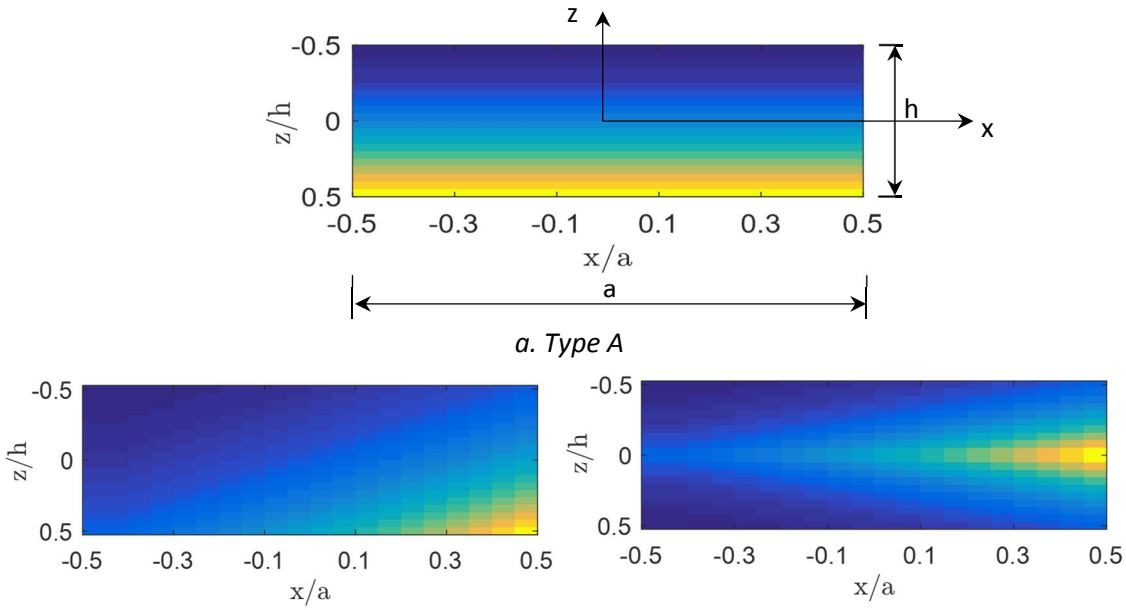

a. Type A

b. Type BD1 *c. Type BD2*

Fig. 4. 1: Co-ordinate and variation of Young's modulus in BDFG beams (n_x=0, n_z=2).

4.3 Kinematics and constitutive relations

The displacement field which includes both transverse shear and normal deformation effects is assumed as follows [137, 138]:

$$u(x,z,t)=U(x,t)-zW_b^{'}(x,t)-f(z)W_s^{'}(x,t) \tag{4. 3a}$$

$$w(x,z,t)=W_b(x,t)+W_s(x,t)+g(z)W_z(x,t) \tag{4. 3b}$$

where U, W_b, W_s and W_z are the mid-plane displacements of the axial, bending, shear and stretching components. $f(z)=\frac{4}{3}\frac{z^3}{h^2}$ and $g(z)=1-\frac{df(z)}{dz}$ are the shape functions of the higher-order and stretching displacements. The non-zero strain components related to the above displacement field are obtained as:

$$\varepsilon_x=U^{'}-zW_b^{''}-f(z)W_s^{''} \tag{4. 4a}$$

$$\varepsilon_z=\frac{\partial g(z)}{\partial z}W_z \tag{4. 4b}$$

$$\gamma_{xz}=g(z)\left(W_s^{'}+W_z^{'}\right) \tag{4. 4c}$$

The rotation vector is expressed as:

$$\theta_y=\frac{1}{2}curl\,\mathbf{u}\big|_{\mathbf{e}_y}=-W_b^{'}-\frac{1}{2}\left[1+\frac{\partial f(z)}{\partial z}\right]W_s^{'}-\frac{1}{2}g(z)W_z^{'} \tag{4. 5a}$$

$$\theta_x=\theta_z=0 \tag{4. 5b}$$

Hence, the non-zero curvature components are given by:

$$\chi_{xy}=\frac{\partial\theta_x}{\partial y}+\frac{\partial\theta_y}{\partial x}=\frac{1}{2}\left\{-W_b^{''}-\frac{1}{2}\left[1+\frac{\partial f(z)}{\partial z}\right]W_s^{''}-\frac{1}{2}g(z)W_z^{''}\right\} \tag{4. 6a}$$

$$\chi_{yz}=\frac{\partial\theta_z}{\partial y}+\frac{\partial\theta_y}{\partial z}=\frac{1}{4}\left[-\frac{\partial^2 f(z)}{\partial z^2}W_s^{'}-\frac{\partial g(z)}{\partial z}W_z^{'}\right] \tag{4. 6b}$$

The linear elastic constitutive relations are expressed for the stress and deviatoric part of couple stress tensors as:

$$\begin{Bmatrix}\sigma_x\\ \sigma_z\\ \sigma_{xz}\end{Bmatrix}=\begin{bmatrix}Q_{11} & Q_{13} & 0\\ & Q_{33} & 0\\ sym. & & Q_{66}\end{bmatrix}\begin{Bmatrix}\varepsilon_x\\ \varepsilon_z\\ \gamma_{xz}\end{Bmatrix} \tag{4. 7a}$$

$$\begin{Bmatrix}m_{yz}\\ m_{xy}\end{Bmatrix}=2l^2\mu\begin{Bmatrix}\chi_{yz}\\ \chi_{xy}\end{Bmatrix} \tag{4. 7b}$$

where $Q_{11}=Q_{33}=\frac{E_0e^{V_x(x)+V_z(z)}}{1-\nu^2}, Q_{13}=\frac{\nu E_0e^{V_x(x)+V_z(z)}}{1-\nu^2}, Q_{66}=\frac{E_0e^{V_x(x)+V_z(z)}}{2(1+\nu)}$, l is the material length scale parameter [36]. The value of l can be determined from experiments, e.g. $l=17.6\mu m$ for homogeneous epoxy beams [7].

By substituting Eqs. (4.4) and (4.6) into Eq. (4.7), the stress and deviatoric part of couple stress tensors are rewritten in terms of displacement components as:

$$\begin{Bmatrix}\sigma_x\\ \sigma_z\\ \sigma_{xz}\end{Bmatrix}=\begin{bmatrix}Q_{11} & Q_{13} & 0\\ & Q_{33} & 0\\ sym. & & Q_{66}\end{bmatrix}\begin{Bmatrix}U^{'}-zW_b^{''}-f(z)W_s^{''}\\ \frac{\partial g(z)}{\partial z}W_z\\ g(z)\left(W_s^{'}+W_z^{'}\right)\end{Bmatrix} \tag{4. 8a}$$

$$\begin{Bmatrix}m_{yz}\\ m_{xy}\end{Bmatrix}=2l^2Q_{66}\begin{Bmatrix}-\frac{1}{4}\frac{\partial^2 f(z)}{\partial z^2}\left(W_s^{'}+W_z^{'}\right)\\ \frac{1}{2}\left\{-W_b^{''}-\frac{1}{2}\left[1+\frac{\partial f(z)}{\partial z}\right]W_s^{''}-\frac{1}{2}g(z)W_z^{''}\right\}\end{Bmatrix} \tag{4. 8b}$$

4.4 Governing equations

Hamilton's principle is employed to obtain the equations of motion:

$$\int_{t_1}^{t_2}\left(\delta U-\delta K\right)dt=0 \tag{4. 9}$$

where δU and δK denote the variation of strain and kinetic energy of the microbeam.

The variation of the strain energy is written in terms of displacements as:

$$\delta U = \int_{-a/2}^{a/2}\int_{-h/2}^{h/2} \left(\sigma_{ij}\delta\varepsilon_{ij} + m_{ij}\delta\chi_{ij}\right)dzdx$$

$$= \int_{-a/2}^{a/2}\int_{-h/2}^{h/2} \left[\sigma_{xx}\delta\varepsilon_{xx} + \sigma_{zz}\delta\varepsilon_{zz} + \sigma_{xz}\delta\gamma_{xz} + 2m_{xy}\delta\chi_{xy} + 2m_{yz}\delta\chi_{yz}\right]dzdx$$

$$= \int_{-a/2}^{a/2} e^{V_x(x)}\left[N_x\delta U' - M_x\delta W_b'' - P_x\delta W_s'' + O_z\delta W_z + \left(Q_{xz} - \frac{1}{2}X_{yz}\right)\left(\delta W_s' + \delta W_z'\right)\right.$$

$$\left. - R_{xy}\delta W_b'' - \left(R_{xy} + S_{xy}\right)\delta W_s'' - T_{xy}\delta W_z''\right]dx \qquad (4.\ 10)$$

where the stress resultants are expressed as:

$$\left(N_x, M_x, P_x\right) = \int_{-h/2}^{h/2} \left(1, z, f\right)\frac{E(z)}{1-\nu^2}\left[U' - zW_b'' - f(z)W_s'' + W_z\right]dz \qquad (4.\ 11a)$$

$$O_z = \int_{-h/2}^{h/2} \frac{\partial g}{\partial z}\frac{E(z)}{1-\nu^2}W_z dz \qquad (4.\ 11b)$$

$$Q_{xz} = \int_{-h/2}^{h/2} g\frac{E(z)}{2(1+\nu)}\left(W_s' + W_z'\right)dz \qquad (4.\ 11c)$$

$$\left(R_{xy}, S_{xy}, T_{xy}\right) = \int_{-h/2}^{h/2} \left(1, \frac{\partial f}{\partial z}, g\right)l^2\frac{E(z)}{1+\nu}\left[-W_b'' - \frac{1}{2}\left(1 + \frac{\partial f}{\partial z}\right)W_s'' - \frac{1}{2}gW_z''\right]dz \qquad (4.\ 11d)$$

$$X_{yz} = \frac{1}{2}\int_{-h/2}^{h/2} \frac{\partial^2 f}{\partial z^2}l^2\frac{E(z)}{1+\nu}\left(-W_s' + W_z'\right)dz \qquad (4.\ 11e)$$

The stress resultants can be rewritten as:

$$N_x = \int_A \sigma_x dA = AU' - BW_b'' - B_sW_s'' + XW_z \qquad (4.\ 12a)$$

$$M_x = \int_A z\sigma_x dA = BU' - DW_b'' - D_sW_s'' + YW_z \qquad (4.\ 12b)$$

$$P_x = \int_A f\sigma_x dA = B_sU' - D_sW_b'' - HW_s'' + Y_sW_z \qquad (4.\ 12c)$$

$$O_z = \int_A \sigma_z\frac{\partial g}{\partial z}dA = XU' - YW_b'' - Y_sW_s'' + ZW_z \qquad (4.\ 12d)$$

$$Q_{xz} = \int_A g\sigma_{xz}dA = A_s\left(W_s' + W_z'\right) \qquad (4.\ 12e)$$

$$R_{xy} = \int_A m_{xy} dA = -A_m W_b'' - \frac{1}{2}\left(A_m + B_m\right) W_s'' - \frac{1}{2} E_m W_z'' \tag{4. 12f}$$

$$S_{xy} = \int_A \frac{\partial f}{\partial z} m_{xy} dA = -B_m W_b'' - \frac{1}{2}\left(B_m + C_m\right) W_s'' - \frac{1}{2} D_m W_z'' \tag{4. 12g}$$

$$T_{xy} = \int_A g m_{xy} dA = -E_m W_b'' - \frac{1}{2}\left(E_m + D_m\right) W_s'' - \frac{1}{2} F_m W_z'' \tag{4. 12h}$$

$$X_{yz} = \int_A \frac{\partial^2 f}{\partial z^2} m_{yz} dA = \frac{1}{2} H_m \left(-W_s' + W_z'\right) \tag{4. 12i}$$

where

$$\left(A, B, B_s, D, D_s, H, Z\right) = \int_{-h/2}^{h/2} \left[1, z, f, z^2, fz, f^2, \left(\frac{dg}{dz}\right)^2\right] \frac{E(z)}{1-\nu^2} dz \tag{4. 13a}$$

$$A_s = \int_{-h/2}^{h/2} g^2 \frac{E(z)}{2(1+\nu)} dz \tag{4. 13b}$$

$$\left(X, Y, Y_s\right) = \int_{-h/2}^{h/2} \left(1, z, f\right) \frac{\partial g}{\partial z} \frac{E(z)}{2(1+\nu)} dz \tag{4. 13c}$$

$$\left[A_m, B_m, C_m, D_m, E_m, F_m, H_m\right] = \int_{-h/2}^{h/2} \frac{E(z)}{1+\nu} l^2 \left[1, \frac{\partial f}{\partial z}, \left(\frac{\partial f}{\partial z}\right)^2, \frac{\partial f}{\partial z} g, g, g^2, \left(\frac{\partial g}{\partial z}\right)^2\right] dz \tag{4. 13d}$$

The variation of the kinetic energy is presented by:

$$\delta K = \int_{-a/2}^{a/2} \int_{-h/2}^{h/2} \rho(x,z)\left(\dot{u}_1 \delta \dot{u}_1 + \dot{u}_3 \delta \dot{u}_3\right) dz dx$$

$$= \int_{-a/2}^{a/2} e^{V_x(x)} \left\{ I_0 \left[\dot{U}\delta\dot{U} + \left(\dot{W}_b + \dot{W}_s\right)\delta\left(\dot{W}_b + \dot{W}_s\right)\right] + J_0 \left[\left(\dot{W}_b + \dot{W}_s\right)\delta\dot{W}_z + \dot{W}_z \delta\left(\dot{W}_b + \dot{W}_s\right)\right] \right.$$

$$-I_1\left(\dot{U}\delta\dot{W}_b' + \dot{W}_s'\delta\dot{U}\right) + I_2 \dot{W}_b'\delta\dot{W}_b' - J_1\left(\dot{U}\delta\dot{W}_s' + \dot{W}_s'\delta\dot{U}\right)$$

$$\left. + K_2 \dot{W}_s'\delta\dot{W}_s' + J_2\left(\dot{W}_b'\delta\dot{W}_s' + \dot{W}_s'\delta\dot{W}_b'\right) + K_0 \dot{W}_z \delta\dot{W}_z \right\} dx \tag{4. 14}$$

where

$$\left(I_0, I_1, I_2, J_0, J_1, J_2, K_0, K_2\right) = \int_{-h/2}^{h/2} \left(1, z, z^2, g, f, zf, g^2, f^2\right) \rho(z) dz \tag{4. 15}$$

Substituting Eqs. (4.10) and (4.14) into Eq. (4.9), integrating by parts and gathering the coefficients of $\delta U, \delta W_b, \delta W_s$ and δW_z, and considering that $V_x(x) = n_x\left(\frac{x}{a}+\frac{1}{2}\right)$, the equations of motion can be obtained:

$$N_x' + \frac{n_x}{a}N_x = I_0\ddot{U} - I_1\ddot{W}_b' - J_1\ddot{W}_s' \tag{4.16a}$$

$$M_x'' + 2\frac{n_x}{a}M_x' + \left(\frac{n_x}{a}\right)^2 M_x + R_{xy}'' + 2\frac{n_x}{a}R_{xy}' + \left(\frac{n_x}{a}\right)^2 R_{xy}$$

$$= I_0\left(\ddot{W}_b + \ddot{W}_s\right) + J_0\ddot{W}_z + \left(\frac{n_x}{a}I_1\ddot{U} + I_1\ddot{U}'\right) - \left(\frac{n_x}{a}I_2\ddot{W}_b' + I_2\ddot{W}_b''\right) - \left(\frac{n_x}{a}J_2\ddot{W}_s' + J_2\ddot{W}_s''\right) \tag{4.16b}$$

$$P_x'' + 2\frac{n_x}{a}P_x' + \left(\frac{n_x}{a}\right)^2 P_x + Q_{xz}' + \frac{n_x}{a}Q_{xz} + \frac{1}{2}\left[R_{xy}'' + 2\frac{n_x}{a}R_{xy}' + \left(\frac{n_x}{a}\right)^2 R_{xy}\right]$$

$$+\frac{1}{2}\left[S_{xy}'' + 2\frac{n_x}{a}S_{xy}' + \left(\frac{n_x}{a}\right)^2 S_{xy}\right] - \frac{1}{2}\left(X_{yz}' + \frac{n_x}{a}X_{yz}\right)$$

$$= J_1\left(\frac{n_x}{a}\ddot{U} + \ddot{U}'\right) + I_0\left(\ddot{W}_b + \ddot{W}_s\right) + J_0\ddot{W}_z - K_2\left(\frac{n_x}{a}\ddot{W}_s' + \ddot{W}_s''\right) - J_2\left(\frac{n_x}{a}\ddot{W}_b' + \ddot{W}_b''\right) \tag{4.16c}$$

$$-O_z + Q_{xz}' + \frac{n_x}{a}Q_{xz} - \frac{1}{2}\left(X_{yz}' + \frac{n_x}{a}X_{yz}\right) + \frac{1}{2}\left[T_{xy}'' + 2\frac{n_x}{a}T_{xy}' + \left(\frac{n_x}{a}\right)^2 T_{xy}\right] = J_0\left(\ddot{W}_b + \ddot{W}_s\right) + K_0\ddot{W}_z \tag{4.16d}$$

The essential BCs are expressed as:

$$\delta W_b : \frac{n_x}{a}M_x + M_x' + \frac{n_x}{a}R_{xy} + R_{xy}' = I_2\omega^2 W_b' + J_2\omega^2 W_s' \tag{4.17a}$$

$$\delta W_b' : M_x + R_{xy} = 0 \tag{4.17b}$$

$$\delta W_s : P_x + Q_{xz} - \frac{1}{2}X_{yz} + \frac{1}{2}\left(\frac{n_x}{a}R_{xy} + R_{xy}'\right) + \frac{1}{2}\left(\frac{n_x}{a}S_{xy} + S_{xy}'\right) = -J_1\omega^2 U + K_2\omega^2 W_s' + J_2\omega^2 W_b' \tag{4.17c}$$

$$\delta W_s' : P_x + \frac{1}{2}\left(R_{xy} + S_{xy}\right) = 0 \tag{4.17d}$$

$$\delta W_z : Q_{xz} - \frac{1}{2}X_{yz} + \frac{1}{2}\left(\frac{n_x}{a}T_{xy} + T_{xy}'\right) = 0 \tag{4.17e}$$

$$\delta W_z' : T_{xy} = 0 \tag{4.17f}$$

The governing equations are expressed in terms of displacements as:

$$\left(AU''-BW_b'''-B_sW_s'''+XW_z'\right)+\frac{n_x}{a}\left(AU'-BW_b''-B_sW_s''+XW_z\right)$$

$$=-I_0\omega^2U+I_1\omega^2W_b'+J_1\omega^2W_s' \qquad \text{(4. 18a)}$$

$$BU'''-DW_b^{(iv)}-D_sW_s^{(iv)}+YW_z''+2\frac{n_x}{a}\left(BU''-DW_b'''-D_sW_s'''+YW_z'\right)$$

$$+\left(\frac{n_x}{a}\right)^2\left(BU'-DW_b''-D_sW_s''+L_{13}W_z\right)-A_mW_b^{(iv)}-\frac{1}{2}\left(A_m+B_m\right)W_s^{(iv)}-\frac{1}{2}E_mW_z^{(iv)}$$

$$+2\frac{n_x}{a}\left[-A_mW_b'''-\frac{1}{2}\left(A_m+B_m\right)W_s'''-\frac{1}{2}E_mW_z'''\right]+\left(\frac{n_x}{a}\right)^2\left[-A_mW_b''-\frac{1}{2}\left(A_m+B_m\right)W_s''-\frac{1}{2}E_mW_z''\right]$$

$$=-I_0\omega^2\left(W_b+W_s\right)-J_0\omega^2W_z-I_1\omega^2\left(\frac{n_x}{a}U+U'\right)+I_2\omega^2\left(\frac{n_x}{a}W_b'+W_b''\right)+J_2\omega^2\left(\frac{n_x}{a}W_s'+W_s''\right) \qquad \text{(4. 18b)}$$

$$B_sU'''-D_sW_b^{(iv)}-HW_s^{(iv)}+Y_sW_z''+2\frac{n_x}{a}\left(B_sU''-D_sW_b'''-HW_s'''+Y_sW_z'\right)$$

$$+\left(\frac{n_x}{a}\right)^2\left(B_sU'-D_sW_b''-HW_s''+Y_sW_z\right)+A_s\left(W_s''+W_z''\right)+\frac{n_x}{a}A_s\left(W_s'+W_z'\right)$$

$$+\frac{1}{2}\left\{\begin{array}{l}-A_mW_b^{(iv)}-\frac{1}{2}\left(A_m+B_m\right)W_s^{(iv)}-\frac{1}{2}E_mW_z^{(iv)}+2\frac{n_x}{a}\left[-A_mW_b'''-\frac{1}{2}\left(A_m+B_m\right)W_s'''-\frac{1}{2}E_mW_z'''\right]\\+\left(\frac{n_x}{a}\right)^2\left[-A_mW_b''-\frac{1}{2}\left(A_m+B_m\right)W_s''-\frac{1}{2}E_mW_z''\right]\end{array}\right\}$$

$$+\frac{1}{2}\left\{\begin{array}{l}-B_mW_b^{(iv)}-\frac{1}{2}\left(B_m+C_m\right)W_s^{(iv)}-\frac{1}{2}D_mW_z^{(iv)}+2\frac{n_x}{a}\left[-B_mW_b'''-\frac{1}{2}\left(B_m+C_m\right)W_s'''-\frac{1}{2}D_mW_z'''\right]\\+\left(\frac{n_x}{a}\right)^2\left[-B_mW_b''-\frac{1}{2}\left(B_m+C_m\right)W_s''-\frac{1}{2}D_mW_z''\right]\end{array}\right\}$$

$$+\frac{1}{4}H_m\left[\left(W_s''-W_z''\right)+\frac{n_x}{a}\left(W_s'-W_z'\right)\right]$$

$$=-J_1\omega^2\left(\frac{n_x}{a}U+U'\right)-I_0\omega^2\left(W_b+W_s\right)-J_0\omega^2W_z+K_2\omega^2\left(\frac{n_x}{a}W_s'+W_s''\right)+J_2\omega^2\left(\frac{n_x}{a}W_b'+W_b''\right) \text{(4. 18c)}$$

$$-XU'+YW_b''+Y_sW_s''-ZW_z+A_s\left(W_s''+W_z''\right)+\frac{n_x}{a}A_s\left(W_s'+W_z'\right)+\frac{1}{2}H_m\left[W_s''-W_z''+\frac{n_x}{a}\left(W_s'-W_z'\right)\right]$$

$$+\frac{1}{2}\left\{\begin{array}{l}-E_mW_b^{(iv)}-\frac{1}{2}\left(E_m+D_m\right)W_s^{(iv)}-\frac{1}{2}F_mW_z^{(iv)}+2\frac{n_x}{a}\left[-E_mW_b'''-\frac{1}{2}\left(E_m+D_m\right)W_s'''-\frac{1}{2}F_mW_z'''\right]\\+\left(\frac{n_x}{a}\right)^2\left[-E_mW_b''-\frac{1}{2}\left(E_m+D_m\right)W_s''-\frac{1}{2}F_mW_z''\right]\end{array}\right\}$$

$$= -J_0\omega^2\left(W_b + W_s\right) - K_0\omega^2 W_z \tag{4. 18d}$$

Using the state space concept, the highest order derivatives of displacements are expressed in terms of the others as:

$$U'' = a_1U + a_2U' + a_3W_b' + a_4W_b'' + a_5W_b''' + a_6W_s' + a_7W_s'' + a_8W_s''' + a_9W_z + a_{10}W_z' \tag{4. 19a}$$

$$W_b^{(iv)} = r_1U + r_2U' + r_3W_b + r_4W_b' + r_5W_b'' + r_6W_b'''$$

$$+ r_7W_s + r_8W_s' + r_9W_s'' + r_{10}W_s''' + r_{11}W_z + r_{12}W_z' + r_{13}W_z'' + r_{14}W_z''' \tag{4. 19b}$$

$$W_s^{(iv)} = s_1U + s_2U' + s_3W_b + s_4W_b' + s_5W_b'' + s_6W_b'''$$

$$+ s_7W_s + s_8W_s' + s_9W_s'' + s_{10}W_s''' + s_{11}W_z + s_{12}W_z' + s_{13}W_z'' + s_{14}W_z''' \tag{4. 19c}$$

$$W_z^{(iv)} = t_1U + t_2U' + t_3W_b + t_4W_b' + t_5W_b'' + t_6W_b'''$$

$$+ t_7W_s + t_8W_s' + t_9W_s'' + t_{10}W_s''' + t_{11}W_z + t_{12}W_z' + t_{13}W_z'' + t_{14}W_z''' \tag{4. 19d}$$

The coefficients in Eq. (4.19) are given in Appendix A. The systems of Eq. (4.19) can be converted into a matrix form using state space approach as:

$$\mathbf{U}'(x) = \mathbf{T}\mathbf{U}(x) \tag{4. 20}$$

where the vector of variables is

$$\mathbf{U}(x) = \left\{U, U', W_b, W_b', W_b'', W_b''', W_s, W_s', W_s'', W_s''', W_z, W_z', W_z'', W_z'''\right\}'; \tag{4. 21}$$

and the non-zero components of matrix **T** are defined as:

$$\mathbf{T} = \begin{bmatrix}
0 & 1 & 0 & 0 & 0 & 0 & 0 & 0 & 0 & 0 & 0 & 0 & 0 & 0 \\
a_1 & a_2 & 0 & a_3 & a_4 & a_5 & 0 & a_6 & a_7 & a_8 & a_9 & a_{10} & 0 & 0 \\
0 & 0 & 0 & 1 & 0 & 0 & 0 & 0 & 0 & 0 & 0 & 0 & 0 & 0 \\
0 & 0 & 0 & 0 & 1 & 0 & 0 & 0 & 0 & 0 & 0 & 0 & 0 & 0 \\
0 & 0 & 0 & 0 & 0 & 1 & 0 & 0 & 0 & 0 & 0 & 0 & 0 & 0 \\
r_1 & r_2 & r_3 & r_4 & r_5 & r_6 & r_7 & r_8 & r_9 & r_{10} & r_{11} & r_{12} & r_{13} & r_{14} \\
0 & 0 & 0 & 0 & 0 & 0 & 0 & 1 & 0 & 0 & 0 & 0 & 0 & 0 \\
0 & 0 & 0 & 0 & 0 & 0 & 0 & 0 & 1 & 0 & 0 & 0 & 0 & 0 \\
0 & 0 & 0 & 0 & 0 & 0 & 0 & 0 & 0 & 1 & 0 & 0 & 0 & 0 \\
s_1 & s_2 & s_3 & s_4 & s_5 & s_6 & s_7 & s_8 & s_9 & s_{10} & s_{11} & s_{12} & s_{13} & s_{14} \\
0 & 0 & 0 & 0 & 0 & 0 & 0 & 0 & 0 & 0 & 0 & 1 & 0 & 0 \\
0 & 0 & 0 & 0 & 0 & 0 & 0 & 0 & 0 & 0 & 0 & 0 & 1 & 0 \\
0 & 0 & 0 & 0 & 0 & 0 & 0 & 0 & 0 & 0 & 0 & 0 & 0 & 1 \\
t_1 & t_2 & t_3 & t_4 & t_5 & t_6 & t_7 & t_8 & t_9 & t_{10} & t_{11} & t_{12} & t_{13} & t_{14}
\end{bmatrix} \tag{4. 22}$$

A formal solution of Eq. (4.20) is given by:

$$\mathbf{U}(x)=\mathbf{e}^{\mathbf{Tx}}\mathbf{K} \tag{4. 23}$$

where $\mathbf{K}$ is a vector which can be solved from the BCs at x=±a/2 and $\mathbf{e}^{\mathbf{Tx}}$ is of the form:

$$\mathbf{e}^{\mathbf{Tx}}=\mathbf{E}\begin{bmatrix} e^{\lambda_1 x} & & 0 \\ & \ddots & \\ 0 & & e^{\lambda_{14} x} \end{bmatrix}\mathbf{E}^{-1} \tag{4. 24}$$

where $\boldsymbol{\lambda}$ and $\mathbf{E}$ are the eigenvalues and columns of eigenvectors, respectively, associated with matrix $\mathbf{T}$. The BCs expressed in terms of displacement variables are described by:

Clamped (C):

$$U=W_b=W_b^{'}=W_s=W_s^{'}=W_z=W_z^{'}=0 \tag{4. 25}$$

Simply supported (S):

$$U=W_b=W_s$$

$$=BU^{'}-\left(D+A_m\right)W_b^{''}-\left[D_s+\frac{1}{2}\left(A_m+B_m\right)\right]W_s^{''}+Y_sW_z-\frac{1}{2}E_mW_z^{''}$$

$$=B_sU^{'}-\left[D_s+\frac{1}{2}\left(A_m+B_m\right)\right]W_b^{''}-\left[H+\frac{1}{4}\left(A_m+2B_m+C_m\right)\right]W_s^{''}+Y_sW_z-\frac{1}{4}\left(E_m+D_m\right)W_z^{''}$$

$$=E_mW_b^{''}+\frac{1}{2}\left(E_m+D_m\right)W_s^{''}+\frac{1}{2}F_mW_z^{''}=0 \tag{4. 26}$$

Free (F):

$$AU^{'}-BW_b^{''}-B_sW_s^{''}+XW_z$$

$$=Ba_1U+B\left(\frac{n_x}{a}+a_2\right)U^{'}$$

$$+\left(Ba_3-I_2\omega^2\right)W_b^{'}+\left[\left(Ba_4-\frac{n_x}{a}\right)D-\frac{n_x}{a}A_m\right]W_b^{''}+\left[\left(Ba_5-D\right)-A_m\right]W_b^{'''}$$

$$+\left(Ba_6-J_2\omega^2\right)W_s^{'}+\left[\left(Ba_7-\frac{n_x}{a}D_s\right)-\frac{1}{2}\frac{n_x}{a}\left(A_m+B_m\right)\right]W_s^{''}+\left[\left(Ba_8-D_s\right)-\frac{1}{2}\left(A_m+B_m\right)\right]W_s^{'''}$$

$$+\left(Ba_9+\frac{n_x}{a}Y\right)W_z+\left(Ba_{10}+Y\right)W_z^{'}-\frac{1}{2}\frac{n_x}{a}E_mW_z^{''}-\frac{1}{2}E_mW_z^{'''}$$

$$=BU^{'}-\left(D+A_m\right)W_b^{''}-\left[D_s+\frac{1}{2}\left(A_m+B_m\right)\right]W_s^{''}+Y_sW_z-\frac{1}{2}E_mW_z^{''}$$

$$=J_1\omega^2U+B_sU^{'}-J_2\omega^2W_b^{'}-\left[D_s+\frac{1}{2}\frac{n_x}{a}\left(A_m+B_m\right)\right]W_b^{''}-\frac{1}{2}\left(A_m+B_m\right)W_b^{'''}$$

$$+\left(A_s+\frac{1}{4}H_m-K_2\omega^2\right)W_s^{'}-\left[H+\frac{1}{4}\frac{n_x}{a}\left(A_m+2B_m+C_m\right)\right]W_s^{''}-\frac{1}{4}\left(A_m+2B_m+C_m\right)W_s^{'''}$$

$$+Y_sW_z+\left(A_s-\frac{1}{4}H_m\right)W_z^{'}-\frac{1}{4}\frac{n_x}{a}\left(E_m+D_m\right)W_z^{''}-\frac{1}{4}\left(E_m+D_m\right)W_z^{'''}$$

$$=B_sU^{'}-\left[D_s+\frac{1}{2}\left(A_m+B_m\right)\right]W_b^{''}-\left[H+\frac{1}{4}\left(A_m+2B_m+C_m\right)\right]W_s^{''}+Y_sW_z-\frac{1}{4}\left(E_m+D_m\right)W_z^{''}$$

$$=-\frac{1}{2}\frac{n_x}{a}E_mW_b^{''}-\frac{1}{2}E_mW_b^{'''}+\left(A_s+\frac{1}{4}H_m\right)W_s^{'}-\frac{1}{4}\frac{n_x}{a}\left(E_m+D_m\right)W_s^{''}-\frac{1}{4}\left(E_m+D_m\right)W_s^{'''}$$

$$+\left(A_s-\frac{1}{4}H_m\right)W_z^{'}-\frac{1}{4}\frac{n_x}{a}F_mW_z^{''}-\frac{1}{4}F_mW_z^{'''}$$

$$=E_mW_b^{''}+\frac{1}{2}\left(E_m+D_m\right)W_s^{''}+\frac{1}{2}F_mW_z^{''}=0 \tag{4. 27}$$

By substituting Eq. (4.23) into Eqs. (4.25-4.27) with the required BCs, a system of equations is obtained as:

$$\boldsymbol{\alpha e^{Tx}K=0} \tag{4. 28}$$

where α comes from the coefficients in Eqs. (4.25-4.27) for the appropriate BCs at x=±a/2. The natural frequencies ω_n of the n^{th} mode of vibration can be obtained by setting $\left|\boldsymbol{\alpha e^{Tx}}\right|=0$. It is noticeable that the iteration procedure [72] is used in this chapter to calculate the natural frequencies. The mode shapes are plotted by solving for **K** from Eq. (4.28) based on the singular value decomposition and calculating the displacement components along the beams after that.

4.5 Numerical examples

A slightly different version of this section has been published recently in Composites Part B: Engineering [139].

In this section, the numerical examples are presented to investigate the size-dependent vibration behaviours of conventional FG and BDFG microbeams using the HOBT and quasi-3D theories. In the first part, the natural frequencies of conventional FG microbeams (Type A) under arbitrary BCs are analysed. The beams are made of SiC (E_c=427GPa, ρ_c=3100kg/m^3, ν_c=0.17) and Al (E_m=70GPa, ρ_m=2702kg/m^3, ν_m=0.3). The non-dimensional natural frequencies are defined as follows: $\bar{\Omega}=\frac{\omega a^2}{h}\sqrt{\frac{\rho_m}{E_m}}$ and $\tilde{\Omega}=\frac{\omega a}{h}\sqrt{\frac{I_{10}}{A_{110}}}$ with $I_{10}=\int_{-h/2}^{h/2}\frac{E_m}{1-\nu_m^2}$ and $A_{110}=\int_{-h/2}^{h/2}\rho_m$. The second part deals with the free vibration response of BDFG microbeams (Types BD1 and BD2). The base material properties in BDFG microbeams are E_0=210GPa, ρ_0=7850kg/m^3 and ν_0=0.3. The

following non-dimensional natural frequency $\hat{\Omega}=\frac{\omega a^2}{h}\sqrt{\frac{\rho_0}{E_0}}$ is used. Since the BDFG beams are not horizontally symmetric as discussed later, it is useful to clarify that the two letters, e.g. C-S, are used to describe the BCs at the left and right ends of the beam, respectively.

4.5.1 Conventional FG microbeams

The natural frequencies of SiC/Al microbeams under various thickness-to-material length scale ratios are given in Table 4.1. The obtained solutions for the C-C and S-S microbeams agree well with those based on the FOBT [87] and HOBT [140]. The effect of BCs on the natural frequencies is also highlighted in this table. It can be seen that the highest frequencies are seen in C-C beams and followed by C-S, F-S, S-S and C-F beams as expected. It is worth noting that the Poisson effect is included in both thickness and longitudinal directions, and the Mori-Tanaka scheme is used in this table. The corresponding formula can be found in [87, 97, 107].

Table 4. 1: Comparisons of non-dimensional natural frequencies $\tilde{\Omega}$ of SiC/Al microbeams for various h/l (a/h=12, n_z=2).

BCs	Theory	h/l					
		1	1.5	2	3	6	10
C–C	HOBT [140]	1.6246	1.2291	1.0642	0.8904	0.7769	0.7454
	FOBT [87]	1.6022	1.2194	1.0416	0.8885	0.7801	0.7548
	HOBT	1.6892	1.2522	1.0565	0.8896	0.7709	0.7427
	Quasi-3D	1.6762	1.2355	1.0373	0.8676	0.7461	0.7171
S–S	HOBT [140]	0.7854	0.5903	0.5042	0.4304	0.3787	0.3662
	FOBT [87]	0.7625	0.5784	0.4968	0.4285	0.3812	0.3701
	HOBT	0.7664	0.5777	0.4948	0.4255	0.3777	0.3666
	Quasi-3D	0.8256	0.6131	0.5145	0.4284	0.3663	0.3517
C-S	HOBT	1.1756	0.8759	0.7426	0.6299	0.5508	0.5323
	Quasi-3D	1.1810	0.8743	0.7355	0.6165	0.5318	0.5118
C-F	HOBT	0.2695	0.2008	1.0426	0.1447	0.1268	0.1227
	Quasi-3D	0.2671	0.1976	0.1666	0.1397	0.1220	0.1177
F-S	HOBT	1.1653	0.8683	0.7361	0.6245	0.5464	0.5282
	Quasi-3D	1.1322	0.8451	0.7140	0.5961	0.5251	0.5062

Further to the C-C microbeams, the difference between the vibration mode shapes predicted by the HOBT and quasi-3D theory is revealed in Fig. 4.2 for the first three modes. It can be seen that the stretching effect is more noticeable for the thick beams and the higher modes. In addition, the axial mode appears in the second mode instead of the third mode as in the case of macrobeams as observed in Ref. [74].

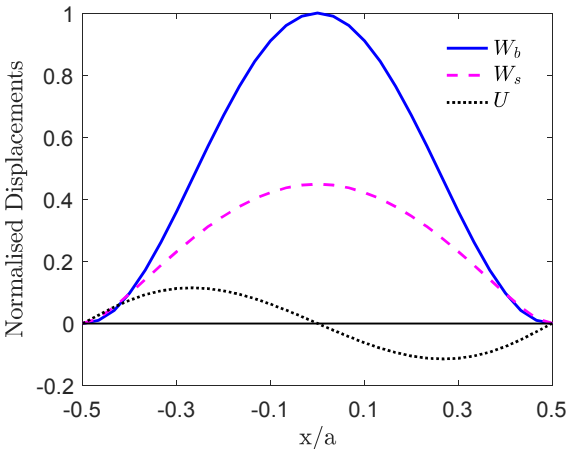

Mode 1: $\bar{\Omega}_1 = 13.2810$

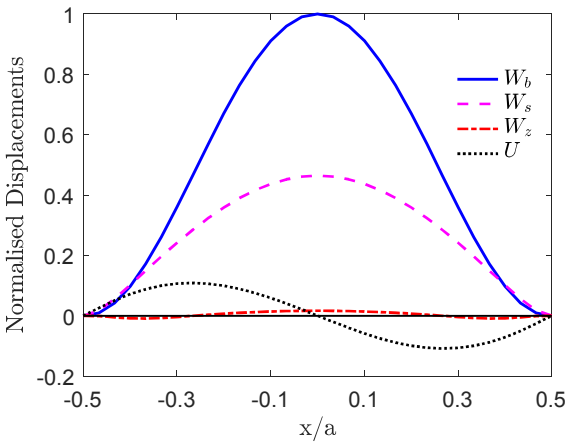

Mode 1: $\bar{\Omega}_1 = 13.3446$

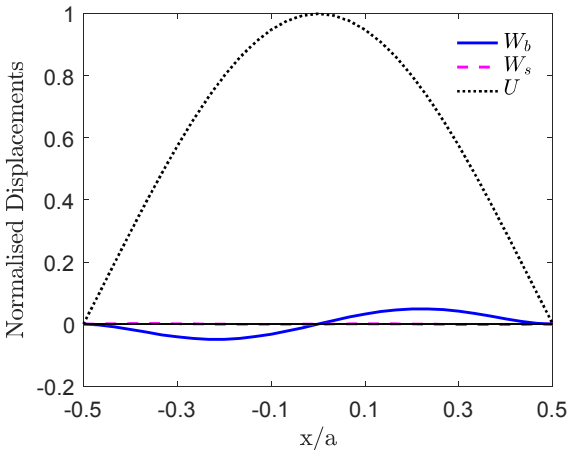

Mode 2: $\bar{\Omega}_2 = 25.1587$

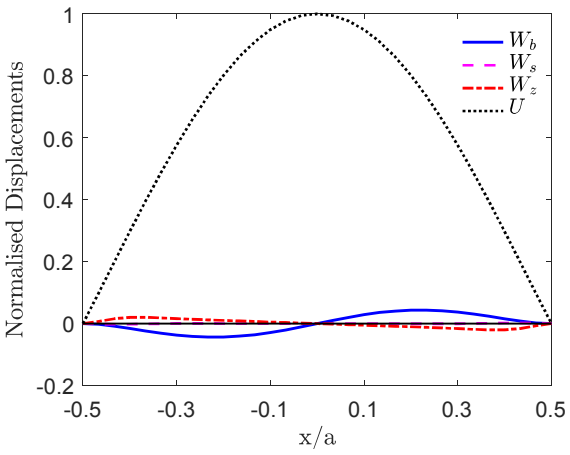

Mode 2: $\bar{\Omega}_2 = 25.8440$

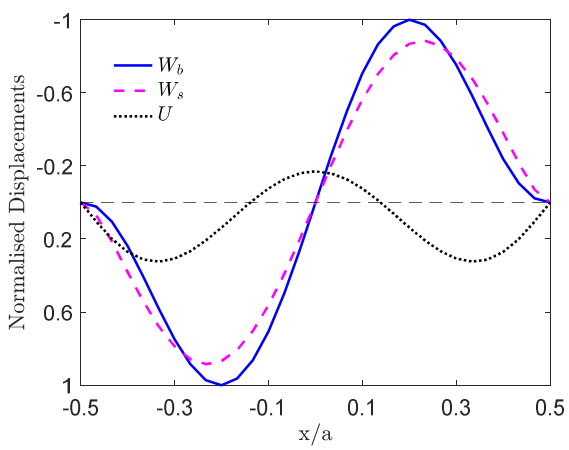

Mode 3: $\bar{\Omega}_3 = 33.6027$

a. HOBT

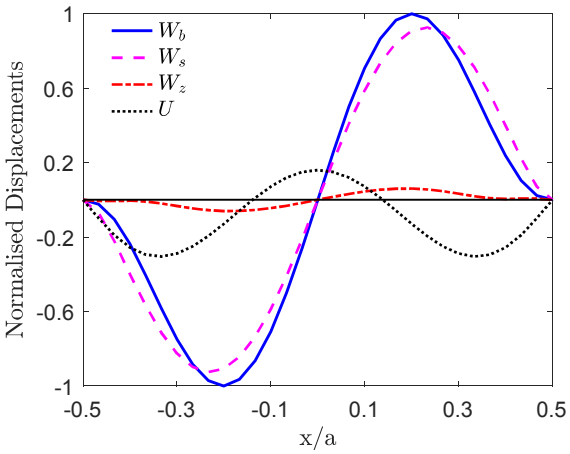

Mode 3: $\bar{\Omega}_3 = 33.6035$

b. Quasi-3D theory

Fig. 4. 2: Vibration mode shapes of SiC/Al microbeams (C-C, a/h=5, h/l=2, n_z=2) using HOBT and quasi-3D theory.

Table 4.2 and Fig. 4.3 examine the effect of the power-law index and the BCs in both micro- and macro- FG beams. As expected, the natural frequencies gradually decrease with a reduction of ceramic volume fraction, which results in a lower Young's modulus.

Table 4. 2: Size effect of frequencies $\overline{\Omega}$ for the SiC/Al beams under various BCs and slenderness ratios.

BCs	h/l	Theory	a/h=5			a/h=20		
			n_z=0	1	10	n_z=0	1	10
S_1-S_1	1	HOBT [107]	15.7140	11.9948	8.0425	-	-	-
		HOBT	15.7140	12.1506	8.1733	16.2251	12.5446	8.4065
		Quasi-3D [107]	15.6249	11.9444	7.9967	-	-	-
		Quasi-3D	15.6833	9.3951	3.9212	16.2228	13.7186	8.9625
S_1-S_2		HOBT	15.7140	11.7745	7.8469	16.2251	12.3911	8.2843
		Quasi-3D	15.6833	9.4005	7.4030	16.2228	12.3681	8.2808
S_1-S_1	5	HOBT	6.8405	5.2905	3.9046	7.1862	5.5598	4.1859
		Quasi-3D	6.8427	5.4276	3.9412	7.1864	5.7077	4.2296
S_1-S_2		HOBT	6.8405	4.9615	3.6775	7.1862	5.2255	3.9508
		Quasi-3D	6.8427	4.9893	3.7046	7.1864	5.2631	3.9827
S_1-S_1	∞	HOBT [107]	6.2025	4.4657	3.3909	-	-	-
		HOBT	6.2009	4.7944	3.6022	6.5441	5.0618	3.9102
		Quasi-3D [107]	6.4615	4.7159	3.5444	-	-	-
		Quasi-3D	6.2069	4.8119	3.6146	6.5445	5.0758	3.9215
S_1-S_2		HOBT	6.2009	4.4404	3.3692	6.5441	4.6954	3.6596
		Quasi-3D	6.2069	4.4865	3.4052	6.5445	4.7382	3.6945
C-C	1	HOBT	33.5290	25.7024	17.4627	36.5871	27.9617	18.7167
		Quasi-3D	33.5390	25.7114	17.4235	36.5928	28.0028	18.7560
	5	HOBT	13.8093	10.2076	7.2212	16.1273	11.7461	8.8328
		Quasi-3D	13.8604	10.3089	7.3016	16.1437	11.8454	8.9182
	∞	HOBT	12.2556	8.9576	6.3403	14.6657	10.5412	8.1522
		Quasi-3D	12.3018	9.0664	6.4268	14.6811	10.6488	8.2419
C-S	1	HOBT	18.1099	14.2757	9.4339	25.2986	19.3299	12.9292
		Quasi-3D	18.3774	14.6234	9.7854	25.2990	19.3553	12.9531
	5	HOBT	10.2151	7.4889	5.4437	11.1866	8.1408	6.1434
		Quasi-3D	10.2396	7.5569	5.4968	11.1924	8.2050	6.1980
	∞	HOBT	9.1925	6.6568	4.9064	10.1823	7.3118	5.6836
		Quasi-3D	9.2208	6.7343	4.9679	10.1879	7.3823	5.7417
C-F	1	HOBT	5.6973	4.3504	2.9127	5.7873	4.4215	2.9559
		Quasi-3D	5.6756	4.3425	2.9191	5.7864	4.4269	2.9622
	5	HOBT	2.5043	1.8236	1.3667	2.5649	1.8655	1.4117
		Quasi-3D	2.5102	1.8425	1.3873	2.5661	1.8804	1.4246
	∞	HOBT	2.2769	1.6362	1.2604	2.3361	1.6765	1.3082
		Quasi-3D	2.2804	1.6544	1.2761	2.3371	1.6926	1.3215
S-F	1	HOBT	18.1099	13.8537	9.1175	25.2960	19.3008	12.9008
		Quasi-3D	18.3774	12.8911	8.8361	25.2718	19.1880	12.8636
	5	HOBT	10.3774	7.4181	5.4633	11.2015	8.1390	6.1505
		Quasi-3D	10.3936	7.4632	5.5363	11.2030	8.1981	6.2029
	∞	HOBT	9.3982	6.6424	5.0073	10.2001	7.3130	5.6963
		Quasi-3D	9.4119	6.7241	5.0785	10.2012	7.3805	5.7517

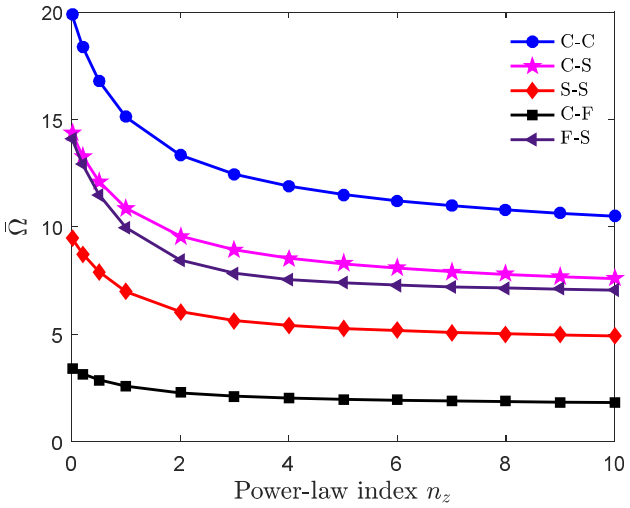

Fig. 4. 3: Variation of natural frequencies $\bar{\Omega}$ with respect to the power-law index n_z (SiC/Al beams, a/h=5, h/l=2).

For simply supported beams, unlike the Navier solution [107], the present approach can be employed to adapt the requirements of both displacement and stress resultants. Therefore, it is applicable to both immovable (S_1) and movable (S_2) simply supported BCs. Using these two BCs (S_1-S_1 and S_1-S_2), the difference between the natural frequencies and the first three mode shapes for microbeams (n_z=2) is shown in Table 4.2 and Fig. 4.4. These two BCs only result in the identical frequencies for the homogeneous beam (n_z=0) as expected, whereas the S_1-S_1 BC leads to the higher values for the FG beams. The difference is more apparent in the higher modes, where the axial modes appear in the movable simply supported beams with quite low frequencies. In the rest of this chapter, the movable simply support is combined with other end conditions, except for the free end that joins with the immovable one. The simply supported beams are assembled by an immovable support at x=-a/2 and a movable one at x=a/2. Comparing various BCs, the higher frequencies are observed in the beams with stiffer ends, i.e. C-C, and with a higher volume of ceramic (smaller n_z). It is interesting that the fundamental frequencies of the S-F beams are nearly the same with those of C-S beams for both micro- and macro-scales.

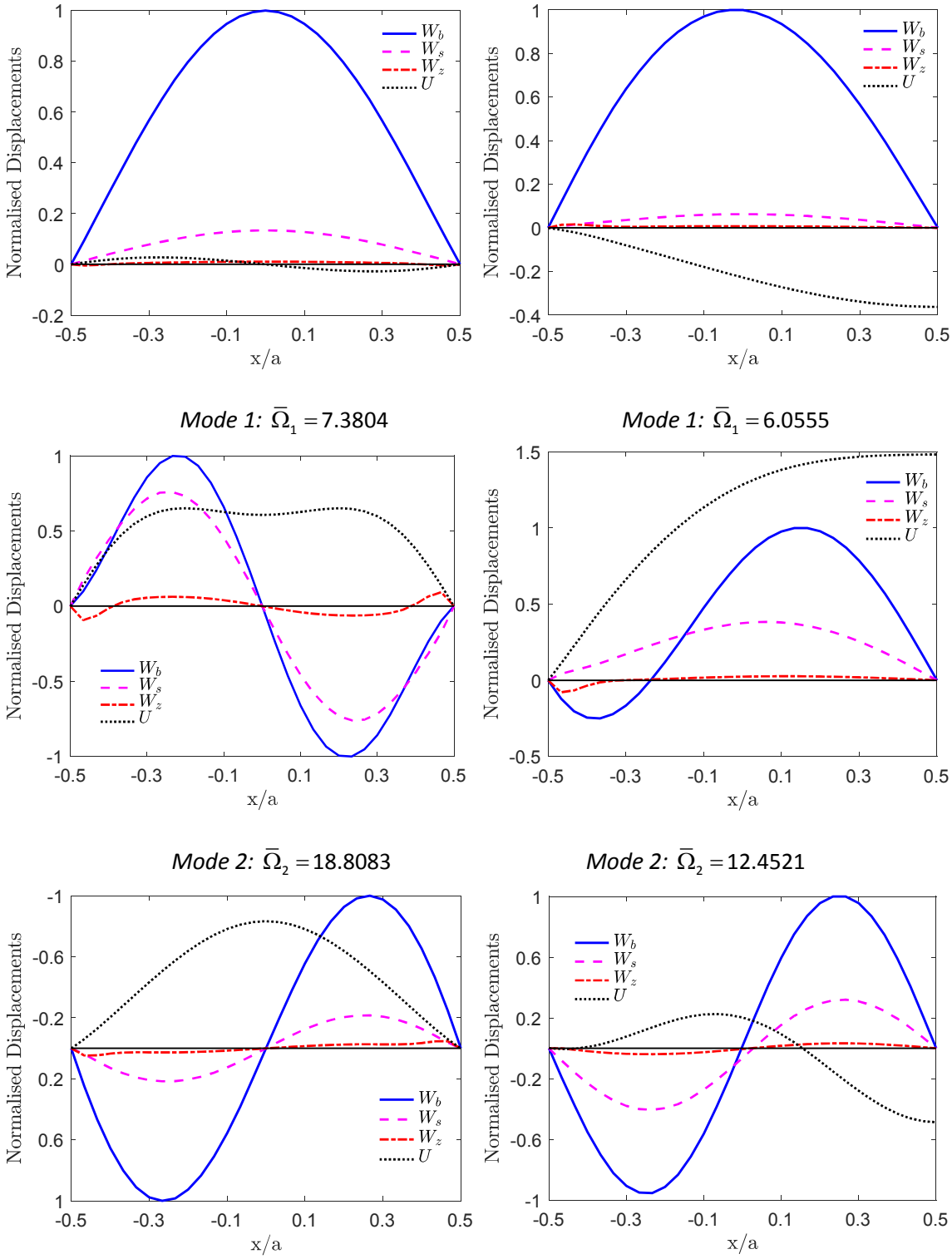

Mode 1: $\bar{\Omega}_1 = 7.3804$ *Mode 1:* $\bar{\Omega}_1 = 6.0555$

Mode 2: $\bar{\Omega}_2 = 18.8083$ *Mode 2:* $\bar{\Omega}_2 = 12.4521$

Mode 3: $\bar{\Omega}_3 = 29.2417$ *Mode 3:* $\bar{\Omega}_3 = 23.1669$

a. Immovable SS beams *b. Movable SS beams*

Fig. 4. 4: Vibration mode shapes of immovable and movable simply supported SiC/Al microbeams (a/h=5, h/l=2, n_z=2).

The difference between the vibration behaviour of macro and microbeams is also seen in the mode shapes. Fig. 4.5 demonstrates the variation of the vibration mode shapes with respect to

the change of the frequencies. These graphs can be used to state the mode shapes where the change of the number of half-sine waves occurs. As can be seen from this figure, for C-C and F-C beams, there is a significant change between the vibration mode shapes in the macrobeams. However, in the microbeams, they are not too prominent to the neighbour status.

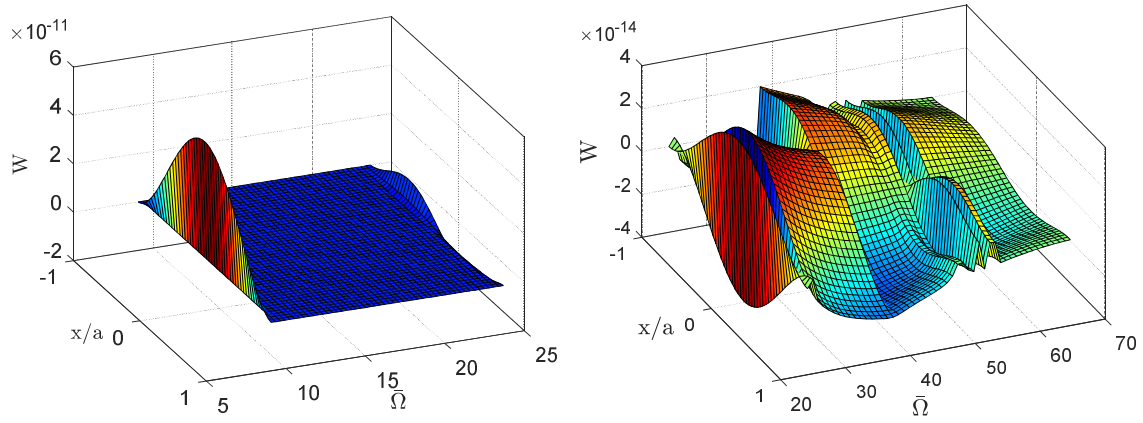

h/l=∞ *h=l*

a. C-C beams

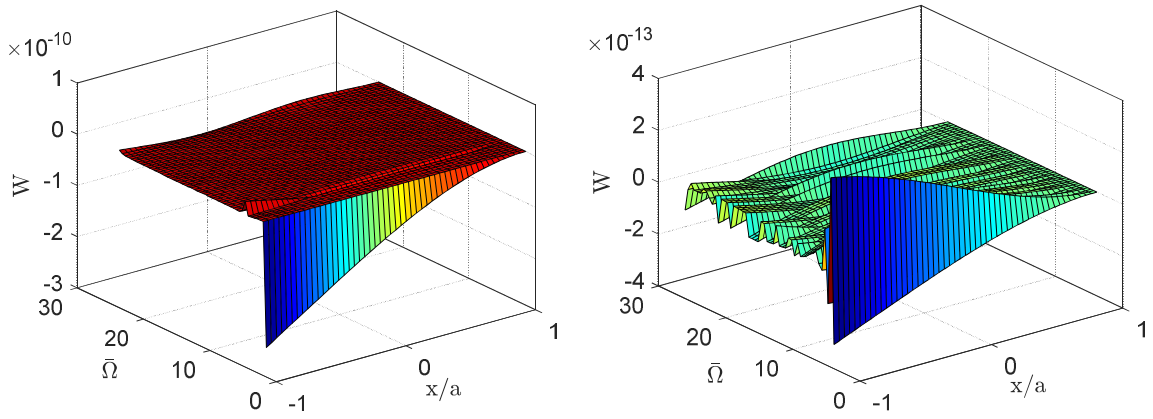

h/l=∞ *h=l*

b. F-C beams

Fig. 4. 5: Variation of mode shapes with respect to the frequencies $\bar{\Omega}$ (SiC/Al beams, a/h=10, n_z=2).

4.5.2 BDFG beams

Tables 4.3-4.6 reveal the fundamental natural frequencies of BDFG beams (Types BD1 and BD2) with respect to different BCs, exponential indices and thickness-to-material length scales. The current results for macrobeams ($h/l=\infty$) agree well with those given by Simsek [126]. The natural frequencies of Types BD1 and BD2 are identical for the conventional FG beams (n_z=0), but they are different for BDFG beams. The lower frequencies are observed with the elevated n_z, but the change is more significant from the symmetric cross-section beams, i.e. Type BD2.

Table 4. 3: Fundamental frequencies of C-C BDFG beams (a/h=5).

h/l	n_x	Theory	Type BD1				Type BD2			
			n_z=0	0.4	0.6	1	n_z=0	0.4	0.6	1
1	0	HOBT	13.8706	13.8720	13.8737	13.8787	13.8706	13.6821	13.5876	13.3996
		Quasi-3D	13.8581	13.8612	13.8650	13.8761	13.8581	13.6680	13.5728	13.3838
	0.4	HOBT	13.8854	13.8868	13.8885	13.8935	13.8854	13.6969	13.6024	13.4143
		Quasi-3D	13.8730	13.8761	13.8798	13.8910	13.8730	13.6829	13.5876	13.3987
	0.6	HOBT	13.9039	13.9053	13.9070	13.9119	13.9039	13.7155	13.6209	13.4328
		Quasi-3D	13.8916	13.8947	13.8984	13.9095	13.8916	13.7015	13.6062	13.4172
	1	HOBT	13.9634	13.9647	13.9664	13.9712	13.9634	13.7749	13.6802	13.4922
		Quasi-3D	13.9513	13.9544	13.9581	13.9690	13.9513	13.7611	13.6658	13.4768
8	0	HOBT	5.4880	5.4711	5.4502	5.3846	5.4880	5.3463	5.2674	5.0963
		Quasi-3D	5.5438	5.5303	5.5135	5.4604	5.5438	5.4003	5.3204	5.1468
	0.4	HOBT	5.4947	5.4778	5.4569	5.3912	5.4947	5.3527	5.2737	5.1023
		Quasi-3D	5.5505	5.5370	5.5201	5.4670	5.5505	5.4068	5.3267	5.1527
	0.6	HOBT	5.5031	5.4862	5.4652	5.3994	5.5031	5.3607	5.2815	5.1097
		Quasi-3D	5.5589	5.5453	5.5285	5.4752	5.5589	5.4148	5.3345	5.1602
	1	HOBT	5.5299	5.5129	5.4919	5.4257	5.5299	5.3864	5.3066	5.1335
		Quasi-3D	5.5857	5.5720	5.5551	5.5015	5.5857	5.4404	5.3595	5.1840
∞	0	CBT [126]	6.3291	6.3056	6.2763	6.1826	-	-	-	-
		FOBT [126]	5.1943	5.1806	5.1630	5.1083	-	-	-	-
		HOBT	5.2308	5.2128	5.1904	5.1202	5.2308	5.0907	5.0110	4.8351
		Quasi-3D	5.2869	5.2725	5.2546	5.1981	5.2869	5.1453	5.0646	4.8865
	0.4	CBT [126]	6.3349	6.3115	6.2822	6.1884	-	-	-	-
		FOBT [126]	5.1982	5.1845	5.1669	5.1123	-	-	-	-
		HOBT	5.2374	5.2193	5.1970	5.1266	5.2374	5.0969	5.0171	4.8409
		Quasi-3D	5.2935	5.2791	5.2612	5.2046	5.2935	5.1515	5.0707	4.8923
	0.6	CBT [126]	6.3427	6.3193	6.288	6.1943	-	-	-	-
		FOBT [126]	5.2041	5.1904	5.1728	5.1181	-	-	-	-
		HOBT	5.2456	5.2275	5.2051	5.1347	5.2456	5.1048	5.0247	4.8481
		Quasi-3D	5.3017	5.2873	5.2693	5.2127	5.3017	5.1594	5.0783	4.8995
	1	CBT [126]	6.3662	6.3427	6.3115	6.2177	-	-	-	-
		FOBT [126]	5.2197	5.2060	5.1884	5.1337	-	-	-	-
		HOBT	5.2719	5.2538	5.2312	5.1604	5.2719	5.1298	5.0491	4.8711
		Quasi-3D	5.3280	5.3135	5.2954	5.2384	5.3280	5.1844	5.1027	4.9225

Table 4. 4: Fundamental frequencies of C-S BDFG beams (a/h=5).

h/l	n_x	Theory	Type BD1				Type BD2			
			n_z=0	0.4	0.6	1	n_z=0	0.4	0.6	1
1	0	HOBT	7.8540	7.8540	7.8540	7.8540	7.8540	7.8540	7.8540	7.8540
		Quasi-3D	8.2332	8.2289	8.2236	8.2075	8.2332	8.2332	8.2332	8.2332
	0.4	HOBT	7.2297	7.2297	7.2297	7.2297	7.2297	7.2297	7.2297	7.2297
		Quasi-3D	7.5787	7.5748	7.5700	7.5553	7.5787	7.5787	7.5787	7.5787
	0.6	HOBT	6.9270	6.9270	6.9270	6.9270	6.9270	6.9270	6.9270	6.9270
		Quasi-3D	7.2614	7.2577	7.2531	7.2392	7.2614	7.2614	7.2614	7.2614
	1	HOBT	6.3414	6.3414	6.3414	6.3414	6.3414	6.3414	6.3414	6.3414
		Quasi-3D	6.6476	6.6442	6.6401	6.6274	6.6476	6.6476	6.6476	6.6476
8	0	HOBT	4.1147	4.1011	4.0843	4.0315	4.1147	3.9743	3.8998	3.7443
		Quasi-3D	4.1406	4.1294	4.1154	4.0714	4.1406	3.9985	3.9231	3.7657
	0.4	HOBT	4.0229	4.0096	3.9931	3.9413	4.0229	3.8834	3.8096	3.6559
		Quasi-3D	4.0484	4.0373	4.0236	3.9803	4.0484	3.9071	3.8324	3.6769
	0.6	HOBT	3.9777	3.9645	3.9481	3.8968	3.9777	3.8386	3.7651	3.6122
		Quasi-3D	4.0029	3.9920	3.9783	3.9354	4.0029	3.8621	3.7877	3.6330
	1	HOBT	3.8878	3.8748	3.8588	3.8085	3.8878	3.7494	3.6765	3.5254
		Quasi-3D	3.9125	3.9017	3.8883	3.8460	3.9125	3.7724	3.6986	3.5456
∞	0	CBT [126]	4.3682	4.3511	4.3304	4.2657	-	-	-	-
		FOBT [126]	3.8779	3.8662	3.8505	3.8037	-	-	-	-
		HOBT	3.9502	3.9359	3.9182	3.8626	3.9502	3.8068	3.7299	3.5680
		Quasi-3D	3.9775	3.9657	3.9510	3.9047	3.9775	3.8321	3.7543	3.5903
	0.4	CBT [126]	4.2486	4.2315	4.2120	4.1485	-	-	-	-
		FOBT [126]	3.7685	3.7568	3.7431	3.6962	-	-	-	-
		HOBT	3.8633	3.8493	3.8320	3.7775	3.8633	3.7207	3.6445	3.4844
		Quasi-3D	3.8902	3.8786	3.8642	3.8186	3.8902	3.7456	3.6684	3.5063
	0.6	CBT [126]	4.1888	4.1729	4.1522	4.0899	-	-	-	-
		FOBT [126]	3.7138	3.7021	3.6865	3.6416	-	-	-	-
		HOBT	3.8206	3.8067	3.7895	3.7355	3.8206	3.6783	3.6023	3.4431
		Quasi-3D	3.8472	3.8357	3.8214	3.7762	3.8472	3.7029	3.6260	3.4648
	1	CBT [126]	4.0704	4.0545	4.0350	3.9752	-	-	-	-
		FOBT [126]	3.6005	3.5908	3.5751	3.5322	-	-	-	-
		HOBT	3.7357	3.7221	3.7052	3.6523	3.7357	3.5939	3.5185	3.3610
		Quasi-3D	3.7618	3.7505	3.7364	3.6919	3.7618	3.6181	3.5417	3.3821

Table 4. 5: Fundamental frequencies of S-S BDFG beams (a/h=5).

h/l	n_x	Theory	Type BD1				Type BD2			
			n_z=0	0.4	0.6	1	n_z=0	0.4	0.6	1
1	0	HOBT	6.5172	6.5078	6.4963	6.4610	6.5172	6.4593	6.4306	6.3745
		Quasi-3D	6.4944	6.4505	6.3978	6.2432	6.4944	6.4369	6.4086	6.3533
	0.4	HOBT	6.5074	6.4999	6.4907	6.4622	6.5074	6.4497	6.4211	6.3652
		Quasi-3D	6.4846	6.4217	6.3499	6.1546	6.4846	6.4274	6.3991	6.3440
	0.6	HOBT	6.4951	6.4882	6.4797	6.4533	6.4951	6.4377	6.4092	6.3536
		Quasi-3D	6.4724	6.3913	6.3044	6.0833	6.4724	6.4154	6.3873	6.3325
	1	HOBT	6.4558	6.4496	6.4420	6.4184	6.4558	6.3992	6.3712	6.3164
		Quasi-3D	6.4334	6.2597	6.1332	5.8673	6.4334	6.3773	6.3496	6.2956
8	0	HOBT	2.7786	2.7679	2.7546	2.7132	2.7786	2.6672	2.6097	2.4924
		Quasi-3D	2.7820	2.7730	2.7618	2.7266	2.7820	2.6698	2.6119	2.4939
	0.4	HOBT	2.7749	2.7643	2.7511	2.7100	2.7749	2.6636	2.6061	2.4889
		Quasi-3D	2.7783	2.7692	2.7580	2.7225	2.7783	2.6662	2.6083	2.4904
	0.6	HOBT	2.7702	2.7597	2.7466	2.7057	2.7702	2.6590	2.6016	2.4845
		Quasi-3D	2.7736	2.7645	2.7532	2.7176	2.7736	2.6616	2.6038	2.4860
	1	HOBT	2.7554	2.7449	2.7319	2.6914	2.7554	2.6444	2.5871	2.4704
		Quasi-3D	2.7587	2.7495	2.7381	2.7021	2.7587	2.6469	2.5893	2.4719
∞	0	CBT [126]	2.8033	2.7911	2.7764	2.7288	-	-	-	-
		FOBT [126]	2.6767	2.6669	2.6533	2.6103	-	-	-	-
		HOBT	2.6774	2.6663	2.6525	2.6096	2.6774	2.5622	2.5024	2.3798
		Quasi-3D	2.6820	2.6728	2.6613	2.6253	2.6820	2.5658	2.5055	2.3820
	0.4	CBT [126]	2.7984	2.7862	2.7716	2.7239	-	-	-	-
		FOBT [126]	2.6728	2.6611	2.6474	2.6044	-	-	-	-
		HOBT	2.6738	2.6628	2.6492	2.6066	2.6738	2.5587	2.4990	2.3764
		Quasi-3D	2.6784	2.6692	2.6577	2.6214	2.6784	2.5623	2.5021	2.3787
	1	CBT [126]	2.7740	2.7618	2.7471	2.6983	-	-	-	-
		FOBT [126]	2.6455	2.6337	2.6201	2.5771	-	-	-	-
		HOBT	2.6552	2.6444	2.6309	2.5889	2.6552	2.5404	2.4809	2.3589
		Quasi-3D	2.6597	2.6504	2.6388	2.6022	2.6597	2.5440	2.4840	2.3611

Table 4. 6: Fundamental frequencies of C-F BDFG beams (a/h=5).

h/l	n_x	Theory	Type BD1				Type BD2			
			n_z=0	0.4	0.6	1	n_z=0	0.4	0.6	1
1	0	HOBT	2.3640	2.3625	2.3605	2.3544	2.3640	2.3433	2.3331	2.3132
		Quasi-3D	2.3513	2.3502	2.3488	2.3445	2.3513	2.3295	2.3188	2.2977
	0.4	HOBT	2.0912	2.0897	2.0879	2.0824	2.0912	2.0728	2.0638	2.0462
		Quasi-3D	2.0788	2.0778	2.0766	2.0727	2.0788	2.0595	2.0500	2.0313
	0.6	HOBT	1.9646	1.9632	1.9616	1.9563	1.9646	1.9473	1.9389	1.9224
		Quasi-3D	1.9525	1.9515	1.9504	1.9467	1.9525	1.9344	1.9254	1.9079
	1	HOBT	1.7303	1.7291	1.7275	1.7228	1.7303	1.7151	1.7076	1.6932
		Quasi-3D	1.7187	1.7178	1.7168	1.7135	1.7187	1.7027	1.6948	1.6793
8	0	HOBT	1.0210	1.0172	1.0126	0.9980	1.0210	0.9765	0.9539	0.9081
		Quasi-3D	1.0267	1.0235	1.0194	1.0067	1.0267	0.9820	0.9592	0.9132
	0.4	HOBT	0.9040	0.9006	0.8965	0.8835	0.9040	0.8644	0.8442	0.8035
		Quasi-3D	0.9094	0.9065	0.9029	0.8915	0.9094	0.8695	0.8492	0.8083
	0.6	HOBT	0.8497	0.8465	0.8426	0.8304	0.8497	0.8123	0.7933	0.7550
		Quasi-3D	0.8548	0.8521	0.8487	0.8380	0.8548	0.8172	0.7981	0.7596
	1	HOBT	0.7489	0.7461	0.7427	0.7319	0.7489	0.7158	0.6990	0.6651
		Quasi-3D	0.7538	0.7513	0.7483	0.7389	0.7538	0.7204	0.7035	0.6694
∞	0	CBT [126]	1.0068	1.0029	0.999	0.9833	-	-	-	-
		FOBT [126]	0.9844	0.9796	0.9735	0.9576	-	-	-	-
		HOBT	0.9854	0.9815	0.9766	0.9615	0.9854	0.9392	0.9156	0.8678
		Quasi-3D	0.9902	0.9869	0.9827	0.9695	0.9902	0.9439	0.9202	0.8723
	0.4	CBT [126]	0.8896	0.8876	0.8818	0.8681	-	-	-	-
		FOBT [126]	0.8709	0.8673	0.8624	0.8486	-	-	-	-
		HOBT	0.8725	0.8690	0.8647	0.8512	0.8725	0.8314	0.8104	0.7679
		Quasi-3D	0.8771	0.8741	0.8704	0.8586	0.8771	0.8358	0.8147	0.7721
	1	CBT [126]	0.7353	0.7333	0.7294	0.7177	-	-	-	-
		FOBT [126]	0.7216	0.7177	0.7138	0.7021	-	-	-	-
		HOBT	0.7229	0.7200	0.7164	0.7052	0.7229	0.6885	0.6710	0.6356
		Quasi-3D	0.7271	0.7246	0.7215	0.7116	0.7271	0.6926	0.6750	0.6394

This correlation is also presented in Fig. 4.6, which illustrates the effect of axial and through-the-thickness exponential indices to the natural frequencies of BDFG microbeams under various BCs. It is seen that the increase of n_z leads to a reduction in frequencies in all cases, whereas the increase of n_x only leads to a reduction in frequencies of C-S, S-S and C-F beams. In order to illustrate solely the effect of material properties in each direction, Fig. 4.7 plots the relationship between the natural frequencies and thickness-to-material length scales for the axial and through-the-thickness FG beams. In both cases, the effect of couple stress is negligible as the thickness is greater than 30l. For the conventional FG beams, the natural frequencies are lower in Type BD2, while they are identical in the axial FG beams as expected.

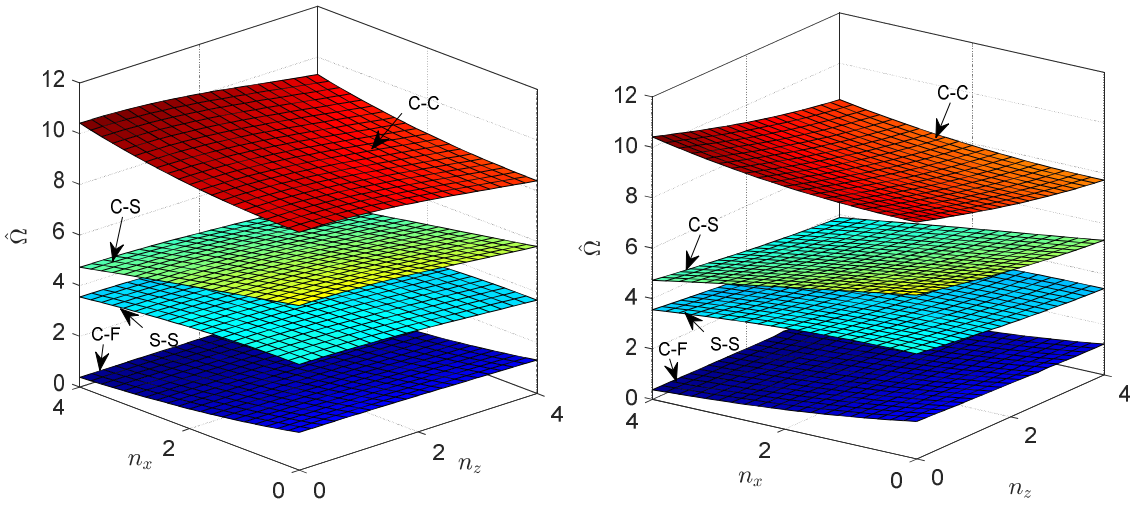

a. Type BD1 *b. Type BD2*

Fig. 4. 6: Variation of fundamental frequencies of BDFG micro-beams (a/h=20, h/l=2) with respect to exponential-indices.

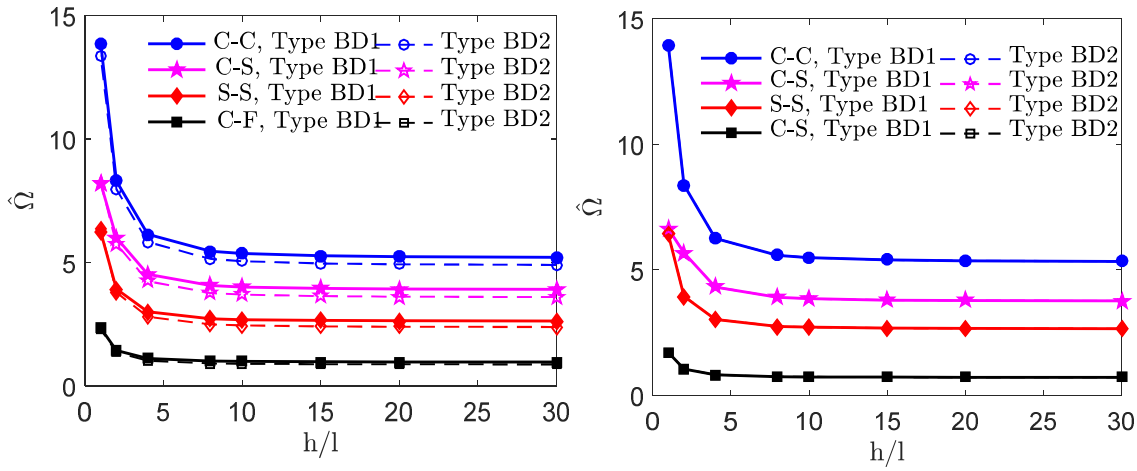

a. Through-the-thickness FG (n_x=0, n_z=1) *b. Axial FG (n_x=1, n_z=0)*

Fig. 4. 7: Difference between Types BD1 and BD2 in BDFG beams (a/h=5).

As mentioned before that the BDFG beams are not horizontally symmetric which means that the switching of the left and right BCs, e.g. C-F and F-C, changes the natural frequencies and vibration mode shapes. An example of switching C-F and C-S BCs is demonstrated in Fig. 4.8. In both cases, the left clamped ends cause lower frequency with the elevated n_x, which is opposite to the right clamped ends do. Indeed, the increase of n_x results in an increase of not only Young's modulus but also the density. When the clamps are placed at the stiffer and heavier ends (the right end), the natural frequencies are maximised.

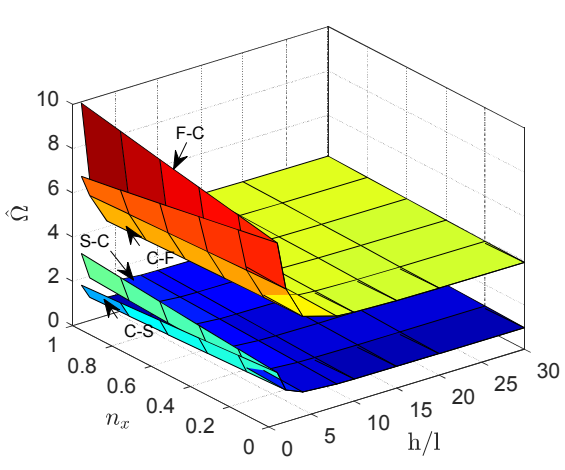

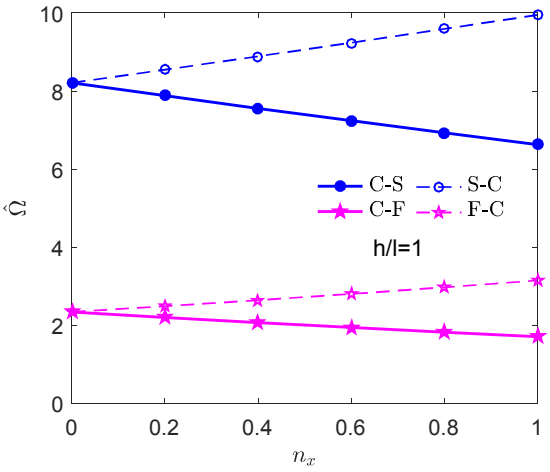

a. $\hat{\Omega} - n_x - h/l$ *b.* $\hat{\Omega} - n_x\left(h/l=1\right)$

Fig. 4. 8: Effect of the left and right ends to the frequencies of BDFG beams (a/h=5, n_z=1).

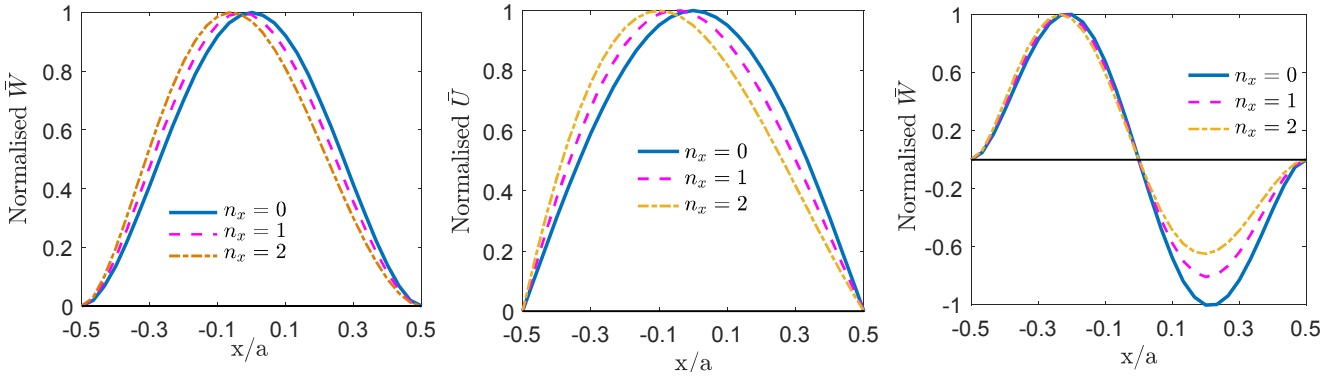

Mode 1 *Mode 2* *Mode 3*

a. C-C beams

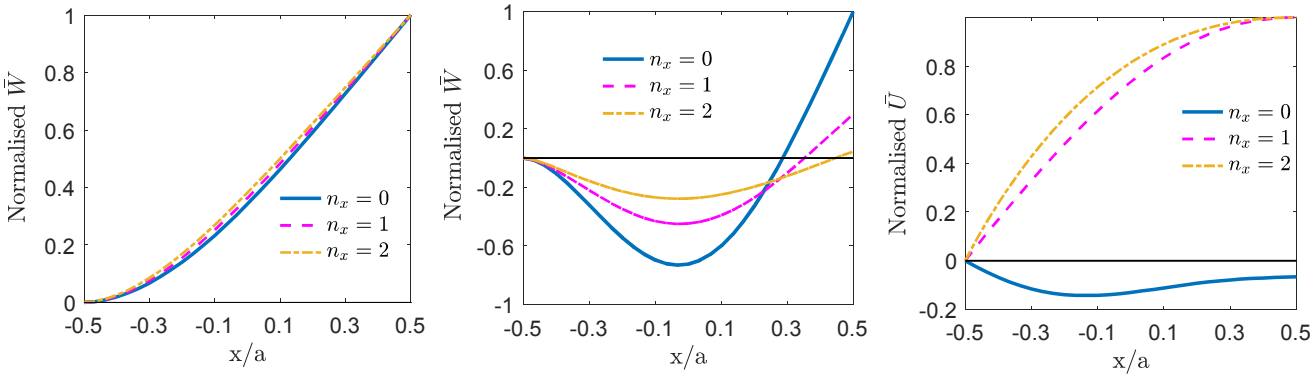

Mode 1 *Mode 2(i)* *Mode 2(ii)*

b. C-F beams

Fig. 4. 9: Effect of the axial exponential index to the vibration mode shapes of BDFG beams (a/h=5, h/l=2, n_z=2).

Finally, the effect of n_x in the mode shapes of several BCs is revealed in Fig. 4.9 with n_z equal to 2. For the C-C beams, the mode shapes are not symmetric for non-zero n_x, where the maximum modal displacement is seen on the left half. For the F-C beams, in which the maximum

displacement occurs at the tip, the small relative magitudes are seen on other points. In addition, the second mode is the flexural mode for through-the-thickness FG beams (n_x=0); however, the axial one for BDFG beams ($n_x \neq 0$).

4.6 Concluding remarks

In this chapter, state-space based solutions are presented for the free vibration behaviour of conventional and BDFG microbeams under arbitrary boundary conditions. Based on the Hamilton's principle and the modified couple stress theory, the governing equations of motion are developed for the quasi-3D theory. The natural frequencies are obtained via an iteration procedure and the corresponding mode shapes are outlined by the singular value decomposition. It is concluded that both the natural frequencies and mode shapes are extensively different between the BDFG macro and microbeams, emphasizing the need of employing the non-classical continua for small-scale structures. The inclusion of the size effect results in a considerable increase in the bending stiffness and the switching between flexural and axial modes. It is also worth noting that due to the asymmetric along the length, the employing of BCs in analysing the BDFG beams needs to perform with the clarification of the left and right ends.

CHAPTER 5

STATIC, FREE VIBRATION AND BUCKLING BEHAVIOURS OF FG-SANDWICH PLATES UNDER MECHANICAL AND THERMAL LOADS

5.1 Introduction

In this section, the review is focused on the development of the MCST for plates based on the classical plate theory (CPT), first-order shear deformation theory (FSDT) and higher-order shear deformation theory (HSDT). Following the theory of the CPT, Tsiatas [141] analysed the bending behaviours of plates with arbitrary shape for the first time. Yin [142] and Jomehzadeh et al. [143] then extended this model for the vibration behaviour of simply support plates [142] and other boundary conditions (BCs) using Levy-type solution [143]. Akgoz and Civalek [144] investigated the size effect on the free vibration of single-layered graphene sheets embedded in an elastic matrix with simply supported conditions. Akgoz and Civalek [145] also included the elastic medium in analysing the static, vibration and buckling behaviours of isotropic microplates. Using extended Kantorovich method, Askari and Tahani [146] obtained the closed-form solutions for free vibration of clamped plates. Simsek et al. [147] examined the size effect on the forced vibration of isotropic plates subject to a moving load. The implicit time integration method of Newmark was applied for the dynamic responses of microplates under various BCs. Asghari [148] developed the formulation for the geometrically nonlinear analysis of microplates with arbitrary shapes. Wang et al. [149, 150] presented a nonlinear model to investigate the size effect on the free vibration [149] and bending behaviours [150] of circular plates. Farokhi and Ghayesh [151] also developed a nonlinear model for the dynamic analysis of isotropic plates which included the initial geometric imperfections. The CPT based MCST was also employed to FG microplates. Ke et al. [152] investigated the static bending, free vibration and buckling behaviours of FG annular microplates with various BCs. The formulations for arbitrary shape and free vibration of FG rectangular microplates were examined by Asghari and Taati [153]. Geometric nonlinearity was considered in Taati's work [154] for buckling and post-buckling behaviours of FG microplates under different BCs using analytical solutions. To overcome the limitation of the CPT, FSDT was proposed by assuming the in-plane displacements vary linearly through the thickness. Thus, a shear correction factor was necessary. Based on the FSDT, Ma et al. [155] presented the closed-form solutions for bending and free vibration problems of simply supported plates for isotropic microplates. Ke et al. [156] employed the *p* version Ritz method for natural frequencies of plates with simply supported and clamped BCs. Roque et al. [157] presented numerical solutions of the MCST coupled with the FSDT model for the static bending analysis of isotropic microplates using

the meshless collocation method with radial basis functions. Regarding the FG microplates, analytical solutions were developed by Thai and Choi [158] for the linear and nonlinear bending, vibration and buckling analysis of simply supported FG microplates. Jung et al. [159, 160] included the elastic foundation in the behaviour of FG microplates. Ansari et al. [161, 162] also developed a nonlinear model for the vibration, bending and post-buckling analysis of FG microplates. In order to eliminate the use of the shear correction factor and obtain a better prediction of responses for thick plates, several HSDTs have been proposed. The MCST based on the third-order shear deformation theory (TSDT) was first developed by Gao et al. [163] for the deflections and natural frequencies of simply supported isotropic plates. These models were applied to investigate bending and free vibration behaviours of FG microplates by Thai and Kim [164] using analytical solutions and annular/circular microplates by Eshraghi [165] using the differential quadrature (DQ) method. Thai and Vo [166] developed a MCST sinusoidal theory for FG microplates and derived analytical solutions for deflections and natural frequencies of simply supported microplates. He et al. [167] presented a MCST four-variable refined plate model using analytical solution for the FG microplates. Lou et al. [168] then developed this model for a unified framework including the von Karman's geometric nonlinearity. It should be noted that in the above studies [26-30], the normal strain or normal deformation, which becomes significant for thick plates, was not included. In order to take into account both shear and normal deformation effects, Nguyen et al. [169] presented a four-variable quasi-3D model to analyse the bending, vibration and buckling behaviours of FG microplates using the isogeometric analysis.

Effect of thermal environment on behaviour of FG microstructures also has been reported in some publications. Reddy and Kim [170] developed theoretical formulation for mechanical and thermal analysis with a general nonlinear model containing cubic and quadratic variations of the in-plane and transverse displacements for FG microplates. They also derived the linear analytical solutions of bending, vibration and buckling behaviours for this model under mechanical loads [171]. Mirsalehi et al. [172] investigated the stability of thin FG microplates under mechanical and thermal loads using CPT based on the spline finite strip method. Using CPT, Ashoori and Vanini [173] also studied thermal buckling of annular FG microplates resting on an elastic medium accounting for geometrically nonlinear effect and snap-through behaviour. Ashoori and Sadough Vanini [174] extended their work [173] to account for geometric nonlinearity on thermal buckling of circular FG microplates. Utilising the DQ method, Eshaghi et al. [175] analysed static bending and free vibration responses of FG annular/circular plates based on the CPT, FSDT and HSDT models.

Based on the MCST, this chapter presents the quasi-3D models for the bending, free vibration and buckling behaviours of FG-sandwich microplates. In the first part, the framework of the MCST is presented to analyse the behaviours of simply supported plates utilising the Navier solution. The refined plate model, which is obtained by degenerating the thickness stretching effect, is applied to examine the difference between the HSDT and quasi-3D solutions. The unified temperature profile is applied to describe the uniform and linear distribution through the thickness. In the second part, the HSDT model is regenerated with more attention to the essential and natural BCs and the numerical results are obtained from the state space based solution for various BCs. The effects of geometries and power-law index along with mechanical loads and various temperature distributions on the size-dependent behaviours of FG-sandwich microplates are also investigated.

5.2 Kinematics and constitutive relations

Consider a FG-sandwich plate with the coordinate and cross-section shown in Fig. 5.1. By applying the MCST, the variation of strain energy is related to both strain and curvature tensors as [36]:

$$\delta\Pi=\int_V\left(\boldsymbol{\sigma}\delta\boldsymbol{\varepsilon}+\mathbf{m}\delta\boldsymbol{\chi}\right)dV \tag{5. 1}$$

where $\boldsymbol{\varepsilon}$ and $\boldsymbol{\chi}$ are the strain and symmetric curvature tensor defined by:

$$\boldsymbol{\varepsilon}=\frac{1}{2}\left(\nabla\mathbf{u}+\left(\nabla\mathbf{u}\right)^T\right) \tag{5. 2a}$$

$$\boldsymbol{\chi}=\frac{1}{2}\left(\nabla\boldsymbol{\theta}+\left(\nabla\boldsymbol{\theta}\right)^T\right) \tag{5. 2b}$$

$\boldsymbol{\sigma}$ and $\mathbf{m}$ are the corresponding stress and deviatoric part of the symmetric couple stress tensors defined by:

$$\boldsymbol{\sigma}=\lambda tr\left(\boldsymbol{\varepsilon}\right)\mathbf{I}+2\mu\boldsymbol{\varepsilon} \tag{5. 3a}$$

$$\mathbf{m}=2l^2\mu\boldsymbol{\chi} \tag{5. 3b}$$

in which, $\lambda=\dfrac{E\nu}{\left(1+\nu\right)\left(1-2\nu\right)}$ and $\mu=\dfrac{E}{2\left(1+\nu\right)}$ are Lame's constants, l is the material length scale parameter [36], $\mathbf{u}=\left(u_1,u_2,u_3\right)$ and $\boldsymbol{\theta}=\left(\theta_x,\theta_y,\theta_z\right)$ are the displacement and rotation vectors expressed below.

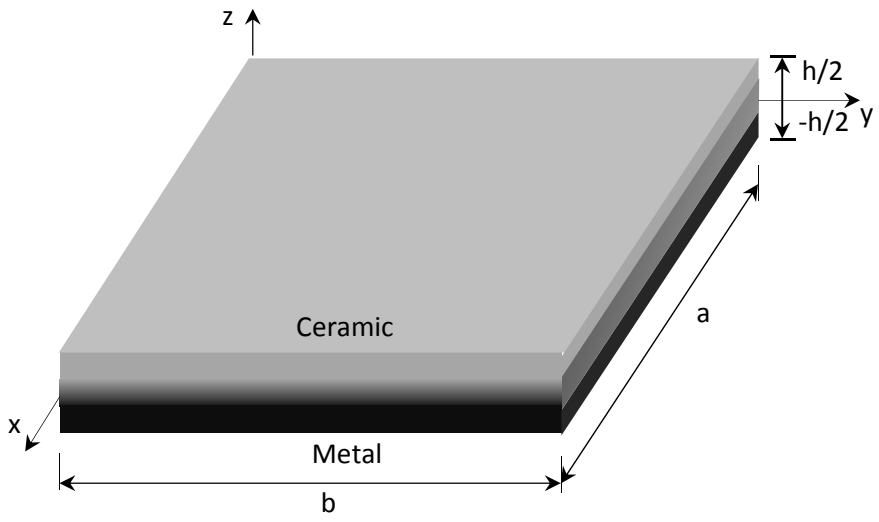

Fig. 5. 1: Geometries and co-ordinate of FG-sandwich plates.

The displacement field which includes the normal stretching effect is assumed to an arbitrary point as:

$$u_1(x,y,z,t)=U(x,y,t)-z\frac{\partial W_b(x,y,t)}{\partial x}-f(z)\frac{\partial W_s(x,y,t)}{\partial x} \tag{5. 4a}$$

$$u_2(x,y,z,t)=V(x,y,t)-z\frac{\partial W_b(x,y,t)}{\partial y}-f(z)\frac{\partial W_s(x,y,t)}{\partial y} \tag{5. 4b}$$

$$u_3(x,y,z,t)=W_b(x,y,t)+W_s(x,y,t)+g(z)W_z(x,y,t) \tag{5. 4c}$$

where U and V are in-plane displacements, W_b, W_s and W_z are bending, shear and stretching displacements of a point on the middle plane. $f(z)$ and $g(z)=1-\frac{df(z)}{dz}$ are the shape functions which distribute the effect of W_s and W_z across the thickness. Two sets of shape functions are applied [119, 176, 177]:

Third-order shear deformation theory (TSDT): $f(z)=\frac{4}{3}\frac{z^3}{h^2}$ (5. 5a)

Sinusoidal shear deformation theory (SSDT): $f(z)=z-\frac{h}{\pi}\sin\frac{\pi z}{h}$ (5. 5b)

The rotation vector is expressed as:

$$\boldsymbol{\theta}=\frac{1}{2}curl\,\mathbf{u}=\frac{1}{2}\left[\left(\frac{\partial u_3}{\partial y}-\frac{\partial u_2}{\partial z}\right)\mathbf{e}_x+\left(\frac{\partial u_1}{\partial z}-\frac{\partial u_3}{\partial x}\right)\mathbf{e}_y+\left(\frac{\partial u_2}{\partial x}-\frac{\partial u_1}{\partial y}\right)\mathbf{e}_z\right] \tag{5. 6a}$$

$$\theta_x = \frac{1}{2} curl\ \mathbf{u}\big|_{\mathbf{e}_x} = \frac{\partial W_b}{\partial y} + \frac{1}{2}\left(1 + \frac{\partial f(z)}{\partial z}\right)\frac{\partial W_s}{\partial y} + \frac{1}{2} g(z)\frac{\partial W_z}{\partial y} \tag{5. 6b}$$

$$\theta_y = \frac{1}{2} curl\,\mathbf{u}\big|_{\mathbf{e}_y} = -\frac{\partial W_b}{\partial x} - \frac{1}{2}\left(1 + \frac{\partial f(z)}{\partial z}\right)\frac{\partial W_s}{\partial x} - \frac{1}{2} g(z)\frac{\partial W_z}{\partial x} \tag{5. 6c}$$

$$\theta_z = \frac{1}{2} curl\ \mathbf{u}\big|_{\mathbf{e}_z} = \frac{1}{2}\left(\frac{\partial \mathrm{V}}{\partial x} - \frac{\partial \mathrm{U}}{\partial y}\right) \tag{5. 6d}$$

The strain components related to above displacement field are presented by substituting Eq. (5.4) to Eq. (5.2a):

$$\varepsilon_{xx} = \frac{\partial U}{\partial x} - z\frac{\partial^2 W_b}{\partial x^2} - f(z)\frac{\partial^2 W_s}{\partial x^2} - \alpha(z,T)\Delta T(x,y,z) \tag{5. 7a}$$

$$\varepsilon_{yy} = \frac{\partial V}{\partial y} - z\frac{\partial^2 W_b}{\partial y^2} - f(z)\frac{\partial^2 W_s}{\partial y^2} - \alpha(z,T)\Delta T(x,y,z) \tag{5. 7b}$$

$$\varepsilon_{zz} = \frac{\partial g(z)}{\partial z} W_z - \alpha(z,T)\Delta T(x,y,z) \tag{5. 7c}$$

$$\gamma_{xy} = 2\varepsilon_{xy} = \frac{\partial U}{\partial y} + \frac{\partial V}{\partial x} - 2z\frac{\partial^2 W_b}{\partial x \partial y} - 2f(z)\frac{\partial^2 W_s}{\partial x \partial y} \tag{5. 7d}$$

$$\gamma_{xz} = 2\varepsilon_{xz} = g(z)\left(\frac{\partial W_s}{\partial x} + \frac{\partial W_z}{\partial x}\right) \tag{5. 7e}$$

$$\gamma_{yz} = 2\varepsilon_{yz} = g(z)\left(\frac{\partial W_s}{\partial y} + \frac{\partial W_z}{\partial y}\right) \tag{5. 7f}$$

and the curvature tensor is given by substituting Eq. (5.4) into Eq. (5.6) and the resulting expression to Eq. (5.2b):

$$\chi_{xx} = \frac{\partial^2 W_b}{\partial y \partial x} + \frac{1}{2}\left(1 + \frac{\partial f(z)}{\partial z}\right)\frac{\partial^2 W_s}{\partial y \partial x} + \frac{1}{2} g(z)\frac{\partial^2 W_z}{\partial y \partial x} \tag{5. 8a}$$

$$\chi_{yy} = -\frac{\partial^2 W_b}{\partial x \partial y} - \frac{1}{2}\left(1 + \frac{\partial f(z)}{\partial z}\right)\frac{\partial^2 W_s}{\partial x \partial y} - \frac{1}{2} g(z)\frac{\partial^2 W_z}{\partial x \partial y} \tag{5. 8b}$$

$$\chi_{zz} = 0 \tag{5. 8c}$$

$$\chi_{xy} = \frac{1}{2}\left[\frac{\partial^2 W_b}{\partial y^2} - \frac{\partial^2 W_b}{\partial x^2} + \frac{1}{2}\left(1 + \frac{\partial f(z)}{\partial z}\right)\left(\frac{\partial^2 W_s}{\partial y^2} - \frac{\partial^2 W_s}{\partial x^2}\right) + \frac{1}{2} g(z)\left(\frac{\partial^2 W_z}{\partial y^2} - \frac{\partial^2 W_z}{\partial x^2}\right)\right] \tag{5. 8d}$$

$$\chi_{xz}=\frac{1}{4}\left[\frac{\partial^2 \mathrm{V}}{\partial x^2}-\frac{\partial^2 \mathrm{U}}{\partial x\partial y}+\frac{\partial^2 f(z)}{\partial z^2}\frac{\partial W_s}{\partial y}+\frac{\partial g(z)}{\partial z}\frac{\partial W_z}{\partial y}\right] \tag{5. 8e}$$

$$\chi_{yz}=\frac{1}{4}\left[\frac{\partial^2 \mathrm{V}}{\partial x\partial y}-\frac{\partial^2 \mathrm{U}}{\partial y^2}-\frac{\partial^2 f(z)}{\partial z^2}\frac{\partial W_s}{\partial x}-\frac{\partial g(z)}{\partial z}\frac{\partial W_z}{\partial x}\right] \tag{5. 8f}$$

Substituting Eqs. (5.7) and (5.8) to Eq. (5.3), the thermal strain, stress and deviatoric part of couple stress tensors are obtained, respectively:

$$\begin{Bmatrix}\sigma_{xx}\\ \sigma_{yy}\\ \sigma_{zz}\\ \sigma_{xz}\\ \sigma_{yz}\\ \sigma_{xy}\end{Bmatrix}=\begin{bmatrix}Q_{11} & Q_{12} & Q_{13} & 0 & 0 & 0\\ & Q_{22} & Q_{23} & 0 & 0 & 0\\ & & Q_{33} & 0 & 0 & 0\\ & & & Q_{44} & 0 & 0\\ & & & & Q_{55} & 0\\ sym. & & & & & Q_{66}\end{bmatrix}\begin{Bmatrix}\frac{\partial U}{\partial x}-z\frac{\partial^2 W_b}{\partial x^2}-f\frac{\partial^2 W_s}{\partial x^2}-\alpha\Delta T(x,y,z)\\ \frac{\partial V}{\partial y}-z\frac{\partial^2 W_b}{\partial y^2}-f\frac{\partial^2 W_s}{\partial y^2}-\alpha\Delta T(x,y,z)\\ \frac{\partial g}{\partial z}W_z-\alpha\Delta T(x,y,z)\\ g\left(\frac{\partial W_s}{\partial x}+\frac{\partial W_z}{\partial x}\right)\\ g\left(\frac{\partial W_s}{\partial y}+\frac{\partial W_z}{\partial y}\right)\\ \frac{\partial U}{\partial y}+\frac{\partial V}{\partial x}-2z\frac{\partial^2 W_b}{\partial x\partial y}-2f\frac{\partial^2 W_s}{\partial x\partial y}\end{Bmatrix} \tag{5. 9a}$$

$$\begin{Bmatrix}m_{xx}\\ m_{yy}\\ m_{zz}\\ m_{xz}\\ m_{yz}\\ m_{xy}\end{Bmatrix}=2l^2\mu\begin{Bmatrix}\frac{\partial^2 W_b}{\partial y\partial x}+\frac{1}{2}\left(1+\frac{\partial f}{\partial z}\right)\frac{\partial^2 W_s}{\partial y\partial x}+\frac{1}{2}g\frac{\partial^2 W_z}{\partial y\partial x}\\ -\frac{\partial^2 W_b}{\partial x\partial y}-\frac{1}{2}\left(1+\frac{\partial f}{\partial z}\right)\frac{\partial^2 W_s}{\partial x\partial y}-\frac{1}{2}g\frac{\partial^2 W_z}{\partial x\partial y}\\ 0\\ \frac{1}{4}\left(\frac{\partial^2 \mathrm{V}}{\partial x^2}-\frac{\partial^2 \mathrm{U}}{\partial x\partial y}+\frac{\partial^2 f}{\partial z^2}\frac{\partial W_s}{\partial y}+\frac{\partial g}{\partial z}\frac{\partial W_z}{\partial y}\right)\\ \frac{1}{4}\left(\frac{\partial^2 \mathrm{V}}{\partial x\partial y}-\frac{\partial^2 \mathrm{U}}{\partial y^2}-\frac{\partial^2 f}{\partial z^2}\frac{\partial W_s}{\partial x}-\frac{\partial g}{\partial z}\frac{\partial W_z}{\partial x}\right)\\ \frac{1}{2}\left[\frac{\partial^2 W_b}{\partial y^2}-\frac{\partial^2 W_b}{\partial x^2}+\frac{1}{2}\left(1+\frac{\partial f}{\partial z}\right)\left(\frac{\partial^2 W_s}{\partial y^2}-\frac{\partial^2 W_s}{\partial x^2}\right)+\frac{1}{2}g\left(\frac{\partial^2 W_z}{\partial y^2}-\frac{\partial^2 W_z}{\partial x^2}\right)\right]\end{Bmatrix} \tag{5. 9b}$$

where Q_{ij} for 2D and quasi-3D models are presented below, respectively:

$$\left[Q_{ii},Q_{ij}\right]=\left[Q_{ii}^{2D},Q_{ij}^{2D}\right]=\begin{cases}\left[\frac{E(z)}{1-\nu^2},\frac{E(z)\nu}{1-\nu^2}\right]\left(\overline{i,j}=\overline{1,3}\right)\\ \left[\frac{E(z)}{2(1+\nu)},0\right]\left(\overline{i,j}=\overline{4,6}\right)\end{cases} \tag{5. 10a}$$

$$\left[Q_{ii},Q_{ij}\right]=\left[Q_{ii}^{3D},Q_{ij}^{3D}\right]=\begin{cases}\left[\dfrac{E(z)[1-\nu]}{(1+\nu)(1-2\nu)},\dfrac{E(z)\nu}{(1+\nu)(1-2\nu)}\right] & \left(\overline{i,j}=\overline{1,3}\right)\\ \left[\dfrac{E(z)}{2(1+\nu)},0\right] & \left(\overline{i,j}=\overline{4,6}\right)\end{cases} \tag{5. 10b}$$

5.3 Variational formulation

The equations of motion are obtained from the Hamilton's principle, which states

$$\int_{t_1}^{t_2}\left(\delta K-\delta \mathrm{U}-\delta V\right)dt \tag{5. 11}$$

where $\delta \mathrm{U}$, δK and δV denote the variation of strain, kinetic energy and work done by external forces.

The variation of strain energy is rewritten in terms of mid-plane displacements as:

$$\delta \mathrm{U}=\int_{A}\int_{-h/2}^{h/2}\left(\sigma_{ij}\delta\varepsilon_{ij}+m_{ij}\delta\chi_{ij}\right)dzdA$$

$$=\int_{A}\int_{-h/2}^{h/2}\Big[\left(\sigma_{xx}\delta\varepsilon_{xx}+\sigma_{yy}\delta\varepsilon_{yy}+\sigma_{zz}\delta\varepsilon_{zz}+\sigma_{xz}\delta\gamma_{xz}+\sigma_{yz}\delta\gamma_{yz}+\sigma_{xy}\delta\gamma_{xy}\right)$$
$$+\left(m_{xx}\delta\chi_{xx}+m_{yy}\delta\chi_{yy}+m_{zz}\delta\chi_{zz}+2m_{xz}\delta\chi_{xz}+2m_{yz}\delta\chi_{yz}+2m_{xy}\delta\chi_{xy}\right)\Big]dzdA$$

$$=\int_{A}\Bigg[\left(N_{xx}\frac{\partial\delta U}{\partial x}-M_{xx}\frac{\partial^2\delta W_b}{\partial x^2}-P_{xx}\frac{\partial^2\delta W_s}{\partial x^2}\right)+\left(N_{yy}\frac{\partial\delta V}{\partial y}-M_{yy}\frac{\partial^2\delta W_b}{\partial y^2}-P_{yy}\frac{\partial^2\delta W_s}{\partial y^2}\right)+O_{zz}\delta W_z$$
$$+Q_{xz}\left(\frac{\partial\delta W_s}{\partial x}+\frac{\partial\delta W_z}{\partial x}\right)+Q_{yz}\left(\frac{\partial\delta W_s}{\partial y}+\frac{\partial\delta W_z}{\partial y}\right)+N_{xy}\left(\frac{\partial\delta U}{\partial y}+\frac{\partial\delta V}{\partial x}\right)-2M_{xy}\frac{\partial^2\delta W_b}{\partial x\partial y}-2P_{xy}\frac{\partial^2\delta W_s}{\partial x\partial y}$$
$$+R_{xx}\left(\frac{\partial^2\delta W_b}{\partial x\partial y}+\frac{1}{2}\frac{\partial^2\delta W_s}{\partial x\partial y}\right)+\frac{1}{2}\left(S_{xx}-S_{yy}\right)\frac{\partial^2\delta W_s}{\partial x\partial y}+\frac{1}{2}\left(T_{xx}-T_{yy}\right)\frac{\partial^2\delta W_z}{\partial x\partial y}-R_{yy}\left(\frac{\partial^2\delta W_b}{\partial x\partial y}+\frac{1}{2}\frac{\partial^2\delta W_s}{\partial x\partial y}\right)$$
$$+\frac{1}{2}R_{xz}\left(\frac{\partial^2 V}{\partial x^2}-\frac{\partial^2 U}{\partial x\partial y}\right)+\frac{1}{2}R_{yz}\left(\frac{\partial^2 V}{\partial x\partial y}-\frac{\partial^2 U}{\partial y^2}\right)+\frac{1}{2}X_{xz}\left(\frac{\partial W_s}{\partial y}+\frac{\partial W_z}{\partial y}\right)-\frac{1}{2}X_{yz}\left(\frac{\partial W_s}{\partial x}+\frac{\partial W_z}{\partial x}\right)$$

$$+\frac{1}{2}R_{xy}\left(\frac{\partial^2 W_b}{\partial y^2}-\frac{\partial^2 W_b}{\partial x^2}+\frac{\partial^2 W_s}{\partial y^2}-\frac{\partial^2 W_s}{\partial x^2}\right)+\frac{1}{2}S_{xy}\left(\frac{\partial^2 W_s}{\partial y^2}-\frac{\partial^2 W_s}{\partial x^2}\right)+\frac{1}{2}T_{xy}\left(\frac{\partial^2 W_z}{\partial y^2}-\frac{\partial^2 W_z}{\partial x^2}\right)\Bigg]dA \tag{5. 12}$$

where the stress resultants are expressed as:

$$\left(N_{ij},M_{ij},P_{ij},Q_{ij},O_{ij}\right)=\int_{-h/2}^{h/2}\left[1,z,f(z),g(z),\frac{\partial g(z)}{\partial z}\right]\sigma_{ij}dz-\left(N_{ij}^{T},M_{ij}^{T},P_{ij}^{T},0,O_{ij}^{T}\right) \tag{5. 13a}$$

$$\left(R_{ij},S_{ij},T_{ij},X_{ij}\right)=\int_{-h/2}^{h/2}\left[1,\frac{\partial f(z)}{\partial z},g(z),\frac{\partial^2 f(z)}{\partial z^2}\right]m_{ij}dz \tag{5. 13b}$$

where

$$\left(N_{ij}^{T},M_{ij}^{T},P_{ij}^{T},O_{ij}^{T}\right)=\int_{-h/2}^{h/2}\left[1,z,f\left(z\right),\frac{\partial g\left(z\right)}{\partial z}\right]\left(Q_{ii}+2Q_{ij}\right)\alpha\left(z,T\right)\Delta T\left(z\right)dz,\left(\overline{i,j}=\overline{1,3}\right) \tag{5. 14}$$

Substituting Eqs. (5.9), (5.10) and (5.14) into Eq. (5.13), the stress resultants can be described in terms of mid-plane displacements as in Appendix B.

The variation of the work done by transverse load *q* and in-plane load *P(w)* is presented as:

$$\delta V=-\int_{A}\left\{\left[P_{x}^{0}\frac{\partial\left(W_{b}+W_{s}\right)}{\partial x}+P_{y}^{0}\frac{\partial\left(W_{b}+W_{s}\right)}{\partial y}\right]\delta\left(W_{b}+W_{s}\right)\right.$$

$$\left.+P_{xy}^{0}\left[\frac{\partial\left(W_{b}+W_{s}\right)}{\partial x}\frac{\partial\delta\left(W_{b}+W_{s}\right)}{\partial y}+\frac{\partial\left(W_{b}+W_{s}\right)}{\partial y}\frac{\partial\delta\left(W_{b}+W_{s}\right)}{\partial x}\right]+q\delta\left(W_{b}+W_{s}+gW_{z}\right)\right\}dA \tag{5. 15}$$

The variation of kinetic energy is presented by:

$$\delta K=\int_{A}\int_{-h/2}^{h/2}\rho\left(z\right)\left(\dot{u}_{1}\delta\dot{u}_{1}+\dot{u}_{2}\delta\dot{u}_{2}+\dot{u}_{3}\delta\dot{u}_{3}\right)dzdA$$

$$=\int_{A}\left\{I_{0}\left[\dot{U}\delta\dot{U}+\dot{V}\delta\dot{V}+\left(\dot{W}_{b}+\dot{W}_{s}\right)\delta\left(\dot{W}_{b}+\dot{W}_{s}\right)\right]+J_{0}\left[\left(\dot{W}_{b}+\dot{W}_{s}\right)\delta\dot{W}_{z}+\dot{W}_{z}\delta\left(\dot{W}_{b}+\dot{W}_{s}\right)\right]\right.$$

$$-I_{1}\left(\dot{U}\frac{\partial\delta\dot{W}_{b}}{\partial x}+\frac{\partial\dot{W}_{s}}{\partial x}\delta\dot{U}+\dot{V}\frac{\partial\delta\dot{W}_{b}}{\partial y}+\frac{\partial\dot{W}_{b}}{\partial y}\delta\dot{V}\right)+I_{2}\left(\frac{\partial\dot{W}_{b}}{\partial x}\frac{\partial\delta\dot{W}_{b}}{\partial x}+\frac{\partial\dot{W}_{b}}{\partial y}\frac{\partial\delta\dot{W}_{b}}{\partial y}\right)$$

$$-J_{1}\left(\dot{U}\frac{\partial\delta\dot{W}_{s}}{\partial x}+\frac{\partial\dot{W}_{s}}{\partial x}\delta\dot{U}+\dot{V}\frac{\partial\delta\dot{W}_{s}}{\partial y}+\frac{\partial\dot{W}_{s}}{\partial y}\delta\dot{V}\right)+K_{2}\left(\frac{\partial\dot{W}_{s}}{\partial x}\frac{\partial\delta\dot{W}_{s}}{\partial x}+\frac{\partial\dot{W}_{s}}{\partial y}\frac{\partial\delta\dot{W}_{s}}{\partial y}\right)$$

$$\left.+J_{2}\left(\frac{\partial\dot{W}_{b}}{\partial x}\frac{\partial\delta\dot{W}_{s}}{\partial x}+\frac{\partial\dot{W}_{s}}{\partial x}\frac{\partial\delta\dot{W}_{b}}{\partial x}+\frac{\partial\dot{W}_{b}}{\partial y}\frac{\partial\delta\dot{W}_{s}}{\partial y}+\frac{\partial\dot{W}_{s}}{\partial y}\frac{\partial\delta\dot{W}_{b}}{\partial y}\right)+K_{0}\dot{W}_{z}\delta\dot{W}_{z}\right\}dA \tag{5. 16}$$

where $\left(I_{0},I_{1},I_{2},J_{0},J_{1},J_{2},K_{0},K_{2}\right)=\int_{-h/2}^{h/2}\left(1,z,z^{2},g\left(z\right),f\left(z\right),zf\left(z\right),g^{2}\left(z\right),f^{2}\left(z\right)\right)\rho\left(z\right)dz$ (5. 17)

Substituting Eqs. (5.12), (5.15) and (5.16) into Eq. (5.11), integrating by parts and gathering the coefficients of $\delta U,\delta V,\delta W_{b},\delta W_{s}$ and δW_{z}, the equations of motion can be obtained:

$$\frac{\partial N_{xx}}{\partial x}+\frac{\partial N_{xy}}{\partial y}+\frac{1}{2}\frac{\partial^{2}R_{xz}}{\partial x\partial y}+\frac{1}{2}\frac{\partial^{2}R_{yz}}{\partial y^{2}}=I_{0}\ddot{U}-I_{1}\frac{\partial\ddot{W}_{b}}{\partial x}-J_{1}\frac{\partial\ddot{W}_{s}}{\partial x} \tag{5. 18a}$$

$$\frac{\partial N_{yy}}{\partial y}+\frac{\partial N_{xy}}{\partial x}-\frac{1}{2}\frac{\partial^{2}R_{xz}}{\partial x^{2}}-\frac{1}{2}\frac{\partial^{2}R_{yz}}{\partial x\partial y}=I_{0}\ddot{V}-I_{1}\frac{\partial\ddot{W}_{b}}{\partial y}-J_{1}\frac{\partial\ddot{W}_{s}}{\partial y} \tag{5. 18b}$$

$$\frac{\partial^2 M_{xx}}{\partial x^2}+\frac{\partial^2 M_{yy}}{\partial y^2}+2\frac{\partial^2 M_{xy}}{\partial x\partial y}-\frac{\partial^2 R_{xx}}{\partial x\partial y}+\frac{\partial^2 R_{yy}}{\partial x\partial y}-\frac{\partial^2 R_{xy}}{\partial y^2}+\frac{\partial^2 R_{xy}}{\partial x^2}+P(w)+q$$

$$=I_0\left(\ddot{W}_b+\ddot{W}_s\right)+J_0\ddot{W}_z+I_1\left(\frac{\partial\ddot{U}}{\partial x}+\frac{\partial\ddot{V}}{\partial y}\right)-I_2\nabla^2\ddot{W}_b-J_2\nabla^2\ddot{W}_s \tag{5. 18c}$$

$$\frac{\partial^2 P_{xx}}{\partial x^2}+\frac{\partial^2 P_{yy}}{\partial y^2}+\frac{\partial Q_{yz}}{\partial y}+\frac{\partial Q_{xz}}{\partial x}+2\frac{\partial^2 P_{xy}}{\partial x\partial y}-\frac{1}{2}\frac{\partial^2 R_{xx}}{\partial x\partial y}-\frac{1}{2}\frac{\partial^2 S_{xx}}{\partial x\partial y}+\frac{1}{2}\frac{\partial^2 R_{yy}}{\partial x\partial y}+\frac{1}{2}\frac{\partial^2 S_{yy}}{\partial x\partial y}$$
$$+\frac{1}{2}\frac{\partial X_{xz}}{\partial y}-\frac{1}{2}\frac{\partial X_{yz}}{\partial x}-\frac{1}{2}\frac{\partial^2 R_{xy}}{\partial y^2}-\frac{1}{2}\frac{\partial^2 S_{xy}}{\partial y^2}+\frac{1}{2}\frac{\partial^2 R_{xy}}{\partial x^2}+\frac{1}{2}\frac{\partial^2 S_{xy}}{\partial x^2}+P(w)+q$$

$$=I_0\left(\ddot{W}_b+\ddot{W}_s\right)+J_0\ddot{W}_z+J_1\left(\frac{\partial\ddot{U}}{\partial x}+\frac{\partial\ddot{V}}{\partial y}\right)-J_2\nabla^2\ddot{W}_b-K_2\nabla^2\ddot{W}_s \tag{5. 18d}$$

$$-O_{zz}+\frac{\partial Q_{xz}}{\partial x}+\frac{\partial Q_{yz}}{\partial y}-\frac{1}{2}\frac{\partial^2 T_{xx}}{\partial x\partial y}+\frac{1}{2}\frac{\partial^2 T_{yy}}{\partial x\partial y}-\frac{1}{2}\frac{\partial X_{xz}}{\partial y}+\frac{1}{2}\frac{\partial X_{yz}}{\partial x}-\frac{1}{2}\frac{\partial^2 T_{xy}}{\partial y^2}+\frac{1}{2}\frac{\partial^2 T_{xy}}{\partial x^2}+gq$$

$$=J_0\left(\ddot{W}_b+\ddot{W}_s\right)+K_0\ddot{W}_z \tag{5. 18e}$$

where $\nabla^2=\frac{\partial^2}{\partial x^2}+\frac{\partial^2}{\partial y^2}$, $P(w)=P_x^0\frac{\partial^2\left(W_b+W_s\right)}{\partial x^2}+P_y^0\frac{\partial^2\left(W_b+W_s\right)}{\partial y^2}+2P_{xy}^0\frac{\partial^2\left(W_b+W_s\right)}{\partial x\partial y}$ (5. 19)

in which P_x^0, P_y^0 and P_{xy}^0 are the in-plane mechanical/thermal equivalent forces (in vibration and buckling analysis).

The governing equations are expressed in terms of displacements as:

$$A_{11}\frac{\partial^2 U}{\partial x^2}+A_{66}\frac{\partial^2 U}{\partial y^2}-\frac{1}{4}A_m\left(\frac{\partial^4 U}{\partial x^2\partial y^2}+\frac{\partial^4 U}{\partial y^4}\right)+\left(A_{12}+A_{66}\right)\frac{\partial^2 V}{\partial x\partial y}+\frac{1}{4}A_m\left(\frac{\partial^4 V}{\partial x^3\partial y}+\frac{\partial^4 V}{\partial x\partial y^3}\right)$$

$$-B_{11}\frac{\partial^3 W_b}{\partial x^3}-\left(B_{12}+2B_{66}\right)\frac{\partial^3 W_b}{\partial x\partial y^2}-B_{11}^s\frac{\partial^3 W_s}{\partial x^3}-\left(B_{12}^s+2B_{66}^s\right)\frac{\partial^3 W_s}{\partial x\partial y^2}+K_{13}\frac{\partial W_z}{\partial x}-\frac{\partial N_{xx}^T}{\partial x}$$

$$=I_0\ddot{U}-I_1\frac{\partial\ddot{W}_b}{\partial x}-J_1\frac{\partial\ddot{W}_s}{\partial x} \tag{5. 20a}$$

$$A_{22}\frac{\partial^2 V}{\partial y^2}+A_{66}\frac{\partial^2 V}{\partial x^2}-\frac{1}{4}A_m\left(\frac{\partial^4 V}{\partial x^4}+\frac{\partial^4 V}{\partial x^2\partial y^2}\right)+\left(A_{12}+A_{66}\right)\frac{\partial^2 U}{\partial x\partial y}+\frac{1}{4}A_m\left(\frac{\partial^4 U}{\partial x^3\partial y}+\frac{\partial^4 U}{\partial x\partial y^3}\right)$$

$$-B_{22}\frac{\partial^3 W_b}{\partial y^3}-\left(B_{12}+2B_{66}\right)\frac{\partial^3 W_b}{\partial x^2\partial y}-B_{22}^s\frac{\partial^3 W_s}{\partial y^3}-\left(B_{12}^s+2B_{66}^s\right)\frac{\partial^3 W_s}{\partial x^2\partial y}+K_{23}\frac{\partial W_z}{\partial y}-\frac{\partial N_{yy}^T}{\partial y}$$

$$=I_0\ddot{V}-I_1\frac{\partial\ddot{W}_b}{\partial y}-J_1\frac{\partial\ddot{W}_s}{\partial y} \tag{5. 20b}$$

$$B_{11}\frac{\partial^3 U}{\partial x^3}+\left(B_{12}+2B_{66}\right)\frac{\partial^3 U}{\partial x\partial y^2}+\left(B_{12}+2B_{66}\right)\frac{\partial^3 V}{\partial x^2\partial y}+B_{22}\frac{\partial^3 V}{\partial y^3}-\left(D_{11}+A_m\right)\frac{\partial^4 W_b}{\partial x^4}$$
$$-\left(2D_{12}+4D_{66}+2A_m\right)\frac{\partial^4 W_b}{\partial x^2\partial y^2}-\left(D_{22}+A_m\right)\frac{\partial^4 W_b}{\partial y^4}-\left[D_{11}^s+\frac{1}{2}\left(A_m+B_m\right)\right]\frac{\partial^4 W_s}{\partial x^4}$$
$$-\left(2D_{12}^s+4D_{66}^s\right)\frac{\partial^4 W_s}{\partial x^2\partial y^2}-\left[D_{22}^s+\frac{1}{2}\left(A_m+B_m\right)\right]\frac{\partial^4 W_s}{\partial y^4}+L_{13}\frac{\partial^2 W_z}{\partial x^2}$$
$$+L_{23}\frac{\partial^2 W_z}{\partial y^2}-\frac{1}{2}E_m\frac{\partial^4 W_z}{\partial x^4}-\frac{1}{2}E_m\frac{\partial^4 W_z}{\partial y^4}+P\left(w\right)+q-\frac{\partial^2 M_{xx}^T}{\partial x^2}-\frac{\partial^2 M_{yy}^T}{\partial y^2}$$
$$=I_0\left(\ddot{W}_b+\ddot{W}_s\right)+I_1\left(\frac{\partial\ddot{U}}{\partial x}+\frac{\partial\ddot{V}}{\partial y}\right)-I_2\nabla^2\ddot{W}_b-J_2\nabla^2\ddot{W}_s+J_0\ddot{W}_z \tag{5. 20c}$$

$$B_{11}^s\frac{\partial^3 U}{\partial x^3}+\left(B_{12}^s+2B_{66}^s\right)\frac{\partial^3 U}{\partial x\partial y^2}+\left(B_{12}^s+2B_{66}^s\right)\frac{\partial^3 V}{\partial x^2\partial y}+B_{22}^s\frac{\partial^3 V}{\partial y^3}$$
$$-\left[D_{11}^s+\frac{1}{2}\left(A_m+B_m\right)\right]\frac{\partial^4 W_b}{\partial x^4}-\left(2D_{12}^s+4D_{66}^s\right)\frac{\partial^4 W_b}{\partial x^2\partial y^2}-\left[D_{22}^s+\frac{1}{2}\left(A_m+B_m\right)\right]\frac{\partial^4 W_b}{\partial y^4}$$
$$+\left(A_{55}^s+\frac{1}{4}H_m\right)\frac{\partial^2 W_s}{\partial x^2}+\left(A_{44}^s+\frac{1}{4}H_m\right)\frac{\partial^2 W_s}{\partial y^2}-\left[H_{11}+\frac{1}{4}\left(A_m+2B_m+C_m\right)\right]\frac{\partial^4 W_s}{\partial x^4}$$
$$-\left(2H_{12}+4H_{66}\right)\frac{\partial^4 W_s}{\partial x^2\partial y^2}-\left[H_{22}+\frac{1}{4}\left(A_m+2B_m+C_m\right)\right]\frac{\partial^4 W_s}{\partial y^4}$$
$$+\left(L_{13}^s+A_{55}^s-\frac{1}{4}H_m\right)\frac{\partial^2 W_z}{\partial x^2}+\left(L_{23}^s+A_{44}^s-\frac{1}{4}H_m\right)\frac{\partial^2 W_z}{\partial y^2}-\frac{1}{4}\left(D_m+E_m\right)\left(\frac{\partial^4 W_z}{\partial x^4}+\frac{\partial^4 W_z}{\partial y^4}\right)$$

$$+P\left(w\right)+q-\frac{\partial^2 P_{xx}^T}{\partial x^2}-\frac{\partial^2 P_{yy}^T}{\partial y^2}=I_0\left(\ddot{W}_b+\ddot{W}_s\right)+J_1\left(\frac{\partial\ddot{U}}{\partial x}+\frac{\partial\ddot{V}}{\partial y}\right)-J_2\nabla^2\ddot{W}_b-K_2\nabla^2\ddot{W}_s+J_0\ddot{W}_z \tag{5. 20d}$$

$$-K_{13}\frac{\partial U}{\partial x}-K_{23}\frac{\partial V}{\partial y}+L_{13}\frac{\partial^2 W_b}{\partial x^2}+L_{23}\frac{\partial^2 W_b}{\partial y^2}-\frac{1}{2}E_m\frac{\partial^4 W_b}{\partial x^4}-\frac{1}{2}E_m\frac{\partial^4 W_b}{\partial y^4}$$
$$+\left(L_{13}^s+A_{55}^s-\frac{1}{4}H_m\right)\frac{\partial^2 W_s}{\partial x^2}+\left(L_{23}^s+A_{44}^s-\frac{1}{4}H_m\right)\frac{\partial^2 W_s}{\partial y^2}-\frac{1}{4}\left(E_m+D_m\right)\frac{\partial^4 W_s}{\partial x^4}$$
$$-\frac{1}{4}\left(E_m+D_m\right)\frac{\partial^4 W_s}{\partial y^4}-Z_{33}W_z+\left(A_{55}^s+\frac{1}{4}H_m\right)\frac{\partial^2 W_z}{\partial x^2}$$

$$+\left(A_{44}^s+\frac{1}{4}H_m\right)\frac{\partial^2 W_z}{\partial y^2}-\frac{1}{4}F_m\left(\frac{\partial^4 W_z}{\partial x^4}+\frac{\partial^4 W_z}{\partial y^4}\right)+gq+O_{zz}^T=J_0\left(\ddot{W}_b+\ddot{W}_s\right)+K_0\ddot{W}_z \tag{5. 20e}$$

5.4 Static, free vibration and buckling behaviours of simply supported FG-sandwich plates under mechanical and thermal loads

5.4.1 Navier solution

Based on the Navier approach, the displacements are expressed in terms of Fourier series as:

$$U\left(x,y\right)=\sum_{n=1}^{\infty}\sum_{m=1}^{\infty}U_{mn}\cos\alpha x\sin\beta y \tag{5. 21a}$$

$$V(x,y)=\sum_{n=1}^{\infty}\sum_{m=1}^{\infty}V_{mn}\sin\alpha x\cos\beta y \tag{5. 21b}$$

$$W_b(x,y)=\sum_{n=1}^{\infty}\sum_{m=1}^{\infty}W_{bmn}\sin\alpha x\sin\beta y \tag{5. 21c}$$

$$W_s(x,y)=\sum_{n=1}^{\infty}\sum_{m=1}^{\infty}W_{smn}\sin\alpha x\sin\beta y \tag{5. 21d}$$

$$W_z(x,y)=\sum_{n=1}^{\infty}\sum_{m=1}^{\infty}W_{zmn}\sin\alpha x\sin\beta y \tag{5. 21e}$$

where $\alpha=m\pi/a,\beta=n\pi/b$ and $(U_{nm},V_{nm},W_{bnm},W_{snm},W_{znm})$ are coefficients. Similarly, mechanical loads and temperature are expanded as:

$$q(x,y)=\sum_{n=1}^{\infty}\sum_{m=1}^{\infty}q_{mn}\sin\alpha x\sin\beta y \tag{5. 22a}$$

$$\Delta T_i(x,y)=\sum_{n=1}^{\infty}\sum_{m=1}^{\infty}\Delta T_{imn}\sin\alpha x\sin\beta y,(i=1,2) \tag{5. 22b}$$

and

$$(q_{mn},\Delta T_{imn})=(q_0,\Delta T_i)\text{ for sinusoidally distributed loads} \tag{5. 23a}$$

$$(q_{mn},\Delta T_{imn})=\frac{16}{nm\pi^2}(q_0,\Delta T_i)\text{ for uniformly distributed loads} \tag{5. 23b}$$

Substituting Eqs. (5.21) and (5.22) to Eq. (5.20), the governing equations can be rewritten as:

$$(k_{ij}-m_{ij}\omega^2)\{u_{jmn}\}=\{F_{jmn}\},\text{where } k_{ij}=k_{ji};m_{ij}=m_{ji}\left(\overline{i,j}=\overline{1,5}\right) \tag{5. 24}$$

where

$$k_{11}=-A_{11}\alpha^2-A_{66}\beta^2-\frac{1}{4}A_m(\alpha^2\beta^2+\beta^4);\ k_{12}=-(A_{12}+A_{66})\alpha\beta+\frac{1}{4}A_m(\alpha^3\beta+\alpha\beta^3);$$

$$k_{13}=B_{11}\alpha^3+(B_{12}+2B_{66})\alpha\beta^2;\ k_{14}=B_{11}^s\alpha^3+(B_{12}^s+2B_{66}^s)\alpha\beta^2;\ k_{15}=K_{13}\alpha$$

$$k_{22}=-A_{22}\beta^2-A_{66}\alpha^2-\frac{1}{4}A_m(\alpha^4+\alpha^2\beta^2);\ k_{23}=B_{22}\beta^3+(B_{12}+2B_{66})\alpha^2\beta;$$

$$k_{24}=B_{22}^s\beta^3+(B_{12}^s+2B_{66}^s)\alpha^2\beta;\ k_{25}=K_{23}\beta$$

$$k_{33}=-(D_{11}+A_m)\alpha^4-(2D_{12}+4D_{66}+2A_m)\alpha^2\beta^2-(D_{22}+A_m)\beta^4-(\alpha^2+\beta^2)P_0$$

$$k_{34}=-\left[D_{11}^{s}+\frac{1}{2}\left(A_m+B_m\right)\right]\alpha^4-\left[2D_{12}^{s}+4D_{66}^{s}+\left(A_m+B_m\right)\right]\alpha^2\beta^2-\left[D_{22}^{s}+\frac{1}{2}\left(A_m+B_m\right)\right]\beta^4$$
$$-\left(\alpha^2+\beta^2\right)P_0;\ k_{35}=-L_{13}\alpha^2-L_{23}\beta^2-\frac{1}{2}E_m\left(\alpha^2+\beta^2\right)^2$$

$$k_{44}=-\left(A_{55}^{s}-\frac{1}{4}H_m\right)\alpha^2-\left(A_{44}^{s}+\frac{1}{4}H_m\right)\beta^2-\left(H_{11}+\frac{1}{4}\left(A_m+2B_m+C_m\right)\right)\alpha^4-\left(2H_{12}+4H_{66}\right)\alpha^2\beta^2$$
$$-\left(H_{22}+\frac{1}{4}\left(A_m+2B_m+C_m\right)\right)\beta^4-\left(\alpha^2+\beta^2\right)P_0$$

$$k_{45}=-\left(L_{13}^{s}+A_{55}^{s}-\frac{1}{4}H_m\right)\alpha^2-\left(L_{23}^{s}+A_{44}^{s}-\frac{1}{4}H_m\right)\beta^2-\frac{1}{4}\left(D_m+E_m\right)\left(\alpha^2+\beta^2\right)^2$$

$$k_{55}=-Z_{33}-\left(A_{55}^{s}+\frac{1}{4}H_m\right)\alpha^2-\left(A_{44}^{s}+\frac{1}{4}H_m\right)\beta^2-\frac{1}{4}F_m\left(\alpha^2+\beta^2\right)^2 \tag{5. 25}$$

$$m_{11}=I_0;\ m_{13}=-I_1\alpha;\ m_{14}=-J_1\alpha;\ m_{22}=I_0;\ m_{23}=-I_1\beta;\ m_{24}=-J_1\beta$$

$$m_{33}=I_0+I_2\left(\alpha^2+\beta^2\right);\ m_{34}=I_0+J_2\left(\alpha^2+\beta^2\right);\ m_{35}=J_0$$

$$m_{44}=I_0+K_2\left(\alpha^2+\beta^2\right);\ m_{45}=J_0;\ m_{45}=K_0;\ m_{12}=m_{15}=m_{25}=0 \tag{5. 26}$$

$$F_j=\left\{F_1,F_2,F_3,F_4,F_5\right\}$$

$$F_1=-\alpha\left(A_t\Delta T_1+B_t\frac{\Delta T_2}{h}\right);\ F_2=-\beta\left(A_t\Delta T_1+B_t\frac{\Delta T_2}{h}\right);\ F_3=\left(\alpha^2+\beta^2\right)\left(B_t\Delta T_1+D_t\frac{\Delta T_2}{h}\right)$$

$$F_4=\left(\alpha^2+\beta^2\right)\left(B_t^{s}\Delta T_1+D_t^{s}\frac{\Delta T_2}{h}\right); \tag{5. 27}$$

For static analysis, the mid-plane displacements are simply calculated by $\left\{u_{jmn}\right\}=k_{ij}\setminus\left\{F_{jmn}\right\}$, where $(m,n)=(1,1)$ for the in-plane sinusoidal temperature and $(m,n)=\left(\overline{1-19},\overline{1-19}\right)$ for the in-plane uniform temperature. It should be noted that the increase of temperature results in the change of material properties and the thermal stress resultants, which leads to the forced vibration and nonlinear buckling analysis. In this chapter, only in-plane thermal resultant (axial force) is considered to solve the problems using eigenvalue algorithm. The thermal vibration and buckling behaviours are similar to mechanical behaviours with consideration paying to the temperature-dependent material properties. Therefore, a trial and error procedure is also needed to obtain the critical buckling temperatures.

5.4.2 Numerical examples

A slightly different version of this section has been published in Composites Part B: Engineering [178].

In this section, numerical investigations are carried out to study the bending, free vibration and buckling behaviours of FG-sandwich microplates under mechanical and thermal loads. First, verification is performed for microplates under mechanical loads and macroplates under thermal loads. Differences between constitutive relations as well as between the TSDT and SSDT are discussed. Parametric study is then carried out to investigate the thermal behaviours of FG-sandwich microplates. In the examples given, effects of geometric configurations and temperatures on microplates are examined using both 2D and quasi-3D models. Apart from the TID form, which is applied to verify the present solution, the TD form is considered in the rest of this chapter. Material properties for mechanical and TD coefficients for thermal analysis are presented in Tables 5.1 and 5.2. Non-dimensional expressions used in this section are as follow:

Bending:

Mechanical load:

$$\text{Deflection: } \bar{w}(z)=\frac{10E_c h^3}{q_0 a^4}u_3\left(\frac{a}{2},\frac{b}{2},z\right) \tag{5. 28}$$

$$\text{Stress: } \bar{\sigma}_{xx}=\frac{h\sigma_{xx}}{aq_0}\ \ \bar{\sigma}_{xz}=\frac{h\sigma_{xz}}{aq_0} \tag{5. 29}$$

Thermal load:

$$\text{Deflection: } \bar{w}(z)=\frac{h}{\alpha_0\Delta T_2 a^2}u_3\left(\frac{a}{2},\frac{b}{2},z\right) \tag{5. 30}$$

$$\text{Stress: } \bar{\sigma}_{xx}=\frac{h^2}{\alpha_0\Delta T_2 E_0 a^2}\sigma_{xx}\left(\frac{a}{2},\frac{b}{2},z\right) \tag{5. 31}$$

where E_0=1GPa, $\alpha_0=10^{-6}\ {}^0C^{-1}$

Vibration:

$$\hat{\omega}=\frac{\omega a^2}{h}\sqrt{\frac{\rho_c}{E_c}},\ \bar{\omega}=\frac{\omega a^2}{h}\sqrt{\frac{\rho_0\left(1-\nu_0^2\right)}{E_0}} \tag{5. 32}$$

Buckling:

$$\bar{P}_{cr}=P_{cr}\frac{a^2}{E_0 h^3} \tag{5. 33}$$

where E_0, ρ_0 and ν_0 are the Young's modulus, mass density and Poisson's ratio of metal at 300K.

Table 5. 1: Material properties of FG plates for mechanical and temperature-independent (TID) thermal analysis.

Material		Material properties			
		E (GPa)	ρ (kg/m^3)	α (1/K)	ν
Metal:	Ti–6A1–4V	66.2	-	10.3e-6	1/3
	Al	70	2700	-	0.3
	Mat_1	14.4	12200	-	0.38
Ceramic:	ZrO_2	117	-	7.11e-6	1/3
	Al_2O_3	380	3800	-	0.3
	Mat_2	1.44	1220	-	0.38

Table 5. 2: Temperature-dependent coefficients of Si_3N_4/SUS304 plates.

Materials	Proprieties	P_0	P_{-1}	P_1	P_2	P_3
Si_3N_4	E (Pa)	348.43e+9	0.0	−3.070e−4	2.160e−7	−8.946e−11
	α (1/K)	5.8723e−6	0.0	9.095e−4	0.0	0.0
	κ (W/mK)	13.723	0.0	−1.032e−3	5.466e−7	−7.876e−11
	ν	0.24	0.0	0.0	0.0	0.0
	ρ (kg/m^3)	2370	0.0	0.0	0.0	0.0
SUS304	E (Pa)	201.04e+9	0.0	3.079e−4	−6.534e−7	0.0
	α (1/K)	12.330e−6	0.0	8.086e−4	0.0	0.0
	κ (W/mK)	15.379	0.0	−1.264e−3	2.092e−6	−7.223e−10
	ν	0.3262	0.0	−2.002e−4	3.797e−7	0.0
	ρ (kg/m^3)	8166	0.0	0.0	0.0	0.0

5.4.2.1 Verification

a. Static analysis

Table 5.3 validates the computed solutions of transverse displacement $\bar{w}$ and normal stress $\bar{\sigma}_{xx}$ under mechanical load for microplates. The sinusoidal mechanical load is applied to Al/Al_2O_3 plate with different slenderness ratios and power-law indices. Under mechanical load, the present quasi-3D results are in good agreement with other quasi-3D ones. Considering 2D models, Lei et al. [179] degenerated quasi-3D to 2D model by setting w_z to zero, which results in a slight difference in stress $\bar{\sigma}_{xx}$ compared to present solutions and those obtained by Thai and Vo [166]. It is also seen that quasi-3D models provide higher deflections for small-scale plates but lower values for thicker plates compared to 2D models. Further verification is presented for thermal bending of FG-sandwich macroplates. By applying the linear temperature through the thickness, the deflections and stresses of Ti-6Al-4V/ZrO_2 plates are presented in Table 5.4. It is seen that the present TSDT and SSDT results are in excellent agreement with those obtained from Tounsi et al. [180] while the quasi-3D ones agree well with those reported by Mantari and Granados [181]. It should be noted that the 2D constitutive relation, i.e. $\left[Q_{ii}^{2D}, Q_{ij}^{2D}\right]$, was applied to the quasi-3D solution in [181]. In this example, applying quasi-3D theories not only increases

the stiffness but also induces the load component F_5 which is caused by z-direction thermal stretching. Therefore, thermal deflections achieved from quasi-3D models together with $\left[Q_{ii}^{3D}, Q_{ij}^{3D}\right]$ are higher than those from 2D models. At the same time, between SSDT and TSDT which are employed to quasi-3D models, the former provides higher stress magnitudes and the difference is much more pronounced in the thermal case. Those values from SSDT quasi-3D model are comparable with the results obtained from 2D solutions. In this chapter, SSDT is applied to static bending behaviours while TSDT is applied to vibration and buckling analysis.

Table 5. 3: Non-dimensional deflections and stresses of Al/Al_2O_3 microplates under sinusoidal loads.

a/h	h/l	Theory	$\bar{w}(a/2,b/2,0)$			$\bar{\sigma}_{xx}(a/2,b/2,h/2)$		
			p=0	1	10	p=0	1	10
5	1	TSDT [179]	0.0569	0.0989	0.2077	0.2321	0.3162	0.6655
		SSDT [166]	0.0588	0.1017	0.2158	0.1800	0.2437	0.5189
		Present TSDT	0.0568	0.0985	0.2099	0.1841	0.2483	0.5294
		Present SSDT	0.0570	0.0988	0.2108	0.1844	0.2488	0.5289
		Quasi-3D (TSDT) [179]	0.0601	0.1031	0.2215	0.1878	0.2603	0.5232
		Present quasi-3D (TSDT)	0.0587	0.1008	0.2171	0.1858	0.2562	0.5228
		Present quasi-3D (SSDT)	0.0589	0.1012	0.2186	0.1968	0.2725	0.5531
	2	TSDT [179]	0.1432	0.2591	0.5113	0.5711	0.8185	1.5491
		Present TSDT	0.1502	0.2715	0.5352	0.4729	0.6702	1.2939
		Present SSDT	0.1506	0.2721	0.5387	0.4740	0.6720	1.2953
		Quasi-3D (TSDT) [179]	0.1564	0.2781	0.5623	0.4888	0.7022	1.3087
		Present quasi-3D (TSDT)	0.1533	0.2731	0.5468	0.4836	0.6930	1.2976
		Present quasi-3D (SSDT)	0.1536	0.2736	0.5505	0.5117	0.7364	1.3733
	4	TSDT [179]	0.2316	0.4363	0.8275	0.9086	1.3660	2.3797
		Present TSDT	0.2586	0.4881	0.9087	0.7891	1.1785	2.0694
		Present SSDT	0.2589	0.4886	0.9141	0.7912	1.1818	2.0759
		Quasi-3D (TSDT) [179]	0.2609	0.4827	0.9245	0.8156	1.2198	2.1200
		Present quasi-3D (TSDT)	0.2583	0.4784	0.9039	0.8105	1.2112	2.0981
		Present quasi-3D (SSDT)	0.2581	0.4781	0.9077	0.8543	1.2824	2.2117
	8	TSDT [179]	0.2740	0.5265	0.9865	1.0685	1.6427	2.7721
		Present TSDT	0.3171	0.6118	1.1243	0.9529	1.4609	2.4657
		Present SSDT	0.3172	0.6119	1.1275	0.9552	1.4648	2.4740
		Quasi-3D (TSDT) [179]	0.3133	0.5916	1.1064	0.9793	1.4953	2.5197
		Present quasi-3D (TSDT)	0.3123	0.5898	1.0963	0.9772	1.4917	2.5077
		Present quasi-3D (SSDT)	0.3115	0.5886	1.0973	1.0276	1.5759	2.6329
10	1	TSDT [179]	0.0530	0.0926	0.1968	0.4836	0.6541	1.3774
		SSDT [166]	0.0552	0.0959	0.2058	0.3749	0.5042	1.0733
		Present TSDT	0.0546	0.0951	0.2043	0.3770	0.5065	1.0787
		Present SSDT	0.0547	0.0951	0.2045	0.3771	0.5067	1.0785
		Quasi-3D (TSDT) [179]	0.0556	0.0960	0.2066	0.3787	0.5184	1.0785
		Present quasi-3D (TSDT)	0.0552	0.0954	0.2054	0.3778	0.5163	1.0785
		Present quasi-3D (SSDT)	0.0552	0.0954	0.2057	0.4018	0.5520	1.1411
	2	TSDT [179]	0.1283	0.2355	0.4577	1.1622	1.6561	3.1516
		Present TSDT	0.1401	0.2556	0.5022	0.9592	1.3542	2.6215
		Present SSDT	0.1402	0.2558	0.5031	0.9598	1.3550	2.6222
		Quasi-3D (TSDT) [179]	0.1419	0.2551	0.5050	0.9672	1.3775	2.6225
		Present quasi-3D (TSDT)	0.1410	0.2537	0.5008	0.9646	1.3728	2.6170
		Present quasi-3D (SSDT)	0.1410	0.2536	0.5015	1.0248	1.4665	2.7684
	4	TSDT [179]	0.1994	0.3837	0.6911	1.7954	2.6893	4.6805
		Present TSDT	0.2313	0.4437	0.7998	1.5683	2.3352	4.1032
		Present SSDT	0.2313	0.4438	0.8012	1.5694	2.3369	4.1066
		Quasi-3D (TSDT) [179]	0.2320	0.4354	0.7933	1.5815	2.3517	4.0981
		Present quasi-3D (TSDT)	0.2313	0.4343	0.7879	1.5790	2.3475	4.0871
		Present quasi-3D (SSDT)	0.2308	0.4335	0.7885	1.6746	2.5036	4.3180
	8	TSDT [179]	0.2314	0.4554	0.7946	2.0799	3.1877	5.3392
		Present TSDT	0.2766	0.5443	0.9455	1.8671	2.8552	4.7946
		Present SSDT	0.2766	0.5443	0.9464	1.8683	2.8572	4.7988
		Quasi-3D (TSDT) [179]	0.2757	0.5288	0.9265	1.8799	2.8567	4.7746
		Present quasi-3D (TSDT)	0.2755	0.5284	0.9240	1.8789	2.8550	4.7687
		Present quasi-3D (SSDT)	0.2747	0.5271	0.9237	1.9908	3.0421	5.0322

Table 5. 4: Deflections and stresses of Ti-6Al-4V/ZrO_2 plates under xy-sinusoidal and z-linear temperature.

p	Theory	z	$\bar{w}(a/2,b/2,z)$			$\bar{\sigma}_{xx}(a/2,b/2,h/2)$		
			FG	FG-core		FG	FG-core	
				1-2-2	1-1-1		1-2-2	1-1-1
0	SSDT [180]		-	0.5446	0.5698	-	-1.7508	-1.6663
	TSDT [180]		-	0.5446	0.5698	-	-1.7508	-1.6663
	Present SSDT		0.4803	0.5446	0.5698	-2.0797	-1.7508	-1.6663
	Present TSDT		0.4803	0.5446	0.5698	-2.0797	-1.7508	-1.6663
	Quasi-3D[(a)] (SSDT) [181]	z=h/2	-	0.5269	0.5526	-	-1.8544	-1.7284
		z=0	-	0.5144	0.5395	-	-	-
	Present quasi-3D[(a)] (SSDT)	z=h/2	0.4616	0.5269	0.5527	-2.2871	-1.8554	-1.7294
		z=0	0.4502	0.5144	0.5395	-	-	-
	Present quasi-3D[(a)] (TSDT)	z=h/2	0.4591	0.5227	0.5492	-1.9369	-1.4456	-1.3174
		z=0	0.4480	0.5103	0.5364	-	-	-
	Present quasi-3D[(b)] (SSDT)	z=h/2	0.4945	0.5673	0.5949	-2.8019	-2.0559	-1.8381
		z=0	0.4823	0.5540	0.5810	-	-	-
	Present quasi-3D[(b)] (TSDT)	z=h/2	0.4897	0.5587	0.5884	-2.0592	-1.1907	-0.9646
		z=0	0.4779	0.5455	0.5747	-	-	-
1	SSDT [180]		-	0.5731	0.5788	-	-1.6745	-1.6646
	TSDT [180]		-	0.5731	0.5788	-	-1.6745	-1.6645
	Present SSDT		0.5798	0.5731	0.5788	-1.5220	-1.6745	-1.6646
	Present TSDT		0.5798	0.5731	0.5788	-1.5220	-1.6745	-1.6645
	Quasi-3D[(a)] (SSDT) [181]	z=h/2	-	0.5561	0.5624	-	-1.7377	-1.7204
		z=0	-	0.5429	0.5490	-	-	-
	Present quasi-3D[(a)] (SSDT)	z=h/2	0.5597	0.5562	0.5624	-1.5307	-1.7388	-1.7215
		z=0	0.5461	0.5430	0.5491		-	-
	Present quasi-3D[(a)] (TSDT)	z=h/2	0.5571	0.5529	0.5593	-1.1158	-1.3257	-1.3097
		z=0	0.5439	0.5400	0.5464		-	-
	Present quasi-3D[(b)] (SSDT)	z=h/2	0.6006	0.5987	0.6055	-1.4865	-1.8563	-1.8267
		z=0	0.5861	0.5847	0.5913			
	Present quasi-3D[(b)] (TSDT)	z=h/2	0.5959	0.5926	0.5999	-0.6062	-0.9800	-0.9520
		z=0	0.5818	0.5789	0.5861	-	-	-
5	SSDT [180]		-	0.5799	0.5807	-	-1.6732	-1.6638
	TSDT [180]		-	0.5799	0.5807	-	-1.6732	-1.6637
	Present SSDT		0.6247	0.5799	0.5807	-1.0700	-1.6732	-1.6638
	Present TSDT		0.6248	0.5799	0.5807	-1.0699	-1.6732	-1.6637
	Quasi-3D[(a)] (SSDT) [181]	z=h/2	-	0.5638	0.5641	-	-1.7318	-1.7156
		z=0	-	0.5505	0.5507	-	-	-
	Present quasi-3D[(a)] (SSDT)	z=h/2	0.6004	0.5638	0.5641	-0.9094	-1.7329	-1.7167
		z=0	0.5853	0.5505	0.5507	-	-	-
	Present quasi-3D[(a)] (TSDT)	z=h/2	0.5990	0.5607	0.5611	-0.4848	-1.3207	-1.3067
		z=0	0.5847	0.5477	0.5482	-	-	-
	Present quasi-3D[(b)] (SSDT)	z=h/2	0.6419	0.6073	0.6071	-0.3865	-1.8475	-1.8182
		z=0	0.6258	0.5931	0.5929	-	-	-
	Present quasi-3D[(b)] (TSDT)	z=h/2	0.6398	0.6016	0.6020	0.5162	-0.9718	-0.9469
		z=0	0.6246	0.5878	0.5881	-	-	-

[(a)]: Results obtained with $\left[Q_{ti}^{2D},Q_{ij}^{2D}\right]$; [(b)]: Results obtained with $\left[Q_{ti}^{3D},Q_{ij}^{3D}\right]$

b. Vibration and buckling analysis

The fundamental frequencies of Al/Al_2O_3 microplates are compared with those of Lei et al. [179] in Table 5.5 and presented in Fig. 5.2 for various slenderness and material length scale ratios. Excellent agreement can be observed. In addition, the natural frequencies reduce with higher material length scale ratios and level out as $h/l \geq 20$. With respect to the thermal effect, the vibration of Si_3N_4/SUS304 macroplates $(a/h = 10)$ under uniform temperature is verified with those given in [182] considering TID and TD forms in Table 5.6. In this example, the equivalent axial load caused by the thermal stress is calculated with/without the transverse thermal stress σ_{zz}^{T} (either $\left[Q_{ii}^{3D}, Q_{ij}^{3D}\right]$ or $\left[Q_{ii}^{2D}, Q_{ij}^{2D}\right]$ is utilised for thermal stress, respectively). The present TSDT results are almost the same with those in [182] while the quasi-3D solution provides lower natural frequencies, especially when σ_{zz}^{T} is included. The TD solution, which describes better the working status of materials, also displays lower natural frequencies compared to TID one.

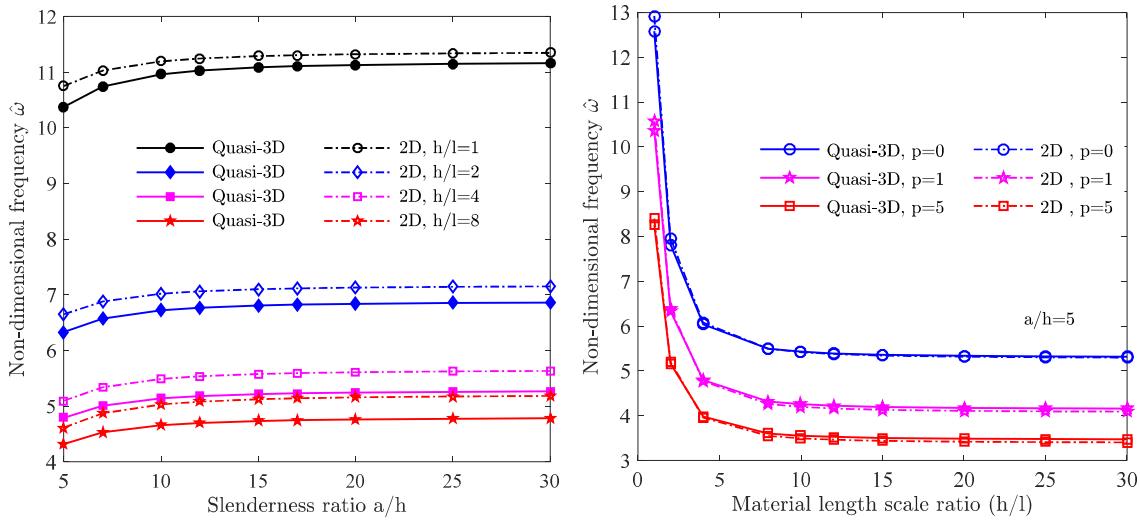

Fig. 5. 2: Non-dimensional frequencies of Al/Al_2O_3 microplates with various slenderness and material length scale ratios.

Table 5. 5: Non-dimensional fundamental frequencies $\hat{\omega}$ of Al/Al_2O_3 microplates.

a/h	h/l	Theory	p				
			0	0.5	1	5	10
5	1	TSDT [179]	12.9565	11.4813	10.5983	8.4762	7.8468
		Present TSDT	13.1645	11.6622	10.7482	8.5714	7.9417
		Quasi-3D (TSDT) [179]	12.4747	11.1097	10.2849	8.2027	7.5480
		Present quasi-3D (TSDT)	12.5865	11.2082	10.3732	8.2599	7.6030
	2	TSDT [179]	8.1759	7.1553	6.5542	5.3491	5.0233
		Present TSDT	8.3177	7.2634	6.6505	5.4479	5.1267
		Quasi-3D (TSDT) [179]	7.7588	6.8328	6.2857	5.1083	4.7628
		Present quasi-3D (TSDT)	7.8212	6.8784	6.3301	5.1591	4.8150
	4	TSDT [179]	6.4393	5.5604	5.0553	4.1718	3.9619
		Present TSDT	6.5027	5.6107	5.0984	4.2352	4.0303
		Quasi-3D (TSDT) [179]	6.0161	5.2220	4.7737	3.9453	3.7260
		Present quasi-3D (TSDT)	6.0397	5.2428	4.7924	3.9796	3.7606
	8	TSDT [179]	5.9205	5.0878	4.6015	3.8080	3.6331
		Present TSDT	5.9413	5.1018	4.6169	3.8310	3.6582
		Quasi-3D (TSDT) [179]	5.4951	4.7406	4.3143	3.5943	3.4113
		Present quasi-3D (TSDT)	5.4983	4.7429	4.3193	3.6038	3.4226
10	1	TSDT [179]	13.6329	12.0824	11.1415	8.9022	8.2367
		Present TSDT	13.7017	12.1439	11.1933	8.9284	8.2615
		Quasi-3D (TSDT) [179]	13.2922	11.8250	10.9199	8.7034	8.0198
		Present quasi-3D (TSDT)	13.3344	11.8606	10.9617	8.7279	8.0421
	2	TSDT [179]	8.7651	7.6413	6.9954	5.7361	5.3998
		Present TSDT	8.8098	7.6774	7.0202	5.7651	5.4330
		Quasi-3D (TSDT) [179]	8.3187	7.3006	6.7130	5.4839	5.1335
		Present quasi-3D (TSDT)	8.3415	7.3148	6.7225	5.5062	5.1525
	4	TSDT [179]	7.0338	6.0428	5.4762	4.5989	4.3928
		Present TSDT	7.0538	6.0534	5.4902	4.6190	4.4186
		Quasi-3D (TSDT) [179]	6.5011	5.6087	5.1293	4.3069	4.0903
		Present quasi-3D (TSDT)	6.5153	5.6282	5.1396	4.3282	4.1092
	8	TSDT [179]	6.5258	5.5750	5.0315	4.2613	4.0974
		Present TSDT	6.5333	5.5692	5.0309	4.2690	4.1078
		Quasi-3D (TSDT) [179]	5.9678	5.1146	4.6442	3.9723	3.7809
		Present quasi-3D (TSDT)	5.9704	5.1197	4.6597	3.9724	3.7955

Table 5. 6: Non-dimensional fundamental frequencies $\overline{\omega}$ of Si_3N_4/SUS304 plates (ΔT=400K, a/h=10).

p	Theory	TID solution			TD solution		
		a/b = 1	a/b = 2	a/b = 3	a/b = 1	a/b = 2	a/b = 3
0	CPT [182]	11.417	30.671	61.696	10.512	29.123	59.048
	FSDT [182]	11.095	29.001	56.078	10.187	27.485	53.584
	TSDT [182]	11.033	28.696	55.121	10.124	27.186	52.652
	Present TSDT	11.170	28.966	55.547	10.302	27.527	53.187
	Present quasi-3D (TSDT) (+)	11.099	28.884	55.571	10.204	27.399	53.139
	Present quasi-3D (TSDT) (++)	10.084	28.139	55.010	8.858	26.459	52.442
0.5	CPT [182]	7.448	20.776	42.166	6.642	19.431	39.870
	FSDT [182]	7.217	19.622	38.330	6.405	18.306	36.174
	TSDT [182]	7.174	19.417	37.694	6.362	18.108	35.563
	Present TSDT	7.264	19.571	37.886	6.479	18.299	35.805
	Present quasi-3D (TSDT) (+)	7.201	19.500	37.905	6.392	18.191	35.769
	Present quasi-3D (TSDT) (++)	6.163	18.781	37.371	4.976	17.295	35.115
1	CPT [182]	6.388	18.142	37.008	5.619	16.863	34.819
	FSDT [182]	6.176	17.099	33.549	5.401	15.848	31.491
	TSDT [182]	6.135	16.909	32.959	5.359	15.662	30.923
	Present TSDT	6.204	17.011	33.057	5.445	15.785	31.039
	Present quasi-3D (TSDT) (+)	6.139	16.932	33.042	5.357	15.673	30.975
	Present quasi-3D (TSDT) (++)	5.088	16.231	32.526	3.902	14.804	30.351
5	CPT [182]	4.969	14.606	30.070	4.266	13.433	28.036
	FSDT [182]	4.776	13.687	27.034	4.063	12.534	25.108
	TSDT [182]	4.732	13.491	26.437	4.015	12.336	24.514
	Present TSDT	4.841	13.675	26.689	4.156	12.556	24.810
	Present quasi-3D (TSDT) (+)	4.757	13.551	26.569	4.042	12.394	24.637
	Present quasi-3D (TSDT) (++)	3.695	12.898	26.104	2.539	11.608	24.094

(+): Exclusion of thermal thickness stress $\left(\sigma_{zz}^{T}=0\right)$,

(++): Inclusion of thermal thickness stress $\left(\sigma_{zz}^{T}\neq 0\right)$

Further verification is carried out for mechanical and thermal buckling behaviours of FG plates in Tables 5.7 and 5.8. As can be seen in Table 5.7, the present results of mechanical buckling agree well with those obtained from refined plate theories (RPT) [167, 169] and quasi-3D theory [169]. It is also shown that the inclusion of normal stretching effect leads to the higher critical buckling loads for macroplates but less significant to microplates. Regarding the thermal buckling behaviour, by applying the linear temperature which is expressed by $T(x,y,z)=305+(1/2+z/h)\Delta T$ [172], a good agreement can be seen for Al/Al_2O_3 macroplates and thin microplates in Table 5.8. This temperature pattern, which assumes the temperature elevation occurs only at the top surface, can lead to a very high difference in the temperature at the bottom and top surfaces; therefore, the temperature distribution described in Eq. (1.8) and the exclusion of σ_{zz}^{T} are considered in the thermal vibration and buckling analysis.

Table 5. 7: Non-dimensional critical buckling loads of Mat_1/Mat_2 microplates.

h/l	Theory	$a/h=5$			$a/h=10$			$a/h=20$		
		p=0	1	10	p=0	1	10	0	1	10
1	RPT [167]	82.694	43.809	15.952	88.542	46.537	16.603	90.180	47.291	16.779
	RPT [169]	78.968	42.039	15.407	87.378	45.998	16.443	89.872	47.149	16.738
	Present TSDT	85.767	45.262	16.272	89.332	46.908	16.605	89.047	47.027	16.319
	Quasi-3D (RPT) [169]	73.693	39.887	14.529	85.604	45.822	16.482	89.402	47.660	17.083
	Present quasi-3D	86.070	45.969	16.576	89.332	47.312	17.009	89.047	47.027	16.319
2	Present TSDT	33.372	16.562	6.517	35.961	17.587	6.885	36.424	17.848	6.540
	Present quasi-3D	34.028	17.420	6.820	36.163	18.394	7.289	36.443	18.665	7.352
4	Present TSDT	19.952	9.321	3.841	22.535	10.212	4.353	23.070	10.545	4.484
	Present quasi-3D	20.937	10.280	4.194	22.939	11.020	4.757	23.474	10.949	4.888
8	Present TSDT	16.504	7.476	3.057	19.197	8.439	3.692	20.020	8.707	3.858
	Present quasi-3D	17.627	8.473	3.423	19.601	9.247	4.146	20.020	9.313	4.262
∞	RPT [167]	15.332	6.861	2.767	18.075	7.828	3.497	18.924	8.114	3.745
	RPT [169]	15.332	6.861	2.770	18.076	7.828	3.498	18.924	8.114	3.745
	Present TSDT	15.332	6.861	2.767	18.075	7.828	3.497	18.924	8.113	3.745
	Quasi-3D (RPT) [169]	15.363	7.391	3.012	18.156	8.540	3.892	18.968	8.864	4.185
	Present quasi-3D	16.527	7.876	3.148	18.489	8.673	3.930	19.037	8.891	4.188

Table 5. 8: Critical buckling temperatures ΔT_{cr} [K] of Al/Al_2O_3 microplates.

p	h/l	Theory	Uniform temperature			Linear temperature		
			a/h=100	20	10	100	20	10
0	∞	HSDT [183]	17.080	421.530	1618.680	24.170	833.070	3227.360
		HSDT [184]	17.089	421.540	1618.750	24.179	833.079	3227.510
		CBT [172]	17.099	-	-	24.198	-	-
		Present TSDT	17.089	421.535	1618.689	24.177	833.073	3227.377
		Present quasi-3D	17.083	423.290	1644.410	24.182	836.576	3278.829
	2	CBT [172]	35.053	-	-	60.107	-	-
		Present TSDT	35.042	870.790	3419.221	60.084	1731.582	6828.442
		Present quasi-3D	35.042	871.571	3431.200	60.086	1733.152	6852.410
	1	CBT [172]	88.916	-	-	167.831	-	-
		Present TSDT	88.902	2215.320	8772.104	167.806	4420.639	17534.209
		Present quasi-3D	88.891	2215.610	8776.800	167.798	4421.229	17543.610
1	∞	HSDT [183]	7.940	196.260	758.390	5.510	358.710	1412.960
		HSDT [184]	7.940	196.267	758.424	5.513	358.715	1413.020
		CBT [172]	7.944	-	-	5.521	-	-
		Present TSDT	7.939	196.266	758.398	5.512	358.713	1412.975
		Present quasi-3D	8.174	202.797	790.829	5.955	370.963	1473.811
	2	CBT [172]	17.852	-	-	24.104	-	-
		Present TSDT	17.846	443.874	1747.416	24.093	823.094	3267.841
		Present quasi-3D	18.082	450.093	1775.366	24.541	834.758	3320.262
	1	CBT [172]	47.577	-	-	79.852	-	-
		Present TSDT	47.571	1185.721	4699.088	79.839	2214.401	8803.603
		Present quasi-3D	47.803	1191.776	4724.691	80.285	2225.760	8851.616
5	∞	HSDT [183]	7.260	178.530	679.310	3.891	298.700	1160.680
		HSDT [184]	7.260	178.516	679.039	3.890	298.672	1160.220
		CBT [172]	7.266	-	-	3.900	-	-
		Present TSDT	7.258	178.535	679.312	3.889	298.704	1160.689
		Present quasi-3D	7.547	186.246	713.734	4.394	311.968	1219.936
	2	CBT [172]	14.692	-	-	16.683	-	-
		Present TSDT	14.687	365.354	1438.925	16.674	620.276	2468.204
		Present quasi-3D	14.971	372.589	1466.682	17.181	632.736	2515.987
	1	CBT [172]	36.971	-	-	55.031	-	-
		Present TSDT	36.967	922.164	3663.791	55.023	1578.709	6297.849
		Present quasi-3D	37.256	929.248	3689.120	55.530	1590.906	6341.446

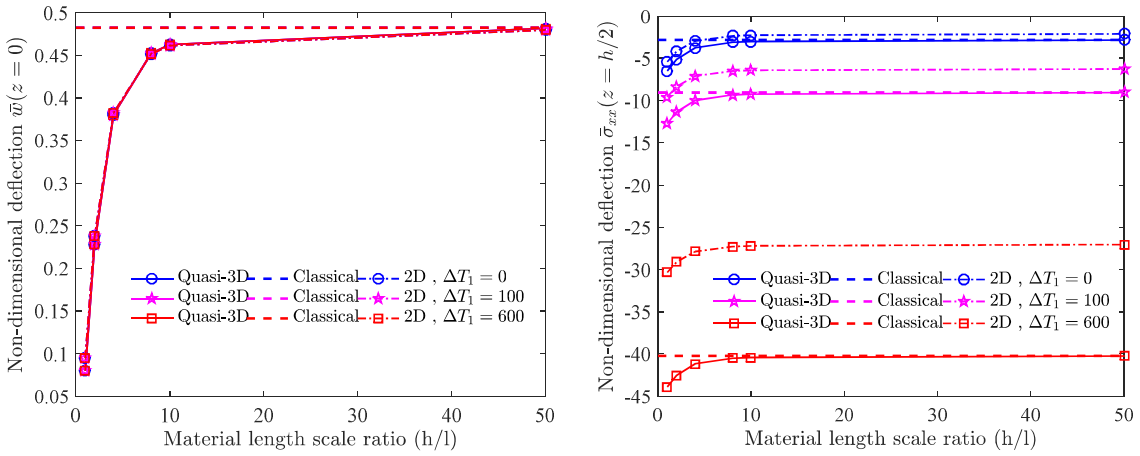

a. p = 0

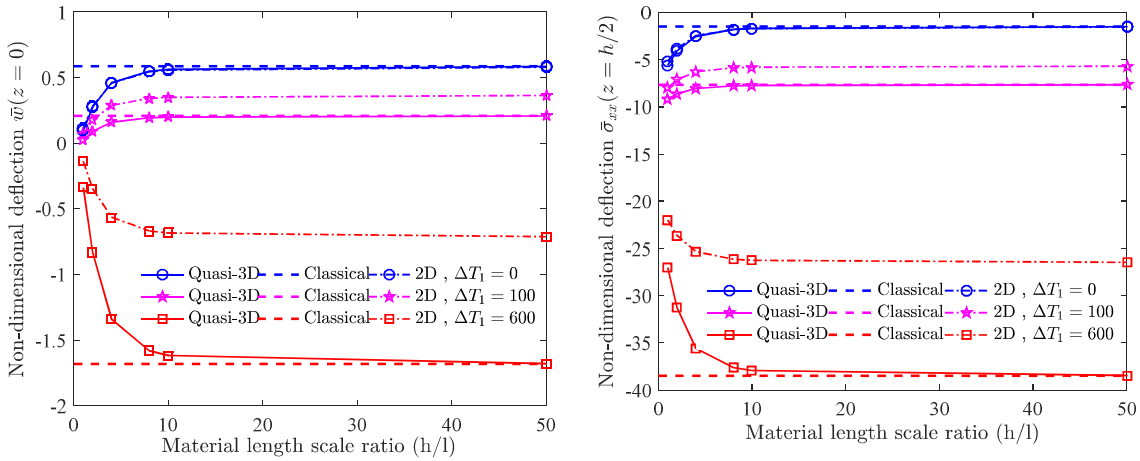

b. p = 1

Fig. 5. 3: Non-dimensional deflections and stresses of Ti-6Al-4V/ZrO_2 microplates for various material length scale ratios and temperatures.

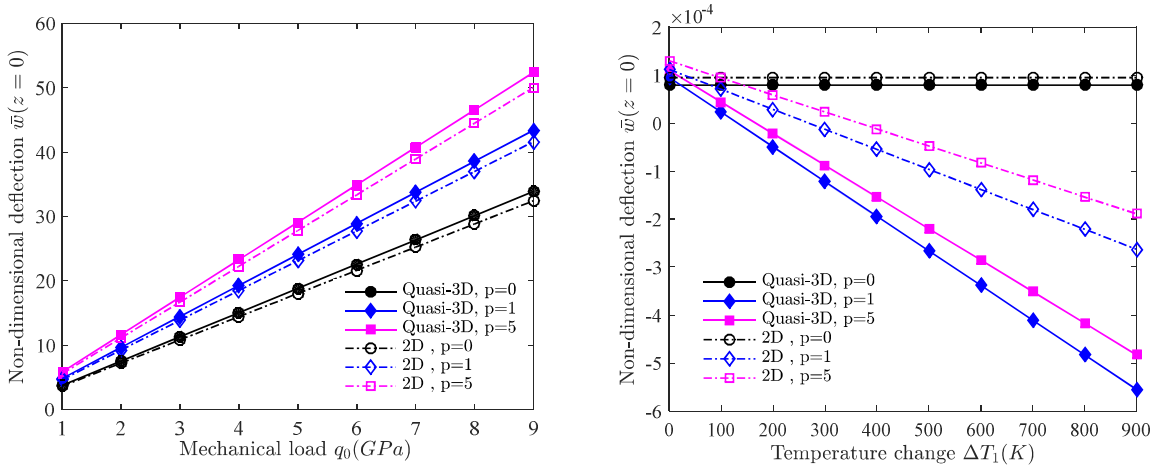

a. h/l=1

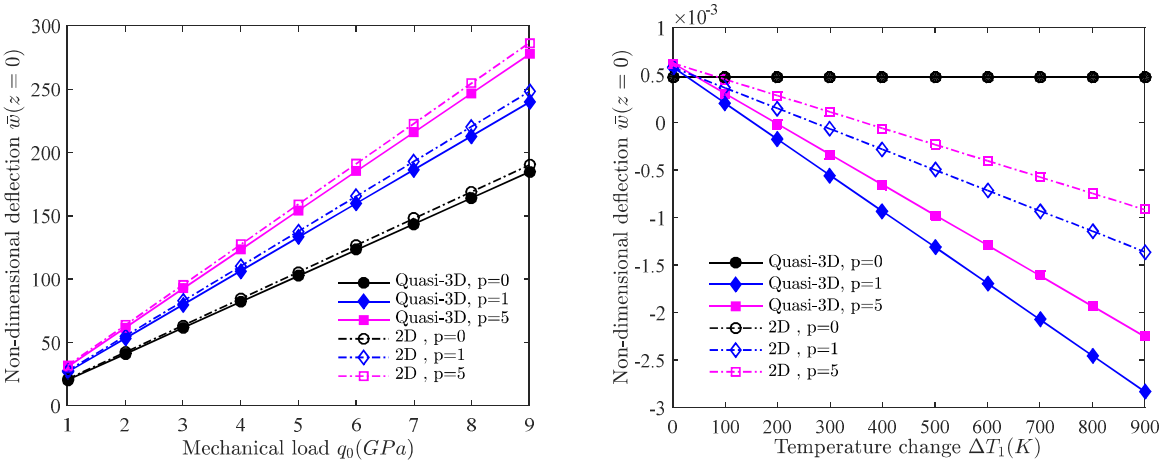

b. Classical

Fig. 5. 4: Non-dimensional deflections of Ti-6Al-4V/ZrO_2 microplates under various mechanical and thermal loads.

5.4.2.2 Parameter study

a. Static analysis

The deflection and stress of Ti-6Al-4V/ZrO_2 plates under various thickness scales and temperatures are presented in Fig. 5.3. In this figure, TID is considered to verify with those obtained from [181] for the macroplates under the higher temperatures. The small-scale effect can be seen for deflection and stress in microplates and is negligible for thicker plates (h≥20l) where a good agreement with those results for macroplates is observed. Regarding the thickness stretching effect, the results from the quasi-3D and 2D models agree well at ambient temperature but the significant difference between them is observed at elevated temperature. In addition, under lower temperature, the positive deflection can be seen while the negative deflection is obtained with increasing temperature. This can be explained by the difference in thermal expansions of Ti-6Al-4V and ZrO_2. At the lower temperature, the linear temperature

causes an expansion on the upper face (ceramic – ZrO_2) whereas the metal has not been heated up. This results in a coupled force pushing the plate upward. At the higher temperature ΔT_1, due to the higher thermal expansion coefficient, the metal surface stretches more than the ceramic one which creates a reverse moment pushing the plate downward. This change is illustrated by the transverse displacements obtained from quasi-3D and 2D models for various thickness scales in Fig. 5.4. It is seen that the difference between these solutions are more profound under thermal loads than under mechanical loads.

Table 5. 9: Non-dimensional deflections of FG and (1-2-2) Si_3N_4/SUS304 sandwich microplates under uniform temperature (a/h=5).

h/l	p	Theory	FG		FG-core		Ceramic-core		Metal-core	
			ΔT_1=300	900	300	900	300	900	300	900
1	0	SSDT	0	0	-0.381	-1.075	0	0	0	0
		Quasi-3D (SSDT)	0	0	-0.435	-2.713	0	0	0	0
	1	SSDT	-0.522	-2.276	-0.653	-2.449	0.170	0.666	-0.202	-0.920
		Quasi-3D (SSDT)	-0.585	-4.523	-0.696	-5.036	0.159	1.094	-0.238	-2.218
	5	SSDT	-0.448	-2.482	-0.769	-3.086	0.250	0.996	-0.238	-0.881
		Quasi-3D (SSDT)	-0.581	-6.179	-0.847	-6.795	0.231	1.910	-0.251	-2.021
5	0	SSDT	0	0	-1.921	-5.863	0	0	0	0
		Quasi-3D (SSDT)	0	0	-2.978	-17.339	0	0	0	0
	1	SSDT	-2.437	-10.724	-3.171	-12.921	0.862	3.658	-0.847	-3.302
		Quasi-3D (SSDT)	-3.530	-23.143	-4.531	-28.813	1.147	7.160	-1.286	-8.828
	5	SSDT	-1.957	-9.930	-3.596	-15.463	1.280	5.948	-1.002	-3.296
		Quasi-3D (SSDT)	-3.057	-25.040	-5.167	-34.746	1.685	12.749	-1.470	-8.910
∞	0	SSDT	0	0	-2.321	-7.219	0	0	0	0
		Quasi-3D (SSDT)	0	0	-3.617	-21.072	0	0	0	0
	1	SSDT	-2.896	-12.774	-3.799	-15.789	1.042	4.508	-0.985	-3.744
		Quasi-3D (SSDT)	-4.221	-27.238	-5.457	-34.458	1.397	8.759	-1.510	-9.975
	5	SSDT	-2.296	-11.478	-4.274	-18.685	1.551	7.490	-1.167	-3.754
		Quasi-3D (SSDT)	-3.598	-28.485	-6.171	-40.844	2.053	15.790	-1.737	-10.190

Table 5. 10: Non-dimensional deflections of FG and (1-2-2) Si_3N_4/SUS304 sandwich microplates under linear temperature (a/h=5).

h/l	p	Theory	FG		FG-core		Ceramic-core		Metal-core	
			ΔT_1=0	300	0	300	0	300	0	300
1	0	SSDT	0.119	0.170	0.155	-0.165	0.119	0.170	0.282	0.403
		Quasi-3D (SSDT)	0.061	0.092	0.087	-0.305	0.061	0.091	0.148	0.251
	1	SSDT	0.189	-0.254	0.177	-0.404	0.181	0.419	0.199	0.085
		Quasi-3D (SSDT)	0.104	-0.422	0.100	-0.541	0.099	0.306	0.103	-0.071
	5	SSDT	0.237	-0.108	0.189	-0.502	0.211	0.537	0.158	-0.010
		Quasi-3D (SSDT)	0.126	-0.372	0.109	-0.675	0.113	0.404	0.083	-0.119
5	0	SSDT	0.571	0.815	0.781	-0.833	0.571	0.816	1.263	1.779
		Quasi-3D (SSDT)	0.553	0.801	0.809	-1.816	0.553	0.802	1.230	1.855
	1	SSDT	0.886	-1.183	0.864	-1.955	0.919	2.128	0.845	0.361
		Quasi-3D (SSDT)	0.886	-2.228	0.885	-3.237	0.938	2.477	0.809	-0.074
	5	SSDT	1.042	-0.476	0.888	-2.336	1.085	2.761	0.677	-0.029
		Quasi-3D (SSDT)	1.019	-1.526	0.910	-3.819	1.109	3.263	0.654	-0.496
∞	0	SSDT	0.683	0.975	0.944	-1.006	0.683	0.975	1.487	2.089
		Quasi-3D (SSDT)	0.676	0.979	0.993	-2.194	0.676	0.979	1.478	2.214
	1	SSDT	1.055	-1.405	1.036	-2.340	1.112	2.575	0.986	0.422
		Quasi-3D (SSDT)	1.075	-2.646	1.079	-3.883	1.152	3.028	0.971	-0.065
	5	SSDT	1.224	-0.560	1.058	-2.774	1.316	3.347	0.792	-0.030
		Quasi-3D (SSDT)	1.224	-1.769	1.102	-4.544	1.363	3.988	0.787	-0.569

Tables 5.9 and 5.10 present the non-dimensional deflection of Si_3N_4/SUS304 sandwich microplates under uniform and linear temperatures through the thickness. No displacement is shown in Table 5.9 for homogeneous plates (FG or homogeneous-core sandwich plate with *p=0*) due to the symmetry of material and thermal stress under uniform temperature. The deflection increases with respect to temperature but in different ways, upward for the ceramic-core plates and downward for the others. Also, less deflection can be observed for smaller scale plates under thermal environment, which is similar to the case of mechanical loads. At the macro scale, the smallest displacement is observed in metal-core plates, especially under uniform temperature. At the micro scale, the homogeneous-core plates induce lower deflection under uniform temperature, but higher deflection under linear temperature compared to the FG/ FG-core plates. To compare the quasi-3D and 2D models in evaluating thermal stresses, Fig. 5.5 displays the through-the-thickness normal and shear stresses of sandwich microplates under thermal environment. The inclusion of stretching effect leads to the higher stresses and this difference is more significant at the top and bottom surfaces for the normal stress and at the middle surface for the shear stress. The stress distributions under uniform and linear temperatures are revealed in Fig. 5.6. The linear temperature results in the higher normal stress at the top surface but the lower at the bottom surface compared to the uniform temperature. In addition, the higher shear stresses are obtained under uniform temperature for FG-core plates but under linear temperature for the homogeneous-core plates. In increasing the material

length scales ratio, the shear stresses reduce significantly and the normal stress also changes the distribution, from higher at the top to higher at the bottom.

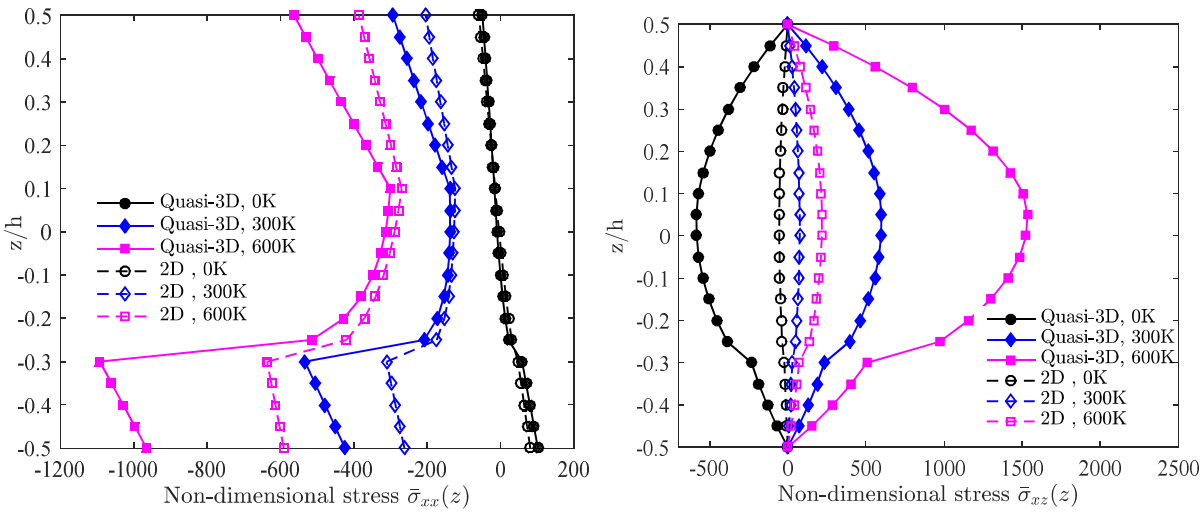

a. FG-core sandwich plates

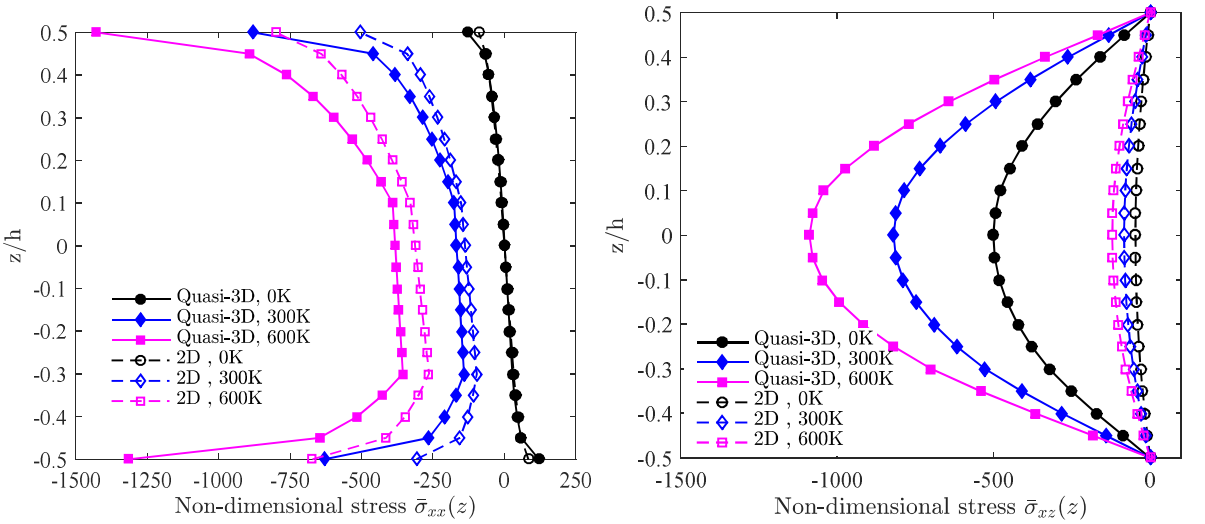

b. Ceramic-core sandwich plates

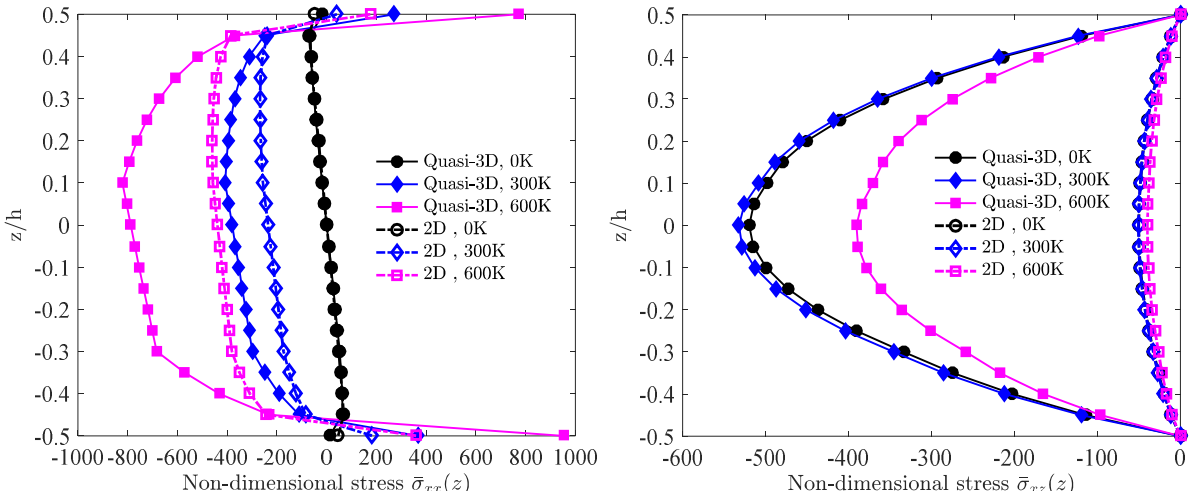

c. Metal-core sandwich plates

Fig. 5. 5: Distribution of non-dimensional stresses of (1-2-2) Si_3N_4/SUS304 microplates through the thickness under various linear temperatures (h/l=1, p=0.2).

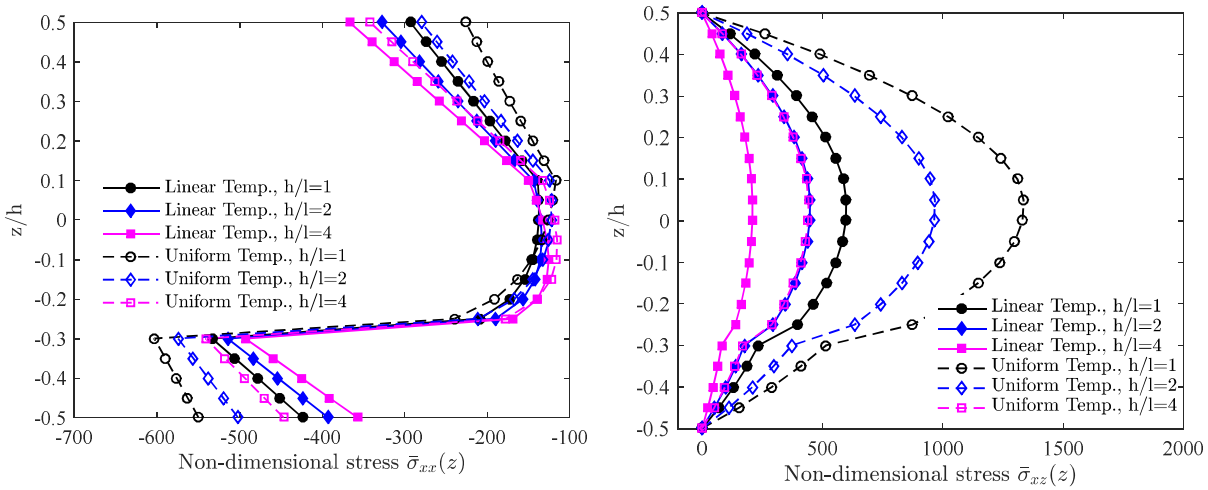

a. FG-core sandwich plates

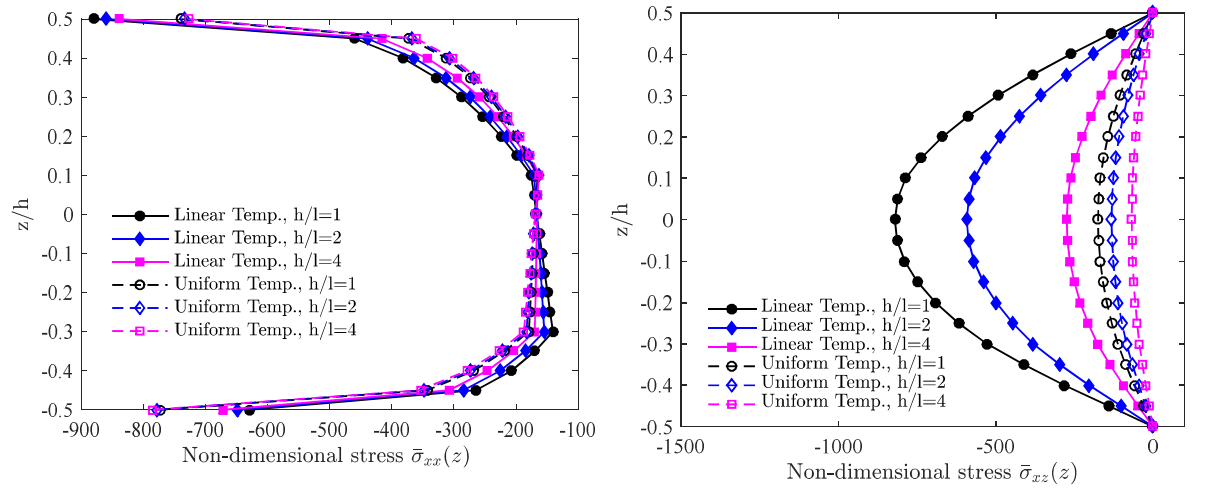

b. Ceramic-core sandwich plates

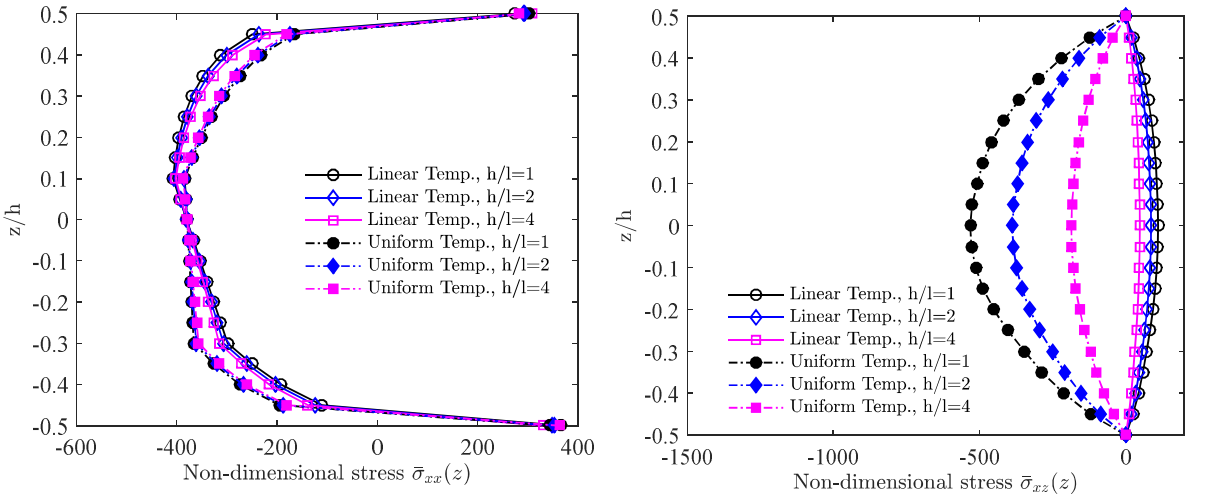

c. Metal-core sandwich plates

Fig. 5. 6: Distribution of non-dimensional stresses of (1-2-2) Si_3N_4/SUS304 microplates through the thickness for various material length scale ratios (p=0.2, ΔT_1 = 300K).

b. Vibration and buckling analysis

The natural frequencies under uniform and linear temperatures are presented for Si_3N_4/SUS304 microplates (a/h=10, p=1) in Fig. 5.7 with TD solution. In this example, $\left[Q_{ii}^{3D}, Q_{ij}^{3D}\right]$ relation is applied for thermal stress in evaluating equivalent axial loads. As expected, the natural frequency decreases as increasing temperature up to zero at the critical buckling temperature. In addition, the difference between the natural frequencies under uniform and linear temperatures is minor, but the difference between 2D and quasi-3D solutions increases with elevated temperature. Considering the small-scale effect, the smaller material length scale ratios are considered, the higher natural frequencies are obtained. This can be explained that including the deviatoric part of the symmetric couple stress tensors in strain energy strengthen the stiffness of the microplates. The natural frequencies of sandwich microplates under thermal environment are presented in Fig. 5.8 and Tables 5.11-5.13 for FG-, ceramic- and metal- core, respectively. Under both uniform and linear temperatures, the highest natural frequencies can be seen in ceramic-core and the lowest in metal-core plates. In addition, the increase of power-law index leads to the lower natural frequencies in FG-core and ceramic-core plates but the higher natural frequencies in metal-core plates.

Table 5. 11: Non-dimensional fundamental frequencies $\overline{\omega}$ of FG-core Si_3N_4/SUS304 microplates under uniform and linear temperatures (a/h=10).

Temp.	h/l	ΔT_1	Theory	1-2-2			1-1-1		
				p=0	1	5	p=0	1	5
Uniform	1	300	TSDT	22.4338	18.6189	16.7630	19.7294	17.1845	15.8297
			Quasi-3D (TSDT)	22.0117	18.2000	16.3504	19.3065	16.7698	15.4215
		600	TSDT	20.9876	17.0665	15.1717	18.2403	15.5951	14.2002
			Quasi-3D (TSDT)	20.5158	16.5776	14.6816	17.7495	15.1040	13.7117
	2	300	TSDT	13.5455	11.2868	10.2184	11.9329	10.4568	9.6866
			Quasi-3D (TSDT)	12.9872	10.7364	9.6809	11.3723	9.9151	9.1571
		600	TSDT	11.9747	9.7006	8.6644	10.3869	8.8846	8.1331
			Quasi-3D (TSDT)	11.2999	8.9945	7.9589	9.6762	8.1757	7.4303
	4	300	TSDT	10.1607	8.4986	7.7354	8.9662	7.9025	7.3584
			Quasi-3D (TSDT)	9.4653	7.8201	7.0824	8.2688	7.2412	6.7212
		600	TSDT	8.2989	6.6680	5.9843	7.1708	6.1178	5.6288
			Quasi-3D (TSDT)	7.3687	5.6853	5.0148	6.1802	5.1373	4.6710
	8	300	TSDT	9.1121	7.6342	6.9647	8.0472	7.1099	6.6341
			Quasi-3D (TSDT)	8.3549	6.8993	6.2634	7.2881	6.3978	5.9539
		600	TSDT	7.0791	5.6485	5.0791	6.0979	5.1835	4.7769
			Quasi-3D (TSDT)	5.9950	4.4900	3.9445	4.9322	4.0308	3.6616
Linear	1	300	TSDT	22.4592	18.6501	16.7943	19.7607	17.2157	15.8591
			Quasi-3D (TSDT)	22.0338	18.2277	16.3784	19.3341	16.7976	15.4477
		600	TSDT	21.0472	17.1390	15.2447	18.3125	15.6678	14.2700
			Quasi-3D (TSDT)	20.5644	16.6387	14.7433	17.8097	15.1653	13.7704
	2	300	TSDT	13.5738	11.3207	10.2520	11.9669	10.4904	9.7183
			Quasi-3D (TSDT)	13.0113	10.7663	9.7106	11.4020	9.9447	9.1850
		600	TSDT	12.0339	9.7689	8.7311	10.4547	8.9517	8.1975
			Quasi-3D (TSDT)	11.3435	9.0473	8.0102	9.7273	8.2272	7.4797
	4	300	TSDT	10.1934	8.5375	7.7734	9.0051	7.9406	7.3941
			Quasi-3D (TSDT)	9.4937	7.8553	7.1168	8.3036	7.2757	6.7535
		600	TSDT	8.3668	6.7443	6.0566	7.2462	6.1911	5.6986
			Quasi-3D (TSDT)	7.4182	5.7447	5.0708	6.2367	5.1941	4.7252
	8	300	TSDT	9.1471	7.6756	7.0049	8.0887	7.1503	6.6718
			Quasi-3D (TSDT)	8.3858	6.9374	6.3005	7.3259	6.4350	5.9887
		600	TSDT	7.1531	5.7309	5.1562	6.1793	5.2621	4.8510
			Quasi-3D (TSDT)	6.0504	4.5573	4.0072	4.9955	4.0947	3.7225

Table 5. 12: Non-dimensional fundamental frequencies $\bar{\omega}$ of ceramic-core Si_3N_4/SUS304 microplates under uniform and linear temperatures (a/h=10).

Temp.	h/l	ΔT_1	Theory	1-2-2			1-1-1		
				p=0	1	5	p=0	1	5
Uniform	1	300	TSDT	28.8114	20.2316	16.9970	28.8114	19.5962	16.2481
			Quasi-3D (TSDT)	28.3804	19.7974	16.5421	28.3804	19.1574	15.7836
		600	TSDT	27.3966	18.6788	15.3814	27.3966	18.0212	14.5935
			Quasi-3D (TSDT)	26.9733	18.1707	14.8047	26.9733	17.4994	13.9915
	2	300	TSDT	17.5032	12.1752	10.2190	17.5032	11.7825	9.7630
			Quasi-3D (TSDT)	16.9854	11.5797	9.5750	16.9854	11.1744	9.0978
		600	TSDT	15.8513	10.5199	8.5980	15.8513	10.1166	8.1234
			Quasi-3D (TSDT)	15.3187	9.7509	7.6754	15.3187	9.3138	7.1393
	4	300	TSDT	13.2177	9.0990	7.6294	13.2177	8.7970	7.2846
			Quasi-3D (TSDT)	12.6045	8.3414	6.7943	12.6045	8.0184	6.4155
		600	TSDT	11.2134	7.1404	5.7616	11.2134	6.8299	5.4041
			Quasi-3D (TSDT)	10.5380	6.0225	4.3372	10.5380	5.6433	3.8379
	8	300	TSDT	11.8927	8.1443	6.8256	11.8927	7.8701	6.5153
			Quasi-3D (TSDT)	11.2411	7.3107	5.8976	11.2411	7.0106	5.5456
		600	TSDT	9.6960	5.9987	4.7925	9.6960	5.7144	4.4689
			Quasi-3D (TSDT)	8.9467	4.6440	2.9635	8.9467	4.2567	2.3797
Linear	1	300	TSDT	28.8116	20.2191	16.9825	28.8116	19.5927	16.2436
			Quasi-3D (TSDT)	28.3806	19.7860	16.5289	28.3806	19.1542	15.7797
		600	TSDT	27.3956	18.6554	15.3549	27.3956	18.0177	14.5891
			Quasi-3D (TSDT)	26.9723	18.1505	14.7823	26.9723	17.4967	13.9887
	2	300	TSDT	17.5028	12.1621	10.2047	17.5028	11.7792	9.7591
			Quasi-3D (TSDT)	16.9849	11.5679	9.5621	16.9849	11.1716	9.0946
		600	TSDT	15.8500	10.4987	8.5764	15.8500	10.1138	8.1199
			Quasi-3D (TSDT)	15.3174	9.7342	7.6595	15.3174	9.3121	7.1382
	4	300	TSDT	13.2169	9.0842	7.6135	13.2169	8.7935	7.2806
			Quasi-3D (TSDT)	12.6036	8.3278	6.7797	12.6036	8.0153	6.4122
		600	TSDT	11.2117	7.1170	5.7392	11.2117	6.8270	5.4005
			Quasi-3D (TSDT)	10.5363	6.0039	4.3210	10.5363	5.6419	3.8380
	8	300	TSDT	11.8916	8.1285	6.8088	11.8916	7.8665	6.5112
			Quasi-3D (TSDT)	11.2400	7.2959	5.8817	11.2400	7.0073	5.5422
		600	TSDT	9.6941	5.9733	4.7686	9.6941	5.7114	4.4652
			Quasi-3D (TSDT)	8.9447	4.6226	2.9440	8.9447	4.2553	2.3807

Table 5. 13: Non-dimensional fundamental frequencies $\bar{\omega}$ of metal-core Si_3N_4/SUS304 microplates under uniform and linear temperatures (a/h=10).

Temp.	h/l	ΔT_1	Theory	1-2-2			1-1-1		
				p=0	1	5	p=0	1	5
Uniform	1	300	TSDT	11.9407	14.9082	17.4338	11.9407	15.2919	18.2617
			Quasi-3D (TSDT)	11.4623	14.5204	17.0666	11.4623	14.9104	17.8979
		600	TSDT	9.9850	13.1901	15.8828	9.9850	13.5931	16.7388
			Quasi-3D (TSDT)	9.3046	12.7394	15.4927	9.3046	13.1591	16.3631
	2	300	TSDT	7.3231	9.2076	10.7613	7.3231	9.4488	11.2728
			Quasi-3D (TSDT)	6.6535	8.7145	10.3174	6.6535	8.9689	10.8405
		600	TSDT	5.5929	7.6072	9.2621	5.5929	7.8549	9.7792
			Quasi-3D (TSDT)	4.4629	6.9703	8.7523	4.4629	7.2510	9.2999
	4	300	TSDT	5.5729	7.0523	8.2421	5.5729	7.2399	8.6342
			Quasi-3D (TSDT)	4.7358	6.4750	7.7334	4.7358	6.6815	8.1427
		600	TSDT	3.7079	5.2892	6.5676	3.7079	5.4778	6.9544
			Quasi-3D (TSDT)	1.7897	4.4490	5.9331	1.7897	4.6918	6.3666
	8	300	TSDT	5.0284	6.3771	7.4544	5.0284	6.5472	7.8088
			Quasi-3D (TSDT)	4.1170	5.7714	6.9264	4.1170	5.9635	7.3006
		600	TSDT	3.0349	4.4826	5.6535	3.0349	4.6516	5.9985
			Quasi-3D (TSDT)	0.0000	3.5267	4.9612	0.0000	3.7666	5.3631
Linear	1	300	TSDT	11.9363	14.9136	17.4425	11.9363	15.2905	18.2615
			Quasi-3D (TSDT)	11.4584	14.5251	17.0747	11.4584	14.9091	17.8977
		600	TSDT	9.9800	13.2033	15.8999	9.9800	13.5913	16.7378
			Quasi-3D (TSDT)	9.3015	12.7506	15.5082	9.3015	13.1575	16.3622
	2	300	TSDT	7.3194	9.2132	10.7694	7.3194	9.4475	11.2723
			Quasi-3D (TSDT)	6.6504	8.7194	10.3250	6.6504	8.9678	10.8400
		600	TSDT	5.5890	7.6177	9.2730	5.5890	7.8537	9.7782
			Quasi-3D (TSDT)	4.4620	6.9779	8.7610	4.4620	7.2500	9.2990
	4	300	TSDT	5.5694	7.0585	8.2507	5.5694	7.2386	8.6335
			Quasi-3D (TSDT)	4.7329	6.4805	7.7416	4.7329	6.6803	8.1420
		600	TSDT	3.7042	5.2992	6.5761	3.7042	5.4767	6.9534
			Quasi-3D (TSDT)	1.7910	4.4556	5.9389	1.7910	4.6910	6.3656
	8	300	TSDT	5.0249	6.3835	7.4633	5.0249	6.5459	7.8080
			Quasi-3D (TSDT)	4.1141	5.7773	6.9349	4.1141	5.9622	7.2998
		600	TSDT	3.0312	4.4925	5.6612	3.0312	4.6506	5.9974
			Quasi-3D (TSDT)	0.0000	3.5333	4.9659	0.0000	3.7659	5.3620

Table 5. 14: Critical buckling temperatures ΔT_{cr} [K] of (1-2-2) Si_3N_4/SUS304 microplates (a/h=20).

Temp.	h/l	Theory	FG core			Ceramic core			Metal core		
			p=0.2	1	5	0.2	1	5	0.2	1	5
Uniform	1	TSDT	1053.28	1005.92	997.92	1095.52	1018.72	979.36	724.78	835.04	977.28
		Quasi-3D	1075.20	1033.60	1052.80	1096.96	1020.80	982.56	725.76	836.32	978.56
	2	TSDT	512.80	481.76	462.56	568.48	497.12	448.48	364.96	422.56	483.36
		Quasi-3D	515.20	486.40	467.20	569.60	498.08	449.60	365.28	423.20	484.16
	4	TSDT	336.80	316.00	304.16	380.64	322.40	284.64	244.32	288.48	332.32
		Quasi-3D	339.20	320.00	307.20	381.92	323.52	285.92	244.96	289.44	333.28
	8	TSDT	287.20	269.60	260.64	327.20	273.12	239.20	211.04	251.68	290.40
		Quasi-3D	291.20	272.00	262.40	328.64	274.40	240.48	212.00	252.64	291.68
	∞	TSDT	270.24	253.92	245.60	308.64	256.16	223.52	199.52	238.88	276.00
		Quasi-3D	272.00	256.00	249.60	310.08	257.44	224.80	200.64	240.00	277.44
Linear	1	TSDT	1041.76	993.76	980.64	1095.84	1021.60	986.08	724.84	833.12	969.82
		Quasi-3D	1064.00	1018.72	1020.96	1097.44	1024.00	989.76	725.44	834.08	970.88
	2	TSDT	515.36	484.64	465.44	567.84	496.48	448.16	364.96	422.88	483.36
		Quasi-3D	520.00	489.60	470.72	568.80	497.44	449.12	365.44	423.36	484.16
	4	TSDT	340.32	319.84	308.00	379.68	321.12	283.68	244.32	289.12	332.96
		Quasi-3D	344.16	324.00	312.48	380.96	322.24	284.64	244.96	289.92	333.92
	8	TSDT	291.04	273.76	264.48	326.24	271.84	237.92	211.04	252.00	291.36
		Quasi-3D	294.88	277.92	268.96	327.52	273.12	239.04	212.00	253.12	292.48
	∞	TSDT	273.76	257.76	249.44	307.68	254.88	222.24	199.84	239.52	276.96
		Quasi-3D	277.92	262.08	254.08	309.12	256.00	223.36	200.64	240.64	278.24

Finally, the critical buckling temperatures are tabulated in Table 5.14 for Si_3N_4/SUS304 microplates. As expected, the higher values are observed for smaller material length scale ratios. The relation between the power-law index and the critical buckling temperature for these sandwich plates is similar to what is observed in vibration behaviours.

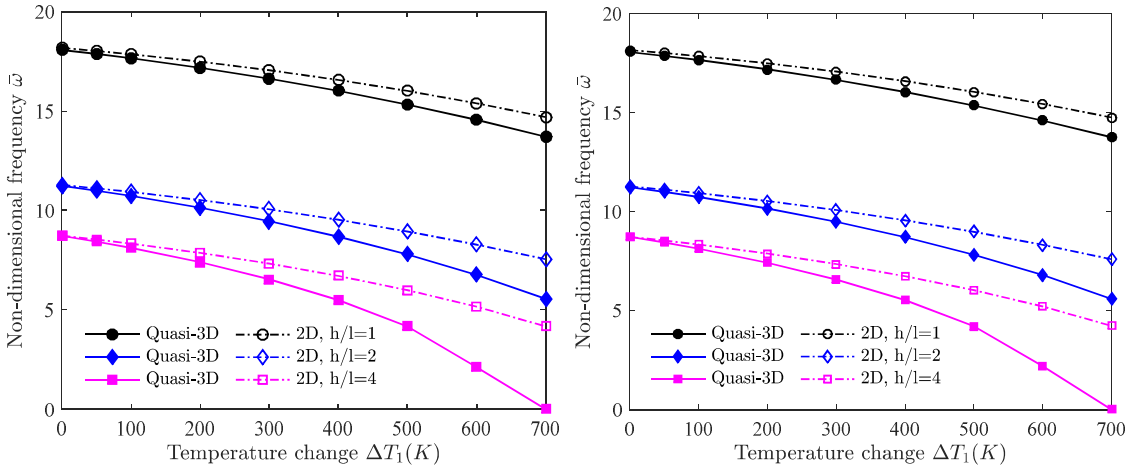

a. Uniform temperature *b. Linear temperature*

Fig. 5. 7: Non-dimensional frequencies of Si_3N_4/SUS304 microplates for various material length scale ratios under uniform and linear temperatures.

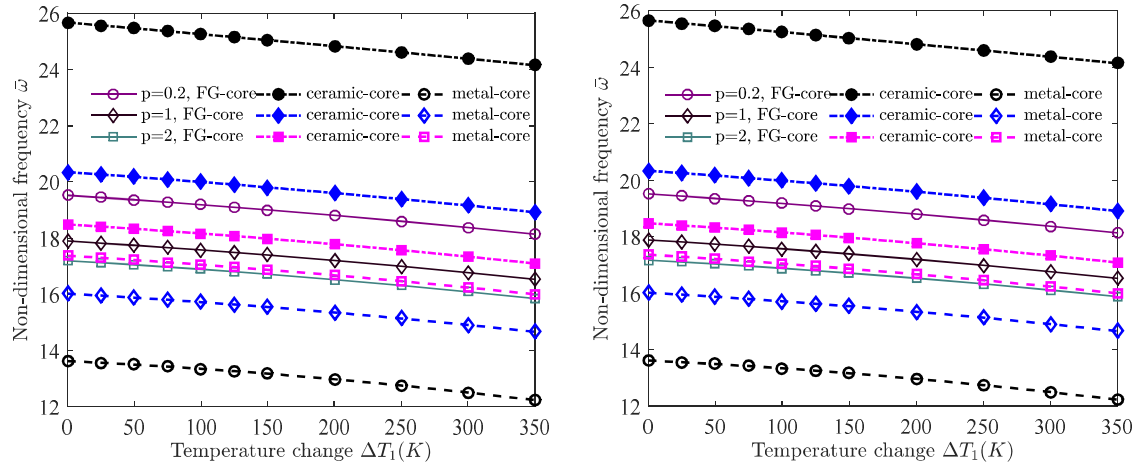

a. Uniform *b. Linear*

Fig. 5. 8: Non-dimensional frequencies of (1-1-1) Si_3N_4/SUS304 microplates for various power-law index under uniform and linear temperature (h/l=1).

5.5 Static, free vibration and buckling behaviours of FG-sandwich plates with various boundary conditions under mechanical loads

5.5.1 State space based solution

The governing equations for HSDT model can be deducted from those for quasi-3D models in Eq. (5.20) by neglecting W_z :

$$A_{11}\frac{\partial^2 U}{\partial x^2}+A_{66}\frac{\partial^2 U}{\partial y^2}-\frac{1}{4}A_m\left(\frac{\partial^4 U}{\partial x^2\partial y^2}+\frac{\partial^4 U}{\partial y^4}\right)+\left(A_{12}+A_{66}\right)\frac{\partial^2 V}{\partial x\partial y}+\frac{1}{4}A_m\left(\frac{\partial^4 V}{\partial x^3\partial y}+\frac{\partial^4 V}{\partial x\partial y^3}\right)$$

$$-B_{11}\frac{\partial^3 W_b}{\partial x^3}-\left(B_{12}+2B_{66}\right)\frac{\partial^3 W_b}{\partial x\partial y^2}-B_{11}^s\frac{\partial^3 W_s}{\partial x^3}-\left(B_{12}^s+2B_{66}^s\right)\frac{\partial^3 W_s}{\partial x\partial y^2}=I_0\ddot{U}-I_1\frac{\partial\ddot{W}_b}{\partial x}-J_1\frac{\partial\ddot{W}_s}{\partial x} \quad (5.34a)$$

$$A_{22}\frac{\partial^2 V}{\partial y^2}+A_{66}\frac{\partial^2 V}{\partial x^2}-\frac{1}{4}A_m\left(\frac{\partial^4 V}{\partial x^4}+\frac{\partial^4 V}{\partial x^2\partial y^2}\right)+\left(A_{12}+A_{66}\right)\frac{\partial^2 U}{\partial x\partial y}+\frac{1}{4}A_m\left(\frac{\partial^4 U}{\partial x^3\partial y}+\frac{\partial^4 U}{\partial x\partial y^3}\right)$$

$$-B_{22}\frac{\partial^3 W_b}{\partial y^3}-\left(B_{12}+2B_{66}\right)\frac{\partial^3 W_b}{\partial x^2\partial y}-B_{22}^s\frac{\partial^3 W_s}{\partial y^3}-\left(B_{12}^s+2B_{66}^s\right)\frac{\partial^3 W_s}{\partial x^2\partial y}=I_0\ddot{V}-I_1\frac{\partial\ddot{W}_b}{\partial y}-J_1\frac{\partial\ddot{W}_s}{\partial y} \quad (5.34b)$$

$$B_{11}\frac{\partial^3 U}{\partial x^3}+\left(B_{12}+2B_{66}\right)\frac{\partial^3 U}{\partial x\partial y^2}+\left(B_{12}+2B_{66}\right)\frac{\partial^3 V}{\partial x^2\partial y}+B_{22}\frac{\partial^3 V}{\partial y^3}-\left(D_{11}+A_m\right)\frac{\partial^4 W_b}{\partial x^4}$$
$$-\left(2D_{12}+4D_{66}+2A_m\right)\frac{\partial^4 W_b}{\partial x^2\partial y^2}-\left(D_{22}+A_m\right)\frac{\partial^4 W_b}{\partial y^4}-\left[D_{11}^s+\frac{1}{2}\left(A_m+B_m\right)\right]\frac{\partial^4 W_s}{\partial x^4}$$
$$-\left(2D_{12}^s+4D_{66}^s\right)\frac{\partial^4 W_s}{\partial x^2\partial y^2}-\left[D_{22}^s+\frac{1}{2}\left(A_m+B_m\right)\right]\frac{\partial^4 W_s}{\partial y^4}+P\left(w\right)+q$$

$$=I_0\left(\ddot{W}_b+\ddot{W}_s\right)+I_1\left(\frac{\partial\ddot{U}}{\partial x}+\frac{\partial\ddot{V}}{\partial y}\right)-I_2\nabla^2\ddot{W}_b-J_2\nabla^2\ddot{W}_s \quad (5.34c)$$

$$B_{11}^s\frac{\partial^3 U}{\partial x^3}+\left(B_{12}^s+2B_{66}^s\right)\frac{\partial^3 U}{\partial x\partial y^2}+\left(B_{12}^s+2B_{66}^s\right)\frac{\partial^3 V}{\partial x^2\partial y}+B_{22}^s\frac{\partial^3 V}{\partial y^3}$$
$$-\left[D_{11}^s+\frac{1}{2}\left(A_m+B_m\right)\right]\frac{\partial^4 W_b}{\partial x^4}-\left(2D_{12}^s+4D_{66}^s\right)\frac{\partial^4 W_b}{\partial x^2\partial y^2}-\left[D_{22}^s+\frac{1}{2}\left(A_m+B_m\right)\right]\frac{\partial^4 W_b}{\partial y^4}$$
$$+\left(A_{55}^s+\frac{1}{4}H_m\right)\frac{\partial^2 W_s}{\partial x^2}+\left(A_{44}^s+\frac{1}{4}H_m\right)\frac{\partial^2 W_s}{\partial y^2}-\left[H_{11}+\frac{1}{4}\left(A_m+2B_m+C_m\right)\right]\frac{\partial^4 W_s}{\partial x^4}$$
$$-\left(2H_{12}+4H_{66}\right)\frac{\partial^4 W_s}{\partial x^2\partial y^2}-\left[H_{22}+\frac{1}{4}\left(A_m+2B_m+C_m\right)\right]\frac{\partial^4 W_s}{\partial y^4}+P\left(w\right)+q$$

$$=I_0\left(\ddot{W}_b+\ddot{W}_s\right)+J_1\left(\frac{\partial\ddot{U}}{\partial x}+\frac{\partial\ddot{V}}{\partial y}\right)-J_2\nabla^2\ddot{W}_b-K_2\nabla^2\ddot{W}_s. \quad (5.34d)$$

The expressions for boundary conditions are described by:

$$\delta U: N_{xx}n_x+N_{xy}n_y+\frac{1}{2}\left(\frac{\partial R_{xz}}{\partial y}+\frac{\partial R_{yz}}{\partial x}\right)n_y \quad (5.35a)$$

$$\delta V : N_{yy} n_y + N_{xy} n_x - \frac{1}{2}\left(\frac{\partial R_{xz}}{\partial x} + \frac{\partial R_{yz}}{\partial y} \right) n_x \tag{5. 35b}$$

$$\delta \frac{\partial V}{\partial x} : R_{xz} n_x + R_{yz} n_y \tag{5. 35c}$$

$$\delta W_b : \frac{\partial M_{xx}}{\partial x} + \frac{\partial M_{xy}}{\partial y} + \frac{\partial R_{xy}}{\partial x} - I_1 \ddot{U} + I_2 \frac{\partial \ddot{W}_b}{\partial x} + J_2 \frac{\partial \ddot{W}_s}{\partial x} + \tilde{P} + \frac{\partial \bar{M}_{ns}}{\partial s} \tag{5. 35d}$$

$$\delta \frac{\partial W_b}{\partial n} : \bar{M}_{nn} \tag{5. 35e}$$

$$\delta W_s : \frac{\partial P_{xx}}{\partial x} + \frac{\partial P_{xy}}{\partial y} + Q_{xz} - \frac{1}{2} X_{yz} + \frac{\frac{1}{2}\partial\left(R_{xy} + S_{xy}\right)}{\partial x} + \frac{\frac{1}{2}\partial\left(R_{yy} + S_{yy}\right)}{\partial y} + \tilde{P} + \frac{\partial \bar{P}_{ns}}{\partial s}$$

$$- J_1 \ddot{U} + J_2 \frac{\partial \ddot{W}_b}{\partial x} + K_2 \frac{\partial \ddot{W}_s}{\partial x} = 0 \tag{5. 35f}$$

$$\delta \frac{\partial W_s}{\partial n} : \bar{P}_{nn} \tag{5. 35g}$$

where

$$\tilde{P} = \left[P_x^0 \frac{\partial\left(W_b + W_s\right)}{\partial x} + P_{xy}^0 \frac{\partial\left(W_b + W_s\right)}{\partial y} \right] n_x + \left[P_{xy}^0 \frac{\partial\left(W_b + W_s\right)}{\partial x} + P_y^0 \frac{\partial\left(W_b + W_s\right)}{\partial y} \right] n_y \tag{5. 36a}$$

$$\bar{M}_{nn} = \left(M_x + R_{xy}\right) n_x^2 + \left(M_y - R_{xy}\right) n_y^2 + \left(2M_{xy} - R_x + R_y\right) n_x n_y \tag{5. 36b}$$

$$\bar{M}_{ns} = \left(M_y - M_x - 2P_{xy}\right) n_x n_y + \left(M_{xy} - R_x\right) n_x^2 - \left(M_{xy} + R_y\right) n_y^2 \tag{5. 36c}$$

$$\bar{P}_{nn} = \left(P_x + \frac{1}{2} R_{xy} + \frac{1}{2} S_{xy} \right) n_x^2 + \left(P_y - \frac{1}{2} R_{xy} - \frac{1}{2} S_{xy} \right) n_y^2$$

$$+ \left(2P_{xy} - \frac{1}{2} R_x - \frac{1}{2} S_x + \frac{1}{2} R_y + \frac{1}{2} S_y \right) n_x n_y \tag{5. 36d}$$

$$\bar{P}_{ns} = \left(P_y - P_x - R_{xy} - S_{xy}\right) n_x n_y + \left(P_{xy} - \frac{1}{2} R_x - \frac{1}{2} S_x \right) n_x^2 - \left(P_{xy} + \frac{1}{2} R_y + \frac{1}{2} S_y \right) n_y^2 \tag{5. 36e}$$

Based on the state space solution for the plate with simply supported BCs at $y = 0$ and $y = b$, the displacements are expressed in terms of Fourier series as:

$$U\left(x, y\right) = \sum_{n=1}^{\infty} U_n\left(x\right) e^{i\omega t} \sin \beta y \tag{5. 37a}$$

$$V\left(x, y\right) = \sum_{n=1}^{\infty} V_n\left(x\right) e^{i\omega t} \sin \beta y \tag{5. 37b}$$

$$W_b(x,y)=\sum_{n=1}^{\infty}W_{bn}(x)e^{i\omega t}\sin\beta y \tag{5. 37c}$$

$$W_s(x,y)=\sum_{n=1}^{\infty}W_{sn}(x)e^{i\omega t}\sin\beta y \tag{5. 37d}$$

where $\beta=n\pi/b$. (5. 38)

By substituting Eq. (5.37) to Eq. (5.34), the highest-order of derivatives are expressed by the lower-order and displacements themselves as follow:

$$\frac{\partial^2 U_n}{\partial x^2}=a_1U_n+a_2\frac{\partial V_n}{\partial x}+a_3\frac{\partial^3 V_n}{\partial x^3}+a_4\frac{\partial W_{bn}}{\partial x}+a_5\frac{\partial^3 W_{bn}}{\partial x^3}+a_6\frac{\partial W_{sn}}{\partial x}+a_7\frac{\partial^3 W_{sn}}{\partial x^3} \tag{5. 39a}$$

$$\frac{\partial^4 V_n}{\partial x^4}=r_1\frac{\partial U_n}{\partial x}+r_2V_x+r_3\frac{\partial^2 V_n}{\partial x^2}+r_4W_{bx}+r_5\frac{\partial^2 W_{bn}}{\partial x^2}+r_6W_{sx}+r_7\frac{\partial^2 W_{sn}}{\partial x^2}+r_8 \tag{5. 39b}$$

$$\frac{\partial^4 W_{bn}}{\partial x^4}=s_1\frac{\partial U_n}{\partial x}+s_2V_x+s_3\frac{\partial^2 V_n}{\partial x^2}+s_4W_{bx}+s_5\frac{\partial^2 W_{bn}}{\partial x^2}+s_6W_{sx}+s_7\frac{\partial^2 W_{sn}}{\partial x^2}+s_8 \tag{5. 39c}$$

$$\frac{\partial^4 W_{sn}}{\partial x^4}=t_1\frac{\partial U_n}{\partial x}+t_2V_x+t_3\frac{\partial^2 V_n}{\partial x^2}+t_4W_{bx}+t_5\frac{\partial^2 W_{bn}}{\partial x^2}+t_6W_{sx}+t_7\frac{\partial^2 W_{sn}}{\partial x^2}+t_8 \tag{5. 39d}$$

The coefficients of Eq. (5.39) are presented in Appendix C.

Eq. (5.39) can be rewritten in the matrix form as:

$$\frac{\partial\mathbf{U}(x)}{\partial x}=\mathbf{T}\mathbf{U}(x)+\mathbf{F}(x) \tag{5. 40}$$

where the vector of variables is

$$\mathbf{U}(x)=\left\{U,\frac{\partial U}{\partial x},V,\frac{\partial V}{\partial x},\frac{\partial^2 V}{\partial x^2},\frac{\partial^3 V}{\partial x^3},W_b,\frac{\partial W_b}{\partial x},\frac{\partial^2 W_b}{\partial x^2},\frac{\partial^3 W_b}{\partial x^3},W_s,\frac{\partial W_s}{\partial x},\frac{\partial^2 W_s}{\partial x^2},\frac{\partial^3 W_s}{\partial x^3}\right\}^{'}; \tag{5. 41}$$

and matrix **T** are defined as:

$$\mathbf{T}=\begin{bmatrix}
0 & 1 & 0 & 0 & 0 & 0 & 0 & 0 & 0 & 0 & 0 & 0 & 0 & 0\\
a_1 & 0 & 0 & a_2 & 0 & a_3 & 0 & a_4 & 0 & a_5 & 0 & a_6 & 0 & a_7\\
0 & 0 & 0 & 1 & 0 & 0 & 0 & 0 & 0 & 0 & 0 & 0 & 0 & 0\\
0 & 0 & 0 & 0 & 1 & 0 & 0 & 0 & 0 & 0 & 0 & 0 & 0 & 0\\
0 & 0 & 0 & 0 & 0 & 1 & 0 & 0 & 0 & 0 & 0 & 0 & 0 & 0\\
0 & r_1 & r_2 & 0 & r_3 & 0 & r_4 & 0 & r_5 & 0 & r_6 & 0 & r_7 & 0\\
0 & 0 & 0 & 0 & 0 & 0 & 0 & 1 & 0 & 0 & 0 & 0 & 0 & 0\\
0 & 0 & 0 & 0 & 0 & 0 & 0 & 0 & 1 & 0 & 0 & 0 & 0 & 0\\
0 & 0 & 0 & 0 & 0 & 0 & 0 & 0 & 0 & 1 & 0 & 0 & 0 & 0\\
0 & s_1 & s_2 & 0 & s_3 & 0 & s_4 & 0 & s_5 & 0 & s_6 & 0 & s_7 & 0\\
0 & 0 & 0 & 0 & 0 & 0 & 0 & 0 & 0 & 0 & 0 & 1 & 0 & 0\\
0 & 0 & 0 & 0 & 0 & 0 & 0 & 0 & 0 & 0 & 0 & 0 & 1 & 0\\
0 & 0 & 0 & 0 & 0 & 0 & 0 & 0 & 0 & 0 & 0 & 0 & 0 & 1\\
0 & t_1 & t_2 & 0 & t_3 & 0 & t_4 & 0 & t_5 & 0 & t_6 & 0 & t_7 & 0
\end{bmatrix} \tag{5. 42}$$

and the force vector in static bending is described by:

$$\mathbf{F}(x)=\{0 \quad 0 \quad 0 \quad 0 \quad 0 \quad r_8 \quad 0 \quad 0 \quad 0 \quad s_8 \quad 0 \quad 0 \quad 0 \quad t_8\}^{'} \tag{5. 43}$$

A formal solution of Eq. (5.40) is given by:

$$\mathbf{U}=\mathbf{e}^{\mathbf{T}x}\mathbf{K}+\int_0^x \mathbf{e}^{-\mathbf{T}\xi}\mathbf{F}(\xi)d\xi \tag{5. 44}$$

where **K** is a vector which can be solved from the BCs at x=±a/2 and $\mathbf{e}^{\mathbf{T}x}$ is of the form:

$$\mathbf{e}^{\mathbf{T}x}=\mathbf{E}\begin{bmatrix} e^{\lambda_1 x} & & 0\\ & \ddots & \\ 0 & & e^{\lambda_{14} x}\end{bmatrix}\mathbf{E}^{-1} \tag{5. 45}$$

where $\boldsymbol{\lambda}$ and **E** are the eigenvalues and columns of eigenvectors, respectively, associated with matrix **T**. The BCs expressed in terms of displacement variables are described by:

Clamped (C):

$$U=V=\frac{\partial V}{\partial x}=W_b=\frac{\partial W_b}{\partial x}=W_s=\frac{\partial W_s}{\partial x}=0 \tag{5. 46}$$

Simply supported (S):

$$U=V=\frac{\partial V}{\partial x}=W_b=W_s$$

$$=B_{11}\frac{\partial U_n}{\partial x}-\beta B_{12}V_n-D_{11}\frac{\partial^2 W_{bn}}{\partial x^2}+\beta^2 D_{12}W_{bn}-D_{11}^s\frac{\partial^2 W_{sn}}{\partial x^2}+\beta^2 D_{12}^s W_{sn}$$

$$-\beta^2 A_m W_{bn}-\frac{1}{2}\beta^2\left(A_m+B_m\right)W_{sn}-A_m\frac{\partial^2 W_{bn}}{\partial x^2}-\frac{1}{2}\left(A_m+B_m\right)\frac{\partial^2 W_{sn}}{\partial x^2}$$

$$= B_{11}\frac{\partial U_n}{\partial x} - \beta B_{12} V_n + \beta^2 \left(D_{12} - A_m\right) W_{bn} - \left(D_{11} + A_m\right)\frac{\partial^2 W_{bn}}{\partial x^2}$$
$$+ \beta^2 \left[D_{12}^s - \frac{1}{2}\left(A_m + B_m\right)\right] W_{sn} - \left[D_{11}^s + \frac{1}{2}\left(A_m + B_m\right)\right]\frac{\partial^2 W_{sn}}{\partial x^2} \qquad (5.47)$$

Free (F):

$$A_{11}\frac{\partial U_n}{\partial x} - \beta A_{12} V_x + \beta^2 B_{12} W_{bx} - B_{11}\frac{\partial^2 W_{bn}}{\partial x^2} + \beta^2 B_{12}^s W_{sx} - B_{11}^s \frac{\partial^2 W_{sn}}{\partial x^2}$$

$$= \left(\beta A_{66} - \frac{1}{4}\beta^3 A_m\right) U_x + \frac{1}{4}\beta A_m \frac{\partial^2 U_n}{\partial x^2} + \left(A_{66} + \frac{1}{4}\beta^2 A_m\right)\frac{\partial V_n}{\partial x} - \frac{1}{4} A_m \frac{\partial^3 V_n}{\partial x^3}$$
$$-2\beta B_{66}\frac{\partial W_{bn}}{\partial x} - 2\beta B_{66}^s \frac{\partial W_{sn}}{\partial x}$$

$$= -\frac{1}{2}\beta A_m \frac{\partial U_n}{\partial x} + \frac{1}{2} A_m \frac{\partial^2 V_n}{\partial x^2} - \frac{1}{2}\beta H_m W_{sx}$$

$$= B_{11}\frac{\partial U_n}{\partial x} - \beta B_{12} V_n - D_{11}\frac{\partial^2 W_{bn}}{\partial x^2} + \beta^2 D_{12} W_{bn} - D_{11}^s \frac{\partial^2 W_{sn}}{\partial x^2} + \beta^2 D_{12}^s W_{sn}$$
$$-\beta^2 A_m W_{bn} - \frac{1}{2}\beta^2 \left(A_m + B_m\right) W_{sn} - A_m \frac{\partial^2 W_{bn}}{\partial x^2} - \frac{1}{2}\left(A_m + B_m\right)\frac{\partial^2 W_{sn}}{\partial x^2}$$

$$= \left(-2\beta^2 B_{66} + \omega^2 I_1 + B_{11} a_1\right) U_x + \left[-\beta\left(B_{12} + 2B_{66}\right) + B_{11} a_2\right]\frac{\partial V_n}{\partial x} + B_{11} a_3 \frac{\partial^3 V_n}{\partial x^3}$$
$$+ \left[\beta^2\left(D_{12} + 4D_{66} + A_m\right) + \left(-\omega^2 I_2 + P_x^0 + P_{xy}^0\right) + B_{11} a_4\right]\frac{\partial W_{bn}}{\partial x} + \left[-\left(D_{11} + A_m\right) + B_{11} a_5\right]\frac{\partial^3 W_{bn}}{\partial x^3}$$
$$+ \left\{\beta^2\left[D_{12}^s + 4D_{66}^s + \frac{1}{2}\left(A_m + B_m\right)\right] + \left(-\omega^2 J_2 + P_x^0 + P_{xy}^0\right) + B_{11} a_6\right\}\frac{\partial W_{sn}}{\partial x}$$
$$+ \left[-D_{11}^s - \frac{1}{2}\left(A_m + B_m\right) + B_{11} a_7\right]\frac{\partial^3 W_{sn}}{\partial x^3}$$

$$= B_{11}\frac{\partial U_n}{\partial x} - \beta B_{12} V_n + \beta^2 \left(D_{12} - A_m\right) W_{bn} - \left(D_{11} + A_m\right)\frac{\partial^2 W_{bn}}{\partial x^2}$$
$$+ \beta^2 \left[D_{12}^s - \frac{1}{2}\left(A_m + B_m\right)\right] W_{sn} - \left[D_{11}^s + \frac{1}{2}\left(A_m + B_m\right)\right]\frac{\partial^2 W_{sn}}{\partial x^2}$$

$$
\begin{aligned}
&=\left(-2\beta^2 B_{66}^s+\omega^2 J_1+B_{11}^s a_1\right)U_n+\left[-\beta\left(B_{12}^s+2B_{66}^s\right)+B_{11}^s a_2\right]\frac{\partial V_n}{\partial x}+B_{11}^s a_3\frac{\partial^3 V_n}{\partial x^3}\\
&+\left[\left(-\omega^2 J_2+P_x^0+P_{xy}^0\right)+\beta^2\left(D_{12}^s+4D_{66}^s+\frac{3}{2}\left(A_m+B_m\right)\right)+B_{11}^s a_4\right]\frac{\partial W_{bn}}{\partial x}\\
&+\left(-D_{11}^s-\frac{1}{2}\left(A_m+B_m\right)+B_{11}^s a_5\right)\frac{\partial^3 W_{bn}}{\partial x^3}\\
&+\left\{\left(-\omega^2 K_2+P_x^0+P_{xy}^0\right)+A_{55}^s+\frac{1}{4}H_m+\beta^2\left[H_{12}+4H_{66}+\frac{3}{4}\left(A_m+2B_m+C_m\right)\right]+B_{11}^s a_6\right\}\frac{\partial W_{sn}}{\partial x}\\
&+\left[-H_{11}-\frac{1}{4}\left(A_m+2B_m+C_m\right)+B_{11}^s a_7\right]\frac{\partial^3 W_{sn}}{\partial x^3}
\end{aligned}
\tag{5.48}
$$

a. Vibration and buckling analysis:

As the force vector is vanished in the vibration and buckling analysis, the general solution in Eq. (5.44) becomes:

$$\mathbf{U}=\mathbf{e}^{\mathbf{T}x}\mathbf{K} \tag{5.49}$$

By substituting Eq. (5.49) into Eqs. (5.46)-(5.48) with the required BCs, a system of equations is obtained as:

$$\boldsymbol{\alpha}\mathbf{e}^{\mathbf{T}x}\mathbf{K}=\mathbf{0} \tag{5.50}$$

where $\boldsymbol{\alpha}$ comes from the coefficients in Eqs. (5.46)-(5.48) for the appropriate BCs at x=±a/2. The natural frequencies ω_n or the buckling loads of the n^{th} mode can be obtained by setting $\left|\boldsymbol{\alpha}\mathbf{e}^{\mathbf{T}x}\right|=0$. It is noticeable that the iteration procedure [72] is used in this chapter to calculate the natural frequencies/ buckling loads. The mode shapes are plotted by solving for **K** from Eq. (5.50) based on the singular value decomposition and calculating the displacement components along the plates after that.

b. Static analysis

The solutions for each value of n, which corresponds to the number of half-sine waves in y-direction can be obtained by substituting Eq. (5.44) to the appropriate BCs at x=±a/2. The displacements are then summed up using Eq. (5.37).

5.5.2 Numerical examples

5.5.2.1 Verification

a. Static analysis

The verification is carried out for macroplates with those published using the finite element method [185] and Levy solution [186]. The numerical results are also validated for microplates under simply-supported boundary conditions solved by Navier's solution. Non-dimensional

deflection $\bar{w}$ for Al/Al_2O_3 plates under uniform loads and various combinations of clamped (C), simply supported (S) and free (F) are presented in Table 5.15. The present results agree well in all BCs and slenderness ratios with those in the literature. Further verification for the FG microplates is presented in Table 5.16 for simply-supported microplates, which was obtained from the Navier's solution. A good agreement between present results and those from analytical solution can be observed for various parameters such as slenderness, thickness to material length scales and power-law indices.

Table 5. 15: Non-dimensional deflection of FG plates under various BCs.

a/h	p	Theory	SCSC	SSSC	SSSS	SFSC	SFSS	SFSF
5	0	HOBT [185]	0.3090	0.4020	0.5381	0.7579	0.9986	1.6153
		HOBT [186]	0.2990	0.3949	0.5354	0.7386	0.9871	1.5857
		Present HOBT	0.3220	0.4181	0.5589	0.7623	1.0110	1.6100
	0.5	HOBT [185]	0.4577	0.6015	0.8120	1.1431	1.5153	2.4570
		HOBT [186]	0.4443	0.5920	0.8085	1.1168	1.4997	2.4165
		Present HOBT	0.4775	0.6228	0.8323	1.1510	1.5273	2.4518
	1	HOBT [185]	0.5857	0.7734	1.0486	1.4728	1.9586	3.1759
		HOBT [186]	0.5714	0.7634	1.0450	1.4439	1.9419	3.1318
		Present HOBT	0.6136	0.7975	1.0569	1.4874	1.9639	3.1767
	2	HOBT [185]	0.7610	1.0028	1.3572	1.9003	2.5253	4.0852
		HOBT [186]	0.7462	0.9927	1.3539	1.8693	2.5080	4.0384
		Present HOBT	0.8022	1.0316	1.3475	1.9271	2.5209	4.0980
	5	HOBT [185]	0.9896	1.2770	1.6973	2.3685	3.1091	4.9908
		HOBT [186]	0.9711	1.2642	1.6929	2.3298	3.0871	4.9317
		Present HOBT	1.0495	1.3249	1.7068	2.4104	3.1214	5.0145
	10	HOBT [185]	1.1365	1.4518	1.9125	2.6697	3.4814	5.5730
		HOBT [186]	1.1121	1.4346	1.9059	2.6195	3.4517	5.4948
		Present HOBT	1.2044	1.5160	1.9574	2.7143	3.5176	5.5922
20	0	HOBT [185]	0.2256	0.3173	0.4521	0.6460	0.8851	1.4692
		HOBT [186]	0.2151	0.3099	0.4494	0.6264	0.8736	1.4396
		Present HOBT	0.2265	0.3216	0.4613	0.6385	0.8859	1.4522
	0.5	HOBT [185]	0.3449	0.4869	0.6956	0.9917	1.3618	2.2594
		HOBT [186]	0.3307	0.4770	0.6921	0.9649	1.3463	2.2189
		Present HOBT	0.3482	0.4922	0.7004	0.9833	1.3581	2.2382
	1	HOBT [185]	0.4448	0.6304	0.9033	1.2838	1.7670	2.9293
		HOBT [186]	0.4297	0.6199	0.8997	1.2543	1.7503	2.8851
		Present HOBT	0.4524	0.6345	0.8921	1.2783	1.7526	2.9102
	2	HOBT [185]	0.5670	0.8058	1.1572	1.6400	2.2615	3.7454
		HOBT [186]	0.5515	0.7954	1.1539	1.6087	2.2443	3.6989
		Present HOBT	0.5808	0.8074	1.1205	1.6395	2.2299	3.7312
	5	HOBT [185]	0.6776	0.9597	1.3747	1.9493	2.6835	4.4427
		HOBT [186]	0.6579	0.9463	1.3703	1.9098	2.6615	4.3837
		Present HOBT	0.6933	0.9641	1.3412	1.9470	2.6524	4.4226
	10	HOBT [185]	0.7521	1.0604	1.5138	2.1525	2.9557	4.8958
		HOBT [186]	0.7252	1.0418	1.5073	2.1006	2.9259	4.8177
		Present HOBT	0.7646	1.0705	1.5066	2.1419	2.9386	4.8609

Table 5. 16: Non-dimensional deflection of simply-supported FG microplates under uniform load.

a/h	l/h	p = 0			p = 1			p = 10		
		FSDT [187]	RFVPT [188]	Present HSDT	FSDT [164]	RFVPT [188]	Present HSDT	FSDT [187]	RFVPT [188]	Present HSDT
5	0.0	0.5147	0.5095	0.5384	1.1536	1.1441	1.1549	2.6273	2.8261	2.8530
	0.2	0.4479	0.4321	0.4674	0.9685	0.9396	0.9742	2.3127	2.3569	2.4162
	0.4	0.3250	0.2974	0.3353	0.6599	0.6120	0.6677	1.7138	1.5900	1.6888
	0.6	0.2268	0.1962	0.2282	0.4395	0.3874	0.4395	1.2163	1.0427	1.1380
	0.8	0.1631	0.1331	0.1577	0.3073	0.2561	0.2977	0.8841	0.7080	0.7852
	1.0	0.1230	0.0942	0.1129	0.2279	0.1784	0.2106	0.6710	0.5026	0.5626
10	0.0	0.4415	0.4403	0.4554	1.0205	1.0184	1.0040	2.2247	2.2756	2.2232
	0.2	0.3844	0.3805	0.3963	0.8567	0.8496	0.8478	1.9593	1.9723	1.9425
	0.4	0.2775	0.2706	0.2853	0.5798	0.5677	0.5800	1.4461	1.4159	1.4213
	0.6	0.1907	0.1829	0.1945	0.3790	0.3658	0.3805	1.0116	0.9677	0.9870
	0.8	0.1335	0.1259	0.1346	0.2573	0.2442	0.2570	0.7171	0.6720	0.6927
	1.0	0.0972	0.0899	0.0964	0.1838	0.1711	0.1814	0.5263	0.4830	0.5011
20	0.0	0.4232	0.4229	0.4346	0.9873	0.9867	0.9662	2.1240	2.1369	2.0647
	0.2	0.3684	0.3674	0.3783	0.8286	0.8269	0.8162	1.8705	1.8739	1.8226
	0.4	0.2655	0.2638	0.2724	0.5595	0.5565	0.5578	1.3781	1.3706	1.3532
	0.6	0.1814	0.1795	0.1858	0.3636	0.3602	0.3654	0.9591	0.9481	0.9485
	0.8	0.1259	0.1240	0.1285	0.2445	0.2417	0.2465	0.6740	0.6627	0.6691
	1.0	0.0906	0.0887	0.0921	0.1724	0.1693	0.1738	0.4888	0.4779	0.4854

b. Vibration and buckling analysis

Regarding the vibration behaviours, the first four natural frequencies of FG macroplates under various BCs are compared with those from the literature. The present fundamental frequencies are in excellent agreement with those published by Thai and Choi [189] using the state space based Levy method for the HSDT while the higher-mode frequencies slightly higher than those reported by Hosseini-Hashemi et al. [190] using another Levy method. This change is due to the increase of strain energy as a result of higher-order shear components.

Table 5. 17: The first four frequencies of Al/Al_2O_3 plates under SCSC and SCSS conditions (a/h=5).

BCs	Mode	Theory	p						
			0	0.5	1	2	5	8	10
SCSC	1	FSDT [190]	6.7663	5.8409	5.3039	4.8032	4.4127	4.2604	4.1865
		HSDT [189]	7.1104	6.1324	5.5509	4.9920	4.5128	-	4.2845
		Present HSDT	7.1104	6.1330	5.5518	4.9931	4.5141	4.3509	4.2859
	2	FSDT [190]	12.0602	10.4202	9.4561	8.5466	7.8331	7.5610	7.4307
		Present HSDT	12.3997	10.7310	9.7147	8.7086	7.8003	7.4978	7.3848
	3	FSDT [190]	13.5011	11.7581	10.7121	9.6759	8.7548	8.3957	8.2345
		Present HSDT	14.3191	12.4804	11.3314	10.1324	8.9301	8.5308	8.3927
	4	FSDT [190]	17.7182	15.4232	14.0402	12.6702	11.4732	11.0112	10.8022
		Present HSDT	18.5667	16.2020	14.7088	13.1346	11.5369	11.0107	10.8323
SCSS	1	FSDT [190]	5.9625	5.1188	4.6356	4.1996	3.8916	3.7746	3.7146
		HSDT [189]	6.1170	5.2500	4.7440	4.2751	3.9103	-	3.7322
		Present HSDT	6.1170	5.2516	4.7475	4.2806	3.9150	3.7893	3.7350
	2	FSDT [190]	11.7862	10.1652	9.2165	8.3310	7.6567	7.4012	7.2768
		Present HSDT	11.9345	10.3115	9.3302	8.3703	7.5253	7.2433	7.1355
	3	FSDT [190]	12.5431	10.8651	9.8739	8.9239	8.1442	7.8438	7.7031
		Present HSDT	12.9036	11.2016	10.1636	9.1169	8.1191	7.7815	7.6583
	4	FSDT [190]	17.1992	14.9302	13.5712	12.2492	11.1422	10.7172	10.5212
		Present HSDT	19.1332	17.1557	15.7412	14.0592	12.3257	11.5688	11.2754

Table 5. 18: The first four frequencies of Al/ZrO_2 plates under SCSF, SSSF and SFSF conditions (a/h=5).

BCs	Mode	Theory	p						
			0	0.5	1	2	5	8	10
SCSF	1	FSDT [190]	3.4383	3.2528	3.1804	3.1651	3.2092	3.2055	3.1936
		HSDT [189]	3.5275	3.3366	3.2598	3.2387	3.2757	3.2740	3.2642
		Present HSDT	3.5275	3.3368	3.2602	3.2393	3.2766	3.2749	3.2652
	2	FSDT [190]	7.7937	7.4170	7.2553	7.1894	7.2183	7.1916	7.1628
		Present HSDT	8.2135	7.8143	7.6329	7.5388	7.5337	7.5156	7.4965
	3	FSDT [190]	9.9541	9.4709	9.2647	9.1833	9.2242	9.1903	9.1533
		Present HSDT	10.0773	9.6010	9.3781	9.2495	9.2152	9.1884	9.1659
	4	FSDT [190]	13.5342	12.9212	12.6432	12.5022	12.4892	12.4262	12.3732
		Present HSDT	14.0120	13.3954	13.0834	12.8591	12.7217	12.6708	12.6428
SSSF	1	FSDT [190]	3.4383	3.2528	3.1804	3.1651	3.2092	3.2055	3.1936
		HSDT [189]	3.2779	3.0987	3.0274	3.0096	3.0478	3.0469	3.0377
		Present HSDT	3.2779	3.1010	3.0321	3.0159	3.0527	3.0504	3.0406
	2	FSDT [190]	7.7937	7.4170	7.2553	7.1894	7.2183	7.1916	7.1628
		Present HSDT	7.1825	6.8210	6.6659	6.6001	6.6244	6.6120	6.5937
	3	FSDT [190]	9.9541	9.4709	9.2647	9.1833	9.2242	9.1903	9.1533
		Present HSDT	9.9848	9.5125	9.2926	9.1672	9.1354	9.1087	9.0860
	4	FSDT [190]	13.5342	12.9212	12.6432	12.5022	12.4892	12.4262	12.3732
		Present HSDT	13.4133	12.8149	12.5209	12.3210	12.2110	12.1635	12.1348
SFSF	1	FSDT [190]	2.7184	2.5672	2.5096	2.5006	2.5429	2.5419	2.5327
		HSDT [189]	2.7330	2.5819	2.5226	2.5094	2.5448	2.5445	2.5367
		Present HSDT	2.7329	2.5821	2.5229	2.5099	2.5454	2.5452	2.5375
	2	FSDT [190]	4.2650	4.0376	3.9474	3.9260	3.9764	3.9710	3.9563
		Present HSDT	4.4344	4.1962	4.0995	4.0716	4.1163	4.1140	4.1019
	3	FSDT [190]	8.8171	8.3769	8.1902	8.1217	8.1770	8.1549	8.1241
		Present HSDT	9.5238	9.0690	8.8586	8.7418	8.7191	8.6952	8.6736
	4	FSDT [190]	9.4629	8.9983	8.8020	8.7282	8.7752	8.7451	8.7101
		Present HSDT	11.1175	10.5975	10.3510	10.2037	10.1562	10.1253	10.1009

The next comparison between the present fundamental frequencies of homogeneous microplates under various BCs and those from Jomehzadeh et al. [143] is depicted in Fig. 5.9. The material properties analyzed in this example are E=1.44GPa, ρ=1220kg/m^3, ν=0.38, a=b=10mm. Excellent agreement can be observed for all the material length scale ratios and boundary conditions. Further verification is presented in Table 5.19 for Mat_1/Mat_2 microplates, whose material properties are presented in Table 5.1. Again, excellent agreement is observed for the first two modes reported by Thai and Choi [158]. The present HSDT model provides slightly higher frequencies compared to the FSDT but smaller values in comparison with the CPT, which neglects the shear deformation effects.

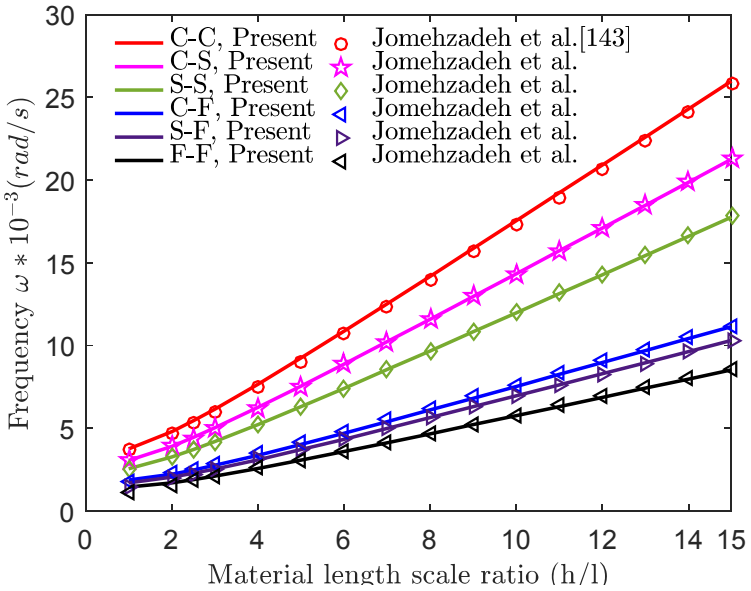

Fig. 5. 9: The size effect in the fundamental frequencies of epoxy plates under various BCs.

Table 5. 19: Size effect in the first two natural frequencies of Mat_1/Mat_2 simply supported plates.

a/h	l/h	p = 0			p = 1			p = 10		
		CPT [158]	FSDT [158]	Present HSDT	CPT [158]	FSDT [158]	Present HSDT	CPT [158]	FSDT [158]	Present HSDT
First mode										
5	0	5.9671	5.3871	5.3884	5.2960	4.8744	4.9097	6.2322	5.5818	5.4216
	0.2	6.3957	5.7797	5.7807	5.7810	5.3239	5.3486	6.6413	5.9551	5.8754
	0.4	7.5366	6.7996	6.8223	7.0383	6.4600	6.4775	7.7399	6.9333	7.0163
	0.6	9.1264	8.1595	8.2702	8.7406	7.9298	8.0025	9.2865	8.2517	8.5428
	0.8	10.9718	9.6451	9.9483	10.6773	9.4998	9.7331	11.0953	9.7045	10.2688
	1	12.9640	11.1311	11.7585	12.7419	11.0451	11.5485	13.0578	11.1666	11.9649
10	0	6.1103	5.9301	5.9302	5.3953	5.2697	5.3179	6.3958	6.1903	6.1851
	0.2	6.5491	6.3559	6.3566	5.8894	5.7518	5.7953	6.8156	6.5967	6.6205
	0.4	7.7174	7.4807	7.4911	7.1702	6.9920	7.0294	7.9431	7.6797	7.7590
	0.6	9.3453	9.0261	9.0712	8.9045	8.6477	8.7014	9.5303	9.1829	9.3365
	0.8	11.2349	10.7848	10.9046	10.8775	10.4942	10.6055	11.3866	10.9066	11.1686
	1	13.2749	12.6360	12.8837	12.9808	12.4128	12.6370	13.4006	12.7303	13.1500
20	0	6.1477	6.0997	6.0982	5.4210	5.3880	5.4392	6.4387	6.3837	6.4425
	0.2	6.5892	6.5376	6.5379	5.9175	5.8812	5.9305	6.8614	6.8026	6.8685
	0.4	7.7646	7.7009	7.7040	7.2044	7.1571	7.1990	7.9965	7.9251	7.9999
	0.6	9.4026	9.3158	9.3289	8.9470	8.8781	8.9192	9.5943	9.4993	9.5878
	0.8	11.3037	11.1801	11.2148	10.9293	10.8255	10.8787	11.4631	11.3303	11.4437
	1	13.3562	13.1786	13.2507	13.0426	12.8871	12.9696	13.4906	13.3030	13.4577
Second mode										
5	0	14.2717	11.6717	11.6852	12.7821	10.7905	10.8213	14.8485	11.9931	11.2750
	0.2	15.2967	12.5737	12.6733	13.9526	11.8256	11.9067	15.8232	12.8505	12.5635
	0.4	18.0253	14.8649	15.2580	16.9870	14.3792	14.6759	18.4408	15.0497	15.6480
	0.6	21.8277	17.8057	18.7916	21.0957	17.5492	18.3756	22.1257	17.9059	19.5692
	0.8	24.2521	20.8542	22.4013	24.2521	20.7470	22.3099	24.2521	20.8971	22.3515
	1	25.8375	23.7023	23.7224	25.8375	23.6723	23.6988	25.8375	23.7146	23.6867
10	0	15.0936	14.0893	14.0907	13.3625	12.6460	12.6809	15.7809	14.6464	14.3136
	0.2	16.1776	15.1064	15.1497	14.5861	13.8057	13.8632	16.8169	15.6144	15.4905
	0.4	19.0634	17.7680	17.9551	17.7583	16.7603	16.9117	19.5989	18.1705	18.4709
	0.6	23.0848	21.3648	21.8442	22.0536	20.6375	21.0265	23.5151	21.6607	22.4815
	0.8	27.7525	25.3657	26.3413	26.9400	24.8597	25.6993	28.0953	25.5744	27.0681
	1	32.7917	29.4588	31.1846	32.1492	29.1174	30.6760	33.0646	29.6009	31.9913
20	0	15.3223	15.0319	15.0292	13.5203	13.3192	13.3571	16.0428	15.7108	15.6456
	0.2	16.4227	16.1108	16.1242	14.7585	14.5378	14.5842	17.0960	16.7416	16.7453
	0.4	19.3522	18.9688	19.0284	17.9681	17.6812	17.7526	19.9241	19.4962	19.6316
	0.6	23.4345	22.9150	23.0701	22.3141	21.8989	22.0409	23.9054	23.3382	23.6370
	0.8	28.1730	27.4365	27.7568	27.2583	26.6355	26.9187	28.5616	27.7739	28.2910
	1	33.2885	32.2374	32.8132	32.5290	31.6012	32.1185	33.6134	32.5074	33.3258

Finally, the comparison is carried out for the buckling behaviour of FG plates. Similar to the vibration behaviour, there are no data for microplates under various BCs, the verification is carried out for macroplates under various BCs and for simply supported microplates. Table 5.20 presents the non-dimensional buckling loads of Al/Al_2O_3 under biaxial loads. The present results are nearly the same with those reported by Thai and Uy [191], which are obtained by the Levy solution and neutral axis concept.

Table 5. 20: Non-dimensional buckling loads of Al/Al_2O_3 plates under various BCs (a/h=5).

BCs	Theory	p					
		0	0.5	1	2	5	10
SCSC	Present HSDT	13.1426	8.8460	6.8778	5.2642	4.0410	3.5278
	HSDT [191]	13.1425	8.8460	6.8778	5.2642	4.0410	3.5278
SCSS	Present HSDT	10.0551	6.7079	5.2014	3.9994	3.1389	2.7657
	HSDT [191]	10.0551	6.7079	5.2014	3.9994	3.1389	2.7657
SSSS	Present HSDT	8.0106	5.3127	4.1122	3.1716	2.5265	2.2403
	HSDT [191]	8.0105	5.3127	4.1122	3.1716	2.5265	2.2403
SCSF	Present HSDT	4.9706	3.2680	2.5230	1.9546	1.5923	1.4259
	HSDT [191]	4.9706	3.2680	2.5231	1.9547	1.5924	1.4260
SSSF	Present HSDT	4.6270	3.0444	2.3556	1.8304	1.4931	1.3355
	HSDT [191]	4.6270	3.0391	2.3457	1.8182	1.4850	1.3313
SFSF	Present HSDT	4.1391	2.7149	2.0946	1.6247	1.3318	1.1959
	HSDT [191]	4.1391	2.7149	2.0946	1.6247	1.3318	1.1959

The size effect in buckling behaviour of Mat_1/Mat_2 plates under biaxial and uniaxial loads is presented for the simply-supported plates in Table 5.21.

Table 5. 21: Size effect in the buckling behaviour of simply supported Mat_1/Mat_2 plates.

a/h	l/h	p = 0			p = 1			p = 10		
		CPT [158]	FSDT [158]	Present HSDT	CPT [158]	FSDT [158]	Present HSDT	CPT [158]	FSDT [158]	Present HSDT
Biaxial buckling ($\gamma_1 = \gamma_2 = -1$)										
5	0	19.2255	15.3228	15.3323	8.2145	6.8576	6.9762	3.8359	2.9979	2.8206
	0.2	22.0863	17.6150	17.6397	9.7879	8.1715	8.2755	4.3560	3.4076	3.3219
	0.4	30.6685	24.2899	24.5529	14.5082	11.9922	12.1282	5.9164	4.6013	4.7614
	0.6	44.9723	34.7856	36.0588	22.3753	17.9838	18.5038	8.5171	6.4804	7.0935
	0.8	64.9976	48.2915	52.1533	33.3892	25.6654	27.3937	12.1581	8.9020	10.3175
	1	90.7444	63.8913	72.8328	47.5499	34.4981	38.7995	16.8393	11.7042	14.4405
10	0	19.2255	18.0746	18.0755	8.2145	7.8273	7.9778	3.8359	3.5853	3.5815
	0.2	22.0863	20.7607	20.7663	9.7879	9.3241	9.4736	4.3560	4.0710	4.1035
	0.4	30.6685	28.7478	28.8352	14.5082	13.7742	13.9362	5.9164	5.5151	5.6345
	0.6	44.9723	41.8271	42.2822	22.3753	21.0597	21.3542	8.5171	7.8802	8.1676
	0.8	64.9976	59.6657	61.0953	33.3892	30.9928	31.7235	12.1581	11.1065	11.6951
	1	90.7444	81.8269	85.2865	47.5499	43.3274	45.0402	16.8393	15.1152	16.2169
20	0	19.2255	18.9243	18.9243	8.2145	8.1142	8.2756	3.8359	3.7700	3.8419
	0.2	22.0863	21.7387	21.7330	9.7879	9.6675	9.8169	4.3560	4.2809	4.3561
	0.4	30.6685	30.1625	30.1768	14.5082	14.3167	14.4571	5.9164	5.8102	5.9028
	0.6	44.9723	44.1369	44.2235	22.3753	22.0292	22.2064	8.5171	8.3472	8.4754
	0.8	64.9976	63.5656	63.9520	33.3892	32.7517	33.0808	12.1581	11.8745	12.1212
	1	90.7444	88.3157	89.2519	47.5499	46.4105	46.9539	16.8393	16.3678	16.7298
Uniaxial buckling ($\gamma_1 = -1, \gamma_2 = 0$)										
5	0	38.4510	30.6456	30.6645	16.4291	13.7153	13.9450	7.6717	5.9959	5.6311
	0.2	44.1725	35.2300	35.2786	19.5759	16.3430	16.5443	8.7120	6.8153	6.6367
	0.4	61.3370	48.5799	49.1043	29.0164	23.9844	24.2523	11.8328	9.2027	9.5190
	0.6	89.9446	69.5711	72.1147	44.7505	35.9677	37.0028	17.0342	12.9607	14.1838
	0.8	129.9952	96.5829	104.3048	66.7784	51.3308	54.7822	24.3161	17.8040	20.6321
	1	181.4888	127.7826	145.6706	95.0998	68.9962	77.5973	33.6786	23.4084	28.8776
10	0	38.4510	36.1492	36.1510	16.4291	15.6547	15.9493	7.6717	7.1707	7.1574
	0.2	44.1725	41.5214	41.5325	19.5759	18.6482	18.9394	8.7120	8.1420	8.2031
	0.4	61.3370	57.4956	57.6783	29.0164	27.5483	27.8646	11.8328	11.0303	11.2768
	0.6	89.9446	83.6543	84.5644	44.7505	42.1194	42.7083	17.0342	15.7605	16.3352
	0.8	129.9952	119.3314	122.1907	66.7784	61.9856	63.4470	24.3161	22.2129	23.3902
	1	181.4888	163.6539	170.5729	95.0998	86.6547	90.0805	33.6786	30.2304	32.4337
20	0	38.4510	37.8485	37.8487	16.4291	16.2284	16.5451	7.6717	7.5400	7.6786
	0.2	44.1725	43.4774	43.4659	19.5759	19.3351	19.6496	8.7120	8.5619	8.7121
	0.4	61.3370	60.3249	60.3535	29.0164	28.6334	28.9457	11.8328	11.6205	11.8371
	0.6	89.9446	88.2739	88.4943	44.7505	44.0584	44.4602	17.0342	16.6945	16.9981
	0.8	129.9952	127.1312	127.9040	66.7784	65.5033	66.1616	24.3161	23.7489	24.1793
	1	181.4888	176.6313	178.5827	95.0998	92.8210	93.9867	33.6786	32.7357	33.4596

5.5.2.2 Parameter study

In this section, numerical examples are presented to analyse the static, vibration and buckling behaviours of FG and FG-sandwich plates. The metal and ceramic used in this section are Al and Al_2O_3 with the material properties presented in Table 5.1.

a. Static analysis

The size-dependent deflection and stress of FG-sandwich plates under several BCs are demonstrated in Fig. 5.10. For both SCSC and SCSF, the non-dimensional deflection decreases

significantly as the thickness reaches to the material length scale parameter (l=17.6μm). Similarly, the normal and shear stresses are also smaller in micro scales, as can be seen in Fig. 5.11 for SCSC and SCSS plates. This is due to the inclusion of couple stress and the corresponding curvatures in the strain energy.

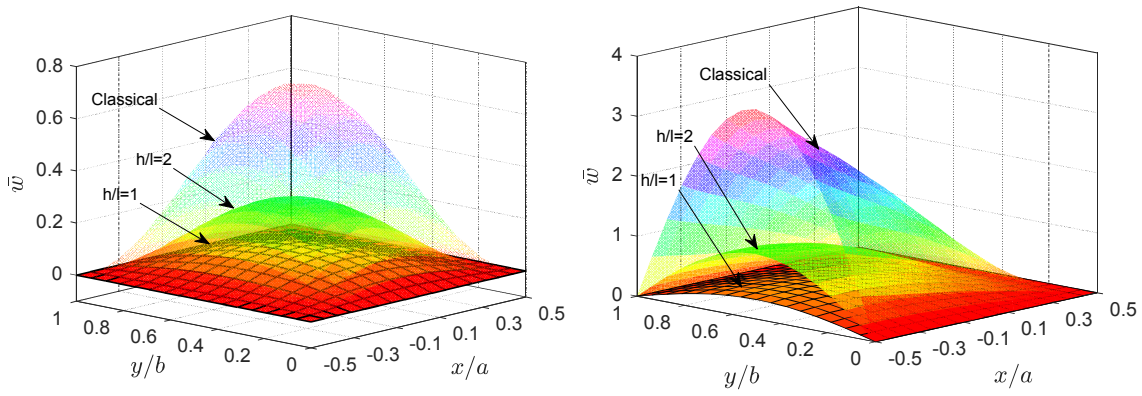

a. SCSC b. SCSF

Fig. 5. 10: Size effect in the deflection of FG-core (1-1-1) plates.

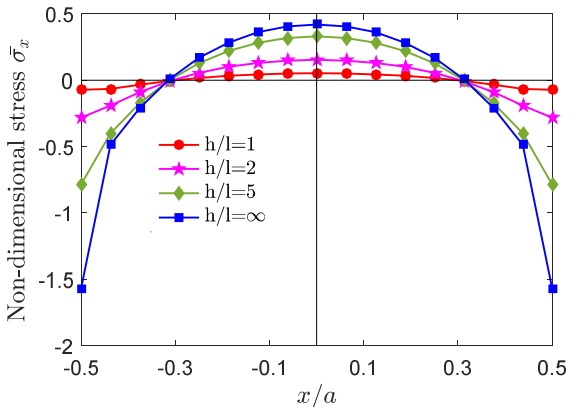

i. SCSC

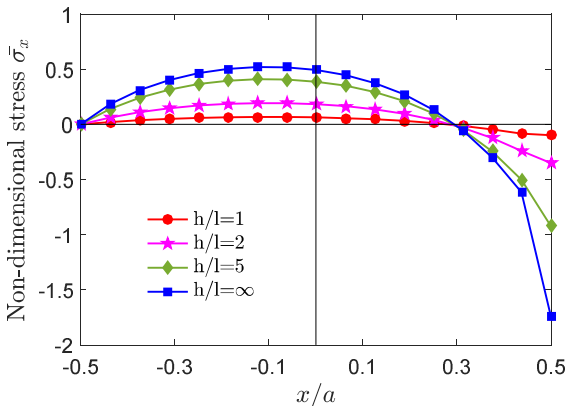

ii. SCSS

a. $\bar{\sigma}_x(x,b/2,h/2)$

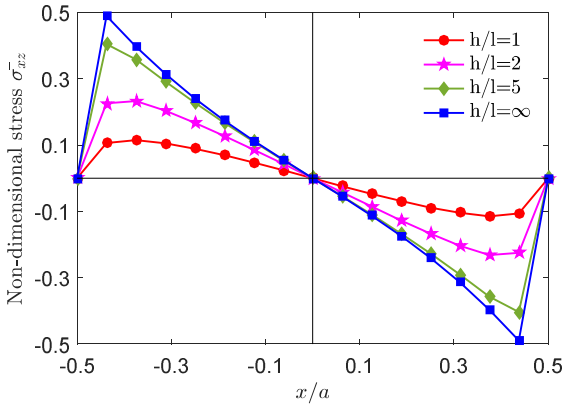

i. SCSC

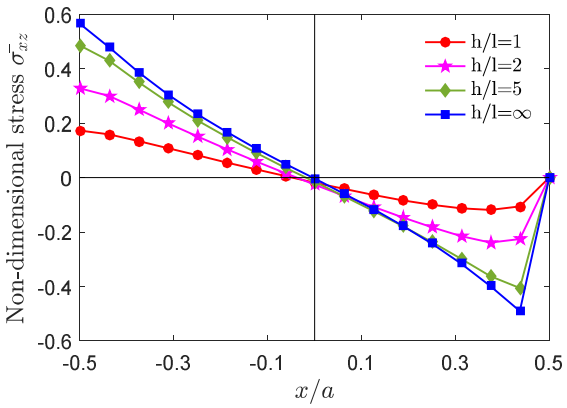

ii. SCSS

b. $\bar{\sigma}_{xz}(x,b/2,0)$

Fig. 5. 11: Size effect in the stresses of ceramic-core (1-1-1) plates (a/h=5).

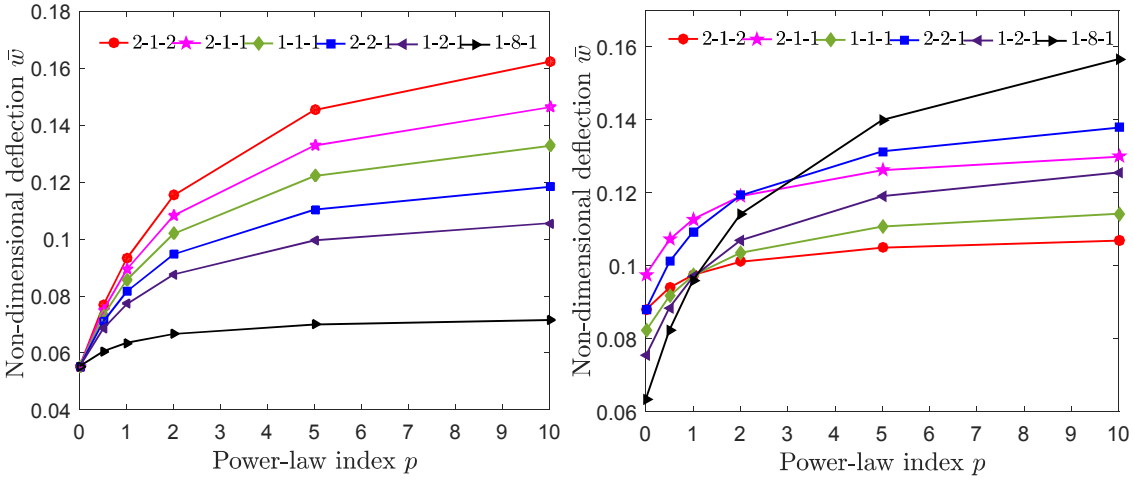

a. Ceramic-core *b. FG-core*

Fig. 5. 12: Non-dimensional deflection of various FG-sandwich plates (a/h=5, h/l=1, SCSC).

Deflection of FG-sandwich SCSC microplates is presented in Fig. 5.12. For both types of sandwich plates, the increase of power-law index, which results in the more prominent volume of metal, leads to the increase of deflection. It is understandable as the Young's modulus of metal is smaller than that of ceramic. This can be seen more clearly in the ceramic-core plates, the smallest deflection is obtained as p=0, and mount up with the higher power-law index. The deflection curve is always highest for the thin core (2-1-2) and lowest for the thick core (1-8-1). In the FG-core plates, there are changes in the deflection values for different schemes as p goes up. The shift approximately occurs at p=1 for symmetric geometries and at p=2 for asymmetric geometries. The benchmark results for the size-dependent bending behaviour of FG-sandwich plates are presented in Tables 5.22-5.27 under various BCs.

Table 5. 22: Non-dimensional deflection and stress of SCSC FG-sandwich plates (a/h=5).

Core	h/l	$\bar{w}(0,b/2)$			$\bar{\sigma}_x(0,b/2,h/2)$			$\bar{\sigma}_y(0,b/2,h/2)$		
		p=0	1	10	p=0	1	10	p=0	1	10
FG	1	0.0820	0.0972	0.1142	0.2320	0.2544	0.2808	0.2051	0.2265	0.2511
	2	0.2272	0.2745	0.3250	0.6780	0.7365	0.7921	0.6174	0.6724	0.7243
	4	0.4188	0.5103	0.6050	1.2871	1.3859	1.4480	1.2078	1.3055	1.3730
	8	0.5348	0.6531	0.7735	1.6560	1.7748	1.8259	1.5832	1.7084	1.7823
	∞	0.5907	0.7218	0.8548	1.8308	1.9583	2.0014	1.7680	1.9082	1.9885
Ceramic	1	0.0554	0.0857	0.1328	0.2050	0.0558	0.0840	0.1795	0.0485	0.0728
	2	0.1455	0.2301	0.3608	0.5385	0.1632	0.2649	0.4862	0.1479	0.2400
	4	0.2461	0.4153	0.7073	0.9018	0.3078	0.5575	0.8459	0.2884	0.5189
	8	0.2987	0.5257	0.9538	1.0843	0.3941	0.7670	1.0429	0.3761	0.7234
	∞	0.3223	0.5785	1.0834	1.1632	0.4345	0.8764	1.1341	0.4189	0.8321

Table 5. 23: Non-dimensional deflection and stress of SCSS FG-sandwich plates (a/h=5).

Core	h/l	$\bar{w}(0,b/2)$			$\bar{\sigma}_x(0,b/2,h/2)$			$\bar{\sigma}_y(0,b/2,h/2)$		
		p=0	1	10	p=0	1	10	p=0	1	10
FG	1	0.1133	0.1349	0.1594	0.2904	0.3265	0.3694	0.2699	0.2962	0.3273
	2	0.3097	0.3730	0.4399	0.8391	0.9327	1.0228	0.7850	0.8449	0.9017
	4	0.5610	0.6763	0.7913	1.5746	1.7285	1.8344	1.4986	1.5933	1.6536
	8	0.7094	0.8534	0.9919	2.0149	2.1973	2.2916	1.9415	2.0554	2.1093
	∞	0.7798	0.9372	1.0861	2.2216	2.4158	2.5008	2.1561	2.2801	2.3328
Ceramic	1	0.0768	0.1179	0.1817	0.2422	0.0660	0.0994	0.2389	0.0648	0.0974
	2	0.1974	0.3142	0.4958	0.6292	0.1905	0.3092	0.6341	0.1925	0.3123
	4	0.3261	0.5619	0.9728	1.0439	0.3565	0.6465	1.0805	0.3686	0.6653
	8	0.3905	0.7069	1.3095	1.2502	0.4550	0.8874	1.3172	0.4767	0.9218
	∞	0.4185	0.7749	1.4852	1.3392	0.5013	1.0132	1.4244	0.5288	1.0574

Table 5. 24: Non-dimensional deflection and stress of SSSS FG-sandwich plates (a/h=5).

Core	h/l	$\bar{w}(0,b/2)$			$\bar{\sigma}_x(0,b/2,h/2)$			$\bar{\sigma}_y(0,b/2,h/2)$		
		p=0	1	10	p=0	1	10	p=0	1	10
FG	1	0.1603	0.1920	0.2277	0.3250	0.3499	0.3803	0.3792	0.4208	0.4697
	2	0.4363	0.5290	0.6261	0.9440	1.0178	1.0878	1.0848	1.1854	1.2815
	4	0.7880	0.9560	1.1148	1.7776	1.9050	1.9786	2.0447	2.2080	2.3123
	8	0.9943	1.2028	1.3862	2.2812	2.4350	2.4879	2.6304	2.8252	2.9140
	∞	1.0906	1.3170	1.5092	2.5239	2.6914	2.7322	2.9070	3.1141	3.1927
Ceramic	1	0.1083	0.1651	0.2533	0.2972	0.0810	0.1222	0.3267	0.0889	0.1338
	2	0.2733	0.4371	0.6938	0.7630	0.2308	0.3745	0.8515	0.2580	0.4185
	4	0.4428	0.7763	1.3619	1.2533	0.4282	0.7775	1.4244	0.4863	0.8801
	8	0.5246	0.9723	1.8314	1.4947	0.5449	1.0648	1.7190	0.6242	1.2126
	∞	0.5592	1.0631	2.0751	1.5984	0.5995	1.2147	1.8497	0.6898	1.3874

Table 5. 25: Non-dimensional deflection and stress of SCSF FG-sandwich plates (a/h=5).

Core	h/l	$\bar{w}(0,b/2)$			$\bar{\sigma}_x(0,b/2,h/2)$			$\bar{\sigma}_y(0,b/2,h/2)$		
		p=0	1	10	p=0	1	10	p=0	1	10
FG	1	0.1956	0.2358	0.2836	0.2871	0.3226	0.3589	0.3877	0.4222	0.4671
	2	0.5733	0.6979	0.8305	0.7331	0.7962	0.8536	1.2346	1.3415	1.4468
	4	1.0718	1.2995	1.5102	1.2440	1.3340	1.3815	2.3712	2.5515	2.6594
	8	1.3603	1.6428	1.8843	1.4763	1.5792	1.6172	3.0209	3.2366	3.3254
	∞	1.4964	1.8049	2.0611	1.5592	1.6675	1.7036	3.3221	3.5564	3.6409
Ceramic	1	0.1349	0.2012	0.3042	0.2303	0.0628	0.0947	0.3612	0.0958	0.1415
	2	0.3622	0.5736	0.8998	0.5614	0.1748	0.2896	0.9962	0.2988	0.4795
	4	0.5977	1.0548	1.8526	0.8429	0.2969	0.5546	1.6551	0.5673	1.0288
	8	0.7119	1.3298	2.5177	0.9517	0.3508	0.6944	1.9725	0.7189	1.4022
	∞	0.7626	1.4583	2.8571	0.9905	0.3701	0.7466	2.1125	0.7884	1.5875

Table 5. 26: Non-dimensional deflection and stress of SSSF FG-sandwich plates (a/h=5).

Core	h/l	$\bar{w}(0,b/2)$			$\bar{\sigma}_x(0,b/2,h/2)$			$\bar{\sigma}_y(0,b/2,h/2)$		
		p=0	1	10	p=0	1	10	p=0	1	10
FG	1	0.2652	0.3195	0.3837	0.3915	0.4472	0.5071	0.5253	0.5691	0.6268
	2	0.7760	0.9405	1.1152	1.0188	1.1296	1.2353	1.6426	1.7657	1.8894
	4	1.4394	1.7281	1.9891	1.7393	1.8985	1.9968	3.1163	3.3010	3.3989
	8	1.8133	2.1616	2.4473	2.0705	2.2490	2.3321	3.9377	4.1405	4.1902
	∞	1.9874	2.3637	2.6597	2.1929	2.3798	2.4586	4.3122	4.5245	4.5549
Ceramic	1	0.1838	0.2725	0.4103	0.3045	0.0827	0.1244	0.4927	0.1308	0.1932
	2	0.4923	0.7806	1.2268	0.7482	0.2311	0.3806	1.3575	0.4056	0.6495
	4	0.8035	1.4332	2.5362	1.1232	0.3945	0.7353	2.2376	0.7665	1.3911
	8	0.9486	1.7999	3.4435	1.2667	0.4676	0.9272	2.6476	0.9672	1.8929
	∞	1.0114	1.9682	3.9014	1.3183	0.4944	1.0014	2.8244	1.0580	2.1401

Table 5. 27: Non-dimensional deflection and stress of SFSF FG-sandwich plates (a/h=5).

Core	h/l	$\bar{w}(0,b/2)$			$\bar{\sigma}_x(0,b/2,h/2)$			$\bar{\sigma}_y(0,b/2,h/2)$		
		p=0	1	10	p=0	1	10	p=0	1	10
FG	1	0.3832	0.4648	0.5637	0.4068	0.4674	0.5296	0.6895	0.7451	0.8237
	2	1.2176	1.4874	1.7798	0.9751	1.0598	1.1348	2.4251	2.6344	2.8538
	4	2.3527	2.8485	3.2835	1.4688	1.5652	1.5952	4.7630	5.1179	5.3132
	8	2.9762	3.5772	4.0434	1.5367	1.6359	1.6552	5.9861	6.3874	6.5026
	∞	3.2601	3.9098	4.3909	1.4934	1.5939	1.6209	6.5178	6.9426	7.0294
Ceramic	1	0.2694	0.3911	0.5802	0.3096	0.0835	0.1248	0.6727	0.1741	0.2527
	2	0.7743	1.2140	1.8871	0.7287	0.2311	0.3872	2.0054	0.5902	0.9326
	4	1.2834	2.3074	4.0918	0.9507	0.3499	0.6798	3.3253	1.1404	2.0686
	8	1.5113	2.9028	5.5973	0.9638	0.3647	0.7437	3.8872	1.4258	2.8034
	∞	1.6104	3.1708	6.3318	0.9466	0.3547	0.7176	4.1225	1.5486	3.1432

b. Vibration and buckling analysis

The vibration and buckling behaviours of FG and FG-sandwich plates are presented in this section. Firstly, the size effect in the natural frequencies of FG plates and the effect of BCs in microplates are presented in Fig. 5.13. As can be seen for the SCSC plates, the inclusion of couple stress results in a significant increase of frequencies for the small-scale plates, i.e. h/l<10. This effect is less important as the thickness of plates is up to h=20l for all the values of power-law index. Considering the plates with the micro thickness (h=l) under various BCs, the order of frequencies coincides with the stiffness of BCs, i.e. highest for SCSC and lowest for SFSF. Further investigation for the microplates is presented in Fig. 5.14 for sandwich plates. Opposite to the bending behaviour, the increase of p results in the lower frequencies in ceramic-core plates, except 1-8-1 scheme. It is worth noting that, the natural frequencies are determined by both the Young's modulus and mass density. The increase of metal volume fraction is equivalent to the lower stiffness and lower mass. These factors lead to the decrease of natural frequencies when the ceramic-core is thin, where the Young's modulus contributes more effect. However, for the plates with very thick ceramic core (1-8-1 scheme), where the stiffness is concentrated

near the neutral axis, the decrease of mass is prominent involving the frequencies. Therefore, the increase of p in this case results in a slight escalation of frequencies. For the FG-core plates, the natural frequencies also depend on the relative thickness of the core. As the core is thick enough, i.e. 1-8-1, 1-2-1 and 2-2-1 plates, the behaviour of these sandwich plates is similar to that of FG plates. In the thin core plates, the increase of metal in the core does not affect the stiffness much while the decrease of mass slightly improves the frequencies. The benchmark results of natural frequencies are presented for some FG-sandwich plates with different slenderness ratios, power-law index and BCs in Tables 5.28 - 5.33. Several mode shapes of FG microplates under SCSC and SFSF are then illustrated in Figs. 5.15 and 5.16.

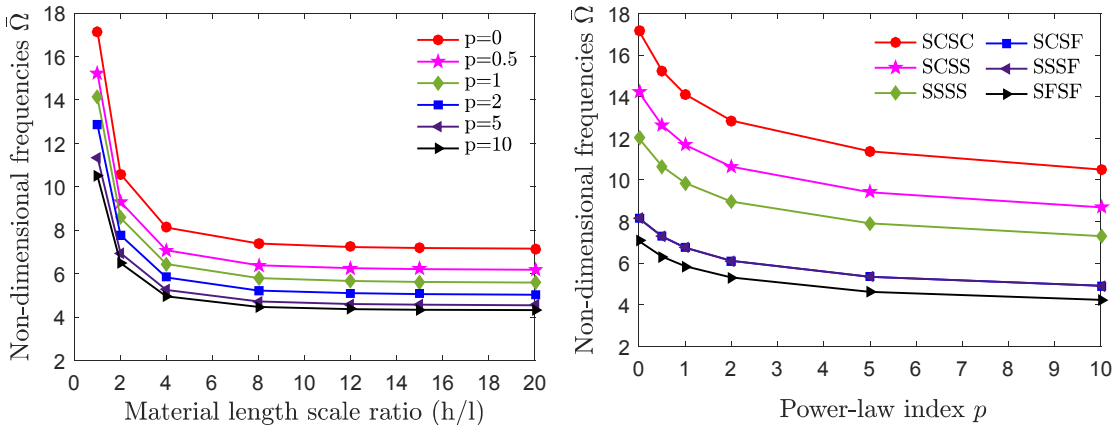

a. SCSC *b.* $h/l=1$

Fig. 5. 13: Effects of power-law index and boundary condition in the vibration of Al/Al_2O_3 plates (a/h=5).

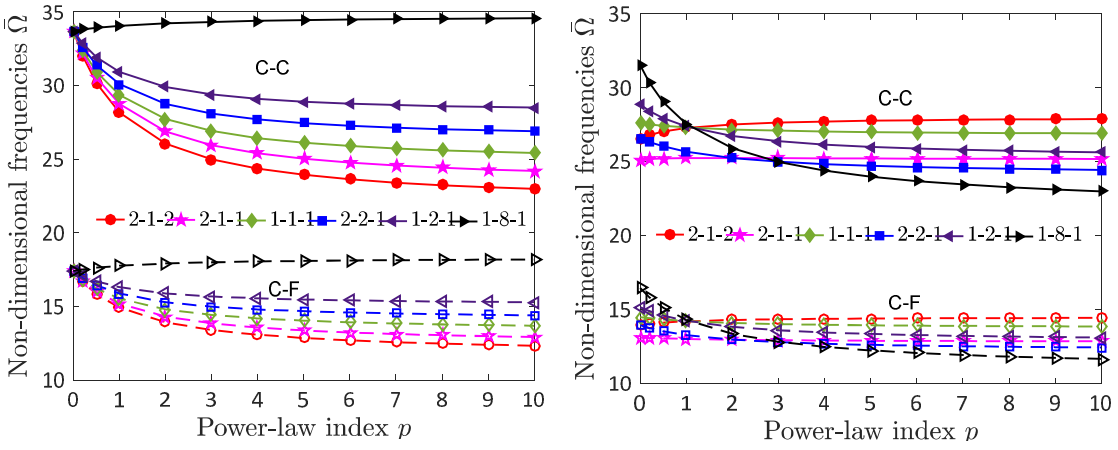

a. Ceramic-core plates *b. FG-core plates*

Fig. 5. 14: Non-dimensional frequencies of Al/Al_2O_3 sandwich microplates (a/h=5, h/l=1).

Table 5. 28: Non-dimensional frequencies of SCSC FG-sandwich plates.

Core	a/h	h/l	Scheme								
			2-1-1			1-1-1			1-2-1		
			p=0	1	10	p=0	1	10	p=0	1	10
Ceramic	5	1	33.7216	28.7547	24.1988	33.7216	29.3627	25.4263	33.7216	30.9303	28.5057
		2	20.7906	17.4513	14.5361	20.7906	17.8440	15.3167	20.7906	18.8231	17.1885
		4	15.9756	12.9530	10.4561	15.9756	13.2457	10.8913	15.9756	14.0610	12.3369
		8	14.5036	11.5064	9.0823	14.5036	11.7642	9.3666	14.5036	12.5433	10.6897
		∞	13.9645	10.9692	8.5632	13.9645	11.2137	8.7850	13.9645	11.9811	10.0649
	20	1	38.7411	33.7095	28.5605	38.7411	34.5036	30.2924	38.7411	36.2504	33.9323
		2	24.2913	20.0890	16.5414	24.2913	20.5526	17.3794	24.2913	21.7545	19.6155
		4	19.0339	14.8133	11.6972	19.0339	15.1430	12.0901	19.0339	16.1907	13.8191
		8	17.4731	13.1626	10.1222	17.4731	13.4490	10.3427	17.4731	14.4642	11.9271
		∞	16.9196	12.5627	9.5385	16.9196	12.8334	9.6875	16.9196	13.8387	11.2238
FG	5	1	25.1288	25.2542	25.1957	27.5819	27.3226	26.9216	28.8806	27.3924	25.6409
		2	14.9157	15.0383	15.1541	16.5312	16.2556	16.0332	17.4393	16.3575	15.3798
		4	10.8691	11.0403	11.1939	12.1478	11.9039	11.7583	12.9496	12.0460	11.3450
		8	9.5738	9.7750	9.9253	10.7409	10.5179	10.4029	11.5214	10.6803	10.0593
		∞	9.0935	9.3059	9.4476	10.2194	10.0049	9.8997	10.9939	10.1757	9.5778
	20	1	28.7888	28.6484	28.5247	31.8999	31.2187	30.5910	33.5114	31.3155	29.0556
		2	17.0320	17.2420	17.5520	18.9074	18.5578	18.4310	20.0445	18.7195	17.7764
		4	12.4594	12.8992	13.4701	13.8546	13.6622	13.8069	14.8635	13.8817	13.5569
		8	11.0220	11.5607	12.2351	12.2668	12.1317	12.3832	13.2519	12.3787	12.2750
		∞	10.4976	11.0768	11.7925	11.6876	11.5742	11.8701	12.6676	11.8345	11.8156

Table 5. 29: Non-dimensional frequencies of SCSS FG-sandwich plates.

Core	a/h	h/l	Scheme								
			2-1-1			1-1-1			1-2-1		
			p=0	1	10	p=0	1	10	p=0	1	10
Ceramic	5	1	25.0912	22.6033	19.4670	25.0912	23.1497	20.7836	25.0912	24.2065	23.1855
		2	17.4407	14.5934	12.1170	17.4407	14.9240	12.7649	17.4407	15.7545	14.3429
		4	13.5861	10.8967	8.7362	13.5861	11.1416	9.0826	13.5861	11.8505	10.3143
		8	12.4285	9.7159	7.6033	12.4285	9.9311	7.8208	12.4285	10.6159	8.9542
		∞	12.0135	9.2820	7.1779	12.0135	9.4861	7.3420	12.0135	10.1643	8.4418
	20	1	31.6987	27.5944	23.3822	31.6987	28.2460	24.8065	31.6987	29.6742	27.7866
		2	19.8978	16.4478	13.5381	19.8978	16.8275	14.2231	19.8978	17.8134	16.0556
		4	15.6092	12.1319	9.5731	15.6092	12.4017	9.8926	15.6092	13.2627	11.3102
		8	14.3374	10.7820	8.2846	14.3374	11.0163	8.4630	14.3374	11.8511	9.7622
		∞	13.8870	10.2919	7.8071	13.8870	10.5123	7.9267	13.8870	11.3392	9.1859
FG	5	1	19.2742	18.9688	18.6143	21.3883	20.8534	20.2368	22.3738	20.8566	19.0330
		2	12.4027	12.5144	12.6260	13.7764	13.5291	13.3387	14.5607	13.6252	12.8087
		4	9.1165	9.3080	9.4986	10.1925	9.9986	9.9168	10.8924	10.1319	9.6101
		8	8.0725	8.3088	8.5244	9.0490	8.8835	8.8502	9.7336	9.0356	8.6160
		∞	7.6892	7.9447	8.1676	8.6288	8.4753	8.4614	9.3099	8.6353	8.2530
	20	1	23.5469	23.4270	23.3227	26.1010	25.5350	25.0147	27.4233	25.6150	23.7573
		2	13.9384	14.1121	14.3693	15.4756	15.1881	15.0855	16.4095	15.3218	14.5520
		4	10.2026	10.5693	11.0473	11.3445	11.1888	11.3142	12.1735	11.3702	11.1158
		8	9.0286	9.4785	10.0455	10.0467	9.9390	10.1545	10.8563	10.1431	10.0746
		∞	8.6004	9.0852	9.6875	9.5742	9.4839	9.7358	10.3780	9.6980	9.7022

Table 5. 30: Non-dimensional frequencies of SSSS FG-sandwich plates.

Core	a/h	h/l	Scheme								
			2-1-1			1-1-1			1-2-1		
			p=0	1	10	p=0	1	10	p=0	1	10
Ceramic	5	1	23.5707	20.2272	17.0441	23.5707	20.6741	17.9803	23.5707	21.7588	20.1507
		2	14.8313	12.3853	10.2699	14.8313	12.6640	10.8059	14.8313	13.3755	12.1521
		4	11.6514	9.2819	7.4220	11.6514	9.4846	7.6892	11.6514	10.1011	8.7462
		8	10.7068	8.2937	6.4705	10.7068	8.4701	6.6243	10.7068	9.0693	7.5997
		∞	10.3723	7.9323	6.1137	10.3723	8.0990	6.2213	10.3723	8.6941	7.1691
	20	1	26.4926	23.0719	19.5577	26.4926	23.6143	20.7428	26.4926	24.8074	23.2345
		2	16.6404	13.7565	11.3313	16.6404	14.0688	11.8882	16.6404	14.8940	13.4211
		4	13.0620	10.1514	8.0227	13.0620	10.3698	8.2675	13.0620	11.0911	9.4536
		8	12.0015	9.0243	6.9488	12.0015	9.2121	7.0726	12.0015	9.9118	8.1599
		∞	11.6246	8.6151	6.5500	11.6246	8.7914	6.6255	11.6246	9.4839	7.6791
FG	5	1	17.3777	17.3549	17.2264	19.2229	18.9012	18.4870	20.1870	18.9630	17.5522
		2	10.5592	10.6657	10.7711	11.7073	11.5142	11.3728	12.3699	11.5945	10.9254
		4	7.8488	8.0445	8.2384	8.7255	8.6028	8.5790	9.3112	8.7132	8.3290
		8	6.9918	7.2351	7.4630	7.7773	7.6878	7.7167	8.3485	7.8138	7.5340
		∞	6.6754	6.9393	7.1808	7.4281	7.3513	7.4017	7.9968	7.4844	7.2448
	20	1	19.7369	19.6452	19.5604	21.8501	21.3978	20.9805	22.9435	21.4593	19.9254
		2	11.7480	11.9096	12.1291	12.9942	12.7927	12.7370	13.7544	12.8956	12.2846
		4	8.6575	8.9838	9.3882	9.5613	9.4820	9.6239	10.2266	9.6217	9.4489
		8	7.6898	8.0862	8.5648	8.4854	8.4508	8.6702	9.1312	8.6080	8.5930
		∞	7.3370	7.7609	8.2688	8.0925	8.0757	8.3255	8.7347	8.2394	8.2856

Table 5. 31: Non-dimensional frequencies of SCSF FG-sandwich plates.

Core	a/h	h/l	Scheme								
			2-1-1			1-1-1			1-2-1		
			p=0	1	10	p=0	1	10	p=0	1	10
Ceramic	5	1	17.4115	15.1927	12.9223	17.4115	15.5346	13.6860	17.4115	16.3062	15.2884
		2	10.3808	8.7861	7.3515	10.3808	8.9912	7.7840	10.3808	9.4739	8.7245
		4	7.9354	6.3097	5.0479	7.9354	6.4522	5.2536	7.9354	6.8716	5.9710
		8	7.2041	5.5314	4.2932	7.2041	5.6528	4.4057	7.2041	6.0603	5.0605
		∞	6.9279	5.2391	4.0081	6.9279	5.3527	4.0846	6.9279	5.7558	4.7164
	20	1	19.3465	17.0642	14.5652	19.3465	17.4711	15.4956	19.3465	18.3173	17.3161
		2	11.4560	9.6479	8.0372	11.4560	9.8741	8.4858	11.4560	10.4207	9.5437
		4	8.6025	6.7444	5.3629	8.6025	6.8957	5.5623	8.6025	7.3624	6.3426
		8	7.7820	5.8573	4.5081	7.7820	5.9848	4.6096	7.7820	6.4368	5.3139
		∞	7.4960	5.5433	4.2016	7.4960	5.6621	4.2652	7.4960	6.1101	4.9434
FG	5	1	13.0971	13.0107	12.8546	14.4816	14.2185	13.8586	15.1609	14.2424	13.1131
		2	7.4245	7.4393	7.4678	8.2772	8.0889	7.9276	8.7426	8.1411	7.5849
		4	5.2723	5.4047	5.5600	5.8937	5.7838	5.7659	6.3079	5.8667	5.6139
		8	4.6037	4.7844	4.9816	5.1474	5.0705	5.1072	5.5508	5.1661	5.0166
		∞	4.3497	4.5472	4.7578	4.8658	4.7997	4.8546	5.2657	4.9003	4.7863
	20	1	14.5707	14.4200	14.2663	16.1596	15.7819	15.3906	16.9420	15.8109	14.5554
		2	8.1819	8.2216	8.3019	9.0895	8.8992	8.7841	9.6072	8.9597	8.4248
		4	5.6757	5.8579	6.1026	6.3116	6.2177	6.2700	6.7606	6.3117	6.1451
		8	4.9074	5.1509	5.4616	5.4593	5.4009	5.5192	5.8971	5.5107	5.4766
		∞	4.6337	4.9006	5.2360	5.1565	5.1112	5.2532	5.5923	5.2275	5.2409

Table 5. 32: Non-dimensional frequencies of SSSF FG-sandwich plates.

Core	a/h	h/l	Scheme								
			2-1-1			1-1-1			1-2-1		
			p=0	1	10	p=0	1	10	p=0	1	10
Ceramic	5	1	16.0456	14.0147	11.9287	16.0456	14.3297	12.6307	16.0456	15.0403	14.1108
		2	9.5669	8.0946	6.7735	9.5669	8.2820	7.1651	9.5669	8.7278	8.0330
		4	7.3391	5.8245	4.6587	7.3391	5.9539	4.8395	7.3391	6.3433	5.5030
		8	6.6834	5.1195	3.9730	6.6834	5.2294	4.0679	6.6834	5.6090	4.6750
		∞	6.4376	4.8567	3.7158	6.4376	4.9597	3.7780	6.4376	5.3356	4.3647
	20	1	17.7053	15.6114	13.3239	17.7053	15.9825	14.1703	17.7053	16.7578	15.8369
		2	10.5061	8.8430	7.3668	10.5061	9.0483	7.7707	10.5061	9.5505	8.7410
		4	7.9085	6.1975	4.9303	7.9085	6.3341	5.1055	7.9085	6.7637	5.8226
		8	7.1659	5.3932	4.1549	7.1659	5.5080	4.2402	7.1659	5.9245	4.8888
		∞	6.9071	5.1099	3.8771	6.9071	5.2165	3.9286	6.9071	5.6302	4.5541
FG	5	1	12.1291	12.0524	11.9171	13.3842	13.1555	12.8461	13.9994	13.1728	12.1564
		2	6.8742	6.8931	6.9237	7.6448	7.4844	7.3493	8.0664	7.5296	7.0322
		4	4.9041	5.0343	5.1845	5.4616	5.3757	5.3740	5.8369	5.4496	5.2341
		8	4.2996	4.4759	4.6668	4.7862	4.7315	4.7812	5.1520	4.8172	4.6986
		∞	4.0703	4.2624	4.4667	4.5324	4.4874	4.5540	4.8956	4.5779	4.4922
	20	1	13.3506	13.2192	13.0830	14.7944	14.4588	14.1109	15.5066	14.4839	13.3474
		2	7.5312	7.5748	7.6517	8.3490	8.1888	8.0953	8.8169	8.2416	7.7649
		4	5.2535	5.4275	5.6543	5.8215	5.7515	5.8115	6.2256	5.8343	5.6944
		8	4.5585	4.7885	5.0754	5.0499	5.0126	5.1330	5.4435	5.1098	5.0905
		∞	4.3117	4.5627	4.8712	4.7770	4.7512	4.8933	5.1687	4.8541	4.8786

Table 5. 33: Non-dimensional frequencies of SFSF FG-sandwich plates.

Core	a/h	h/l	Scheme								
			2-1-1			1-1-1			1-2-1		
			p=0	1	10	p=0	1	10	p=0	1	10
Ceramic	5	1	13.8910	12.2205	10.4375	13.8910	12.4989	11.0708	13.8910	13.1056	12.3599
		2	8.0274	6.8250	5.7292	8.0274	6.9853	6.0733	8.0274	7.3551	6.8017
		4	6.1085	4.8388	3.8667	6.1085	4.9482	4.0236	6.1085	5.2727	4.5749
		8	5.5690	4.2515	3.2907	5.5690	4.3445	3.3735	5.5690	4.6621	3.8790
		∞	5.3674	4.0371	3.0813	5.3674	4.1243	3.1370	5.3674	4.4387	3.6259
	20	1	14.9603	13.2411	11.3227	14.9603	13.5577	12.0544	14.9603	14.2071	13.4636
		2	8.7270	7.3796	6.1648	8.7270	7.5532	6.5161	8.7270	7.9659	7.3223
		4	6.5161	5.1095	4.0657	6.5161	5.2242	4.2189	6.5161	5.5772	4.8091
		8	5.9061	4.4410	3.4161	5.9061	4.5375	3.4923	5.9061	4.8810	4.0267
		∞	5.6988	4.2126	3.1916	5.6988	4.3032	3.2405	5.6988	4.6435	3.7559
FG	5	1	10.5560	10.4584	10.3117	11.6591	11.4410	11.1477	12.1889	11.4505	10.5271
		2	5.7768	5.7758	5.7887	6.4360	6.2868	6.1575	6.7906	6.3233	5.8825
		4	4.0463	4.1536	4.2861	4.5205	4.4378	4.4343	4.8401	4.5028	4.3246
		8	3.5434	3.6926	3.8631	3.9575	3.9024	3.9454	4.2703	3.9779	3.8860
		∞	3.3575	3.5196	3.7010	3.7510	3.7043	3.7614	4.0612	3.7835	3.7187
	20	1	11.3079	11.1767	11.0409	12.5418	12.2439	11.9282	13.1421	12.2623	11.2691
		2	6.2607	6.2806	6.3304	6.9552	6.8065	6.7097	7.3457	6.8495	6.4271
		4	4.3001	4.4371	4.6227	4.7819	4.7102	4.7494	5.1215	4.7811	4.6548
		8	3.7209	3.9072	4.1455	4.1390	4.0952	4.1870	4.4717	4.1790	4.1563
		∞	3.5221	3.7253	3.9824	3.9188	3.8845	3.9947	4.2493	3.9726	3.9849

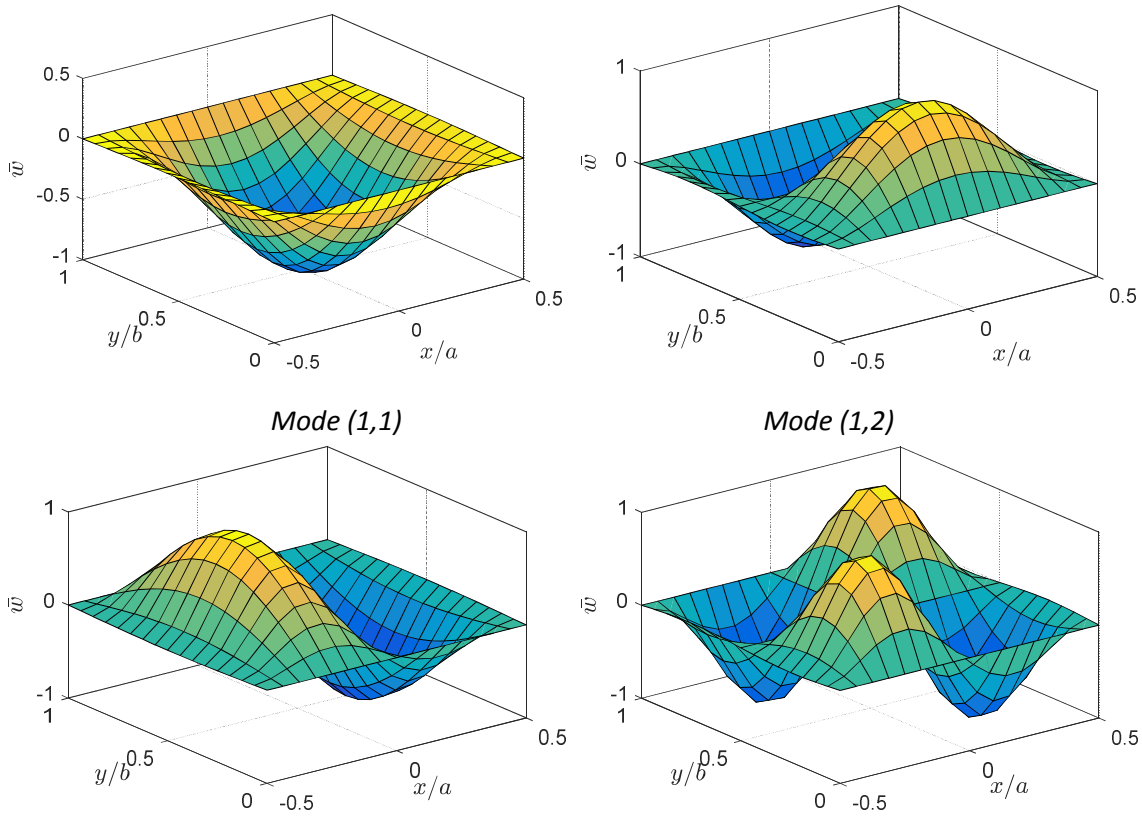

Fig. 5. 15: The first four mode shapes of SCSC FG microplates (a/h=10, h/l=2).

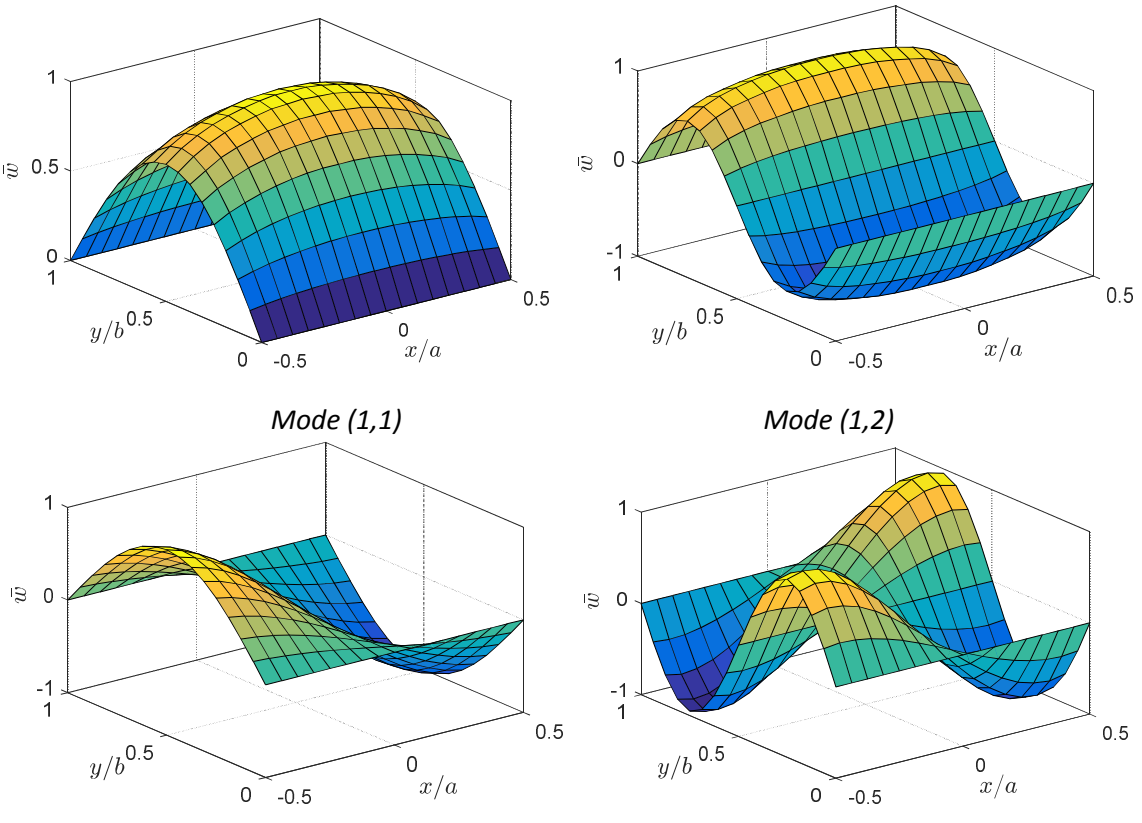

Fig. 5. 16: The first four mode shapes of SFSF FG microplates (a/h=10, h/l=2).

Finally, the critical buckling loads of various ceramic- and FG-core micro plates under axial loads are investigated. The size dependent effect on buckling behaviours is presented in Tables 5.34 - 5.39 for various FG-core and ceramic-core plates. As expected, the critical buckling loads always decrease with an increase of metal volume fraction for all the schemes (Fig. 5.17). It is worth nothing that, they only depend on the stiffness, therefore, their variations are more significant in thicker FG layers.

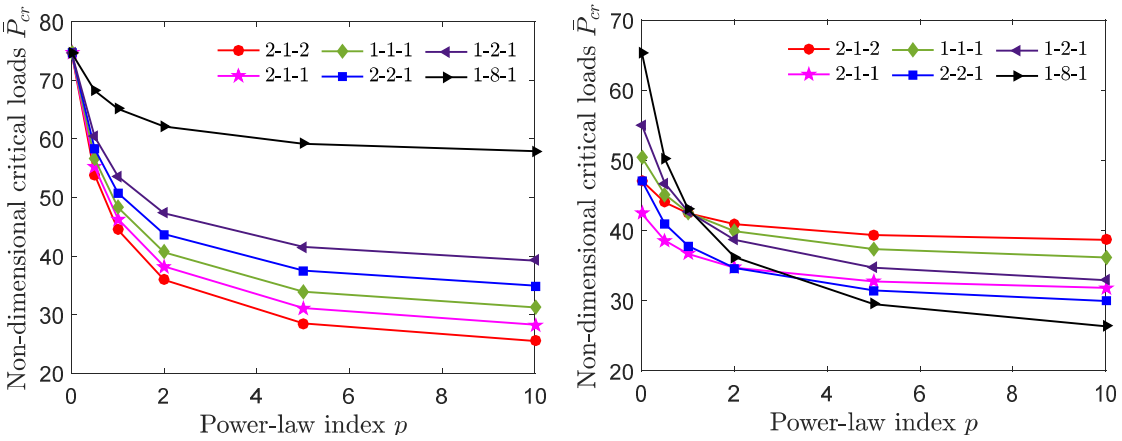

a. Ceramic core *b. FG core*

Fig. 5. 17: Non-dimensional buckling loads of Al/Al_2O_3 sandwich microplates (a/h=5, h/l=1).

Table 5. 34: Non-dimensional buckling loads of SCSC FG-sandwich plates.

Core	a/h	h/l	Scheme								
			2-1-1			1-1-1			1-2-1		
			p=0	1	10	p=0	1	10	p=0	1	10
Ceramic	5	1	74.6429	46.2857	28.2857	74.6429	48.2857	31.2143	74.6429	53.5714	39.2143
		2	28.5357	17.2500	10.3571	28.5357	18.0357	11.5000	28.5357	20.0357	14.4643
		4	16.9821	9.5893	5.4107	16.9821	10.0357	5.8750	16.9821	11.3036	7.5357
		8	14.0982	7.6250	4.1161	14.0982	7.9732	4.3750	14.0982	9.0536	5.6964
		∞	13.1425	6.9573	3.6713	13.1425	7.2751	3.8618	13.1425	8.3021	5.0680
	20	1	95.6571	61.9429	38.3238	95.6571	64.9143	43.1238	95.6571	71.6571	54.0952
		2	37.6381	22.0000	12.8571	37.6381	23.0286	14.1905	37.6381	25.8095	18.0762
		4	23.1333	11.9714	6.4286	23.1333	12.5143	6.8667	23.1333	14.3048	8.9714
		8	19.5048	9.4571	4.8190	19.5048	9.8714	5.0286	19.5048	11.4238	6.6905
		∞	18.2971	8.6195	4.2801	18.2971	8.9947	4.4153	18.2971	10.4621	5.9263
FG	5	1	42.4214	36.6786	31.8357	50.4571	42.5429	36.1786	55.0571	42.6929	32.9286
		2	14.9643	12.9571	11.3786	18.2571	15.1036	12.7536	20.2393	15.2714	11.7214
		4	8.0143	7.0250	6.2214	9.9554	8.1679	6.8946	11.2696	8.3518	6.3982
		8	6.2563	5.5420	4.9205	7.8313	6.4170	5.4295	8.9768	6.6071	5.0607
		∞	5.6680	5.0475	4.4853	7.1163	5.8309	4.9412	8.2061	6.0234	4.6140
	20	1	52.9143	44.8000	38.2857	64.9143	53.1810	44.0381	71.6190	53.4857	39.6952
		2	18.5143	16.2286	14.4952	22.8190	18.8000	15.9810	25.6381	19.1238	14.8762
		4	9.9143	9.0952	8.5524	12.2571	10.1905	8.9810	14.1048	10.5238	8.6571
		8	7.7667	7.3095	7.0619	9.6095	8.0429	7.2286	11.2143	8.3714	7.1048
		∞	7.0491	6.7146	6.5647	8.7309	7.3259	6.6457	10.2534	7.6569	6.5883

Table 5. 35: Non-dimensional buckling loads of SCSS FG-sandwich plates.

Core	a/h	h/l	Scheme								
			2-1-1			1-1-1			1-2-1		
			p=0	1	10	p=0	1	10	p=0	1	10
Ceramic	5	1	53.5000	33.4286	20.5000	53.5000	34.9286	22.6429	53.5000	38.7143	28.5000
		2	20.9286	12.5714	7.5000	20.9286	13.1429	8.3214	20.9286	14.6429	10.5000
		4	12.7857	7.0536	3.9286	12.7857	7.3929	4.2500	12.7857	8.3571	5.4821
		8	10.7321	5.6339	2.9911	10.7321	5.8929	3.1696	10.7321	6.7321	4.1518
		∞	10.0550	5.1599	2.6760	10.0550	5.3924	2.7987	10.0550	6.1864	3.6973
	20	1	66.7048	43.2381	26.7429	66.7048	45.2952	30.0952	66.7048	49.9810	37.7905
		2	26.3048	15.3714	8.9714	26.3048	16.0762	9.9048	26.3048	18.0190	12.6095
		4	16.1905	8.3619	4.4857	16.1905	8.7333	4.7905	16.1905	9.9905	6.2571
		8	13.6619	6.6048	3.3619	13.6619	6.8952	3.5048	13.6619	7.9810	4.6667
		∞	12.8235	6.0219	2.9858	12.8235	6.2837	3.0786	12.8235	7.3123	4.1344
FG	5	1	30.2143	26.0214	22.5214	36.1643	30.3214	25.6500	39.5571	30.4429	23.3143
		2	10.8107	9.3750	8.2571	13.2357	10.9250	9.2250	14.7214	11.0643	8.5036
		4	5.8786	5.2089	4.6768	7.3000	6.0054	5.1179	8.3018	6.1571	4.7929
		8	4.6277	4.1643	3.7759	5.7768	4.7589	4.0893	6.6545	4.9152	3.8625
		∞	4.2078	3.8160	3.4743	5.2631	4.3410	3.7463	6.1001	4.4987	3.5522
	20	1	36.8762	31.2000	26.6667	45.2571	37.0667	30.6667	49.9429	37.2952	27.6571
		2	12.9143	11.3143	10.1143	15.9048	13.1048	11.1429	17.8857	13.3333	10.3810
		4	6.9238	6.3524	5.9810	8.5524	7.1143	6.2762	9.8476	7.3524	6.0571
		8	5.4238	5.1143	4.9524	6.7095	5.6190	5.0571	7.8333	5.8524	4.9810
		∞	4.9254	4.7000	4.6078	6.0982	5.1201	4.6531	7.1649	5.3530	4.6209

Table 5. 36: Non-dimensional buckling loads of SSSS FG-sandwich plates.

Core	a/h	h/l	Scheme								
			2-1-1			1-1-1			1-2-1		
			p=0	1	10	p=0	1	10	p=0	1	10
Ceramic	5	1	41.1429	25.8571	15.8571	41.1429	27.0000	17.5714	41.1429	29.9286	22.1429
		2	16.3214	9.7500	5.7857	16.3214	10.2143	6.4286	16.3214	11.3929	8.1071
		4	10.0893	5.5000	3.0536	10.0893	5.7500	3.2679	10.0893	6.5179	4.2321
		8	8.5268	4.4018	2.3214	8.5268	4.5982	2.4375	8.5268	5.2679	3.2054
		∞	8.0105	4.0354	2.0812	8.0105	4.2086	2.1542	8.0105	4.8444	2.8571
	20	1	50.2095	32.5714	20.1524	50.2095	34.1333	22.6667	50.2095	37.6381	28.4571
		2	19.8095	11.5810	6.7619	19.8095	12.1143	7.4476	19.8095	13.5810	9.4857
		4	12.2095	6.3048	3.3905	12.2095	6.5810	3.6000	12.2095	7.5238	4.7143
		8	10.3095	4.9857	2.5476	10.3095	5.1952	2.6381	10.3095	6.0143	3.5095
		∞	9.6763	4.5445	2.2645	9.6763	4.7328	2.3163	9.6763	5.5091	3.1115
FG	5	1	23.3071	20.0429	17.3286	27.9286	23.3857	19.7571	30.5571	23.4786	17.9357
		2	8.4714	7.3750	6.5107	10.3214	8.5607	7.2607	11.4679	8.6643	6.7000
		4	4.6929	4.1929	3.7911	5.7554	4.7893	4.1268	6.5232	4.9036	3.8804
		8	3.7277	3.3920	3.1071	4.5804	3.8286	3.3393	5.2518	3.9473	3.1714
		∞	3.4005	3.1208	2.8752	4.1814	3.5027	3.0726	4.8223	3.6237	2.9318
	20	1	27.9238	23.6571	20.1905	34.1714	28.0381	23.2381	37.6762	28.1905	20.9524
		2	9.8857	8.6857	7.7714	12.0952	10.0190	8.5714	13.5429	10.1714	7.9619
		4	5.3714	4.9429	4.6476	6.5429	5.5048	4.8857	7.4857	5.6667	4.7143
		8	4.2429	4.0143	3.8810	5.1619	4.3810	3.9762	5.9714	4.5429	3.9048
		∞	3.8570	3.6913	3.6126	4.6927	3.9952	3.6605	5.4642	4.1601	3.6262

Table 5. 37: Non-dimensional buckling loads of SCSF FG-sandwich plates.

Core	a/h	h/l	Scheme								
			2-1-1			1-1-1			1-2-1		
			p=0	1	10	p=0	1	10	p=0	1	10
Ceramic	5	1	34.5714	22.4286	14.0000	34.5714	23.5000	15.6429	34.5714	25.8571	19.5714
		2	11.9643	7.3929	4.5000	11.9643	7.7500	5.0714	11.9643	8.6071	6.3571
		4	6.7500	3.6607	2.0357	6.7500	3.8393	2.2143	6.7500	4.3393	2.8571
		8	5.4375	2.7411	1.4286	5.4375	2.8661	1.5000	5.4375	3.2946	1.9821
		∞	4.9706	2.4273	1.2267	4.9706	2.5345	1.2724	4.9706	2.9313	1.6970
	20	1	30.2857	29.7143	18.8571	43.8095	31.2381	21.5238	43.8095	34.2857	26.8571
		2	14.0952	8.7619	5.3333	14.0952	9.1429	5.9048	14.0952	10.1905	7.5238
		4	7.5238	4.0000	2.1905	7.5238	4.1429	2.3333	7.5238	4.7143	3.0476
		8	6.0476	2.9048	1.4762	6.0476	3.0476	1.5714	6.0476	3.5238	2.0476
		∞	5.5659	2.6027	1.2880	5.5659	2.7157	1.3272	5.5659	3.1624	1.7835
FG	5	1	20.1500	17.0071	14.3857	24.2857	20.1643	16.7214	26.4500	20.1857	14.9714
		2	6.2821	5.3571	4.6464	7.7679	6.3393	5.2607	8.6214	6.4036	4.8000
		4	3.0429	2.7232	2.4911	3.7768	3.1125	2.6821	4.3089	3.1982	2.5411
		8	2.2548	2.0786	1.9524	2.8000	2.3262	2.0500	3.2452	2.4119	1.9786
		∞	1.9827	1.8503	1.7542	2.4657	2.0543	1.8250	2.8801	2.1396	1.7749
	20	1	25.5238	21.1429	17.7143	31.4286	25.5238	20.7619	34.2857	25.5238	18.4762
		2	7.3333	6.2857	5.4286	9.0476	7.4286	6.1905	10.0952	7.5238	5.6190
		4	3.2857	3.0000	2.7619	4.0952	3.3810	2.9524	4.6667	3.4762	2.8095
		8	2.3810	2.2381	2.1905	2.9524	2.4762	2.2381	3.4762	2.5714	2.1905
		∞	2.1291	2.0365	2.0037	2.6349	2.2141	2.0171	3.0976	2.3157	2.0075

Table 5. 38: Non-dimensional buckling loads of SSSF FG-sandwich plates.

Core	a/h	h/l	Scheme								
			2-1-1			1-1-1			1-2-1		
			p=0	1	10	p=0	1	10	p=0	1	10
Ceramic	5	1	31.2143	20.2857	12.6429	31.2143	21.1429	14.0714	31.2143	23.3571	17.6429
		2	10.8214	6.7143	4.0714	10.8214	7.0357	4.6071	10.8214	7.7857	5.7500
		4	6.1964	3.3571	1.8750	6.1964	3.5000	2.0179	6.1964	3.9821	2.6071
		8	5.0357	2.5268	1.3125	5.0357	2.6429	1.3839	5.0357	3.0357	1.8214
		∞	4.6270	2.2535	1.1389	4.6270	2.3514	1.1780	4.6270	2.7211	1.5720
	20	1	30.2857	26.6667	16.7619	39.2381	27.8095	19.0476	39.2381	30.6667	23.8095
		2	12.7619	7.9048	4.7619	12.7619	8.2857	5.3333	12.7619	9.1429	6.7619
		4	6.8571	3.6190	2.0000	6.8571	3.8095	2.1429	6.8571	4.3333	2.8095
		8	5.5238	2.6667	1.3333	5.5238	2.7619	1.4286	5.5238	3.2381	1.9048
		∞	5.1387	2.4037	1.1915	5.1387	2.5067	1.2248	5.1387	2.9189	1.6461
FG	5	1	18.2643	15.4714	13.1214	21.9357	18.2786	15.2214	23.8786	18.2929	13.6500
		2	5.7321	4.8929	4.2464	7.0607	5.7786	4.8107	7.8250	5.8357	4.3857
		4	2.8107	2.5214	2.3071	3.4732	2.8732	2.4839	3.9554	2.9500	2.3518
		8	2.1048	1.9452	1.8286	2.6000	2.1714	1.9190	3.0071	2.2476	1.8524
		∞	1.8608	1.7403	1.6524	2.3019	1.9265	1.7177	2.6828	2.0047	1.6715
	20	1	22.8571	19.0476	16.0000	28.0000	22.8571	18.6667	30.6667	22.8571	16.5714
		2	6.6667	5.7143	4.9524	8.2857	6.7619	5.6190	9.1429	6.8571	5.1429
		4	3.0476	2.7619	2.5714	3.7619	3.0952	2.7143	4.2857	3.1905	2.6190
		8	2.1905	2.0952	2.0000	2.7143	2.2857	2.0476	3.1905	2.3810	2.0476
		∞	1.9893	1.9043	1.8723	2.4488	2.0664	1.8869	2.8707	2.1584	1.8765

Table 5. 39: Non-dimensional buckling loads of SFSF FG-sandwich plates.

Core	a/h	h/l	Scheme								
			2-1-1			1-1-1			1-2-1		
			p=0	1	10	p=0	1	10	p=0	1	10
Ceramic	5	1	29.7143	19.5000	12.2143	29.7143	20.3571	13.6429	29.7143	22.4286	17.0714
		2	9.6429	5.9643	3.7143	9.6429	6.3214	4.1786	9.6429	7.0000	5.2500
		4	5.4464	2.9464	1.6250	5.4464	3.0714	1.7679	5.4464	3.5000	2.2857
		8	4.4821	2.2321	1.1607	4.4821	2.3393	1.2143	4.4821	2.6875	1.6071
		∞	4.1390	2.0054	1.0094	4.1390	2.0936	1.0457	4.1390	2.4244	1.3967
	20	1	30.2857	24.9524	16.0000	36.5714	26.2857	18.0952	36.5714	28.7619	22.6667
		2	11.3333	7.1429	4.2857	11.3333	7.4286	4.8571	11.3333	8.2857	6.0952
		4	6.0476	3.1905	1.7619	6.0476	3.3333	1.9048	6.0476	3.8095	2.4286
		8	4.9048	2.3333	1.1905	4.9048	2.4762	1.2381	4.9048	2.8571	1.6667
		∞	4.5437	2.1235	1.0504	4.5437	2.2157	1.0824	4.5437	2.5803	1.4549
FG	5	1	17.6286	14.9214	12.6143	21.1214	17.6214	14.6857	22.9500	17.6143	13.1357
		2	5.1393	4.3607	3.7607	6.3429	5.1750	4.2821	7.0214	5.2214	3.8893
		4	2.4393	2.1857	2.0054	3.0304	2.4964	2.1536	3.4607	2.5661	2.0429
		8	1.8381	1.7024	1.6095	2.2833	1.9000	1.6810	2.6500	1.9714	1.6286
		∞	1.6385	1.5360	1.4659	2.0357	1.6988	1.5161	2.3807	1.7707	1.4807
	20	1	21.5238	17.7143	14.8571	26.2857	21.5238	17.5238	28.7619	21.5238	15.4286
		2	6.0000	5.1429	4.3810	7.4286	6.0000	5.0476	8.1905	6.0952	4.5714
		4	2.6190	2.3810	2.2381	3.2857	2.7143	2.3810	3.7619	2.7619	2.2381
		8	1.9524	1.8095	1.7619	2.3810	2.0000	1.8095	2.8095	2.0952	1.7619
		∞	1.7371	1.6621	1.6363	2.1496	1.8064	1.6464	2.5275	1.8896	1.6392

5.6 Concluding remarks

In this chapter, general quasi-3D and higher-order shear deformation models are developed to study the mechanical and thermal behaviours of FG sandwich microplates. Governing

equations are derived from the variational principle based on the framework of the modified couple stress theory. In the first part, the Navier solutions are applied to examine the bending, vibration and buckling behaviours of microplates under mechanical and thermal loads. These solutions reveal that the inclusion of small-scale effect increases the microplates' stiffness, especially for those with the thickness h < 20l. In addition, comprising thickness stretching strain in mechanical analysis results in higher stiffness for FG plates which leads to smaller deflection and higher natural frequencies as well as critical buckling loads, compared with the higher-order 2D models. Moreover, thickness stretching thermal strain also induces the out-of-plane thermal load in the thermal analysis which leads to the higher deflections, stresses as well as lower natural frequency and critical buckling temperature. Utilising the state space approach, the second part copes with the analysis of the plates with simply supports at two opposite edges and various BCs for other edges. The effects of boundary conditions, geometric and material properties as well as the graded schemes to the static bending, free vibration and buckling behaviours of FG-sandwich microplates are examined.

CHAPTER 6

CONCLUSIONS AND RECOMMENDATIONS

6.1 Conclusions

In this thesis, the variational principle is applied to derive the governing equations of motion for the size-dependent static, free vibration and buckling behaviours of functionally graded (FG) sandwich beams and plates using different higher-order shear deformation theories and the modified couple stress theory (MCST). According to the results of the present work, the following conclusions can be drawn:

a. The Navier and state space methods are found to be appropriate and efficient in analysing the static, free vibration and buckling behaviours of FG and FG-sandwich beams and plates in both macro and micro scales. While the Navier method is applicable to the structures embedded in simply supported BCs, the state space approach can be used to analyse the beams with arbitrary BCs and the plates with simply-supported BCs on two opposite edges and various BCs on the others.

b. Utilising the state space based method for beams at the macro scales, an iterative procedure needs to be applied for the natural frequencies and critical buckling loads due to the present of these quantities in the analytical formulation themselves. Although the coupling between the axial displacement and the bending components is presented in the vibration analysis, the general form of eigenvalues and eigenvectors can be employed. However, the absence of eigen-frequency in the formulation of buckling behaviour leads to the multiplicity of eigen values, which requires a Jordan canonical treatment for general solutions. The singular value decomposition is employed at the modal frequencies/buckling loads to plot the corresponding mode shapes and buckling shapes. The state space approach is also developed for the vibration and buckling behaviours of FG beams under mechanical and thermal loads. The effects of temperature-dependent material properties on the natural frequencies and critical buckling loads are also considered under the uniform, linear and nonlinear temperature distribution across the thickness of FG beams. It is also found that the variation of material properties along with the elevated temperatures is essential to take into account in analysing the vibration and buckling behaviours of FG beams.

c. The governing equations of motion and the relating boundary conditions for FG-sandwich microbeams are developed and verified by the excellent agreement of present results with those in the literature. Navier method is applied successfully to analyse the

static, vibration and buckling behaviours of simply supported beams. The state space method is developed to investigate the free vibration behaviour of bidirectional FG microbeams, which can be used to study the FG microbeams and BDFG macrobeams by setting an appropriate material length scale ratio and material power/exponential index.

Using the MCST to capture the size-dependent effects of the small-scale beams, the numerical examples reveal that the increase of material length scale ratio leads to the growth in beams' stiffness. Consequently, there is a decrease in displacement and an increase in the natural frequency and critical buckling load of the microbeams.

d. The governing equations of motion and the relating boundary conditions for FG-sandwich microplates are developed and verified with those in the literature. Both Navier and state space methods are employed to analyse the static, vibration and buckling behaviours of these plates. The behaviours of FG-sandwich microplates under uniform and linear temperature distributions are also carried out in this thesis. Again, the behaviours of FG macroplates can be considered by setting the material length scale ratio to an infinity.

   The effects of material length scale ratio to the structural behaviours of FG-sandwich microplates are similar to the case of microbeams, which highlights the importance of employing the higher-order continuum theories such as MCST to analyse small-scale structures. In applying the state space method for microplates, the general form of eigenvalues and eigenvectors can be employed because all the eigenvalues are distinct. Different from the applications for vibration and buckling behaviours, the solution for static behaviour can be obtained directly without the need of an iterative procedure, which makes the state space approach a closed form solution.

6.2 Recommendations

Following are the recommendations concerning the extensions of the proposed models for future research:

a. Eigen values for the general solutions are repetitive with up to four degrees in analysing the static and buckling behaviours of FG microbeams, which results in an expensive computational cost using Jordan canonical form. Therefore, the state space based solution for the static bending and buckling behaviours of microbeams need to be further developed with a higher level of multiplicity in eigen values of the general solution.

b. Present theoretical models and solutions can be extended to analyse the curve beams and shells, and laminated composite structures.
c. These analytical methods can be developed for other non-classical continua such as the strain gradient theory and non-local elasticity to analyse different small scales of structures.
d. The state space based solution can be combined with other strong form solutions, e.g. differential quadrature method and dynamic stiffness matrix, to achieve 3D solutions and more complex geometries and boundary conditions.

APPENDICES

Appendix A

The coefficients in Eq. (4.19):

$$a_1=\frac{-I_0\omega^2}{A_{11}};a_2=\frac{-\frac{n_x}{a}A_{11}}{A_{11}};a_3=\frac{I_1\omega^2}{A_{11}};a_4=\frac{\frac{n_x}{a}B_{11}}{A_{11}};a_5=\frac{B_{11}}{A_{11}};$$

$$a_6=\frac{J_1\omega^2}{A_{11}};a_7=\frac{\frac{n_x}{a}B_{11}^s}{A_{11}};a_8=\frac{B_{11}^s}{A_{11}};a_9=\frac{-\frac{n_x}{a}K_{13}}{A_{11}};a_{10}=\frac{-K_{13}}{A_{11}}. \quad \text{(A1)}$$

$$r_1=\left[c_3f_2e_4-e_3f_2c_4+f_3\left(e_2c_4-c_2e_4\right)\right]/C_0;$$
$$r_2=\left[c_3\left(f_2e_5-e_2f_4\right)-e_3\left(f_2c_5-c_2f_4\right)+f_3\left(e_2c_5-c_2e_5\right)\right]/C_0;$$
$$r_3=\left[c_3\left(f_2e_6-e_2f_5\right)-e_3\left(f_2c_6-c_2f_5\right)+f_3\left(e_2c_6-c_2e_6\right)\right]/C_0;$$
$$r_4=\left[c_3f_2e_7-e_3f_2c_7+f_3\left(e_2c_7-c_2e_7\right)\right];$$
$$r_5=\left[c_3\left(f_2e_8-e_2f_6\right)-e_3\left(f_2c_8-c_2f_6\right)+f_3\left(e_2c_8-c_2e_8\right)\right]/C_0;$$
$$r_6=\left[c_3\left(f_2e_9-e_2f_7\right)-e_3\left(f_2c_9-c_2f_7\right)+f_3\left(e_2c_9-c_2e_9\right)\right]/C_0;$$
$$r_7=\left[c_3\left(f_2e_{10}-e_2f_8\right)-e_3\left(f_2c_{10}-c_2f_8\right)+f_3\left(e_2c_{10}-c_2e_{10}\right)\right]/C_0;$$
$$r_8=\left[c_3\left(f_2e_{11}-e_2f_9\right)-e_3\left(f_2c_{11}-c_2f_9\right)+f_3\left(e_2c_{11}-c_2e_{11}\right)\right]/C_0;$$
$$r_9=\left[c_3\left(f_2e_{12}-e_2f_{10}\right)-e_3\left(f_2c_{12}-c_2f_{10}\right)+f_3\left(e_2c_{12}-c_2e_{12}\right)\right]/C_0;$$
$$r_{10}=\left[c_3\left(f_2e_{13}-e_2f_{11}\right)-e_3\left(f_2c_{13}-c_2f_{11}\right)+f_3\left(e_2c_{13}-c_2e_{13}\right)\right]/C_0;$$
$$r_{11}=\left[c_3\left(f_2e_{14}-e_2f_{12}\right)-e_3\left(f_2c_{14}-c_2f_{12}\right)+f_3\left(e_2c_{14}-c_2e_{14}\right)\right]/C_0;$$
$$r_{12}=\left[c_3\left(f_2e_{15}-e_2f_{13}\right)-e_3\left(f_2c_{15}-c_2f_{13}\right)+f_3\left(e_2c_{15}-c_2e_{15}\right)\right]/C_0;$$
$$r_{13}=\left[c_3\left(f_2e_{16}-e_2f_{14}\right)-e_3\left(f_2c_{16}-c_2f_{14}\right)+f_3\left(e_2c_{16}-c_2e_{16}\right)\right]/C_0;$$
$$r_{14}=\left[c_3\left(f_2e_{17}-e_2f_{15}\right)-e_3\left(f_2c_{17}-c_2f_{15}\right)+f_3\left(e_2c_{17}-c_2e_{17}\right)\right]/C_0. \quad \text{(A2)}$$
$$s_1=\left[c_1f_3e_4-e_1f_3c_4+f_1\left(e_3c_4-c_3e_4\right)\right]/C_0;$$
$$s_2=\left[c_1\left(f_3e_5-e_3f_4\right)-e_1\left(f_3c_5-c_3f_4\right)+f_1\left(e_3c_5-c_3e_5\right)\right]/C_0;$$
$$s_3=\left[c_1\left(f_3e_6-e_3f_5\right)-e_1\left(f_3c_6-c_3f_5\right)+f_1\left(e_3c_6-c_3e_6\right)\right]/C_0;$$
$$s_4=\left[c_1f_3e_7-e_1f_3c_7+f_1\left(e_3c_7-c_3e_7\right)\right]/C_0;$$
$$s_5=\left[c_1\left(f_3e_8-e_3f_6\right)-e_1\left(f_3c_8-c_3f_6\right)+f_1\left(e_3c_8-c_3e_8\right)\right]/C_0;$$
$$s_6=\left[c_1\left(f_3e_9-e_3f_7\right)-e_1\left(f_3c_9-c_3f_7\right)+f_1\left(e_3c_9-c_3e_9\right)\right]/C_0;$$
$$s_7=\left[c_1\left(f_3e_{10}-e_3f_8\right)-e_1\left(f_3c_{10}-c_3f_8\right)+f_1\left(e_3c_{10}-c_3e_{10}\right)\right]/C_0;$$
$$s_8=\left[c_1\left(f_3e_{11}-e_3f_9\right)-e_1\left(f_3c_{11}-c_3f_9\right)+f_1\left(e_3c_{11}-c_3e_{11}\right)\right]/C_0;$$
$$s_9=\left[c_1\left(f_3e_{12}-e_3f_{10}\right)-e_1\left(f_3c_{12}-c_3f_{10}\right)+f_1\left(e_3c_{12}-c_3e_{12}\right)\right]/C_0;$$

$$s_{10}=\left[c_1\left(f_3e_{13}-e_3f_{11}\right)-e_1\left(f_3c_{13}-c_3f_{11}\right)+f_1\left(e_3c_{13}-c_3e_{13}\right)\right]/C_0;$$
$$s_{11}=\left[c_1\left(f_3e_{14}-e_3f_{12}\right)-e_1\left(f_3c_{14}-c_3f_{12}\right)+f_1\left(e_3c_{14}-c_3e_{14}\right)\right]/C_0;$$
$$s_{12}=\left[c_1\left(f_3e_{15}-e_3f_{13}\right)-e_1\left(f_3c_{15}-c_3f_{13}\right)+f_1\left(e_3c_{15}-c_3e_{15}\right)\right]/C_0;$$
$$s_{13}=\left[c_1\left(f_3e_{16}-e_3f_{14}\right)-e_1\left(f_3c_{16}-c_3f_{14}\right)+f_1\left(e_3c_{16}-c_3e_{16}\right)\right]/C_0;$$
$$s_{14}=\left[c_1\left(f_3e_{17}-e_3f_{15}\right)-e_1\left(f_3c_{17}-c_3f_{15}\right)+f_1\left(e_3c_{17}-c_3e_{17}\right)\right]/C_0. \quad \text{(A3)}$$

$$t_1=\left[-c_1f_2e_4+e_1f_2c_4+f_1\left(c_2e_4-e_2c_4\right)\right]/C_0;$$
$$t_2=\left[c_1\left(e_2f_4-f_2e_5\right)-e_1\left(c_2f_4-f_2c_5\right)+f_1\left(c_2e_5-e_2c_5\right)\right]/C_0;$$
$$t_3=\left[c_1\left(e_2f_5-f_2e_6\right)-e_1\left(c_2f_5-f_2c_6\right)+f_1\left(c_2e_6-e_2c_6\right)\right];$$
$$t_4=\left[-c_1f_2e_7+e_1f_2c_7+f_1\left(c_2e_7-e_2c_7\right)\right]/C_0;$$
$$t_5=\left[c_1\left(e_2f_6-f_2e_8\right)-e_1\left(c_2f_6-f_2c_8\right)+f_1\left(c_2e_8-e_2c_8\right)\right]/C_0;$$
$$t_6=\left[c_1\left(e_2f_7-f_2e_9\right)-e_1\left(c_2f_7-f_2c_9\right)+f_1\left(c_2e_9-e_2c_9\right)\right]/C_0;$$
$$t_7=\left[c_1\left(e_2f_8-f_2e_{10}\right)-e_1\left(c_2f_8-f_2c_{10}\right)+f_1\left(c_2e_{10}-e_2c_{10}\right)\right]/C_0;$$
$$t_8=\left[c_1\left(e_2f_9-f_2e_{11}\right)-e_1\left(c_2f_9-f_2c_{11}\right)+f_1\left(c_2e_{11}-e_2c_{11}\right)\right]/C_0;$$
$$t_9=\left[c_1\left(e_2f_{10}-f_2e_{12}\right)-e_1\left(c_2f_{10}-f_2c_{12}\right)+f_1\left(c_2e_{12}-e_2c_{12}\right)\right]/C_0;$$
$$t_{10}=\left[c_1\left(e_2f_{11}-f_2e_{13}\right)-e_1\left(c_2f_{11}-f_2c_{13}\right)+f_1\left(c_2e_{13}-e_2c_{13}\right)\right]/C_0;$$
$$t_{11}=\left[c_1\left(e_2f_{12}-f_2e_{14}\right)-e_1\left(c_2f_{12}-f_2c_{14}\right)+f_1\left(c_2e_{14}-e_2c_{14}\right)\right]/C_0;$$
$$t_{12}=\left[c_1\left(e_2f_{13}-f_2e_{15}\right)-e_1\left(c_2f_{13}-f_2c_{15}\right)+f_1\left(c_2e_{15}-e_2c_{15}\right)\right]/C_0;$$
$$t_{13}=\left[c_1\left(e_2f_{14}-f_2e_{16}\right)-e_1\left(c_2f_{14}-f_2c_{16}\right)+f_1\left(c_2e_{16}-e_2c_{16}\right)\right]/C_0; \quad \text{(A4)}$$

where $C_0=c_1\left(e_2f_3-e_3f_2\right)-c_2\left(e_1f_3-e_3f_1\right)+c_3\left(e_1f_2-e_2f_1\right).$

$$b_1=D_{11}+A_m;b_2=D_{11}^s+\frac{1}{2}\left(A_m+B_m\right);b_3=\frac{1}{2}E_m;b_4=\frac{n_x}{a}I_1\omega^2;b_5=\left(\frac{n_x}{a}\right)^2B_{11}+I_1\omega^2;b_6=2\frac{n_x}{a}B_{11};$$
$$b_7=B_{11};b_8=I_0\omega^2;b_9=-\frac{n_x}{a}I_2\omega^2;b_{10}=-\left(\frac{n_x}{a}\right)^2\left(D_{11}+A_m\right)-I_2\omega^2;b_{11}=-2\frac{n_x}{a}\left(D_{11}+A_m\right);$$
$$b_{12}=I_0\omega^2;b_{13}=-\frac{n_x}{a}J_2\omega^2;b_{14}=-\left(\frac{n_x}{a}\right)^2\left[D_{11}^s+\frac{1}{2}\left(A_m+B_m\right)\right]-J_2\omega^2;b_{15}=-\frac{n_x}{a}\left[2D_{11}^s+\left(A_m+B_m\right)\right];$$
$$b_{16}=\left(\frac{n_x}{a}\right)^2L_{13}+J_0\omega^2;b_{17}=2\frac{n_x}{a}L_{13};b_{18}=L_{13}-\frac{1}{2}\left(\frac{n_x}{a}\right)^2E_m;b_{19}=-\frac{n_x}{a}E_m. \quad \text{(A5)}$$

$$c_1=b_1-b_7a_5;c_2=b_2-b_7a_8;c_3=b_3;c_4=b_4+b_6a_1+b_7a_2a_1;c_5=b_5+b_6a_2+b_7a_1+b_7a_2a_2;$$
$$c_6=b_8;c_7=b_9+b_6a_3+b_7a_2a_3;c_8=b_{10}+b_6a_4+b_7a_3+b_7a_2a_4;c_9=b_{11}+b_6a_5+b_7a_4+b_7a_2a_5$$
$$c_{10}=b_{12};c_{11}=b_{13}+b_6a_6+b_7a_2a_6;c_{12}=b_{14}+b_6a_7+b_7a_6+b_7a_2a_7;c_{13}=b_{15}+b_6a_8+b_7a_7+b_7a_2a_8$$
$$c_{14}=b_{16}+b_6a_9+b_7a_2a_9;c_{15}=b_{17}+b_6a_{10}+b_7a_9+b_7a_2a_{10};c_{16}=b_{18}+b_7a_{10};c_{17}=b_{19} \quad \text{(A6)}$$
$$d_1=D_{11}^s+\frac{1}{2}\left(A_m+B_m\right);d_2=H_{11}+\frac{1}{4}\left(A_m+2B_m+C_m\right);d_3=\frac{1}{4}\left(E_m+D_m\right);d_4=\frac{n_x}{a}J_1\omega^2;$$

$$d_5=\left(\frac{n_x}{a}\right)^2 B_{11}^s+J_1\omega^2;d_6=2\frac{n_x}{a}B_{11}^s;d_7=B_{11}^s;d_8=I_0\omega^2;d_9=-\frac{n_x}{a}J_2\omega^2;$$

$$d_{10}=-\left(\frac{n_x}{a}\right)^2\left[D_{11}^s+\frac{1}{2}\left(A_m+B_m\right)\right]-J_2\omega^2;d_{11}=-\frac{n_x}{a}\left[2D_{11}^s+\left(A_m+B_m\right)\right];d_{12}=I_0\omega^2;$$

$$d_{13}=\frac{n_x}{a}\left(A_{55}^s+\frac{1}{4}H_m-K_2\omega^2\right);d_{14}=A_{55}^s-\left(\frac{n_x}{a}\right)^2 H_{11}-\frac{1}{4}\left(\frac{n_x}{a}\right)^2\left(A_m+2B_m+C_m\right)+\frac{1}{4}H_m-K_2\omega^2;$$

$$d_{15}=-2\frac{n_x}{a}H_{11}-\frac{1}{2}\frac{n_x}{a}\left(A_m+2B_m+C_m\right);d_{16}=\left(\frac{n_x}{a}\right)^2 L_{13}^s+J_0\omega^2;d_{17}=2\frac{n_x}{a}L_{13}^s+\frac{n_x}{a}A_{55}^s-\frac{1}{4}\frac{n_x}{a}H_m;$$

$$d_{18}=L_{13}^s+A_{55}^s-\frac{1}{4}\left(\frac{n_x}{a}\right)^2\left(E_m+D_m\right)-\frac{1}{4}H_m;d_{19}=-\frac{1}{2}\frac{n_x}{a}\left(E_m+D_m\right); \quad \text{(A7)}$$

$$e_1=d_1-d_7a_5;e_2=d_2-d_7a_8;e_3=d_3;e_4=d_4+d_6a_1+d_7a_2a_1;e_5=d_5+d_6a_2+d_7a_1+d_7a_2a_2;$$
$$e_6=d_8;e_7=d_9+d_6a_3+d_7a_2a_3;e_8=d_{10}+d_6a_4+d_7a_3+d_7a_2a_4;e_9=d_{11}+d_6a_5+d_7a_4+d_7a_2a_5;$$
$$e_{10}=d_{12};e_{11}=d_{13}+d_6a_6+d_7a_2a_6;e_{12}=d_{14}+d_6a_7+d_7a_6+d_7a_2a_7;e_{13}=d_{15}+d_6a_8+d_7a_7+d_7a_2a_8;$$
$$e_{14}=d_{16}+d_6a_9+d_7a_2a_9;e_{15}=d_{17}+d_6a_{10}+d_7a_9+d_7a_2a_{10};e_{16}=d_{18}+d_7a_{10};e_{17}=d_{19}. \quad \text{(A8)}$$

$$f_1=\frac{1}{2}E_m;f_2=\frac{1}{4}\left(E_m+D_m\right);f_3=\frac{1}{4}F_m;f_4=-K_{13};f_5=J_0\omega^2;f_6=L_{13}-\frac{1}{2}\left(\frac{n_x}{a}\right)^2 E_m;f_7=-\frac{n_x}{a}E_m;$$

$$f_8=J_0\omega^2;f_9=\frac{n_x}{a}A_{55}^s+\frac{1}{4}\frac{n_x}{a}H_m;f_{10}=L_{13}^s+A_{55}^s+\frac{1}{4}H_m-\frac{1}{4}\left(\frac{n_x}{a}\right)^2\left(E_m+D_m\right);f_{11}=-\frac{1}{2}\frac{n_x}{a}\left(E_m+D_m\right);$$

$$f_{12}=-Z_{33}+K_0\omega^2;f_{13}=\frac{n_x}{a}A_{55}^s-\frac{1}{4}\frac{n_x}{a}H_m;f_{14}=A_{55}^s-\frac{1}{4}H_m-\frac{1}{4}\left(\frac{n_x}{a}\right)^2 F_m;f_{15}=-\frac{1}{2}\frac{n_x}{a}F_m; \quad \text{(A9)}$$

Appendix B

The stress resultants in Eq. (5.13):

$$N_{xx} = A_{11}\frac{\partial U}{\partial x} + A_{12}\frac{\partial V}{\partial y} - B_{11}\frac{\partial^2 W_b}{\partial x^2} - B_{12}\frac{\partial^2 W_b}{\partial y^2} - B_{11}^s\frac{\partial^2 W_s}{\partial x^2} - B_{12}^s\frac{\partial^2 W_s}{\partial y^2} + K_{13}W_z - \left(A_t T_1 + B_t\frac{T_2}{h}\right) \tag{B1}$$

$$N_{yy} = A_{12}\frac{\partial U}{\partial x} + A_{22}\frac{\partial V}{\partial y} - B_{12}\frac{\partial^2 W_b}{\partial x^2} - B_{22}\frac{\partial^2 W_b}{\partial y^2} - B_{12}^s\frac{\partial^2 W_s}{\partial x^2} - B_{22}^s\frac{\partial^2 W_s}{\partial y^2} + K_{23}W_z - \left(A_t T_1 + B_t\frac{T_2}{h}\right) \tag{B2}$$

$$N_{xy} = A_{66}\left(\frac{\partial U}{\partial y} + \frac{\partial V}{\partial x}\right) - 2B_{66}\frac{\partial^2 W_b}{\partial x\partial y} - 2B_{66}^s\frac{\partial^2 W_s}{\partial x\partial y} \tag{B3}$$

$$M_{xx} = B_{11}\frac{\partial U}{\partial x} + B_{12}\frac{\partial V}{\partial y} - D_{11}\frac{\partial^2 W_b}{\partial x^2} - D_{12}\frac{\partial^2 W_b}{\partial y^2} - D_{11}^s\frac{\partial^2 W_s}{\partial x^2} - D_{12}^s\frac{\partial^2 W_s}{\partial y^2} + L_{13}W_z - \left(B_t T_1 + D_t\frac{T_2}{h}\right) \tag{B4}$$

$$M_{yy} = B_{12}\frac{\partial U}{\partial x} + B_{22}\frac{\partial V}{\partial y} - D_{12}\frac{\partial^2 W_b}{\partial x^2} - D_{22}\frac{\partial^2 W_b}{\partial y^2} - D_{12}^s\frac{\partial^2 W_s}{\partial x^2} - D_{22}^s\frac{\partial^2 W_s}{\partial y^2} + L_{23}W_z - \left(B_t T_1 + D_t\frac{T_2}{h}\right) \tag{B5}$$

$$M_{xy} = B_{66}\left(\frac{\partial U}{\partial y} + \frac{\partial V}{\partial x}\right) - 2D_{66}\frac{\partial^2 W_b}{\partial x\partial y} - 2D_{66}^s\frac{\partial^2 W_s}{\partial x\partial y} \tag{B6}$$

$$P_{xx} = B_{11}^s\frac{\partial U}{\partial x} + B_{12}^s\frac{\partial V}{\partial y} - D_{11}^s\frac{\partial^2 W_b}{\partial x^2} - D_{12}^s\frac{\partial^2 W_b}{\partial y^2} - H_{11}\frac{\partial^2 W_s}{\partial x^2} - H_{12}\frac{\partial^2 W_s}{\partial y^2} + L_{13}^s W_z - \left(B_t^s T_1 + D_t^s\frac{T_2}{h}\right) \tag{B7}$$

$$P_{yy} = B_{12}^s\frac{\partial U}{\partial x} + B_{22}^s\frac{\partial V}{\partial y} - D_{12}^s\frac{\partial^2 W_b}{\partial x^2} - D_{22}^s\frac{\partial^2 W_b}{\partial y^2} - H_{12}\frac{\partial^2 W_s}{\partial x^2} - H_{22}\frac{\partial^2 W_s}{\partial y^2} + L_{23}^s W_z - \left(B_t^s T_1 + D_t^s\frac{T_2}{h}\right) \tag{B8}$$

$$P_{xy} = B_{66}^s\left(\frac{\partial U}{\partial y} + \frac{\partial V}{\partial x}\right) - 2D_{66}^s\frac{\partial^2 W_b}{\partial x\partial y} - 2H_{66}\frac{\partial^2 W_s}{\partial x\partial y} \tag{B9}$$

$$O_{zz} = K_{13}\frac{\partial U}{\partial x} + K_{23}\frac{\partial V}{\partial y} - L_{13}\frac{\partial^2 W_b}{\partial x^2} - L_{23}\frac{\partial^2 W_b}{\partial y^2} - L_{13}^s\frac{\partial^2 W_s}{\partial x^2} - L_{23}^s\frac{\partial^2 W_s}{\partial y^2} + Z_{33}W_z - \left(C_t T_1 + C_t^s\frac{T_2}{h}\right) \tag{B10}$$

$$Q_{xz} = A_{55}^s\left(\frac{\partial W_s}{\partial x} + \frac{\partial W_z}{\partial x}\right) \tag{B11}$$

$$Q_{yz} = A_{44}^s\left(\frac{\partial W_s}{\partial y} + \frac{\partial W_z}{\partial y}\right) \tag{B12}$$

$$R_{xx} = 2A_m\frac{\partial^2 W_b}{\partial x\partial y} + \left(A_m + B_m\right)\frac{\partial^2 W_s}{\partial x\partial y} + E_m\frac{\partial^2 W_z}{\partial x\partial y} \tag{B13}$$

$$R_{yy} = -2A_m\frac{\partial^2 W_b}{\partial x\partial y} - \left(A_m + B_m\right)\frac{\partial^2 W_s}{\partial x\partial y} - E_m\frac{\partial^2 W_z}{\partial x\partial y} \tag{B14}$$

$$R_{xy}=A_m\left(\frac{\partial^2 W_b}{\partial y^2}-\frac{\partial^2 W_b}{\partial x^2}\right)+\frac{1}{2}\left(A_m+B_m\right)\left(\frac{\partial^2 W_s}{\partial y^2}-\frac{\partial^2 W_s}{\partial x^2}\right)+\frac{1}{2}E_m\left(\frac{\partial^2 W_z}{\partial y^2}-\frac{\partial^2 W_z}{\partial x^2}\right) \tag{B15}$$

$$R_{xz}=\frac{1}{2}A_m\frac{\partial^2 V}{\partial x^2}-\frac{1}{2}A_m\frac{\partial^2 U}{\partial x\partial y}-\frac{1}{2}G_m\frac{\partial W_s}{\partial y}+\frac{1}{2}G_m\frac{\partial W_z}{\partial y} \tag{B16}$$

$$R_{yz}=\frac{1}{2}A_m\frac{\partial^2 V}{\partial x\partial y}-\frac{1}{2}A_m\frac{\partial^2 U}{\partial y^2}+\frac{1}{2}G_m\frac{\partial W_s}{\partial x}-\frac{1}{2}G_m\frac{\partial W_z}{\partial x} \tag{B17}$$

$$S_{xx}=2B_m\frac{\partial^2 W_b}{\partial x\partial y}+\left(B_m+C_m\right)\frac{\partial^2 W_s}{\partial x\partial y}+D_m\frac{\partial^2 W_z}{\partial x\partial y} \tag{B18}$$

$$S_{yy}=-2B_m\frac{\partial^2 W_b}{\partial x\partial y}-\left(B_m+C_m\right)\frac{\partial^2 W_s}{\partial x\partial y}-D_m\frac{\partial^2 W_z}{\partial x\partial y} \tag{B19}$$

$$S_{xy}=B_m\left(\frac{\partial^2 W_b}{\partial y^2}-\frac{\partial^2 W_b}{\partial x^2}\right)+\frac{1}{2}\left(B_m+C_m\right)\left(\frac{\partial^2 W_s}{\partial y^2}-\frac{\partial^2 W_s}{\partial x^2}\right)+\frac{1}{2}D_m\left(\frac{\partial^2 W_z}{\partial y^2}-\frac{\partial^2 W_z}{\partial x^2}\right) \tag{B20}$$

$$T_{xx}=2E_m\frac{\partial^2 W_b}{\partial x\partial y}+\left(E_m+D_m\right)\frac{\partial^2 W_s}{\partial x\partial y}+F_m\frac{\partial^2 W_z}{\partial x\partial y} \tag{B21}$$

$$T_{yy}=-2E_m\frac{\partial^2 W_b}{\partial x\partial y}-\left(E_m+D_m\right)\frac{\partial^2 W_s}{\partial x\partial y}-F_m\frac{\partial^2 W_z}{\partial x\partial y} \tag{B22}$$

$$T_{xy}=E_m\left(\frac{\partial^2 W_b}{\partial y^2}-\frac{\partial^2 W_b}{\partial x^2}\right)+\frac{1}{2}\left(E_m+D_m\right)\left(\frac{\partial^2 W_s}{\partial y^2}-\frac{\partial^2 W_s}{\partial x^2}\right)+\frac{1}{2}F_m\left(\frac{\partial^2 W_z}{\partial y^2}-\frac{\partial^2 W_z}{\partial x^2}\right) \tag{B23}$$

$$X_{xz}=-\frac{1}{2}G_m\frac{\partial^2 V}{\partial x^2}+\frac{1}{2}G_m\frac{\partial^2 U}{\partial x\partial y}+\frac{1}{2}H_m\frac{\partial W_s}{\partial y}-\frac{1}{2}H_m\frac{\partial W_z}{\partial y} \tag{B24}$$

$$X_{yz}=-\frac{1}{2}G_m\frac{\partial^2 V}{\partial x\partial y}+\frac{1}{2}G_m\frac{\partial^2 U}{\partial y^2}-\frac{1}{2}H_m\frac{\partial W_s}{\partial x}+\frac{1}{2}H_m\frac{\partial W_z}{\partial x} \tag{B25}$$

where

$$\left(A_{ij},A_{ij}^s,B_{ij},B_{ij}^s,D_{ij},D_{ij}^s,H_{ij}\right)=\int_{-h/2}^{h/2}\left[1,g^2\left(z\right),z,f\left(z\right),z^2,f\left(z\right)z,f^2\left(z\right)\right]Q_{ij}dz \tag{B26}$$

$$\left(K_{ij},L_{ij},L_{ij}^s,Z_{ij}\right)=\int_{-h/2}^{h/2}\left[1,z,f\left(z\right),\frac{\partial g\left(z\right)}{\partial z}\right]\frac{\partial g\left(z\right)}{\partial z}Q_{ij}dz \tag{B27}$$

$$\begin{aligned}&\left(A_m,B_m,C_m,D_m,E_m,F_m,G_m,H_m\right)\\&=\int_{-h/2}^{h/2}I^2\mu\left(1,\frac{\partial f\left(z\right)}{\partial z},\left[\frac{\partial f\left(z\right)}{\partial z}\right]^2,\frac{\partial f\left(z\right)}{\partial z}g\left(z\right),g\left(z\right),\left[g\left(z\right)\right]^2,\frac{\partial g\left(z\right)}{\partial z},\left[\frac{\partial g\left(z\right)}{\partial z}\right]^2\right)dz\end{aligned} \tag{B28}$$

Appendix C:

The coefficients in Eq. (5.39):

$$a_1=\frac{\beta^2A_{66}+\frac{1}{4}\beta^4A_m-I_0\omega^2}{A_{11}+\frac{1}{4}\beta^2A_m};a_2=\frac{\beta\left(A_{12}+A_{66}\right)-\frac{1}{4}\beta^3A_m}{A_{11}+\frac{1}{4}\beta^2A_m};a_3=\frac{\frac{1}{4}\beta A_m}{A_{11}+\frac{1}{4}\beta^2A_m};$$

$$a_4=\frac{-\beta^2\left(B_{12}+2B_{66}\right)+I_1\omega^2}{A_{11}+\frac{1}{4}\beta^2A_m};a_5=\frac{B_{11}}{A_{11}+\frac{1}{4}\beta^2A_m};a_6=\frac{-\beta^2\left(B_{12}^s+2B_{66}^s\right)+J_1\omega^2}{A_{11}+\frac{1}{4}\beta^2A_m};$$

$$a_7=\frac{B_{11}^s}{A_{11}+\frac{1}{4}\beta^2A_m}. \tag{C1}$$

$$\begin{aligned}
r_1&=\left[c_3\left(e_4h_2-e_2h_4\right)-e_3\left(c_4h_2-c_2h_4\right)+h_3\left(c_4e_2-c_2e_4\right)\right]/C_0\\
r_2&=\left[c_3\left(e_5h_2-e_2h_5\right)-e_3\left(c_5h_2-c_2h_5\right)+h_3\left(c_5e_2-c_2e_5\right)\right]/C_0\\
r_3&=\left[c_3\left(e_6h_2-e_2h_6\right)-e_3\left(c_6h_2-c_2h_6\right)+h_3\left(c_6e_2-c_2e_6\right)\right]/C_0\\
r_4&=\left[c_3\left(e_7h_2-e_2h_7\right)-e_3\left(c_7h_2-c_2h_7\right)+h_3\left(c_7e_2-c_2e_7\right)\right]/C_0\\
r_5&=\left[c_3\left(e_8h_2-e_2h_8\right)-e_3\left(c_8h_2-c_2h_8\right)+h_3\left(c_8e_2-c_2e_8\right)\right]/C_0\\
r_6&=\left[c_3\left(e_9h_2-e_2h_9\right)-e_3\left(c_9h_2-c_2h_9\right)+h_3\left(c_9e_2-c_2e_9\right)\right]/C_0\\
r_7&=\left[c_3\left(e_{10}h_2-e_2h_{10}\right)-e_3\left(c_{10}h_2-c_2h_{10}\right)+h_3\left(c_{10}e_2-c_2e_{10}\right)\right]/C_0\\
r_8&=\left[c_3\left(e_{11}h_2-e_2h_{11}\right)+e_3c_2h_{11}-h_3c_2e_{11}\right]/C_0
\end{aligned} \tag{C2}$$

$$\begin{aligned}
s_1&=\left[c_1\left(e_4h_3-e_3h_4\right)-e_1\left(c_4h_3-c_3h_4\right)+h_1\left(c_4e_3-c_3e_4\right)\right]/C_0\\
s_2&=\left[c_1\left(e_5h_3-e_3h_5\right)-e_1\left(c_5h_3-c_3h_5\right)+h_1\left(c_5e_3-c_3e_5\right)\right]/C_0\\
s_3&=\left[c_1\left(e_6h_3-e_3h_6\right)-e_1\left(c_6h_3-c_3h_6\right)+h_1\left(c_6e_3-c_3e_6\right)\right]/C_0\\
s_4&=\left[c_1\left(e_7h_3-e_3h_7\right)-e_1\left(c_7h_3-c_3h_7\right)+h_1\left(c_7e_3-c_3e_7\right)\right]/C_0\\
s_5&=\left[c_1\left(e_8h_3-e_3h_8\right)-e_1\left(c_8h_3-c_3h_8\right)+h_1\left(c_8e_3-c_3e_8\right)\right]/C_0\\
s_6&=\left[c_1\left(e_9h_3-e_3h_9\right)-e_1\left(c_9h_3-c_3h_9\right)+h_1\left(c_9e_3-c_3e_9\right)\right]/C_0\\
s_7&=\left[c_1\left(e_{10}h_3-e_3h_{10}\right)-e_1\left(c_{10}h_3-c_3h_{10}\right)+h_1\left(c_{10}e_3-c_3e_{10}\right)\right]/C_0\\
s_8&=\left[c_1\left(e_{11}h_3-e_3h_{11}\right)+e_1c_3h_{11}-h_1c_3e_{11}\right]/C_0
\end{aligned} \tag{C3}$$

$$t_1=\left[c_1\left(e_2h_4-h_2e_4\right)-e_1\left(c_2h_4-h_2c_4\right)+h_1\left(c_2e_4-e_2c_4\right)\right]/C_0$$
$$t_2=\left[c_1\left(e_2h_5-h_2e_5\right)-e_1\left(c_2h_5-h_2c_5\right)+h_1\left(c_2e_5-e_2c_5\right)\right]/C_0$$
$$t_3=\left[c_1\left(e_2h_6-h_2e_6\right)-e_1\left(c_2h_6-h_2c_6\right)+h_1\left(c_2e_6-e_2c_6\right)\right]/C_0$$
$$t_4=\left[c_1\left(e_2h_7-h_2e_7\right)-e_1\left(c_2h_7-h_2c_7\right)+h_1\left(c_2e_7-e_2c_7\right)\right]/C_0$$
$$t_5=\left[c_1\left(e_2h_8-h_2e_8\right)-e_1\left(c_2h_8-h_2c_8\right)+h_1\left(c_2e_8-e_2c_8\right)\right]/C_0$$
$$t_6=\left[c_1\left(e_2h_9-h_2e_9\right)-e_1\left(c_2h_9-h_2c_9\right)+h_1\left(c_2e_9-e_2c_9\right)\right]/C_0$$
$$t_7=\left[c_1\left(e_2h_{10}-h_2e_{10}\right)-e_1\left(c_2h_{10}-h_2c_{10}\right)+h_1\left(c_2e_{10}-e_2c_{10}\right)\right]/C_0$$
$$t_8=\left[c_1\left(e_2h_{11}-h_2e_{11}\right)-e_1c_2h_{11}+h_1c_2e_{11}\right]/C_0 \qquad \text{(C4)}$$

$$b_1=\frac{\beta\left(A_{12}+A_{66}\right)-\frac{1}{4}\beta^3A_m}{\frac{1}{4}A_m};b_2=\beta;b_3=\frac{-\beta^2A_{22}+I_0\omega^2}{\frac{1}{4}A_m};b_4=\frac{A_{66}+\frac{1}{4}\beta^2A_m}{\frac{1}{4}A_m};$$

$$b_5=\frac{\beta^3B_{22}-\beta I_1\omega^2}{\frac{1}{4}A_m};b_6=\frac{-\beta\left(B_{12}+2B_{66}\right)}{\frac{1}{4}A_m};b_7=\frac{\beta^3B_{22}^s-\beta J_1\omega^2}{\frac{1}{4}A_m};b_8=\frac{-\beta\left(B_{12}^s+2B_{66}^s\right)}{\frac{1}{4}A_m}. \qquad \text{(C5)}$$

$$c_1=1-a_3b_2;c_2=-a_5b_2;c_3=-a_7b_2;c_4=b_1+a_1b_2;c_5=b_3;$$

$$c_6=a_2b_2+b_4;c_7=b_5;c_8=a_4b_2+b_6;c_9=b_7;c_{10}=a_6b_2+b_8. \qquad \text{(C6)}$$

$$d_1=\left(D_{11}+A_m\right);d_2=\left[D_{11}^s+\frac{1}{2}\left(A_m+B_m\right)\right];d_3=\left[-\beta^2\left(B_{12}+2B_{66}\right)+I_1\omega^2\right];d_4=B_{11};$$
$$d_5=\left(\beta^3B_{22}-\beta I_1\omega^2\right);d_6=-\beta\left(B_{12}+2B_{66}\right);d_7=\left[-\beta^4\left(D_{22}+A_m\right)+I_0\omega^2+\beta^2I_2\omega^2-\gamma_2P_0\beta^2\right];$$
$$d_8=\left[\beta^2\left(2D_{12}+4D_{66}+2A_m\right)-I_2\omega^2+\gamma_1P_0\right];$$
$$d_9=\left\{-\beta^4\left[D_{22}^s+\frac{1}{2}\left(A_m+B_m\right)\right]+I_0\omega^2+\beta^2J_2\omega^2-\gamma_2P_0\beta^2\right\};$$

$$d_{10}=\left[\beta^2\left(2D_{12}^s+4D_{66}^s\right)-J_2\omega^2+\gamma_1P_0\right];d_{11}=Q_m \qquad \text{(C7)}$$

$$g_1=D_{11}^s+\frac{1}{2}\left(A_m+B_m\right);g_2=H_{11}+\frac{1}{4}\left(A_m+2B_m+C_m\right);g_3=-\beta^2\left(B_{12}^s+2B_{66}^s\right)+J_1\omega^2;g_4=B_{11}^s;$$
$$g_5=\beta^3B_{22}^s-\beta J_1\omega^2;g_6=-\beta\left(B_{12}^s+2B_{66}^s\right);g_7=-\beta^4\left[D_{22}^s+\frac{1}{2}\left(A_m+B_m\right)\right]+I_0\omega^2+\beta^2J_2\omega^2-\gamma_2P_0\beta^2;$$
$$g_8=\beta^2\left(2D_{12}^s+4D_{66}^s\right)-J_2\omega^2+\gamma_1P_0;$$
$$g_9=-\beta^4\left[H_{22}+\frac{1}{4}\left(A_m+2B_m+C_m\right)\right]-\beta^2\left(A_{44}^s+\frac{1}{4}H_m\right)+I_0\omega^2+\beta^2K_2\omega^2-\gamma_2P_0\beta^2;$$

$$g_{10}=\left(A_{55}^s+\frac{1}{4}H_m\right)+\beta^2\left(2H_{12}+4H_{66}\right)-K_2\omega^2+\gamma_1P_0;g_{11}=Q_m \qquad \text{(C8)}$$

$$h_1 = a_3 g_4; h_2 = \left(g_1 - a_5 g_4\right); h_3 = \left(g_2 - a_7 g_4\right); h_4 = \left(a_1 g_4 + g_3\right); h_5 = g_5;$$

$$h_6 = \left(a_2 g_4 + g_6\right); h_7 = g_7; h_8 = \left(a_4 g_4 + g_8\right); h_9 = g_9; h_{10} = \left(a_6 g_4 + g_{10}\right); h_{11} = g_{11}. \quad \text{(C9)}$$

LIST OF PUBLICATIONS

Peer-reviewed papers:

1. **Trinh LC**, Vo TP, Thai H-T, Trung-Kien Nguyen. Size-dependent vibration of bi-directional functionally graded microbeams with arbitrary boundary conditions. *Composites Part B: Engineering* 2017, In press.
2. **Trinh LC**, Vo TP, Thai H-T, Mantari JL. Size-dependent behaviour of functionally graded sandwich microplates under mechanical and thermal loads. *Composites Part B: Engineering* 2017; 124:218-41.
3. **Trinh LC**, Vo TP, Thai H-T, Nguyen T-K. An analytical method for the vibration and buckling of functionally graded beams under mechanical and thermal loads. *Composites Part B: Engineering* 2016; 100:152-63.
4. **Trinh LC**, Nguyen HX, Vo TP, Nguyen T-K. Size-dependent behaviour of functionally graded microbeams using various shear deformation theories based on the modified couple stress theory. *Composite Structures* 2016; 154:556-72.
5. **Trinh LC**, Vo TP, Osofero AI, Lee J. Fundamental frequency analysis of functionally graded sandwich beams based on the state space approach. *Composite Structures* 2016; 156:263-75.

Conference Presentations:

1. **Trinh LC**, Vo TP. Size-dependent vibration and buckling behaviours of functionally graded plates using a Levy-type solution. 20th International conference on Composite Structures, 4-7 September 2017, Paris, France.
2. **Trinh LC**, Vo TP. Vibration and Buckling behaviours of functionally graded microbeams based on a state space approach. 3rd International Conference on Mechanics of Composites, 4-7 July 2017, Bologna, Italy.
3. **Trinh LC**, Vo TP, Analytical solution for thermal buckling analysis of functionally graded sandwich beams. Vibrations and Buckling, 7-9 March 2016, Porto, Portugal.
4. **Trinh LC**, Osofero AI, Vo TP, Nguyen T-K. Free vibration analysis of functionally graded Euler-Bernoulli and Timoshenko beams using Levy-type solution. 2nd International Conference on Agriculture, Biotechnology, Science and Engineering, 28-29 August 2015, Ho Chi Minh City, Vietnam.
5. **Trinh LC**, Vo TP. Levy-type solution for vibration and buckling analysis of functionally graded sandwich plates based on quasi-3D theory. 18th International conference on Composite Structures, 15-18 June 2015, Lisbon, Portugal.

REFERENCES

[1] Koizumi M. FGM activities in Japan. Composites Part B. 1997;28B:1-4.

[2] Tobioka M. ACE COAT AC 15 aluminum oxide coated cutting tool for highly efficient machining. Technical Report "Sumitomodenki". 1989;135:190-6.

[3] Gasik MM. Functionally graded materials: bulk processing techniques. International Journal of Materials and Product Technology. 2010;39:20-9.

[4] Miyamoto Y, Kaysser W, Rabin B, Kawasaki A, Ford R. Functionally graded materials: design, processing and applications: Springer Science & Business Media; 2013.

[5] Fleck NA, Muller GM, Ashby MF, Hutchinson JW. Strain gradient plasticity: Theory and experiment. Acta Metallurgica et Materialia. 1994;42(2):475-87.

[6] Stolken JS, Evans AG. A microbend test method for measuring the plasticity length scale. Acta Metall Mater. 1998;46:5109-15.

[7] Lam DCC, Yang F, Chong ACM, Wang J, Tong P. Experiments and theory in strain gradient elasticity. Journal of the Mechanics and Physics of Solids. 2003;51(8):1477-508.

[8] Koizumi M. The concept of FGM. Ceramic Transactions, Functionally Gradient Materials. 1993;34:3-10.

[9] Hill R. The Elastic Behaviour of a Crystalline Aggregate. Proceedings of the Physical Society Section A. 1952;65(5):349.

[10] Kim HS, Hong SI, Kim SJ. On the rule of mixtures for predicting the mechanical properties of composites with homogeneously distributed soft and hard particles - - Sun Ig Hong - Sun Jae Kim .pdf>. Journal of Materials Processing Technology. 2001;112:109-13.

[11] Gupta A, Talha M. Recent development in modeling and analysis of functionally graded materials and structures. Progress in Aerospace Sciences. 2015;79:1-14.

[12] Mori T, Tanaka K. Average stress in matrix and average elastic energy of materials with misfitting inclusions. Acta Metallurgica. 1973;21(5):571-4.

[13] Malekzadeh P, Monajjemzadeh SM. Dynamic response of functionally graded beams in a thermal environment under a moving load. Mechanics of Advanced Materials and Structures. 2015;23(3):248-58.

[14] Shen H-S, Wang Z-X. Nonlinear analysis of shear deformable FGM beams resting on elastic foundations in thermal environments. International Journal of Mechanical Sciences. 2014;81:195-206.

[15] Cosserat E, Cosserat F. Theory of deformable bodies (Translated by D.H. Delphenich). Paris: Sorbonne: Herman and Sons; 1909.

[16] Thai H-T, Vo TP, Nguyen T-K, Kim S-E. A review of continuum mechanics models for size-dependent analysis of beams and plates. Composite Structures. 2017;177:196-219.

[17] Eringen AC. Simple microfluids. International Journal of Engineering Science. 1964;2:205-17.

[18] Eringen AC, Suhubi ES. Nonlinear theory of simple microelastic solid-II. International Journal of Engineering Science. 1964;2:389–404.

[19] Eringen AC. Linear theory of micropolar elasticity Journal of Mathematics and Mechanics. 1966;15(6):909-23.

[20] Eringen AC. Micropolar fluids with stretch. International Journal of Engineering Science. 1969;7:115-27.

[21] Eringen AC. Microcontinuum field theories I: Foundation and solids. Newyork: Springer Science+Business Media, LLC; 1999.

[22] Eringen AC. Microcontinuum field theories: II. Fuent Media: Springer; 2001.

[23] Ansari R, Bazdid-Vahdati M, Shakouri AH, Norouzzadeh A, Rouhi H. Micromorphic prism element. Math Mech Solids. 2017;22(6):1438-61.

[24] Ansari R, Shakouri AH, Bazdid-Vahdati M, Norouzzadeh A, Rouhi H. A Nonclassical Finite Element Approach for the Nonlinear Analysis of Micropolar Plates. J Comput Nonlin Dyn. 2017;12(1).

[25] Ansari R, Bazdid-Vahdati M, Shakouri A, Norouzzadeh A, Rouhi H. Micromorphic first-order shear deformable plate element. Meccanica. 2016;51(8):1797-809.
[26] Kröner E. Elasticity theory of materials with long range cohesive forces. International Journal of Solids and Structures. 1967;3(5):731-42.
[27] Eringen AC. Linear theory of nonlocal elasticity and dispersion of plane waves. International Journal of Engineering Science. 1972;10(5):425-35.
[28] Eringen AC. Nonlocal polar elastic continua. International Journal of Engineering Science. 1972;10(1):1-16.
[29] Eringen AC, Edelen DGB. On nonlocal elasticity. International Journal of Engineering Science. 1972;10(3):233-48.
[30] Mindlin RD. Micro-structure in linear elasticity. Archives of Rational Mechanics and Analysis. 1964;16:51-78.
[31] Mindlin RD. Second gradient of strain and surface tension in linear elasticity. Archive for Rational Mechanics and Analysis. 1965;16:51-78.
[32] Toupin RA. Elastic materials with couple stresses. Archives of Rational of Mechanical and Analysis. 1962;11:385–414.
[33] Toupin RA. Theory of elasticity with couple stresses. Archives of Rational Mechanics and Analysis. 1964;17:85-112.
[34] Mindlin RD, Tiersten HF. Effects of couple-stresses in linear elasticity. Archives of Rational Mechanics and Analysis. 1962;11:415–48.
[35] Koiter WT. Couple stresses in the theory of elasticity. I and II Proc K Ned Akad Wet 1964;B(67):17-44.
[36] Yang F, Chong ACM, Lam DCC, Tong P. Couple stress based strain gradient theory for elasticity. International Journal of Solids and Structures. 2002;39:2731–43.
[37] Alshorbagy AE, Eltaher MA, Mahmoud FF. Free vibration characteristics of a functionally graded beam by finite element method. Applied Mathematical Modelling. 2011;35(1):412-25.
[38] Şimşek M, Kocatürk T. Free and forced vibration of a functionally graded beam subjected to a concentrated moving harmonic load. Composite Structures. 2009;90(4):465-73.
[39] Jin C, Wang X. Accurate free vibration analysis of Euler functionally graded beams by the weak form quadrature element method. Composite Structures. 2015;125:41-50.
[40] Aydogdu M, Taskin V. Free vibration analysis of functionally graded beams with simply supported edges. Materials & Design. 2007;28(5):1651-6.
[41] Su H, Banerjee JR, Cheung CW. Dynamic stiffness formulation and free vibration analysis of functionally graded beams. Composite Structures. 2013;106:854-62.
[42] Su H, Banerjee JR. Development of dynamic stiffness method for free vibration of functionally graded Timoshenko beams. Computers & Structures. 2015;147:107-16.
[43] Nguyen T-K, Vo TP, Thai H-T. Static and free vibration of axially loaded functionally graded beams based on the first-order shear deformation theory. Composites Part B: Engineering. 2013;55:147-57.
[44] Sina SA, Navazi HM, Haddadpour H. An analytical method for free vibration analysis of functionally graded beams. Materials & Design. 2009;30(3):741-7.
[45] Thai H-T, Vo TP. Bending and free vibration of functionally graded beams using various higher-order shear deformation beam theories. International Journal of Mechanical Sciences. 2012;62(1):57-66.
[46] Wattanasakulpong N, Gangadhara Prusty B, Kelly DW, Hoffman M. Free vibration analysis of layered functionally graded beams with experimental validation. Materials & Design. 2012;36:182-90.
[47] Pradhan KK, Chakraverty S. Free vibration of Euler and Timoshenko functionally graded beams by Rayleigh–Ritz method. Composites Part B: Engineering. 2013;51:175-84.
[48] Pradhan KK, Chakraverty S. Effects of different shear deformation theories on free vibration of functionally graded beams. International Journal of Mechanical Sciences. 2014;82:149-60.

[49] Şimşek M. Fundamental frequency analysis of functionally graded beams by using different higher-order beam theories. Nuclear Engineering and Design. 2010;240(4):697-705.
[50] Mashat DS, Carrera E, Zenkour AM, Al Khateeb SA, Filippi M. Free vibration of FGM layered beams by various theories and finite elements. Composites Part B: Engineering. 2014;59:269-78.
[51] Vo TP, Thai H-T, Nguyen T-K, Maheri A, Lee J. Finite element model for vibration and buckling of functionally graded sandwich beams based on a refined shear deformation theory. Engineering Structures. 2014;64:12-22.
[52] Nguyen T-K, Nguyen TT-P, Vo TP, Thai H-T. Vibration and buckling analysis of functionally graded sandwich beams by a new higher-order shear deformation theory. Composites Part B: Engineering. 2015;76:273-85.
[53] Bui TQ, Khosravifard A, Zhang C, Hematiyan MR, Golub MV. Dynamic analysis of sandwich beams with functionally graded core using a truly meshfree radial point interpolation method. Engineering Structures. 2013;47:90-104.
[54] Chehel Amirani M, Khalili SMR, Nemati N. Free vibration analysis of sandwich beam with FG core using the element free Galerkin method. Composite Structures. 2009;90(3):373-9.
[55] Yang Y, Lam CC, Kou KP, Iu VP. Free vibration analysis of the functionally graded sandwich beams by a meshfree boundary-domain integral equation method. Composite Structures. 2014;117:32-9.
[56] Murín J, Aminbaghai M, Kutiš V. Exact solution of the bending vibration problem of FGM beams with variation of material properties. Engineering Structures. 2010;32(6):1631-40.
[57] Hsu J-C, Lai H-Y, Chen Co-K. An innovative eigenvalue problem solver for free vibration of uniform Timoshenko beams by using the Adomian modified decomposition method. Journal of Sound and Vibration. 2009;325(1-2):451-70.
[58] Sari Me, Butcher EA. Natural frequencies and critical loads of beams and columns with damaged boundaries using Chebyshev polynomials. International Journal of Engineering Science. 2010;48(10):862-73.
[59] Sari Me, Butcher EA. Free vibration analysis of non-rotating and rotating Timoshenko beams with damaged boundaries using the Chebyshev collocation method. International Journal of Mechanical Sciences. 2012;60(1):1-11.
[60] Şimşek M, Cansız S. Dynamics of elastically connected double-functionally graded beam systems with different boundary conditions under action of a moving harmonic load. Composite Structures. 2012;94(9):2861-78.
[61] Shahba A, Attarnejad R, Marvi MT, Hajilar S. Free vibration and stability analysis of axially functionally graded tapered Timoshenko beams with classical and non-classical boundary conditions. Composites Part B: Engineering. 2011;42(4):801-8.
[62] Wattanasakulpong N, Mao Q. Dynamic response of Timoshenko functionally graded beams with classical and non-classical boundary conditions using Chebyshev collocation method. Composite Structures. 2015;119:346-54.
[63] Sankar BV, Tzeng JT. Thermal Stresses in Functionally Graded Beams. AIAA Journal. 2002;40(6):1228-32.
[64] Esfahani SE, Kiani Y, Eslami MR. Non-linear thermal stability analysis of temperature dependent FGM beams supported on non-linear hardening elastic foundations International Journal of Mechanical Sciences. 2013;69:10-20.
[65] Ghiasian SE, Kiani Y, Eslami MR. Nonlinear thermal dynamic buckling of FGM beams. European Journal of Mechanics - A/Solids. 2015;54:232-42.
[66] Sun Y, Li S-R, Batra RC. Thermal buckling and post-buckling of FGM Timoshenko beams on nonlinear elastic foundation. Journal of Thermal Stresses. 2016;39(1):11-26.
[67] Wattanasakulpong N, Gangadhara Prusty B, Kelly DW. Thermal buckling and elastic vibration of third-order shear deformable functionally graded beams. International Journal of Mechanical Sciences. 2011;53(9):734-43.

[68] Khdeir AA, Reddy JN. Free vibration of cross-ply laminated beams with arbitrary boundary conditions. International Journal of Engineering Science. 1994;32(12):1971-80.
[69] Khdeir AA, Reddy JN. An exact solution for the bending of thin and thick cross-ply laminated beams. Composite Structures. 1997;37:195-203.
[70] Khdeir AA. Dynamic response of antisymmetric cross-ply laminated composite beams with arbitrary boundary conditions. Int Z Engng Sci. 1996;34(1):9-19.
[71] Reddy JN. A simple higher-order theory for laminated composite plates. J Appl Mech. 1984;51 (4):745-52.
[72] Thai HT, Kim SE. Levy-type solution for free vibration analysis of orthotropic plates based on two variable refined plate theory. Applied Mathematical Modelling. 2012;36(8):3870-82.
[73] Trinh LC, Vo TP, Osofero AI, Lee J. Fundamental frequency analysis of functionally graded sandwich beams based on the state space approach. Composite Structures. 2016;156:263-75.
[74] Trinh LC, Vo TP, Thai H-T, Nguyen T-K. An analytical method for the vibration and buckling of functionally graded beams under mechanical and thermal loads. Composites Part B: Engineering. 2016;100:152-63.
[75] Pradhan KK, Chakraverty S. Generalized power-law exponent based shear deformation theory for free vibration of functionally graded beams. Applied Mathematics and Computation. 2015;268:1240-58.
[76] Li S-R, Batra RC. Relations between buckling loads of functionally graded Timoshenko and homogeneous Euler–Bernoulli beams. Composite Structures. 2013;95:5-9.
[77] Fazzolari FA. Stability analysis of FGM sandwich plates by using variable-kinematics Ritz models. Mechanics of Advanced Materials and Structures. 2016;23(9):1104-13.
[78] Reddy JN, Chin CD. Thermomechanical Analysis of Functionally Graded Cylinders and Plates. Journal of Thermal Stresses. 1998;21(6):593-626.
[79] Ebrahimi F, Salari E. Thermal buckling and free vibration analysis of size dependent Timoshenko FG nanobeams in thermal environments. Composite Structures. 2015;128:363-80.
[80] Ebrahimi F, Salari E. Nonlocal thermo-mechanical vibration analysis of functionally graded nanobeams in thermal environment. Acta Astronautica. 2015;113:29-50.
[81] Park SK, Gao XL. Bernoulli–Euler beam model based on a modified couple stress theory. Journal of Micromechanics and Microengineering. 2006;16(11):2355-9.
[82] Kong S, Zhou S, Nie Z, Wang K. The size-dependent natural frequency of Bernoulli–Euler micro-beams. International Journal of Engineering Science. 2008;46(5):427-37.
[83] Xia W, Wang L, Yin L. Nonlinear non-classical microscale beams: Static bending, postbuckling and free vibration. International Journal of Engineering Science. 2010;48(12):2044-53.
[84] Ma H, Gao X, Reddy J. A microstructure-dependent Timoshenko beam model based on a modified couple stress theory. Journal of the Mechanics and Physics of Solids. 2008;56(12):3379-91.
[85] Asghari M, Ahmadian MT, Kahrobaiyan MH, Rahaeifard M. On the size-dependent behavior of functionally graded micro-beams. Materials & Design. 2010;31(5):2324-9.
[86] Ke L-L, Wang Y-S. Size effect on dynamic stability of functionally graded microbeams based on a modified couple stress theory. Composite Structures. 2011;93(2):342-50.
[87] Ke L-L, Wang Y-S, Yang J, Kitipornchai S. Nonlinear free vibration of size-dependent functionally graded microbeams. International Journal of Engineering Science. 2012;50(1):256-67.
[88] Dehrouyeh-Semnani AM, Mostafaei H, Nikkhah-Bahrami M. Free flexural vibration of geometrically imperfect functionally graded microbeams. International Journal of Engineering Science. 2016;105:56-79.
[89] Reddy JN. Microstructure-dependent couple stress theories of functionally graded beams. Journal of the Mechanics and Physics of Solids. 2011;59(11):2382-99.

[90] Şimşek M, Kocatürk T, Akbaş ŞD. Static bending of a functionally graded microscale Timoshenko beam based on the modified couple stress theory. Composite Structures. 2013;95:740-7.
[91] Kahrobaiyan MH, Asghari M, Ahmadian MT. A Timoshenko beam element based on the modified couple stress theory. International Journal of Mechanical Sciences. 2014;79:75-83.
[92] Thai H-T, Vo TP, Nguyen T-K, Lee J. Size-dependent behaviour of functionally graded sandwich microbeams based on the modified couple stress theory. Composite Structures. 2014.
[93] Nateghi A, Salamat-talab M. Thermal effect on size dependent behavior of functionally graded microbeams based on modified couple stress theory. Composite Structures. 2013;96:97-110.
[94] Akgöz B, Civalek Ö. Free vibration analysis of axially functionally graded tapered Bernoulli–Euler microbeams based on the modified couple stress theory. Composite Structures. 2013;98:314-22.
[95] Nateghi A, Salamat-talab M, Rezapour J, Daneshian B. Size dependent buckling analysis of functionally graded micro beams based on modified couple stress theory. Applied Mathematical Modelling. 2012;36(10):4971-87.
[96] Salamat-talab M, Nateghi A, Torabi J. Static and dynamic analysis of third-order shear deformation FG micro beam based on modified couple stress theory. International Journal of Mechanical Sciences. 2012;57(1):63-73.
[97] Ansari R, Gholami R, Faghih Shojaei M, Mohammadi V, Sahmani S. Size-dependent bending, buckling and free vibration of functionally graded Timoshenko microbeams based on the most general strain gradient theory. Composite Structures. 2013;100:385-97.
[98] Sahmani S, Ansari R. Size-dependent buckling analysis of functionally graded third-order shear deformable microbeams including thermal environment effect. Applied Mathematical Modelling. 2013;37(23):9499-515.
[99] Mohammad-Abadi M, Daneshmehr AR. Size dependent buckling analysis of microbeams based on modified couple stress theory with high order theories and general boundary conditions. International Journal of Engineering Science. 2014;74:1-14.
[100] Şimşek M, Reddy JN. Bending and vibration of functionally graded microbeams using a new higher order beam theory and the modified couple stress theory. International Journal of Engineering Science. 2013;64:37-53.
[101] Akgöz B, Civalek Ö. Thermo-mechanical buckling behavior of functionally graded microbeams embedded in elastic medium. International Journal of Engineering Science. 2014;85:90-104.
[102] Akgöz B, Civalek Ö. Shear deformation beam models for functionally graded microbeams with new shear correction factors. Composite Structures. 2014;112:214-25.
[103] Darijani H, Mohammadabadi H. A new deformation beam theory for static and dynamic analysis of microbeams. International Journal of Mechanical Sciences. 2014;89:31-9.
[104] Al-Basyouni KS, Tounsi A, Mahmoud SR. Size dependent bending and vibration analysis of functionally graded micro beams based on modified couple stress theory and neutral surface position. Composite Structures. 2015;125:621-30.
[105] Arbind A, Reddy JN. Nonlinear analysis of functionally graded microstructure-dependent beams. Composite Structures. 2013;98:272-81.
[106] Arbind A, Reddy JN, Srinivasa AR. Modified Couple Stress-Based Third-Order Theory for Nonlinear Analysis of Functionally Graded Beams. Latin American journal of solids and structures. 2014;11:459-87.
[107] Trinh LC, Nguyen HX, Vo TP, Nguyen T-K. Size-dependent behaviour of functionally graded microbeams using various shear deformation theories based on the modified couple stress theory. Composite Structures. 2016;154:556-72.
[108] Eringen AC. On differential equations of nonlocal elasticity and solutions of screw dislocation and surface waves. Journal of Applied Physics. 1983;54:4703-10.

[109] Romanoff J, Reddy JN, Jelovica J. Using non-local Timoshenko beam theories for prediction of micro- and macro-structural responses. Composite Structures. 2015.
[110] Reddy JN, El-Borgi S, Romanoff J. Non-linear analysis of functionally graded microbeams using Eringen's non-local differential model. International Journal of Non-Linear Mechanics. 2014;67:308-18.
[111] Apuzzo A, Barretta R, Canadija M, Feo L, Luciano R, Marotti de Sciarra F. A closed-form model for torsion of nanobeams with an enhanced nonlocal formulation. Composites Part B: Engineering. 2017;108:315-24.
[112] Romano G, Barretta R. Stress-driven versus strain-driven nonlocal integral model for elastic nano-beams. Composites Part B: Engineering. 2017;114:184-8.
[113] Romano G, Barretta R, Diaco M. Micromorphic continua: non-redundant formulations. Continuum Mechanics and Thermodynamics. 2016;28(6):1659-70.
[114] Barretta R, Feo L, Luciano R, Marotti de Sciarra F. Application of an enhanced version of the Eringen differential model to nanotechnology. Composites Part B: Engineering. 2016;96:274-80.
[115] Barretta R, Feo L, Luciano R, Marotti de Sciarra F, Penna R. Functionally graded Timoshenko nanobeams: A novel nonlocal gradient formulation. Composites Part B: Engineering. 2016;100:208-19.
[116] Barretta R, Feo L, Luciano R, Marotti de Sciarra F. An Eringen-like model for Timoshenko nanobeams. Composite Structures. 2016;139:104-10.
[117] Fleck NA, Hutchinson JW. A reformulation of strain gradient plasticity. Journal of the Mechanics and Physics of Solids. 2001;49:2245–71.
[118] Asghari M, Rahaeifard M, Kahrobaiyan MH, Ahmadian MT. The modified couple stress functionally graded Timoshenko beam formulation. Materials & Design. 2011;32(3):1435-43.
[119] Vo TP, Thai H-T, Nguyen T-K, Inam F, Lee J. A quasi-3D theory for vibration and buckling of functionally graded sandwich beams. Composite Structures. 2015;119:1-12.
[120] Vo TP, Thai H-T, Nguyen T-K, Inam F, Lee J. Static behaviour of functionally graded sandwich beams using a quasi-3D theory. Composites Part B: Engineering. 2015;68:59-74.
[121] Thai H-T, Vo TP, Bui TQ, Nguyen T-K. A quasi-3D hyperbolic shear deformation theory for functionally graded plates. Acta Mechanica. 2013;225(3):951-64.
[122] Şimşek M, Reddy JN. A unified higher order beam theory for buckling of a functionally graded microbeam embedded in elastic medium using modified couple stress theory. Composite Structures. 2013;101:47-58.
[123] Dehrouyeh-Semnani AM, Nikkhah-Bahrami M. A discussion on incorporating the Poisson effect in microbeam models based on modified couple stress theory. International Journal of Engineering Science. 2015;86:20-5.
[124] Lü CF, Chen WQ, Xu RQ, Lim CW. Semi-analytical elasticity solutions for bi-directional functionally graded beams. International Journal of Solids and Structures. 2008;45(1):258-75.
[125] Lezgy-Nazargah M. Fully coupled thermo-mechanical analysis of bi-directional FGM beams using NURBS isogeometric finite element approach. Aerospace Science and Technology. 2015;45:154-64.
[126] Şimşek M. Bi-directional functionally graded materials (BDFGMs) for free and forced vibration of Timoshenko beams with various boundary conditions. Composite Structures. 2015;133:968-78.
[127] Şimşek M. Buckling of Timoshenko beams composed of two-dimensional functionally graded material (2D-FGM) having different boundary conditions. Composite Structures. 2016;149:304-14.
[128] Hao D, Wei C. Dynamic characteristics analysis of bi-directional functionally graded Timoshenko beams. Composite Structures. 2016;141:253-63.
[129] Huynh TA, Lieu XQ, Lee J. NURBS-based modeling of bidirectional functionally graded Timoshenko beams for free vibration problem. Composite Structures. 2017;160:1178-90.

[130] Karamanlı A. Elastostatic analysis of two-directional functionally graded beams using various beam theories and Symmetric Smoothed Particle Hydrodynamics method. Composite Structures. 2017;160:653-69.
[131] Karamanlı A. Bending behaviour of two directional functionally graded sandwich beams by using a quasi-3d shear deformation theory. Composite Structures. 2017;174:70-86.
[132] Nejad MZ, Hadi A. Eringen's non-local elasticity theory for bending analysis of bi-directional functionally graded Euler–Bernoulli nano-beams. International Journal of Engineering Science. 2016;106:1-9.
[133] Nejad MZ, Hadi A. Non-local analysis of free vibration of bi-directional functionally graded Euler–Bernoulli nano-beams. International Journal of Engineering Science. 2016;105:1-11.
[134] Nejad MZ, Hadi A, Rastgoo A. Buckling analysis of arbitrary two-directional functionally graded Euler–Bernoulli nano-beams based on nonlocal elasticity theory. International Journal of Engineering Science. 2016;103:1-10.
[135] Shafiei N, Kazemi M. Buckling analysis on the bi-dimensional functionally graded porous tapered nano-/micro-scale beams. Aerospace Science and Technology. 2017;66:1-11.
[136] Shafiei N, Mirjavadi SS, MohaselAfshari B, Rabby S, Kazemi M. Vibration of two-dimensional imperfect functionally graded (2D-FG) porous nano-/micro-beams. Computer Methods in Applied Mechanics and Engineering. 2017;322:615-32.
[137] Vo TP, Thai H-T, Nguyen T-K, Lanc D, Karamanli A. Flexural analysis of laminated composite and sandwich beams using a four-unknown shear and normal deformation theory. Composite Structures. 2017;176:388-97.
[138] Vo TP, Thai H-T, Aydogdu M. Free vibration of axially loaded composite beams using a four-unknown shear and normal deformation theory. Composite Structures. 2017.
[139] Trinh LC, Vo TP, Thai H-T, Nguyen T-K. Size-dependent vibration of bi-directional functionally graded microbeams with arbitrary boundary conditions. Composites Part B: Engineering. 2017.
[140] Ansari R, Shojaei MF, Gholami R. Size-dependent nonlinear mechanical behavior of third-order shear deformable functionally graded microbeams using the variational differential quadrature method. Composite Structures. 2016;136:669-83.
[141] Tsiatas GC. A new Kirchhoff plate model based on a modified couple stress theory. International Journal of Solids and Structures. 2009;46(13):2757-64.
[142] Yin L, Qian Q, Wang L, Xia W. Vibration analysis of microscale plates based on modified couple stress theory. Acta Mechanica Solida Sinica. 2010;23(5):386-93.
[143] Jomehzadeh E, Noori HR, Saidi AR. The size-dependent vibration analysis of micro-plates based on a modified couple stress theory. Physica E: Low-dimensional Systems and Nanostructures. 2011;43(4):877-83.
[144] Akgöz B, Civalek Ö. Free vibration analysis for single-layered graphene sheets in an elastic matrix via modified couple stress theory. Materials & Design. 2012;42:164-71.
[145] Akgöz B, Civalek Ö. Modeling and analysis of micro-sized plates resting on elastic medium using the modified couple stress theory. Meccanica. 2012;48(4):863-73.
[146] Askari AR, Tahani M. Analytical determination of size-dependent natural frequencies of fully clamped rectangular microplates based on the modified couple stress theory. Journal of Mechanical Science and Technology. 2015;29(5):2135-45.
[147] Şimşek M, Aydın M, Yurtcu HH, Reddy JN. Size-dependent vibration of a microplate under the action of a moving load based on the modified couple stress theory. Acta Mechanica. 2015;226(11):3807-22.
[148] Asghari M. Geometrically nonlinear micro-plate formulation based on the modified couple stress theory. International Journal of Engineering Science. 2012;51:292-309.
[149] Wang Y-G, Lin W-H, Liu N. Large amplitude free vibration of size-dependent circular microplates based on the modified couple stress theory. International Journal of Mechanical Sciences. 2013;71:51-7.

[150] Wang Y-G, Lin W-H, Zhou C-L. Nonlinear bending of size-dependent circular microplates based on the modified couple stress theory. Archive of Applied Mechanics. 2013;84(3):391-400.
[151] Farokhi H, Ghayesh MH. Nonlinear dynamical behaviour of geometrically imperfect microplates based on modified couple stress theory. International Journal of Mechanical Sciences. 2015;90:133-44.
[152] Ke LL, Yang J, Kitipornchai S, Bradford MA. Bending, buckling and vibration of size-dependent functionally graded annular microplates. Composite Structures. 2012;94(11):3250-7.
[153] Asghari M, Taati E. A size-dependent model for functionally graded micro-plates for mechanical analyses. Journal of Vibration and Control. 2012;19(11):1614-32.
[154] Taati E. Analytical solutions for the size dependent buckling and postbuckling behavior of functionally graded micro-plates. International Journal of Engineering Science. 2016;100:45-60.
[155] Ma HM, Gao XL, Reddy JN. A non-classical Mindlin plate model based on a modified couple stress theory. Acta Mechanica. 2011;220(1-4):217-35.
[156] Ke L-L, Wang Y-S, Yang J, Kitipornchai S. Free vibration of size-dependent Mindlin microplates based on the modified couple stress theory. Journal of Sound and Vibration. 2012;331(1):94-106.
[157] Roque CMC, Ferreira AJM, Reddy JN. Analysis of Mindlin micro plates with a modified couple stress theory and a meshless method. Applied Mathematical Modelling. 2013;37(7):4626-33.
[158] Thai H-T, Choi D-H. Size-dependent functionally graded Kirchhoff and Mindlin plate models based on a modified couple stress theory. Composite Structures. 2013;95:142-53.
[159] Jung W-Y, Han S-C, Park W-T. A modified couple stress theory for buckling analysis of S-FGM nanoplates embedded in Pasternak elastic medium. Composites Part B: Engineering. 2014;60:746-56.
[160] Jung W-Y, Park W-T, Han S-C. Bending and vibration analysis of S-FGM microplates embedded in Pasternak elastic medium using the modified couple stress theory. International Journal of Mechanical Sciences. 2014;87:150-62.
[161] Ansari R, Faghih Shojaei M, Mohammadi V, Gholami R, Darabi MA. Nonlinear vibrations of functionally graded Mindlin microplates based on the modified couple stress theory. Composite Structures. 2014;114:124-34.
[162] Ansari R, Gholami R, Faghih Shojaei M, Mohammadi V, Darabi MA. Size-dependent nonlinear bending and postbuckling of functionally graded Mindlin rectangular microplates considering the physical neutral plane position. Composite Structures. 2015;127:87-98.
[163] Gao XL, Huang JX, Reddy JN. A non-classical third-order shear deformation plate model based on a modified couple stress theory. Acta Mechanica. 2013;224(11):2699-718.
[164] Thai H-T, Kim S-E. A size-dependent functionally graded Reddy plate model based on a modified couple stress theory. Composites Part B: Engineering. 2013;45(1):1636-45.
[165] Eshraghi I, Dag S, Soltani N. Consideration of spatial variation of the length scale parameter in static and dynamic analyses of functionally graded annular and circular micro-plates. Composites Part B: Engineering. 2015;78:338-48.
[166] Thai H-T, Vo TP. A size-dependent functionally graded sinusoidal plate model based on a modified couple stress theory. Composite Structures. 2013;96:376-83.
[167] He L, Lou J, Zhang E, Wang Y, Bai Y. A size-dependent four variable refined plate model for functionally graded microplates based on modified couple stress theory. Composite Structures. 2015;130:107-15.
[168] Lou J, He LW, Du JK. A unified higher order plate theory for functionally graded microplates based on the modified couple stress theory. Composite Structures. 2015;133:1036-47.
[169] Nguyen HX, Nguyen TN, Abdel-Wahab M, Bordas SPA, Nguyen-Xuan H, Vo TP. A refined quasi-3D isogeometric analysis for functionally graded microplates based on the modified

couple stress theory. Computer Methods in Applied Mechanics and Engineering. 2017;313:904-40.
[170] Reddy JN, Kim J. A nonlinear modified couple stress-based third-order theory of functionally graded plates. Composite Structures. 2012;94(3):1128-43.
[171] Kim J, Reddy JN. Analytical solutions for bending, vibration, and buckling of FGM plates using a couple stress-based third-order theory. Composite Structures. 2013;103:86-98.
[172] Mirsalehi M, Azhari M, Amoushahi H. Stability of thin FGM microplate subjected to mechanical and thermal loading based on the modified couple stress theory and spline finite strip method. Aerospace Science and Technology. 2015;47:356-66.
[173] Ashoori AR, Sadough Vanini SA. Thermal buckling of annular microstructure-dependent functionally graded material plates resting on an elastic medium. Composites Part B: Engineering. 2016;87:245-55.
[174] Ashoori AR, Sadough Vanini SA. Nonlinear thermal stability and snap-through behavior of circular microstructure-dependent FGM plates. European Journal of Mechanics - A/Solids. 2016;59:323-32.
[175] Eshraghi I, Dag S, Soltani N. Bending and free vibrations of functionally graded annular and circular micro-plates under thermal loading. Composite Structures. 2016;137:196-207.
[176] Zenkour AM, Alghamdi NA. Thermoelastic bending analysis of functionally graded sandwich plates. Journal of Materials Science. 2008;43(8):2574-89.
[177] Thai H-T, Kim S-E. A simple quasi-3D sinusoidal shear deformation theory for functionally graded plates. Composite Structures. 2013;99:172-80.
[178] Trinh LC, Vo TP, Thai H-T, Mantari JL. Size-dependent behaviour of functionally graded sandwich microplates under mechanical and thermal loads. Composites Part B: Engineering. 2017;124:218-41.
[179] Lei J, He Y, Zhang B, Liu D, Shen L, Guo S. A size-dependent FG micro-plate model incorporating higher-order shear and normal deformation effects based on a modified couple stress theory. International Journal of Mechanical Sciences. 2015;104:8-23.
[180] Tounsi A, Houari MSA, Benyoucef S, Adda Bedia EA. A refined trigonometric shear deformation theory for thermoelastic bending of functionally graded sandwich plates. Aerospace Science and Technology. 2013;24(1):209-20.
[181] Mantari JL, Granados EV. Thermoelastic analysis of advanced sandwich plates based on a new quasi-3D hybrid type HSDT with 5 unknowns. Composites Part B: Engineering. 2015;69:317-34.
[182] Ungbhakorn V, Wattanasakulpong N. Thermo-elastic vibration analysis of third-order shear deformable functionally graded plates with distributed patch mass under thermal environment. Applied Acoustics. 2013;74(9):1045-59.
[183] Bouiadjra MB, Ahmed Houari MS, Tounsi A. Thermal Buckling of Functionally Graded Plates According to a Four-Variable Refined Plate Theory. Journal of Thermal Stresses. 2012;35(8):677-94.
[184] Akavci SS. Thermal Buckling Analysis of Functionally Graded Plates on an Elastic Foundation According to a Hyperbolic Shear Deformation Theory. Mech Compos Mater. 2014;50(2):197-212.
[185] Thai H-T, Choi D-H. Finite element formulation of various four unknown shear deformation theories for functionally graded plates. Finite Elements in Analysis and Design. 2013;75:50-61.
[186] Demirhan PA, Taskin V. Levy solution for bending analysis of functionally graded sandwich plates based on four variable plate theory. Composite Structures. 2017;177:80-95.
[187] Thai HT, Choi DH. Size-dependent functionally graded Kirchhoff and Mindlin plate models based on a modified couple stress theory. Composite Structures. 2013;95:142-53.
[188] Abazid MA, Sobhy M. Thermo-electro-mechanical bending of FG piezoelectric microplates on Pasternak foundation based on a four-variable plate model and the modified couple stress theory. Microsystem Technologies. 2017.

[189] Thai HT, Choi DH. Levy solution for free vibration analysis of functionally graded plates based on a refined plate theory. Ksce J Civ Eng. 2014;18(6):1813-24.
[190] Hosseini-Hashemi S, Fadaee M, Atashipour SR. A new exact analytical approach for free vibration of Reissner–Mindlin functionally graded rectangular plates. International Journal of Mechanical Sciences. 2011;53(1):11-22.
[191] Thai HT, Uy B. Levy solution for buckling analysis of functionally graded plates based on a refined plate theory. P I Mech Eng C-J Mec. 2013;227(12):2649-64.